UNIVERSITÀ
DEGLI STUDI
DI PADOVA

Sede Amministrativa Università degli Studi di Padova
Dipartimento di Ingegneria Industriale

Scuola di Dottorato in Ingegneria Industriale
Indirizzo Ingegneria Chimica, dei Materiali e della Produzione
Ciclo XXVI

High-throughput Human Cell Reprogramming through Substrate and Microfluidics Integration

Direttore della Scuola: Ch.mo Prof. Paolo Colombo

Coordinatore d'Indirizzo: Ch.mo Prof. Enrico Savio

Supervisore: Dr. Nicola Elvassore

Dottorando: Stefano Giulitti

Foreword

All the material reported in this dissertation is original unless explicit references to studies carried out by other people are indicated.

During this PhD program the following publications have been produced:

- Dupont S, Morsut L, Aragona M, Enzo E, Giulitti S, Cordenonsi M, Zanconato F, Le Digabel J, Forcato M, Bicciato S and others. 2011. Role of YAP/TAZ in mechanotransduction. Nature. 474(7350):179-U212.

- Cimetta E, Franzoso M, Trevisan M, Serena E, Zambon A, Giulitti S, Barzon L, Elvassore N. 2012. Microfluidic-driven viral infection on cell cultures: theoretical and experimental study. Biomicrofluidics. 6, 024127.

- Lamberti F, Giulitti S, Giomo M, Elvassore N. 2013. Biosensing with electroconductive biomimetic soft materials. Journal of Materials Chemistry B. 1: 5083-5091.

- Aragona M, Panciera T, Manfrin M, Giulitti S, Michielin F, Elvassore N, Dupont S, Piccolo S. 2013. A Mechanical Checkpoint Controls Multicellular Growth through YAP/TAZ Regulation by Actin-Processing Factors. Cell. 154(5):1047-1059.

- Giulitti S, Magrofuoco E, Prevedello L, Elvassore N. 2013. Optimal periodic perfusion strategy for robust long-term microfluidic cell culture. Lab on a Chip. 13:4430-4441.

Following publications are submitted or under submission:

- Luni C*, Giulitti S*, Serena E, Zambon A, Gagliano O, Michielin F, Elvassore N. One-step high-throughput reprogramming and differentiation on a chip.

- Zatti S, Serena E, Giulitti S, Mattei N, Elvassore N. Engineered 3D muscle fibers for *in vivo* reconstruction.

Part of this work have been presented at the following national and international conference:

- F. Michielin, S. Giulitti, G.G. Giobbe, N. Elvassore. Sviluppo di una piattaforma microfluidica automatizzata per la coltura e il differenziamento di cellule staminali umane. GRICU 2012. Pescara, Italy, September 16th – 19th 2012.

- S. Giulitti, A. Zoso, A. Zambon, N. Elvassore. Foto-pattern in situ per l'adesione e la coltura selettiva di cellule in microfluidica. GRICU 2012. Pescara, Italy, September 16th – 19th 2012.

- F.Michielin, E. Serena, S. Giulitti, P. Pavan, N. Elvassore. Cyclic Mechanical Stretch Affects Membrane Integrity During Myogenesis. GNB 2012 – 3rd National Congress of Italian Group of Bioengineering. Rome, Italy, June 26th – 29th 2012.

- F. Lamberti, S. Giulitti, M. Giomo, N. Elvassore. Biosensing with electroconductive biomimetic soft material. GEI-ERA 2012. Santa Marina Salina (ME), Italy, June 17th – 21st 2012.

- F. Michielin, E. Serena, S. Giulitti, P. Pavan, N. Elvassore. Cyclic mechanical stretch affects membrane integrity during myogenesis. 3rd International Conference on Stem Cell Engineering. Seattle, Washington (USA), April 29th – May 2nd 2012.

- F. Michielin, C. Luni, S. Giulitti, N. Elvassore. Efficient adenoviral transduction in stem cells through cyclic microfuidic-assisted infections at low MOI. 3rd International Conference on Stem Cell Engineering. Seattle, Washington (USA), April 29th – May 2nd 2012.

- E. Serena, S. Zatti, E. Cimetta, A. Zoso, F. Lo Verso, A. Zambon, S. Giulitti, F. Michielin, N. Elvassore. Engineering 13:4430-4441 an in vitro model of

human muscle dystrophy for highthroughput screenings and development of therapeutic strategies. Riva del Garda (TN), Italy March 7th – 9th 2011.

- S. Giulitti, A. Zoso, F. Michielin, S. Martewicz, E. Serena, M. Flaibani, E. Magrofuoco, A. Zambon, F. Lamberti, N. Elvassore. Microfluidic technologies for biotechnology applications. SAB visit. Venetian Institute of Molecular Medicine. Padova, Italy. February 20th-21st 2011.

- S. Martewicz, E. Serena, S. Giulitti, E. Cimetta, T. Pavan, N. Elvassore. hESC-CM maturation is driven by the cell-substrate interaction. SAB visit Venetian Institute of Molecular Medicine, Padova, Italy. February 20th-21st 2011.

- S. Zatti, E. Serena, A. Zoso, F. Lo Verso, S. Giulitti, E. Cimetta, N. Elvassore. Engineering an in vitro model of human muscle distrophy suitable for the development of new therapeutic strategies. SAB visit. Venetian Institute of Molecular Medicine, Padova, Italy. February 20th-21st 2011.

Sommario

Cellule e tessuti umani sono sistemi essenziali per lo studio della biologia e fisiologia del corpo umano e per lo sviluppo di nuove strategie e farmaci per la cura di varie patologie. Il coinvolgimento di persone in casi studio di ricerca e testing farmacologici espone i soggetti ad elevato rischio e introduce problematiche tecniche ed etiche non facilmente risolvibili. Lo sviluppo di nuove strategie *in vitro* è di fondamentale importanza per ricavare informazioni sull'organismo umano e limitare l'uso di sistemi animali non pienamente predittivi. La richiesta di sistemi efficaci, rappresentativi e a basso costo in campo clinico ed industriale è indubbiamente in aumento.

I sistemi convenzionali per colture cellulari sono normalmente costituiti da recipienti con dimensioni caratteristiche dell'ordine dei centimetri. I nutrienti sono veicolati alle cellule tramite mezzi di coltura liquidi che contengono buffer salini e oligoelementi. Un quantitativo di medium minimo è necessario per garantire un battente omogeneo al di sopra della coltura cellulare e deve essere sostituito periodicamente per apportare nuovi nutrienti e rimuovere i prodotti di scarto. Molti studi e applicazioni richiedono reagenti costosi e sono soggetti a una ridotta capacità di ricavare dati. La scoperta del processo di riprogrammazione cellulare da parte del Premio Nobel 2012 Yamanaka hanno aperto nuove esaltanti prospettive in ambito di ricerca e applicazioni cliniche. In tale processo, da una biopsia cutanea di un paziente è possibile ricavare cellule staminali pluripotenti indotte (iPSC) e derivare nuovi tessuti per una riparazione autologa *ad hoc* dei tessuti.

Ad oggi, le iPSC umane (hiPSC) non sono ancora state utilizzate in ambito clinico a causa di aspetti sulla loro derivazione non ancora pienamente caratterizzati, di metodologie non a livello clinico e del costo significativo della derivazione di hiPSC per singolo paziente. La micronizzazione del processo di riprogrammazione può dare

un'opportunità notevole per la derivazione di hiPSC a basso costo e per ottenere tessuti umani *in vitro*.

Scopo di questa tesi è lo sviluppo di una piattaforma per la riprogrammazione di cellule umane in microscala. Per la sua realizzazione, abbiamo focalizzato la ricerca sullo sviluppo di un microambiente cellulare che tenga conto sia dell'ambiente solubile che dei componenti solidi per l'adesione cellulare.

Durante questo dottorato, sono stati sviluppati degli idrogel sintetici e biodegradabili. La produzione su larga scala di substrati a rigidità variabile a base di poliacrilammide è stata fondamentale per rivelare le interazioni tra la rigidità del substrato e il comportamento e destino cellulare. L'ingegnerizzazione di idrogel biodegradabili ha rivelato il potenziale nello sviluppare tessuti *in vitro* funzionali e la loro integrazione nel paziente. Il *know-how* acquisito sulle modifiche chimiche è stato trasferito al controllo della topologia del substrato e all'interno dell'ambiente microfluidico.

L'ambiente microfluidico e la sua amministrazione sono stati ottimizzati per garantire l'adesione e la crescita cellulare a lungo-termine e registrare importanti fenomeni biologici. Le proteine di adesione fondamentali per la crescita delle cellule sono state modificate e integrate in un ambiente in microscala. In microfluidica, poiché il medium necessario alle colture viene perfuso all'interno del ciruito, un flusso continuo o periodico possono essere applicati. Abbiamo così studiato l'amministrazione della distribuzione del medium per determinare le migliori strategie per colture a lungo termine in microfluidica.

I risultati ottenuti nello sviluppo dei substrati e ambienti microfluidici per colture cellulari sono stati applicati alla generazione di una nuova piattaforma per la derivazione delle hiPSC, differenziamento e validazione in microscala. Per la prima volta in letteratura, è possibile ottenere cloni hiPSC in microfluidica con una riduzione sostanziale dei requisiti minimi (materiali, reagenti, spese globali).

La produzione di hiPSC a basso costo può portare a una produzione di massa di tessuti caratterizzati e funzionali che possono in seguito essere integrati in supporti 3D e servire come valida fonte di derivazione per lo sviluppo di nuovi farmaci. La nostra piattaforma apre nuove prospettive nello studio e trattamento di malattie diffuse e rare coinvolgendo scienziati e imprenditori.

Summary

Human cells and tissues are key systems to study human biology and physiology, and to develop new strategies and targeting drugs for human diseases. Since the study and testing on human beings may not be acceptable due to exposure to risks and practical and ethical concerns, *in vitro* strategies are of paramount importance to rely on human organism and avoid non-fully predictive animal models. The demand of research in clinical and industrial fields for effective, representative and affordable strategies is undoubtedly increasing.

Conventional cell culture systems and drug discovery are normally performed in vessels with a characteristic dimension in the order of centimeters. Nutrients are delivered to cells through liquid media containing balanced saline buffers and oligo-elements. A reasonable amount of medium is necessary to homogeneously cover a cell layer and must exchanged with fresh media to maintain a proper amount of available nutrients and remove released waste products. Many studies and applications require expensive reagents and are subjected to limited data throughput. The discovery of reprogramming process by 2012 Nobel Prize Yamanaka opened breakthrough new perspective on research and clinical applications. Basically, from a patient's skin biopsy it is now possible to derive induced pluripotent stem cells (iPSC) and to obtain new tissues for an *ad hoc* self-repair. So far, human iPSC (hiPSC) have not been applied to clinics due to some unexplored aspects on their derivation, non clinical-grade methods and the significative cost of hiPSC derivation *per* patient. The down-scale of reprogramming process could provide an unique opportunity to derive cost-effective hiPSC and obtain valuable human in *vitro* tissues.

The aim of this thesis is the development of a comprehensive platform for the reprogramming of human cells at the microscale. To this end, we focused on the

development of cell microenvironment which is composed by both soluble and solid components.

During this thesis, synthetic and biodegradable hydrogels were developed. The large-scale production of mechanically-tunable poly-acrylamide-based substrates were fundamental to reveal the interaction occurring between substrate stiffness and cell behavior and fate. Engineering of biodegradable hydrogels has revealed the potential to develop *in vitro* functional tissues and to integrate them at a later stage in patients. Chemical modifications were transferred to topological substrate control and in turn in microfluidic platforms.

Microfluidic chip environment and management was designed in order to allow long-term adhesion, culture and biologically relevant cell behaviors. Adhesion proteins fundamental for cell attachment and growth were modified and integrated with the micronized substrates. Since medium for microfluidic cell culture relies on perfusion, continuous or periodic flow could be applied. Thus, we studied the management of media delivery in order to determine the best strategy for long-term cell cultures.

The achievements obtained with both substrate and microfluidic cell culture development was applied to the generation of a new platform for hiPSC derivation, differentiation and testing at the microscale. For the first time, it is possible to obtain human iPSC clones in microfluidics with a remarked reduction of minimum requirements (materials, reagents, overall expenses).

The production of cost effective hiPSC can lead to a mass production of characterized and functional tissues that can be either integrated in 3D developed constructs and serve as valuable tissue source derivation for drug development. Our platform opens new perspectives in studying and treating both abundant and rare diseases involving both scientists and entrepreneurs.

Contents

Chapter 1

Engineering the Generation of Human Pluripotent Stem Cells

Human somatic cells of an adult can be reprogrammed to an embryonic-like state through the subministration of defined molecular factors. In this state, cells have the potential to generate all the cell of an adult organism, the so called *pluripotency*. Reprogrammed cells, namely Induced Pluripotent Stem Cells (iPSC), can be programmed further to indefinitely obtain different desired somatic cell types [1–3]. For this finding, prof. Shynia Yamanaka has been awarded for the Nobel Prize in 2013. Since the original publication in 2006, the reprogramming efficiency has been revealed as a barrier to an intense application of iPSC. Despite recent efforts and new technology available, many other barriers limit the use of iPSC both in research and preclinical approaches.

Nowadays, the reprogramming process is unfeasible and not affordable for more than a few tens of people [4]. In the standard process, before, during and after the reprogramming phase, cells must be expanded, evaluated to assess the proper phenotype, stored for cells banking and programmed towards adult phenotypes. For a few samples from a single patient, thousands of euros and a full-time dedicated expert are required over a 1-2 months period. Hence, big efforts have to be invested to scale-up the iPSC production.

1.1 Introduction

The majority of the cells in a adult human body are terminally differentiated cells with defined properties and functions to support the activities of different tissues and organs. A very low number of partially specified cells, namely adult stem cells (ASC), support the renewal of differentiated cells undergoing senescence and death [5]. Other than these somatic cells, germ cells (GC) (i.e. spermatozoa and egg cells) are specialized for the generation of a new individual.

When an egg is fertilized, several cell divisions occur ending up with a hollow structure, the blastocyst (Figure 1.1.1A). The inner cell mass (ICM) is surrounded by cells of the trophoblast, which are responsible for the placenta development. The ICM cells are defined as pluripotent since they account for the formation of all the cells necessary for the development of the embryo and finally of the adult. When a part of the ICM is cultured *in vitro*, the cultured cells maintain the pluripotent state under specific conditions. This cells are called human Embryonic Stem Cells (hESC) (Figure 1.1.1A).

The 2012 Nobel prize Shynia Yamanaka and colleagues evidenced that differentiated cells from ad adult, can be reprogrammed back to a state similar to hESC. Thanks to the forced-expression of genetic regulators of the pluripotent state (OCT4, SOX2, KLF4, c-MYC) *via* viral vectors, human iPSC (hiPSC) were derived from differentiated fibroblasts [2]. Since hiPSC can be derived from cells of an adult tissue, they can solve ethical problems rising from the use of hESC and they offer the opportunity for a theoretical unlimited source of pluripotent stem cells (Figure 1.1.1B).

The means to derive hiPSC have extended in the past 5 years [2, 4, 6–9]. Despite little is known of the reprogramming and its players during the whole process, some common aspects have been defined: for instance, the ectopic forced-expression of a 'consensus' class of factors is necessary [10, 11]. These transcription factors are recapitulated by a list of four, comprising OCT4, SOX2, KLF4, c-MYC and more defined cocktails and variants can be found in the literature. The delivery method of these factors account for part of the process efficiency. Viral vectors were the first to be used thanks to they ability to transfer genes inside the cell. Both genome-integrating and transient viruses were used. Firsts efforts to develop non-

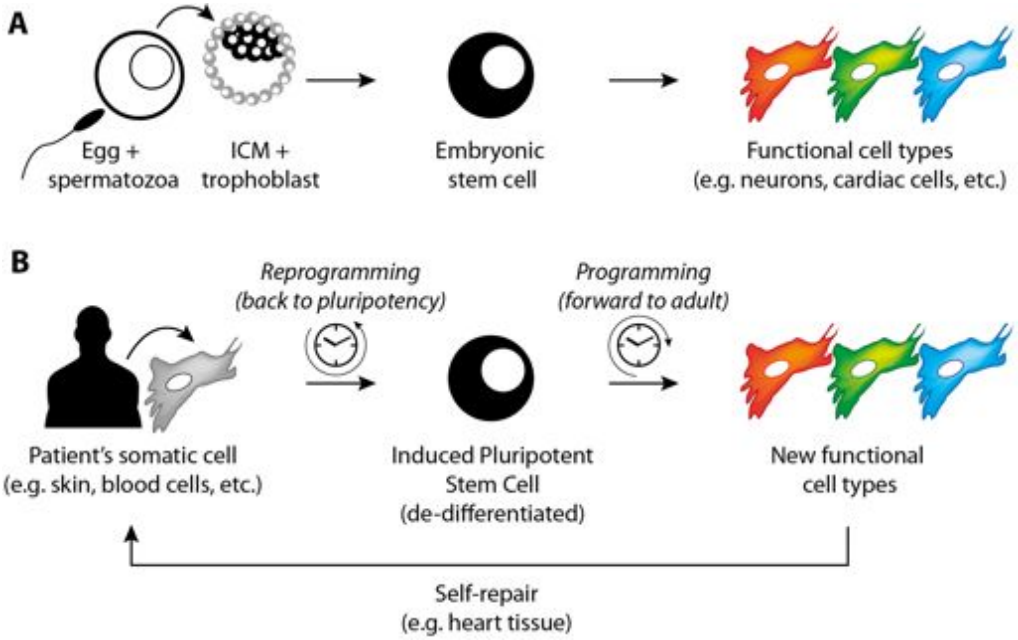

Figure 1.1.1 – Pluripotent stem cells. (A) The egg fertilization produce a globular cell structure (the blastocyst, here sectioned) that is the source for embryonic stem cells. Cells depicted in grey form the trophoblast and the ICM is facing inside (black). The ICM cells are defined as pluripotent stem cells since they can produce all the differentiated cells in our body (e.g. neurons, cardiac cells, etc.). (B) Patient's derived cells (e.g. a skin biopsy or blood sample) can be turn *back in time* through a reprogramming process that erase actual cell functions. The delivery of Yamanaka's factors induce pluripotency in cells leading to an analog state of embryonic stem cells. This cells being pluripotent can generate new cell types valid for the self-repair (autologous) of patient's tissues.

viral vectors (e.g. proteins, mRNAs, chemical compounds, etc.) have offered limited reprogramming efficiency [12, 13]. Recently, modified mRNAs (mmRNAs) and small synthetic molecules emerged as a powerful and potentially clinical-grade tool for the reprogramming of human cells [9, 14].

Since the various steps towards the iPSC depend on the sustained delivery and expression of the reprogramming factors - which is not fully efficient - , and on the state of each individual cell, the target cells to be reprogrammed do not show the same capacity to enter and complete the process [15]. Beyond others, an evident morphological cell rearrangement (mesenchymal-epithelial transition, MET) and an epigenetic reorganization of the genome are key factors of the process concomitant with cell sustained proliferation [16]. A recent study shows that cells can be deterministically reprogrammed by abolishing defined key factors [17]. However, only cells that are transfected with the reprogramming factors enter the process.

Significative advances have been introduced to ameliorate the reprogramming of human cells but the overall process remains far to be extensively applicable. In this Chapter, we introduce the key aspects to develop cost effective and clinical-grade solutions for the reprogramming of human cells. Advantages of substrate engineering and microfluidic technology will be evidenced and their development will be reported for the efficient generation of hiPSC.

1.2 Motivation for technology development

Since cell continuously interact with their microenvironment, its control is crucial to drive cell behavior and fate. Soluble and solid biochemical species are the two major components surrounding cells, thus, the understanding and modeling of their dynamics can effectively impact on tightly balanced biological processes such as reprogramming.

1.2.1 Mechanical control and physical barriers - substrates

Besides soluble components of the cell niche, the adhesion substrate has a key role on cell behavior and is continuously modeled to accomplish different biochemical and mechanical roles [5]. Rigidity, topology and chemical properties of the substrate

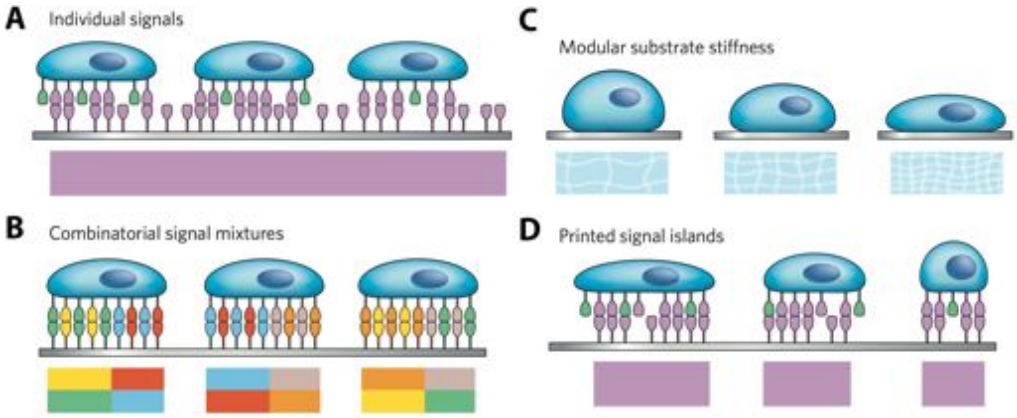

Figure 1.2.1 – Engineering 2D artificial stem-cell niches. (A) Surfaces can be functionalized with pro-adhesion molecules of the ECM that specificaly bind cellular receptors exposed at the surface. (B) Different types of ECM molecules can be used to trigger differential pathways and signals. (C) Substrate stiffness can be tuned in order to elicit different mechanical stimuli on cells. Stiffer substrates promote cell spreading and flattening. (D) Surface can be functionalized in order to allow cell adhesion on defined patterned regions exposing ECM components. Image adapted from [18].

are recognized by adhesion proteins and receptors at the cell surface and can trigger either direct mechanical or biomolecular soluble transduction to various cell compartments (Figure 1.2.1) [18].

Cells can vary their gene expression in order to respond to the substrate stimulus. Various examples of the mechanical importance of substrates were demonstrated in non-pluripotent cells, comprising cell maturation [19], functional activity [20], growth and death [21]. Conversely, little is known regarding the interaction of hPSC with their culture substrate.

A new way to control the pluripotency state through substrates may reduce the need of expensive soluble factors and reduce the operations and time required to maintain culture purity and remove spontaneous events of differentiation [18, 22, 23]. Moreover, substrates mechanics, topology and biochemical features can influence the reprogramming process [8, 24]. The imposition of a hPSC-like shape or the biochemical composition of the substrate may favor the remodeling of differentiated cells fastening the transition to pluripotency.

1.2.2 Soluble control and micronization - microfluidics

The reprogramming process is tightly controlled by cell internal events and external surroundings. Outside the cell, extrinsic factors play as environmental stimuli which

occur at a few cell distances. Figure 1.2.2A illustrates the major players in the so called "cell niche". As described in the previous section 1.2.1, the extracellular matrix substrate has a part in affecting some biological processes. Many other stimuli are soluble factors that are released by neighboring cells (paracrine) or by the cell itself (autocrine) [5]. These factors account for endogenous (EnF) signals while exogenous (ExF) ones are derived from the culture medium supplemented to the cells. Biochemical pathways are activated upon the recognition of these extrinsic factors by receptors at the cell membrane (Figure 1.2.2A).

Since many soluble factors can act at the same time and insist on even redundant pathways, the control of the soluble environment is crucial to support proper stimulation of cell under reprogramming. Typically, established protocols suggest daily medium changes in order to prevent the accumulation of toxic signals (EnF) and continuously stimulate cells with fresh exogenous and controlled factors (ExF). Deprivation of nutrients and accumulation of waste products of cell metabolism and cell turnover can trigger cell death or induce differentiation of non terminally differentiated cell types. Figure 1.2.2B-C shows a comparison of medium usage between conventional vessels and emerging microfluidic technology. Standard culture systems like Petri dishes require a minimum amount of medium volume over a 24 h cycle in order to:

- provide a minimum height to homogeneously cover the entire culture surface;
- reduce the concentration of medium components due to evaporation at 37 °C;
- provide nutrients to high-demanding cells like hPSC;
- dilute waste and unwanted cell product.

Microfluidics represents a way to deliver tiny amounts of media (nanoliters to microliters) over a cell layer with homogeneous distribution and tight control of cell species inside the fluidic environment both in space and time (Figure 1.2.2B-C) [25]. Adjusting the perfusion rate of media through the channels it would be possible to control the balance of the extrinsic factors either produced by cells or carried within the fresh medium (Figure 1.2.2C).

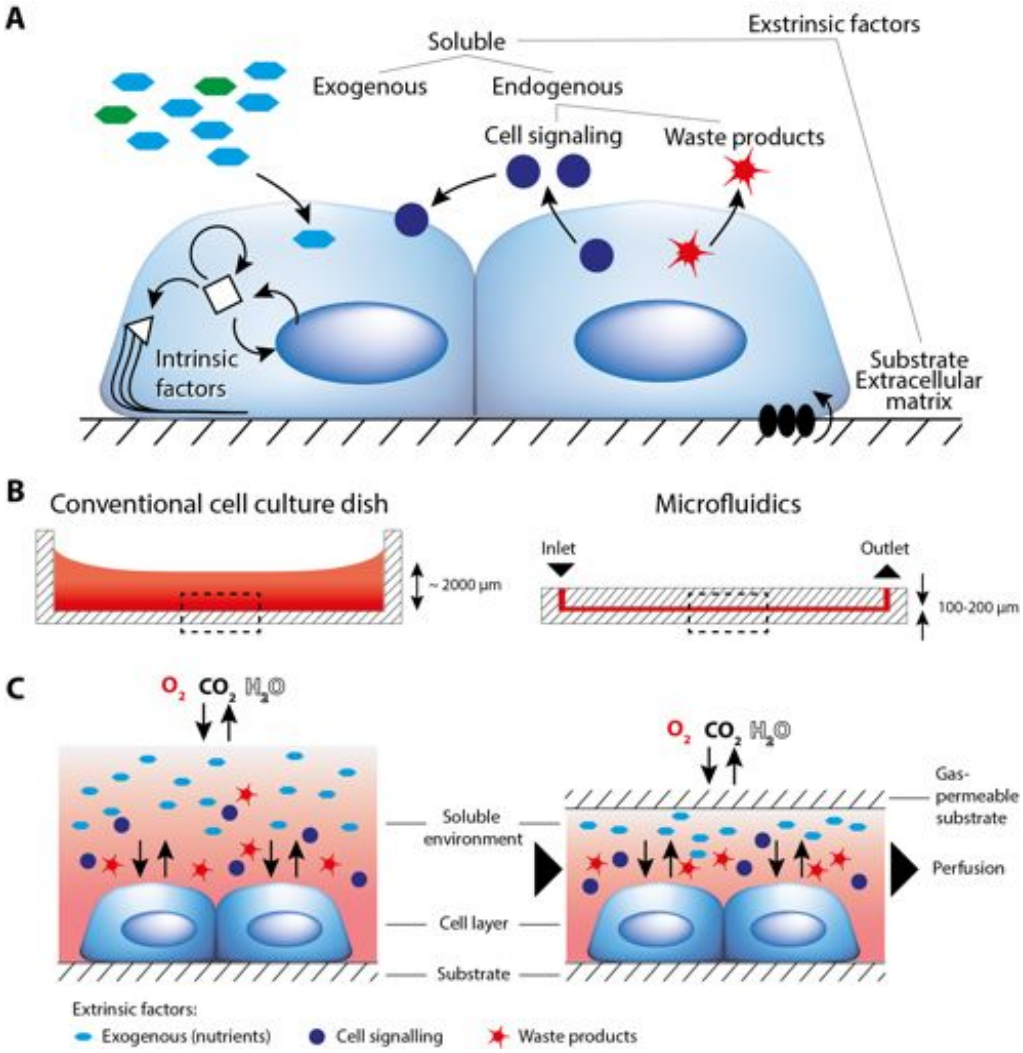

Figure 1.2.2 – Cell niche and comparison between conventional cell culture environment and microfluidics. (A) Cell biology is based on extrinsic (outside the cells) and intrinsic (inside the cell) signals of the microenvironment. While intrinsic signals directly acts on internal cell system, extrinsic signals can be further classified. Besides the interaction with the substrate where cells adhere, soluble environment is bases on exogenous molecules (e.g. provided nutrients) and cell-produced molecules such important cell signaling species or by-products and waste. (B) Longitudinal sections of a common culture dish and a microfluidic chip. Most used cell culture vessels require some milliliters of culture medium in order to provide a homogeneous and sufficient height above cells. In a common 35-mm-wide Petri dish this consist in 2 ml of media (∼2 mm height). Microfluidic chips have inlets and outlet for media delivery into channels. Channels height ranges from 100 to 200 micrometers, a tenth of conventional vessels. (C) Micro-environments at the cell culture surface. Large amounts of media in conventional vessels allow a nutrients supply for 1-4 days, depending on the cell type and density. Cell metabolism produces biochemical signals (e.g. cytokines, hormones, etc.) important for cell communications and to sustain cell proliferation and activities. Since waste products are also produced medium exchange is necessary to avoid toxic effects. Oxygen, carbon dioxide and water vapor diffuse across the medium-air interface. Excessive evaporation leads to unbalanced osmotic pressure in the medium that can dramatically affect cell viability. Microfluidic liquid environment results in a tiny volume above the cell layer. The perfusion of the channel allow to apport fresh nutrients while washing out waste products. Since perfusion may also alter the balance of factors secreted by cells a proper strategy should be defined using living systems. Gases and vapor can diffuse through the roof of the channel based on permeable polymers. Due to the small amount of medium, osmotic pressure must be tightly monitored.

Culture components for hPSC are considerably expensive compared to other cell lines and may limit the use of these pluripotent cells. For these reasons, a reduced volume for culture reagents and a homogeneous long-term hPSC culture system are fundamental. A such micronized system would benefit of a controlled and automated liquid handling integration.

Microfluidic derivation and expansion of hiPSC can guarantee a new system to match the precise requirements of hPSC and to boost their applicability with cost-effective and automated production and maintenance.

1.3 State of the art

1.3.1 Reprogramming

The scientific community is pursuing a translational approach for human pluripotent stem cells (Center for Commercialization of Research Medicine, Toronto, Canada) [26]. Overcoming the ethical issue of hESC, hiPSC derivation capabilities have been improving in the latest years. Despite the present process efficiency may not sustain a full translational procedure, safe and clean ways have been introduced to prove the feasibility of clinical grade operations and materials [14, 27].

After the first selection of optimal reprogramming factors by Yamanaka's group, others concentrated on the optimal stoichiometry of each factor [10, 28, 29] and on the expansion of the original pool of factors [30, 31]. Other groups evidenced other components and pathways affecting the reprogramming process and the morphological evolution of transforming cells [6, 15, 16, 32–35].

Figure 1.3.1 illustrates the major classes of reprogramming tools to deliver exogenous factors that initiate the process.

Various reprogramming efforts have adopted genome-integrating viruses to deliver Yamanaka-like factors [2, 7, 10, 15, 16, 36]. Modified retroviruses and lentiviruses have the ability to infect a cell, to integrate within its genome and to use the cell machinery to produce *ad hoc* factors [7, 28]. However, a permanent random genome integration of viral nucleic information can lead to alterations and instability of the cell genome and related activities. Non-integrating viruses have been modified to

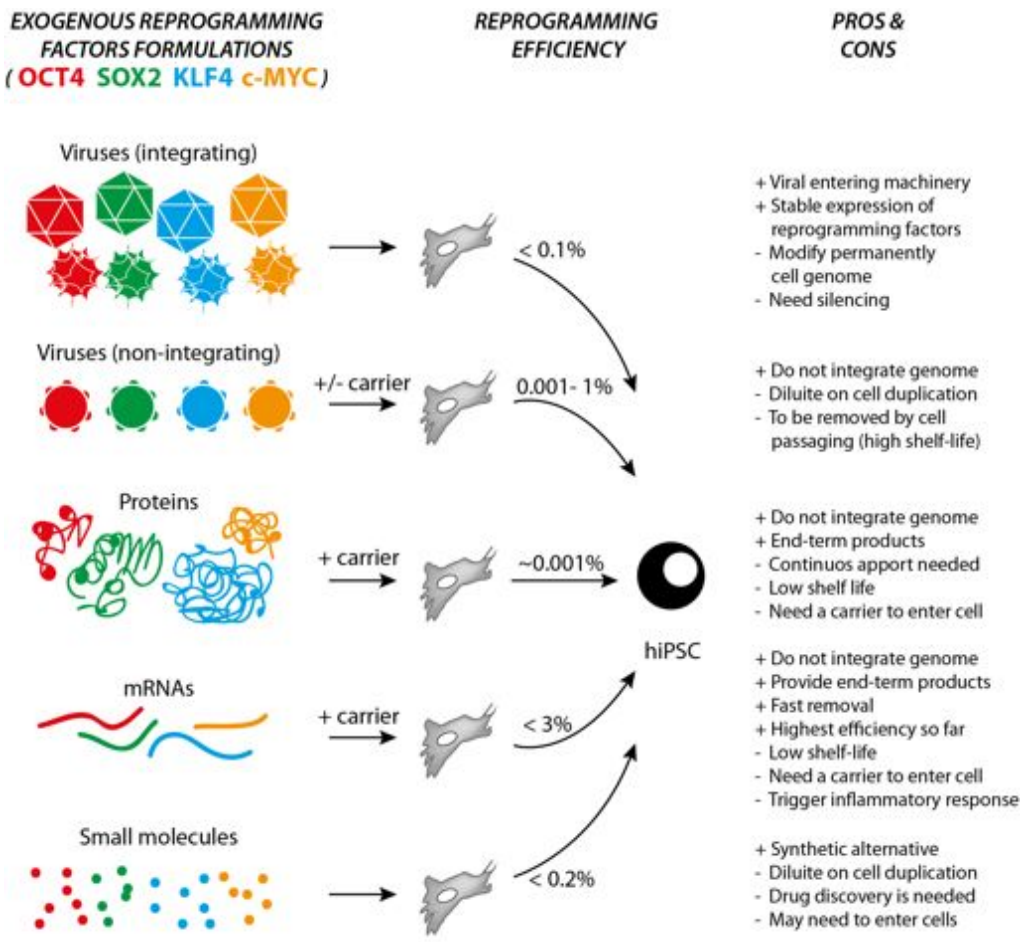

Figure 1.3.1 – Exogenous factors for cell reprogramming. Various biochemical approaches have been used to deliver reprogramming factors inside cell. Genome-integrating viruses have been the most used system since it is easy to take advantage of their innate capacity of infecting cells; major limits of this system are the modification of host genome and the low reprogramming efficiency. Non-integrating viruses such Sendai have significant higher efficiency and do not integrate in the cell genome. Proteins of the reprogramming factors can directly be delivered inside cells. They require at least a modification with a tag sequence to enter cells and must be provided repeatedly since they are naturally degraded. Modified mRNAs are being commercialized as the method with highest yeald. They need a lipophilic vesicle in order to enter cells and an protectant must be provided to block the activation of immune cellular response. Small chemicals can offer a new frontier to reprogram cells in a fully defined and synthetic way. These molecules can act either as activators or repressors of biological functions to elicit the reprogrammig.

prevent replication [37, 38]. After cell infection, they rely in the cell cytoplasm and are diluted during the progress of cell divisions. Adenoviruses and Sendai virus (SeV) are based on DNA and RNA, respectively. Adenovirus have a short transient expression and require various transfections during the reprogramming window, whereas SeV is retained for various weeks after a single transfection with a reprogramming efficiencies up to 1% of the starting transfected cells [39].

In order to avoid the virus-mediated delivery of reprogramming factors, three ways have been explored:

- direct proteins subministration;
- modified mRNAs delivery;
- chemicals.

Recombinant proteins with tagged epitopes can enter the cell and directly operate as transcription factors [40, 41]. The total amount and stoichiometry needed is a major limitation to promote an efficient reprogramming. Modified RNA messengers (mmRNA) have been introduced in the last 2 years and provide the most efficient methodology to produce hiPSC (up to 3% of efficiency) [9, 14, 42]. Chemicals are being improved and tested in order to provide the most elegant way to revert differentiated cells into iPSC. Chemicals were mostly used for the reprogramming of murine cells [12, 13, 43]. Using degradable chemicals in the same way we take drugs, no biological derivates will be adopted without leaving any footprint of the delivery of the reprogramming factors.

Since mouse embryonic stem cells (mESC) represent a different and earlier stage of embryonic development compared to hESC, mouse and human induced pluripotent stem cells recapitulate different stages [44]. Mouse pluripotent cells have different requirements in terms of culture conditions and are the typical case study in literature. hPSCs require more restrictive conditions both at the maintenance and at the reprogramming phase. For example, hPSC require additional cells that help in supporting the pluripotency or defined media with stimulating degradable factors (i.e. cytokines) that sustain their state. In this context, the mechanisms underlying the relationship between hPSC and their environment are poorly characterized.

1.3.2 Substrates for cell culture

Cell cultures are normally performed on tissue-culture-treated poly-styrene plates with different dimensions and shapes. *In vivo,* cells experience a complex niche made of various biochemical species, structural proteins and polysaccharides that cooperate to the peculiar biochemical and biophysical properties of each tissue [20, 45–48].

Advantages in substrate development to study cell behavior in physiological environment have been obtained in the past on different cell types. Discher and Engler were pioneers in using compliant matrices for muscular cells and underlining the interplay between stiffness and biological activities [19, 49, 50]. Physical contribution to biological activities has been termed *mechanotransduction* since external forces are transferred through the cell's anchor sites binding the ECM to the internal cellular cytoskeleton and converted in biochemical soluble signals down to the nuclear regulation [51–56].

Although a multitude of studies have been published on the relationship between substrates and cells dynamics, little is still known on how hPSCs relate to substrates [18, 57]. Research groups have focused on two issues: the intrinsic mechanical properties of PSC compared to other cells [58–64] and the effect of different substrates on PSC maintenance (both for mouse and human) [22, 57, 65–74].

Little is known about the implications of substrates on the reprogramming process [8, 24, 54, 75, 76]. The use of defined substrates may significantly contribute to remove machanotransduction barriers that naturally prevent cell transformation and determine a reprogramming pathway in cultured cells. In the future, this studies may also shed light on the role of substrate in tumor formation and metastases which gain independence from the original substrate.

1.3.3 Cell culture in microfluidics

Microfluidics offers an unique way to deliver nanoliters to microliters over a fluidic circuit. It has expanded both in research and industry thanks to the availability of technology and the cost reduction of components and machinery to build fluidic chips. Microfluidic devices are being used for low cost and high-throughput biomolecular

assays and chemical reactions [77–84], however the integration of living systems is still at the beginning. Despite interesting properties such efficient mass transport and low volumes, some drawback may impair the integration of cell and tissues cultures [85, 86].

Cells need a balanced soluble environment, with fresh nutrients, removal of waste products, defined pH and osmolarity (Figure 1.2.2). For instance, at the microscale, evaporation and medium exchange, can significantly affect these issues [85, 87]. In order to acquire the advantages of the microscale and to look at biological system from a new perspective, microfluidics must sustain viable and healthy cell cultures for prolonged periods. Despite various authors proposed long-term culture systems for particular purposes [68, 82, 83, 87–93], no clear and comprehensive advance has been proposed for long-term cell cultures in the last decade.

Various groups focused on the integration of chip tools and add-ons [87] but poorly characterized the role of the soluble environment at different conditions. Among others, pluripotent stem cells are particularly sensitive to an unbalanced environment and precise medium management must be found in order to preserve their phenotype. As depicted in a review by Voldman and colleagues [86], before being widely adopted, microfluidic system for robust long-term cell cultures must be developed.

The translation of cell cultures from open macroscopic vessels to non directly accessible microfluidic circuits undoubtedly requires a comprehensive study of material adoption, medium management and environmental conditions. In this thesis, we propose an advance for long-term cell cultures, pointing out the importance of medium management strategies and adhesion substrates at the microscale.

1.4 Rationale of substrate and microfluidic development for the high-throughput generation of hiPSC

Expectations on new ways of drug development and regenerative medicine are considerably high because of the social and economical impact. The classical way of drug development and commercialization results in a long process which can span

over 15 years [81]. Even if the screening of molecular candidates may be accelerated in some phases by bioinformatic means, the testing on animal or human candidates still requires a lot of effort in terms of time, money and proper testers.

The development of new technologies and biological tools can dramatically favor this process:

- first, new lab-on-a-chip technology aims to improve and extend the possibilities of bioassays, cell biology and biomedical research by mimicking the environment and the physics of biological tissues [80, 81, 94–96];
- second, hiPSC are a promising and unlimited source for the *in vitro* derivation of adult-like cells and tissues [97, 98].

Up to the in vivo early trials for drug discovery, hiPSC may represent the key to a better, safer, faster and parallelized description of the drug-related human biology and physiology, rather than animal models or adult people. Additionally, self-derived hiPSC can offer a attractive way to easily sustain the development of personal drug therapies. Community of regenerative medicine is expecting great promise o hiPSC and it is deepening into translational approaches for clinical applications. hiPSC not only represent a possible source for autologous tissue regeneration, but can provide extended informations related to human development and disease outcomes.

In this perspective, the high-throughput generation of hiPSC can represent a paramount advance in drug discovery and regenerative medicine. The development of defined substrates controlling cell shape and behavior, and the automated management of defined soluble micro-engineered environments can resolve the technical issues that currently limit hiPSC adoption.

1.5 Aim of the thesis

This thesis aims at the developing of technological tools for the generation of human induced pluripotent stem cells (hPSC), a promising source for tissue engineering and pharmaceutical development and assays. Since hPSC generation (reprogramming), maintenance and differentiation are highly amenable to soluble microenvironment and culture substrate, and require considerable efforts, microfluidic cell culturing

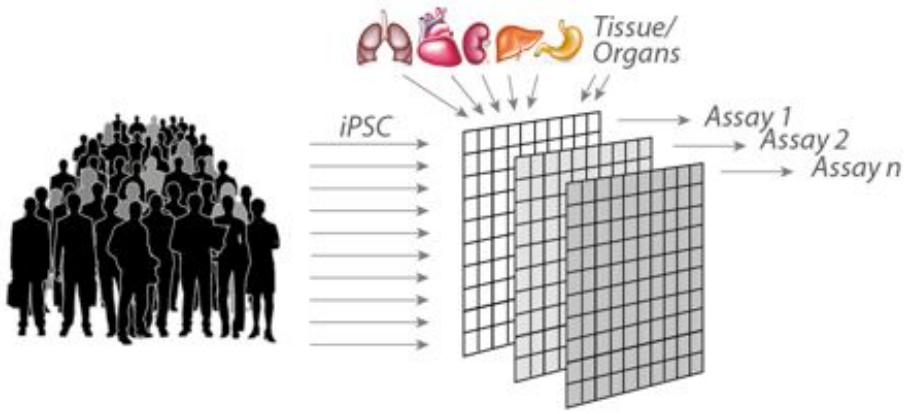

Figure 1.5.1 – Aim of the thesis. A platform for high-throughput reprogramming and programming at population scale. Cells derived from hundreds of patients can be reprogrammed in order to produce a comprehensive library of hiPSC. These cells, beside being expanded, can be directly differentiated in order to provide additional libraries on various tissues. Each of them could be used for assays such as drug screening, and biological and medical research.

and biomimetic materials were developed to provide a defined microenvironment with a considerable reduction in costs and manual labour.

Since substrates determine the behavior of adherent cell cultures we focused on the development of hydrogels to study the role of mechanical and biochemical properties exerted on cells. The microscale culturing offers consistent reagents reduction and flow control but requires unique management to permit restrictive cell culture conditions. Cell cultures were integrated in microfluidic devices specifically aiming at the implementation of robust, healthy and long-term culture conditions and at the efficient delivery of biochemicals for reprogramming process. Optimal management of culture conditions revealed as a mandatory requirement for subsequent studies on reprogramming at the microscale. Achievements gained with the engineering of cell microenvironments allowed to build a reprogramming platform of human patient cells at the microscale. Figure 1.5.1 depicts the final aim of the entire thesis. By producing hiPSC in a cost effective and high-throughput manner, derived cells can be programmed further to adult tissues of various organs to provide a population-scale library of functional cells. This library can be then used to perform population-scale assays valuable for drug discovery, screening and disease characterization. Thanks to the clinical-grade approaches and reduced requirements and expenses hiPSC can be easily be adopted in medical tissue engineering.

In this thesis, the development of substrates and microfluidic systems to control cell behavior is proposed as follows:

- in Chapter 2, substrates have been developed to study the relations of cells and their adhesion support;
- in Chapter 3, the long-term integration for cell cultures in microfluidics is illustrated;
- in Chapter 4, the advances in substrate-optimized microfluidic cell cultures are adopted to derive hiPSC at the microscale for the first time;
- in Chapter 5, early results on the use of substrates to promote reprogramming are introduced.
- in Chapter 6, the perspectives on microscale tissue an organ development.

1.6 Conclusions

The development of *in vitro* screenings strongly based on human biology and physiology is a future step for *ad hoc* biomedical applications and pre-clinical pharmaceutical screenings. In this perspective, new tools and technologies are emerging to obtain reliable system and provide faster high-throughput data. Human pluripotent stem cells, especially hiPSC, are a promising source for unlimited personal screenings and self-regeneration of our tissues. Engineered microenvironments can be designed to finely control both adhesive and soluble properties of *in vitro* cell cultivation. The synergic implementation of these two fields can unleash the potential of hiPSC that has never been translated in clinical or industrial applications so far.

Thanks to the substantial cost reduction, delivery efficiency and chemically defined surfaces, microfluidics and substrates can massively expand hiPSC clone production and obtain new differentiated cell lines at a low cost - an affordable process for limited samples nowadays. Parallelized one-step processes to obtain newly generated tissues can provide a platform to perform breakthrough screenings at the population level, shortening the finding of new biological pathways and drug targets, and making attractive the development of compounds for rare diseases.

Chapter 2

Substrate development

This chapter introduces to the development of substrates for cell cultures. Different types of substrates have been developed for different purposes in 2D and 3D applications: polymeric substrates presented in this chapter form tunable hydrogels with biologically relevant physical and chemical properties. As a second task, we focused on the functionalization of surfaces in order to control cell adhesion, shape and behavior. The knowledge gained with this part of the thesis revealed crucial to control cell behavior at the microscale for the reprogramming purpose presented in Chapter 4 and 5.

2.1 Motivations

Tissues in our body are made of different type of cells embedded in a network of a secreted extracellular matrix (Figure 2.1.1A) [45]. This external skeleton of proteins, glycoproteins and polysaccharides, retains water and other soluble substances that form the interstitial fluid. Since the composition of the ECM varies between tissues and each bio-polymer has its own functionality and physical-chemical properties each tissue displays a different global stiffness (Figure 2.1.1B). Since cells exert their functions in a compliant microenvironment pairing defined chemical-mechanical properties (Figure 2.1.1C), it is necessary to develop substrates that mimic the natural matrix *in vitro* [50, 99].

Cells actuate complex interaction with the extracellular substrate that is prevalently composed by structural proteins and glycosilated polymers which define the

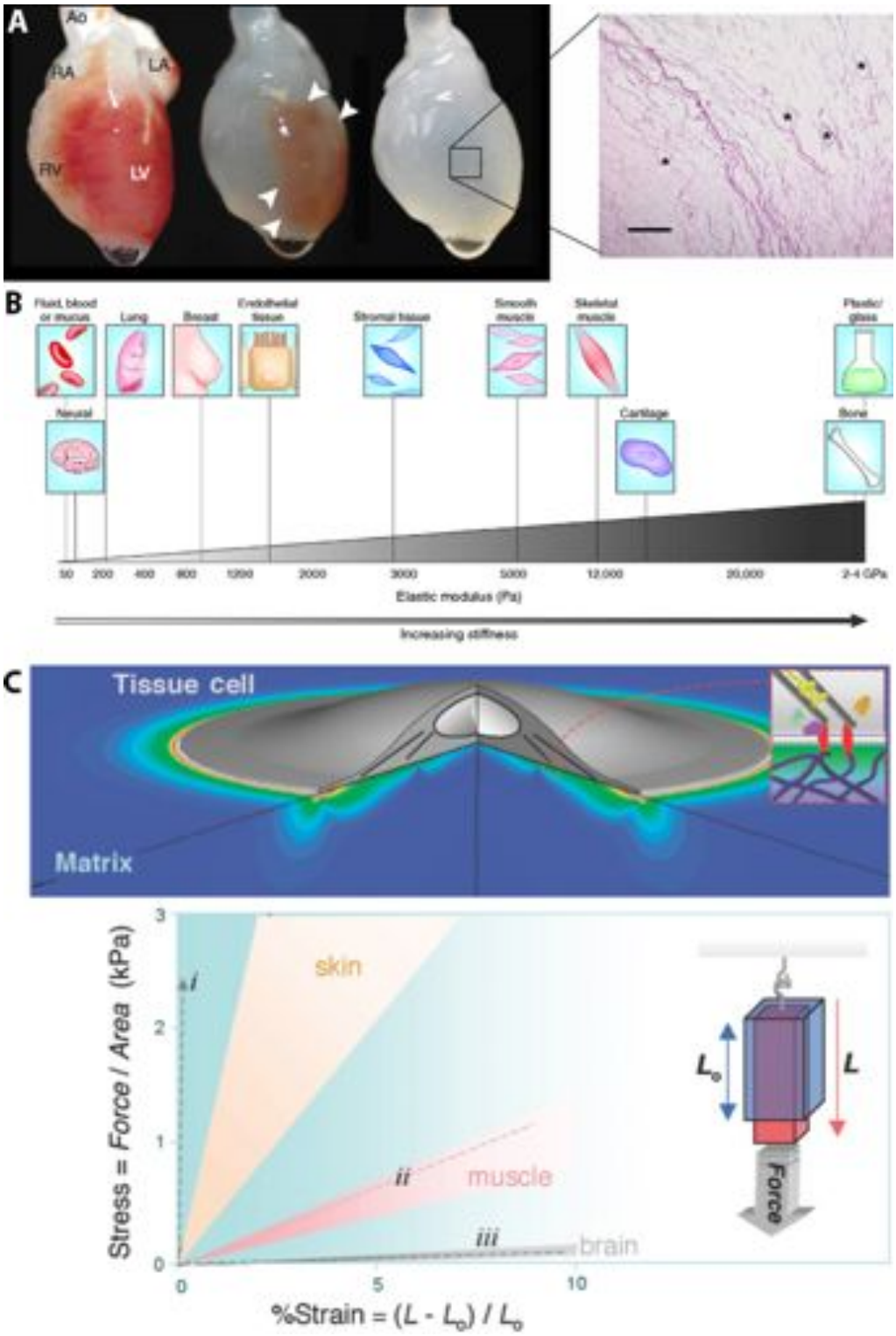

Figure 2.1.1 – Matrix mechanics. (A) Decellularization process reveal the extracellular matrix is a major component of living tissues (adapted from [47]). (B) Each tissue has its own stiffness. Bone and cartilage have high percentages of deposited matrix and result particularly stiff. Muscles have a medium living stiffness in order to provide elasticity, strength and power stroke. Softer tissues such brain and fat do not require particular mechanical properties. (C) Each cell attached to a substrate exerts forces by organizing its internal cytoskeletal architecture (adapted from [99]).

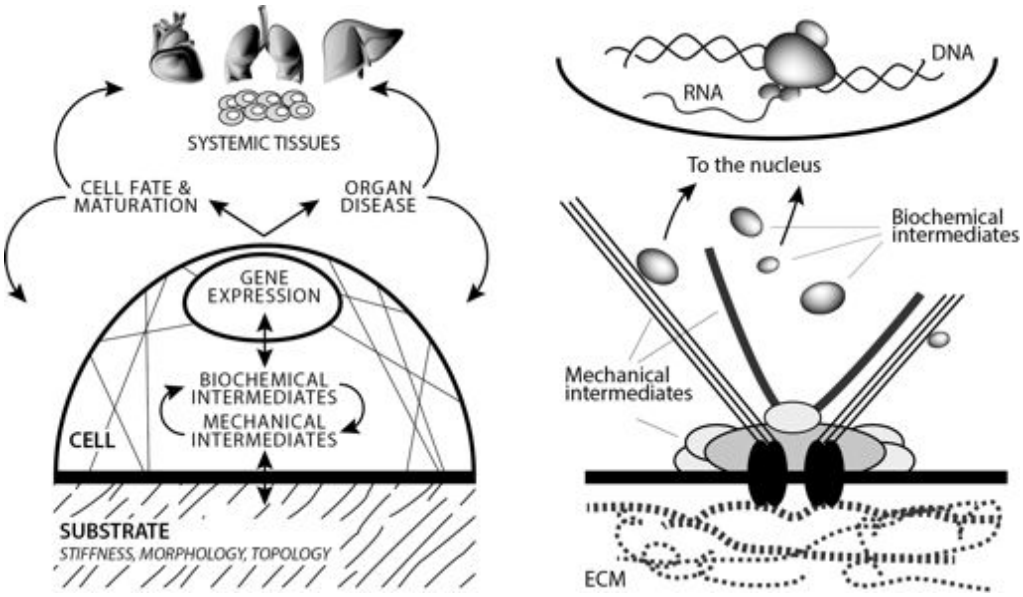

Figure 2.1.2 – Cell and substrate interaction. Cells sense the chemistry, stiffness, morphology and topology of the substrate by mechanical intermediates that in turn act on soluble biochemical players that control gene expression, cell fate, maturation and eventually local or systemic diseases.

extracellular matrix (ECM). The physical and biochemical properties of the ECM directly influence cells through a direct interaction with mechanical intermediates connected to the internal cellular cytoskeleton (Figure 2.1.2). These players communicate in turn with soluble biochemical intermediates that trigger regulatory pathways ending in defined cell behaviors and eventually in local or systemic diseases.

In the last decades, *de facto* standards for *in vitro* culture system has remained unchanged resulting in a poor mimicking of *in vivo* ECM. Conventional cell cultures are mainly performed on treated poly-styrene (PS) that can be molded in different types of open vessels. The treatment performed *via* plasma-oxidation turns the internal surface hydrophilic and more attractive for the adsorption of ECM proteins and for cell ligands such as integrins [100, 101]. Each cell type may show affinity for a particular subset of ECM components, requiring the adsorption of certain proteins on the PS prior the cell seeding. When the material to support cell culture is changed (e.g. glass), attention should be placed on the compatibility with the protein previously used on PS. Changes in treating concentration, time, and operative conditions may be necessary prior to a change in ECM components.

Besides the advantage in using cheap plastic supports with various formats and

the condition of *de facto* support for cell culture, PS shows some drawbacks:

- PS is not compatible with diffused fluorescent-based applications due to intrinsic autofluorescence;
- it is rigid, with a stiffness of a few GPa [102], 10^6-times the physiological range [45, 50];
- it limits the diffusion of soluble components to the apical-lateral portion of cells.

The development of new substrates for cell cultures is an active field, with the aim of expanding current methodologies and mimic the *in vivo* extracellular environment. Particular efforts have been made for the development of 3D scaffolds aimed at tissue reconstruction and to provide an *in vitro* model to understand tissue dynamics [103, 104].

Among the abundance of materials applied to cell cultures (polymers, resins, ceramics etc.), hydrogels emerged as unique opportunity to couple the chemical properties of the surface with the physical properties of the gel. Hydrogels are based on a solid non-soluble network dispersed in a water environment: in their hydrated state they allow solute to diffuse within the matrix accordingly to the cutoff of the mesh. Since the major component is water, these substrate can be extremely soft and stiffness can be tuned depending on the water/matrix ratio.

In the following sections, we report the achievements on substrate development. In particular we focus the attention on:

- mechanically tunable biocompatible substrates to perform large studies on the mechanotransduction cell behaviors.
- mechanically tunable substrates to be directly used as biosensors of cellular activities.
- mechanically tunable biodegradable substrates for tissue engineering and *in vivo* applications.
- chemistry for long-term and topological control of cell adhesion.

2.2 Mechanically tunable biocompatible substrates

This section describes the development of synthetic substrates able to resemble the mechanics of different tissues. Important results based on the formulation of these substrates are presented.

Various studies revealed that the culture substrate can affect the behavior of differentiated cell types [19, 50, 62, 105–108]. Beyond chemistry composition, the stiffness revealed an important co-factor for cell maturation. Soft substrate may also be used to study the earlier stages of human developmental process, tissue and organ growth and the single-cell behavior. In this perspective, we wanted to study the mechanotransduction behavior on immature cells like mesenchymal stem cells, which are a key component of human body development.

In order to study mechano-related issues on cell cultures soft materials mimicking the physiological *in vivo* stiffness were chosen. Here we describe the approach and a summary of the obtained results. Extensive informations can be found in Appendix A and B.

Biocompatibility of materials results from various aspects such as the release of toxic species and the cellular recognition of antigens triggering an inflammatory response [109]. First, we focused on substrates that results bio-compatible with a large number of cell types. Starting from the pioneeristic work of Pelham and colleagues [110], we introduced bidimensional poly-acrylamide hydrogels in our activities. These gels are well known in molecular biology since - when dissolved in defined buffer solution - they have been used as a support for high-resolution electrophoresis for decades. They result in a cross-linked matrix of linear poly-acrylamide fibers that is not degraded by the enzymatic activity of cells. Although acrylamide molecules alone are toxic and carcinogenic, the polymerization process produces inert macromolecules bridging with bis-acrylamide. Free monomers that can interfere with biological processes are eventually extracted in a water bath.

Varying the proportions of acrylamide, bis-acrylamide and water it is possible to change the stiffness of the gel and the diffusivity of species inside the matrix according to their hydrodynamic radius. Although some guidelines report the stiffness values associated with defined proportions of the three species [111], others report

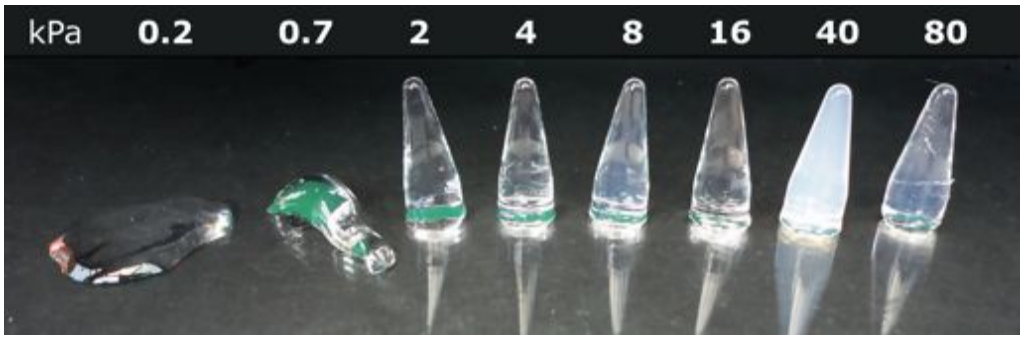

Figure 2.2.1 – Poly-acrylamide hydrogels at various nominal stiffnesses. Tuning the proportion of acrylamide and bis-acrylamide it is possible to obtain soft and hard gels. Softer hydrogels below 1 kPa have more than 97% of water and do not retain the shape of the tube were they have been polymerized. Optical features can also be altered varying the ratio between acrylamide and bis-acrylamide (see 40 kPa).

discordant values [112]: most of the times, details and procedures applied for the measurements are not reported. Atomic force microscopy (AFM) is tool for measuring the stiffness based on the deflection of a cantilever tapping the surface of the material [113]: when we had the opportunity to measure the stiffness of our hydrogels, softer gels were even impossible to detect even by an expert technician.

Due to the softness of the hydrogels, a glass coverslip is always used as a support and treated for the adhesion of the acrylamide. Different chemistries can be used to bound the gel to the glass surface and terminally-functionalized silanes are used as a bridge. The height of the hydrogel above the glass must be considered since cells on the top can feel differences in stiffness down to several micrometers [114].

A particular aspect when performing extensive experiments regarding many condition to be tested and spanning various months of work is the consistency of each produced piece within the lot and between lots. With this in mind, protocols are normally defined for the production of a dozen of hydrogels. Due to the high demand of our experiments (100-200 pieces at once per week) we rearranged the current available protocols to produce consistent hydrogels over months. Since poly-acrylamide prevents proteins from adsorbing on its surface and in turn results cell-repellent, the coating procedures with ECM proteins have been revisited.

Using hydrogels namely from 0.2 to 120 kPa, after a total of 5000 produced pieces, we were able to resemble a physiological or pathological stiffness, controlling the cell spreading, overall shape and in turn to study biological processes affecting cell

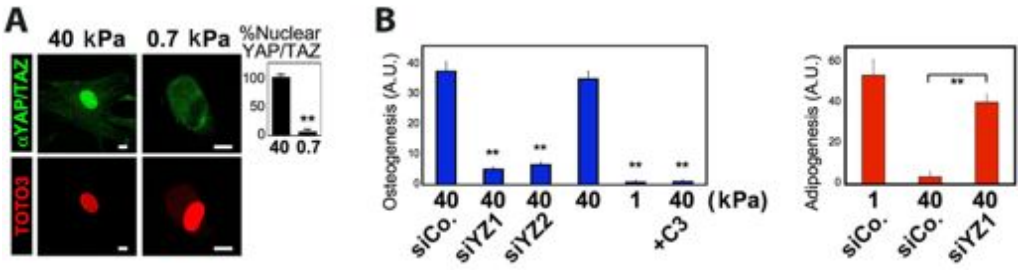

Figure 2.2.2 – Role of YAP/TAZ in mechanotransduction. (A). On relatively rigid substrates, cell and tissue growth controllers YAP/TAZ localize in the nucleus to promote cell activity (active). YAP/TAZ immunofluorescence signal co-localizes with the nuclear marker TOTO3. When cells are cultured on soft substrates below 1 kPa, YAP/TAZ localization is prominently sparse in the cell cytoplasm (inactive). (B) When stem cells are cultured on 1 kPa and 40 kPa different differentiation pathways occur. On 40 kPa hydrogels, cells preferentially differentiate towards an osteogenic pathways mimicking the *in vivo* stiffness of bones morphogenesis. Osteogenic markers are not identified on soft substrates or when YAP/TAZ activity is blocked (siYT and C3). Adipogenesis occurs on soft gels and it is not significantly present on stiff substrates. When YAP/YAZ are inactivated (siYT), cells do not sense the rigid stiffness and adipogenesis is promoted.

behavior. Details on bidimensional hydrogel production are reported in Appendix G.1. Appendix A reports the achievements obtained with these hydrogels and the collaboration with Stefano Piccolo's lab. It was found that substrate mechanics can act as a master control over certain biochemical pathways and cells - perceiving their microenvironment - remodel their overall shape and fate (Figure 2.2.2A). This discovery opens implications on how our tissue and organs regulate their expansion and homeostasis when subjected to mechanical forces and on how changes in ECM composition and mechanical cues may be linked to differentiation and cancer (Figure 2.2.2B).

The same hydrogel technology also served another publication reported in Appendix B, pushing a step further the first research. A series of proteins have been identified as transducers of the mechanical-responsiveness of transcription factors (YAP/TAZ) responsible of the genetic activity and cell behavior (Figure 2.2.3). Again, we gained evidence on how substrates mechanical properties can affect cellular behavior *in vitro* and can be juxtaposed to physiological and pathological phenomena occurring in our body.

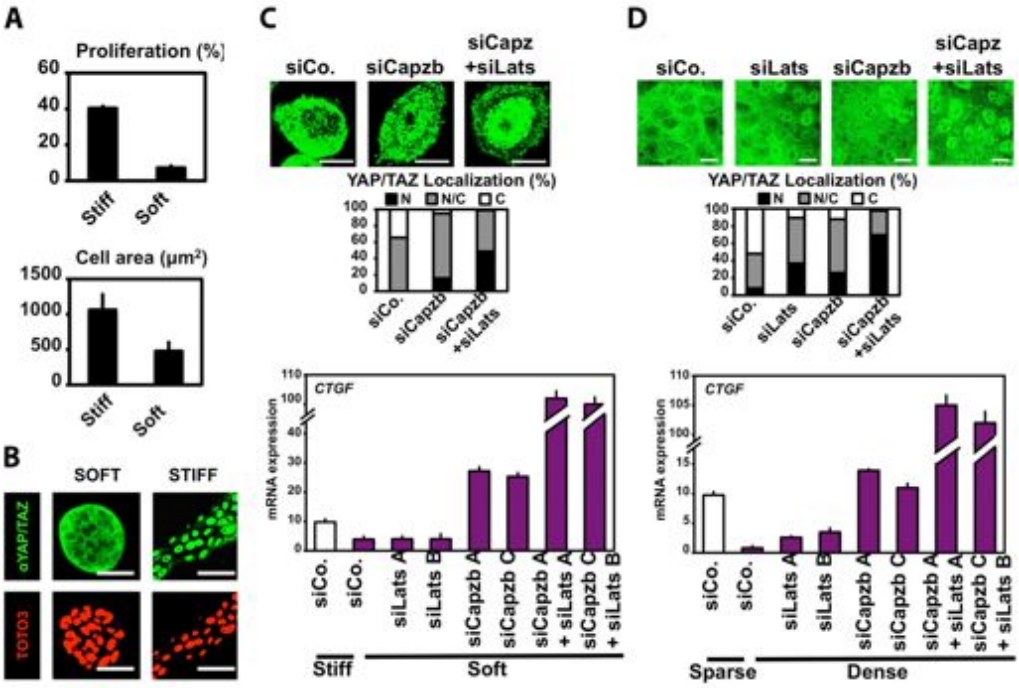

Figure 2.2.3 – Mechanical players drive cell fate. (A) Substrate stiffness affects proliferation and cell shape. Softer hydrogels limit cell duplication and spreading on the substrate. (B) When cells are included in a 3D matrix, soft gels induce a cell clustering with inactive YAP/TAZ out of the nucleus (TOTO3). Stiff gels induce the speading of single cells and the protrusion of the tissue. (C-D) Mechanical players inside the cells are responsible for the ECM mechanotransduction. When cells are cultured of soft hydrogels (C), Capz, a protein controlling cytoskeletal architecture, drive the inactivation of YAP/TAZ. When Capz activity is abolished (siCapzb) YAP/TAZ activity is restored. Analog results were obtained using cell confluence as YAP/TAZ inhibitor (D), demonstrating that cells perceive their physical environment in different manner and these signals affect cell biochemistry and fate.

2.3 Mechanically tunable electroconductive substrates

Previously described hydrogels are used as scaffolds to integrate cell cultures. We next thought to hydrogels as a compliant substrate to send stimuli and collect data from cells in real-time.

Muscle cells exert contractions after the depolarization of the cell membrane and the calcium influx. These cells are also implicated in high-impact pathologies such as diabetes being a major player in the glucose-uptake and metabolism [115]. Cultivating these cells on a substrate capable of detecting the membrane potential or the glucose consumption would be a direct tool to study pathological conditions.

With this perspective, we integrated the previously developed hydrogels with the biosensors expertise in our lab. Carbon single-walled nanotubes (SWNTs) are

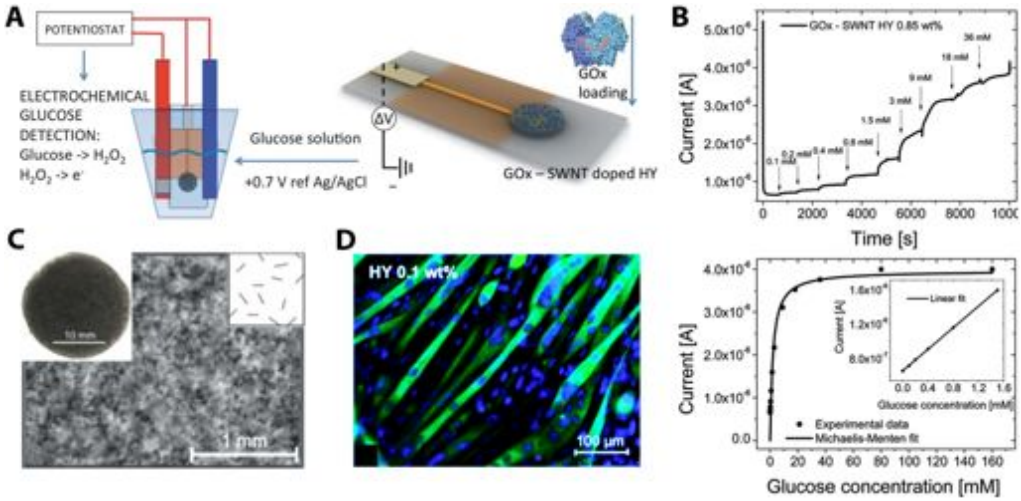

Figure 2.3.1 – SWNT-doped hydrogels for biosensing. (A) Representation of biosensor with a terminal hydrogel-based detector. (B) Evolution of concentration-dependent signal of oxidized glucose by GOx. Conversion of oxidized glucose follow a Michaelis-Menten profile. (C) SWNTs-doped hydrogel with nanotubes distribution. (D) Muscle cells are able to differentiate properly on SWNT-doped hydrogels.

extremely conductive fibers meaning that a non-invasive doping procedure of the hydrogel may be performed [116]. In the publication reported in Appendix C we show that a proper electron network could be successfully used to acquire electrons from a redox enzymatic reaction that takes place within soft biomaterials. Figure 2.3.1 reports an hydrogel biosensor that enzymatically process glucose producing an electron transfer through SWNTs. The sensor detects different glucose concentrations within a biologically relevant range. Muscular precursors were successfully cultivated and differentiated on SWNT-doped compliant poly-acrylamide hydrogels, finalizing the perspective of integrating a soft biosensor for dynamically monitoring metabolic activity.

The use of SWNTs within the hydrogel matrix revealed effective without dramatically altering the mechanical properties of the substrates and allowing the cell viability and maturation as normally performed in conventional methods. Thus, this approach can allow the real time monitoring of detectable activities at the cell niche in a compliant environment.

2.4 Chemistry for long term cell adhesion

Poly-acrylamide hydrogels are a tunable tool to cultivate cells on a defined stiffness. Since the hydrogel results in a repellent surface for standard ECM protein adsorption, ECM species must be incubated for a few hours to result partially entrapped in the superficial matrix mesh and allow cell attachment and propagation.

When hydrogel are used for short-term experiments and cells do not exert substantial force on the substrate, the physical adsorption/absorption of ECM molecules is a convenient and fast way to finalize substrate ready for seeding. However, in our experience, long-term experiments and cells with particularly active locomotion (e.g. contracting muscle cells) necessitate an anchored and stable adhesive layer.

As stated in section 2.2, poly-acrylamide gels are established electrophoresis supports in molecular biology for their inertness versus proteins. A covalent coupling of ECM proteins requires the surface activation with new reactive groups. Although *ad hoc* commercially available UV-active cross-linkers can be used, they are expensive, offer poor scalability in large hydrogel production, have poor solubility, rapid decrease of cross-linking activity when solubilized, limited shelf life, and dependence on UV lamp power and positioning [117]. Other techniques involve carbodiimide or the straightforward inclusion of 6-((acryloyl)amino) hexanoic acid during the polymerization of acrylamide: the N-hydroxysuccinimide ester reacts with amines exposed by proteins, however only cross-linker molecules exposed on the surface can react. Although in line with a limited hydrogel production, Damljanovic and colleagues proposed a convenient alternative to functionalize poly-acrylamide, derived from the fabrication process of oligonucleotide microchips: amide groups, once reduced by highly reactive hydrazine hydrate can be coupled to oxidized proteins [117].

Since the hydrogel production and functionalization can be executed *a priori* and protein oxidation revealed stable for weeks, the translation of this technique to our large and frequent lot production was successfully adopted. Even after several vigorous washes of the functionalize surface, poly-acrylamide hydrogel offered good adhesion capability to different cell types. Cardiac and muscle cells were successfully cultivated for various weeks on activated hydrogels (Figure 2.4.1). Tested techniques and hydrazine protocol modification are reported in Appendix G.2.

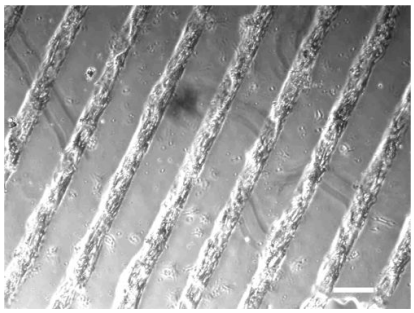

Figure 2.4.1 – Beating cardiac rat cardiomyocytes on long-term functionalized hydrogels. Bar 250 μm.

Hydrazine chemistry revealed a cost effective alternative for the cross-linking of fibronectin or laminin on poly-acrylamide surfaces and allows stable integration of cells on soft gels.

2.5 Substrate development for large-scale studies

The production of large number of hydrogels at one time is extremely useful when various conditions have to be tested along with technical replicates. However:

- hydrogel surface is usually limited to few square centimeters and certain applications require a large number of cells to be analyzed in the same sample;
- part of the cells are wasted because of hydrogel is attached to a glass support that can not completely fit the entire plastic vessel; this point reveal particularly tricky with cell obtained from precious and limited sources;
- acrylamide polymerization relies on a radical reaction that is inhibited by oxygen; the outer ring of the hydrogel exposed to the air do not polymerize leaving a thin glass adhesive surface for the attachment of cellular outliers not cultured on a soft matrix (Figure 2.5.1A). These cells can interfere with the analysis of the whole sample dynamics. Dedicated hypoxic working boxes would prevent radical transfer inhibition.

Poly-acrylamide hydrogels covering the entire surface of common biological Petri dishes and multiwell plates are now commercially available (Matrigen Life Technologies, USA) but were ineffective when we tried to replicate results reported in section 2.2 and Appendix A and B. Maintaining the same hydrogel formulation

in our hands, we tried to develop a similar tool on conventional biological dishes made in poly-styrene. Details of fabrication are reported in Appendix G.3. A brief description of results is reported here.

Although the priming of PS through an oxidation step is simple, plastic can effectively adsorb free molecular oxygen [118], preventing the coupling of acrylamide at the PS level and previously used cross-linkers may not efficiently cover the surface in a manner comparable to glass. In fact, various techniques and molecular bridges failed to couple the hydrogel on the PS (diazonium salts, acryl-terminated silanes, methacrylic anhydride), and in many cases the pre-polymer solution did not reacted few micrometers above PS even after a degassing step of prepolymer solution (Figure 2.5.1B). Even with a lower efficiency, the same technique used with glass supports in our previous works [108, 119] was effective when we considerably incremented the concentration and reaction time of each coupling reagent and during the polymerization process. This supports are now being used for extended proteomic and gene expression analysis for mechanotransduction and metabolic studies with $\sim 10^6$ cells per sample. Previously performed assays evidenced same cell behavior of smaller glass-supported hydrogels.

The opportunity to culture cell on conventional vessels but with a compliant stiffness at the bottom can allow to dissect the behavior of an entire cell population instead of looking at a few hundreds representative cells. These substrate could also be applied to reprogramming studies to investigate the role of stiffness in hiPSC generation. Large surface are an indispensable prerequisite for statistical evaluation of sporadic hiPSC colonies rising from differentiated cells cultured on a single stiffness. Preliminary studies are reported in Chapter 5.

2.6 Mechanically tunable biodegradable substrates

Poly-acrylamide hydrogels are considerably useful since a broad range of biologically-relevant stiffnesses can be explored. Some applications may require substrates that can also actively interact with the cells. Since poly-acrylamide can not be degraded by the cells, new hydrogel-based biodegradable polymers should be developed aiming also at new research targets. Due to the continuous remodeling of ECM components

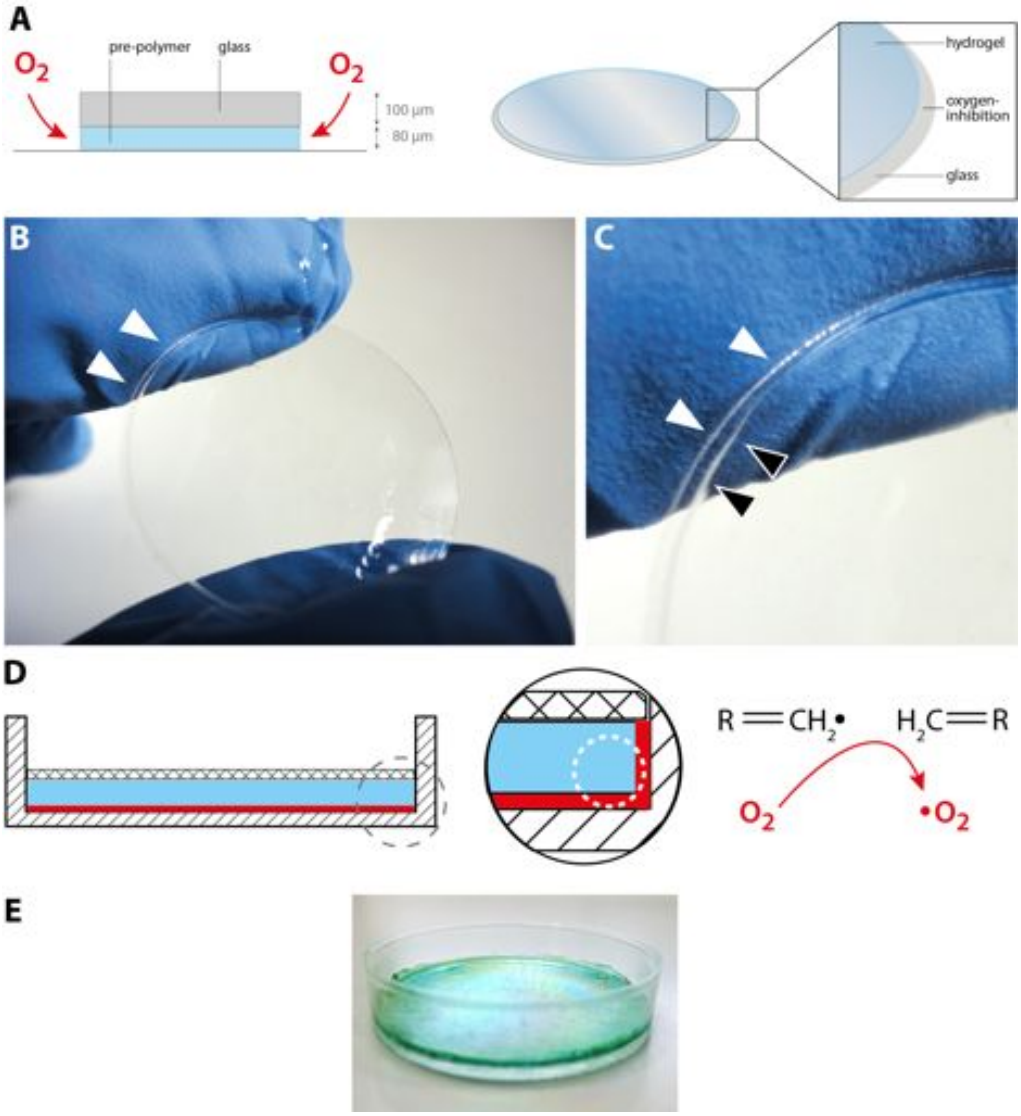

Figure 2.5.1 – Soft hydrogels on standard Petri dishes. (A-C) Oxygen inhibition of radical reaction is normally experienced at the air interface of the solution under polymerization. (B-C) Arrows show glass (white) and hydrogel limit (black). (D) Oxygen inhibition occurs also at surfaces that adsorb/absorb oxigen such plastics and rubbers. (E) Convalently bonded hydrogel stained with a green dye

by cells and the culture in three-dimensional scaffolds, biodegradable hydrogels can further improve the *in vitro* microenvironment for a better mimicking of *in vivo* tissues. In our experience of muscle tissue engineering, various substrate cues have been proven to optimally drive *in vitro* tissue maturation [108, 119, 120].

Before seeking at synthetic polymers that can be degraded we focused on a biomolecule known for implications on cell regeneration, the hyaluronic acid (HA). HA is an unique non-sulfonated poly-saccharide based on D-glucuronic acid and D-N-acetyl-glucosamine (NAG) present throughout the body. It is synthesized by cells directly in the pericellular space with an sustained daily turnover and serves different biological functions [121, 122]. Depending on the chain length, different roles have been address to HA, even if some of them remain putative [98, 123]. Global cosmetic industry has revamped HA for body and facial creams with the potential of skin renewal. HA has also found commercial applications in biomedical rehabilitation and tissue repair with Fidia Farmaceutici s.p.a. located in Padova, Italy. HA chemical derivates are also sold as hydrogel precursors for the maintenance of human stem cells in 3D environments (Glycosan, Biotime, Inc., USA) [98, 123–125].

Since HA is a natural linear polymer, its hydrogel formulation would require an inter-molecular cross-link (Figure 2.6.1). Current strategies presented by researchers and companies propose a modification of HA backbone in order to bridge two macromolecules with an additional cross-linker [126, 127]. Since additional cross-likers may not be fully degradable, we studied the opportunity of synthesizing an hydrogel only based on modified HA and that can eventually be further functionalized with other biomolecules, ending with a more complex biomimetic microenvironment (Figure 2.6.1).

Here we present the main results aimed at obtaining a new concept of an *in vitro* biodegradable scaffold with geometrically controlled features for *in vivo* tissue regeneration. A scaffold for the generation of bundled muscle fibers and subsequent integration in a damaged muscle was engineered. Protocols and additional informations are available in Appendix G.4.

Starting from a method available in the literature [124, 125, 127], we derived a methacrylated form (MeHA) of a naive 700 kDa HA produced by Fidia Farmaceutici

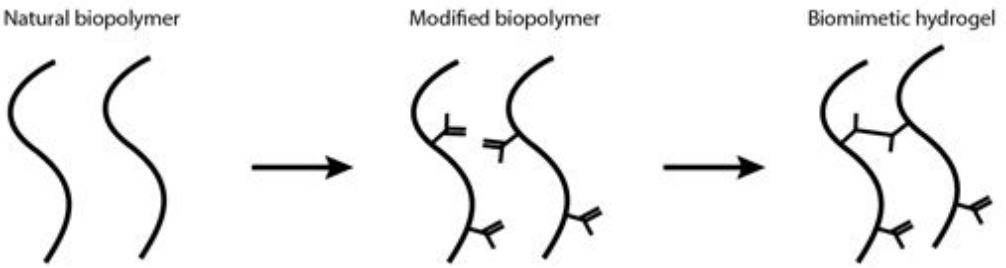

Figure 2.6.1 – Native and modified biopolymers. (A) Polymers produced by cells can be used to improve the biological responsiveness in an *in vitro* environment. Natural polymeric chains can be derived by chemically introducing new functional groups that are able to cross-link together in defined conditions forming a soft hydrogel with active biological functionality. (B) Hyaluronic acid have been derived with methacrylic groups to obtain UV- or APS/TEMED-activatable hydrogels as well as poly-acrylamide gels.

s.p.a.. Since two methacrylated groups can react together forming a stable chemical bond, a MeHA chain can be recursively cross-linked with neighbors, thus, forming a hydrogel. Although we did not have the opportunity to characterize the gel, comparing it with poly-acrylamide gels, its *bona fide* stiffness ranges from $\sim$0.2 to $<$10 kPa depending on the percentage in water.

Using a 3D mold with an array of fibers, we were able to produce a three-dimensional hydrogel with a bundle of channels for the *in vitro* reconstruction of muscle precursors. Figure 2.6.2A shows the main steps for the in vivo integration of engineed muscle fibers. Cells can directly interact with HA through the receptors CD44 and CD138 located on the plasma membrane but we experienced poor long-term adhesion and spreading (data not shown). Thus, we further improved the architecture of this 3D device cross-linking ECM proteins on the surface of each channel (Figure 2.6.2 and 2.6.3A-C). Arranging the MeHA derivation protocol, we adapted the reagents for the derivation of methacryated proteins such as gelatin or collagen .

The *in vitro* degradability experienced with MeHA constructs was comparable to literature with the use of additional cross-linkers [128]. Due to the high viscosity of HA at $>$2% w/v, a minor percentage (0.5% v/v) of poly-ethylene-glycole di-acrylate (PEGDA) was added to increase the cross-linking ratio and the stiffness up to the physiological level of the muscle. Well-differentiated myotube fibers integrated with the 3D hydrogel were obtained (Figure 2.6.3D). At this stage, the hydrogel platform was mechanically laminated from the glass support for the *in vitro* cultivation and

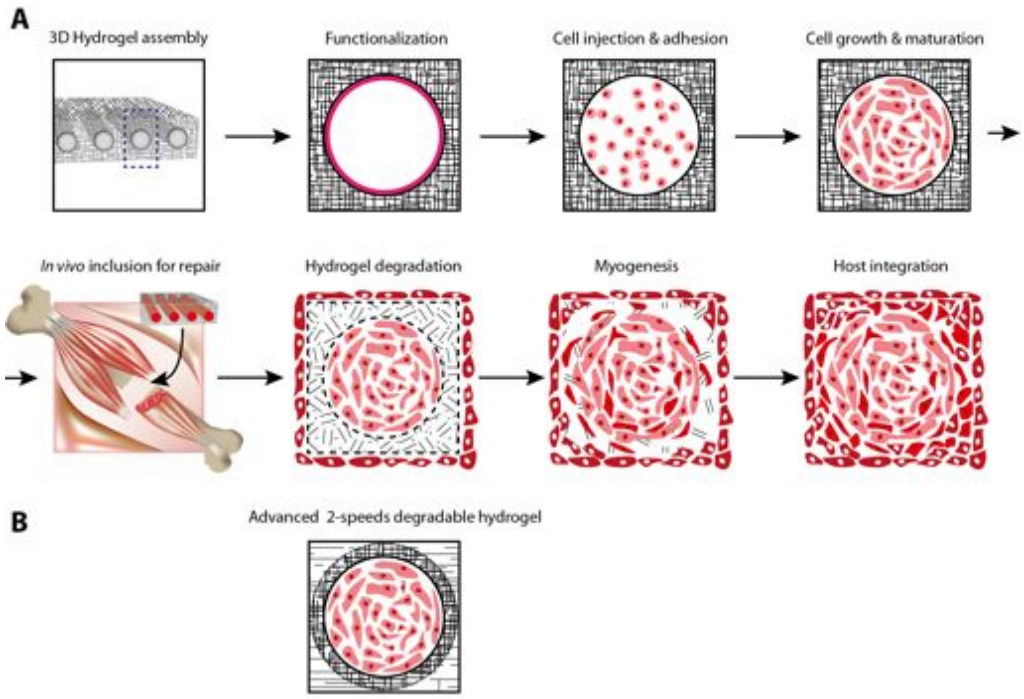

Figure 2.6.2 – Three-dimensional construct for the *in vitro* development of integrable arrays of muscle fibers in patients. (A) A 3D scaffold is produced and coated with bioreactive molecules that allow the attachment of muscle cell precursors. These cells propagate inside each channel, aligning a differentiate into myotube fibers. Mature constructs are transferred in damaged muscle to promote its regeneration. Once *in vivo*, HA matrix is progressively degraded and promote the proliferation of silent cell both from the *in vitro* fibers and the damaged muscle. When degradation is complete both cell type can interact each other in a regenerated muscle. (B) As a proof of concept, these constructs have been successfully integrated in mice with damaged-tibial muscle.

transferred inside an ablated muscle in a mice's leg (Figure 2.6.3G). The construct perfectly integrated with the host muscle promoting its regeneration (Figure 2.6.3H). Again, *in vivo* we experienced a lower degradation than expected and the *in vitro* muscle fibers remained isolated.

In parallel, we tried a Fidia's proprietary new HA formulation. In this case, the hydrogel had fast degradability botj *in vitro* and *in vivo* (Figure 2.6.3I), but not enough to allow proper development of *in vitro* muscle fibers. In the next future, we aim at integrating both hydrogels: MeHA will constitute the core shell to support the proper formation of *in vitro* fibers and the bulk will be formed by the fast degradable formulation (Figure 2.6.2B).

These results evidence the potential of HA in promoting controlled maturation of *in vitro* tissues and in allowing the *in vivo* integration to promote tissue regeneration. Exhancement of available chemistry protocols allowed the generation of 3D hydrogel

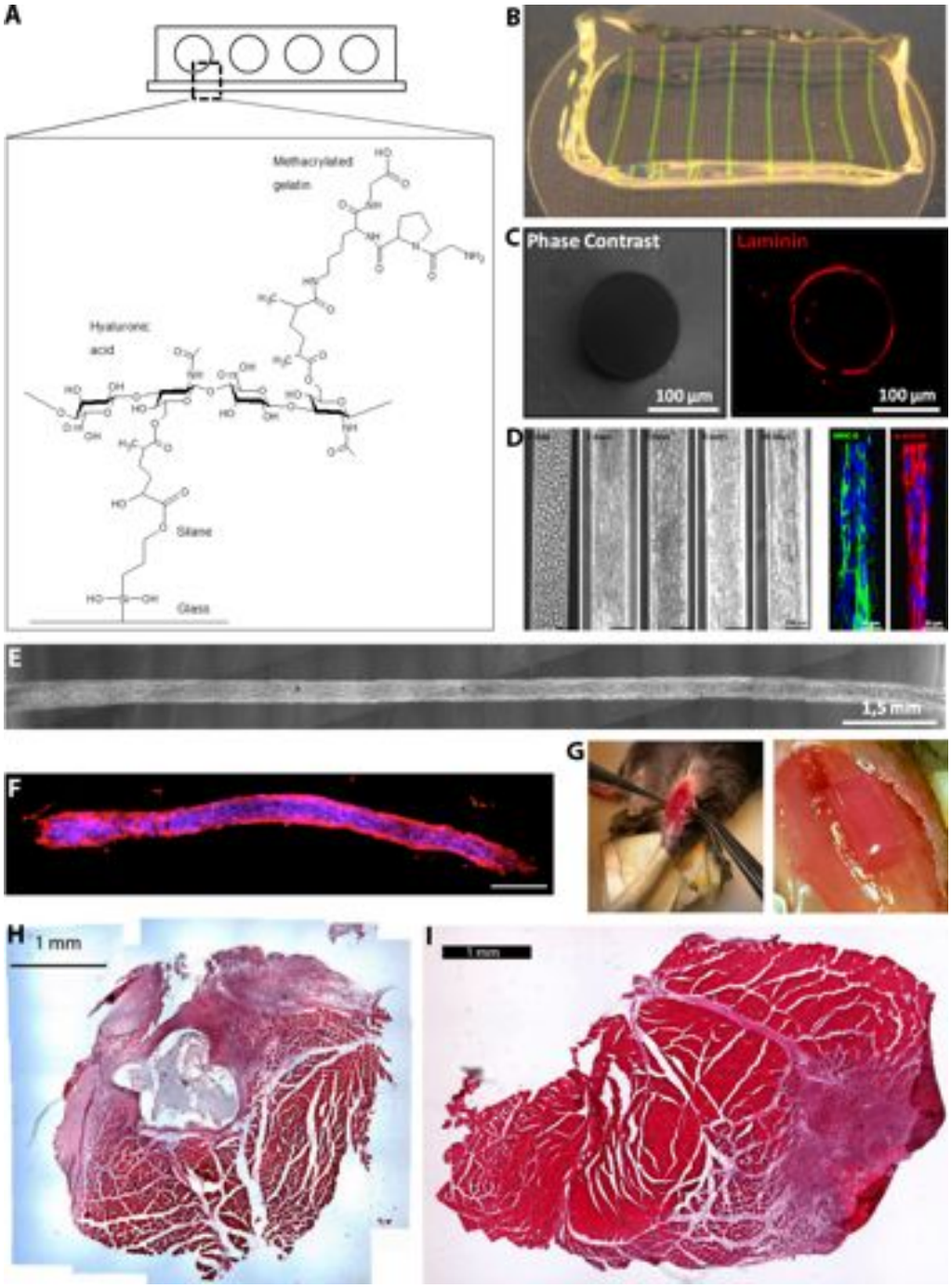

Figure 2.6.3 – 3D biodegradable hydrogel constructs. (A) Different chemical functionalizations were performed in order to obtain an optimal scaffold for in vitro differentiation of muscle cell precursors. Methacrylated HA and gelatin were used to produce the hydrogel and the permanent ECM coating, respectively. HA was bind to a glass slide with a methacrylic terminated silane. (B) An hydrogel prototype with channels filled with a green fluorescent tracer. (C) Transversal section of a 100-µm-wide channel and the detection of ECM protein on the walls with fluorescent-tagged antibody. (D) Evolution of cell culture, from cell injection to maturation in myotubes. Immunofluorescent analysis shows expression of mature muscular markers MHC-II and a-actinin (right). (E) One fiber extracted from the hydrogel after 10 days and (F) MHC-II immunofluorescence of an extracted fiber. (G) *In vivo* implants of 3D constructs with fibers on mice with ablated muscles. (H) Section of a muscle 2 weeks after implant. Hydrogel is degrading and favoring muscle regeneration. (I) Section of a muscle 2 weeks after implant using a the commercial hyaluronic acid derivate. Hydrogel was completely degraded with concurrent muscle regeneration.

scaffolds and the control of cell adhesion and maturation. Engineered muscle fibers can support the host regeneration together with a stimulating biomimetic scaffold.

The chemical control of native biomolecules here presented will be used for the microscale substrate enginering in microfluidic environments in Chapter 4.

2.7 Topological control

Previous sections depicted how substrate mechanics can influence and drive cell behavior, transducing signals from mechanical to soluble biochemical intermediates. As reported in Appendix A and [129], mechanotransduction pathways also sense cell morphology and spreading over the substrate. topological control of adhesive substrates can complete the tools in out hands to control cell behavior *in vitro*.

Substrate topology has been controlled in many ways [108, 129–138] and detailed experience in micro-contact printing (mCP) was gained during this thesis. However, mCP results an unpractical way to topologically define a large number of samples. Thanks to the experience achieved in this thesis, UV-activatable surfaces can be exposed for few seconds to transfer geometric patterns from a photomask. In section 2.2, the poly-acrylamide surface was described problematic for the repellent action versus proteins and cells. To topologically control cell adhesion, we turned in favor this property saturating selected regions for cell-exclusion and leaving pro-adhesive areas free for cell landing (Figure 2.7.1).

Instead of using a branched polymer as previously described, linear chains of poly-acrylamide can be produced as well; in the first case, cell-exclusion is based both on the chemical nature of the polymer and on the physical discontinuity of a wall with defined height. In the second case, one side of poly-acrylamide chain is anchored leaving the other fluctuate: the length of polymer is affected by the rate of radical catalysis, the faster is catalysis the shorter will be the chain lenght, and *viceversa*.

Since radical polymerization of acrylamide can be actuated either by the well established chemical initiation/catalysis of APS/TEMED (see Appendix 2.2) or by UV photo-activation different strategies can be followed. Stamps or other relief have to be placed in conformal contact with a flat surface to guide patterned chemical

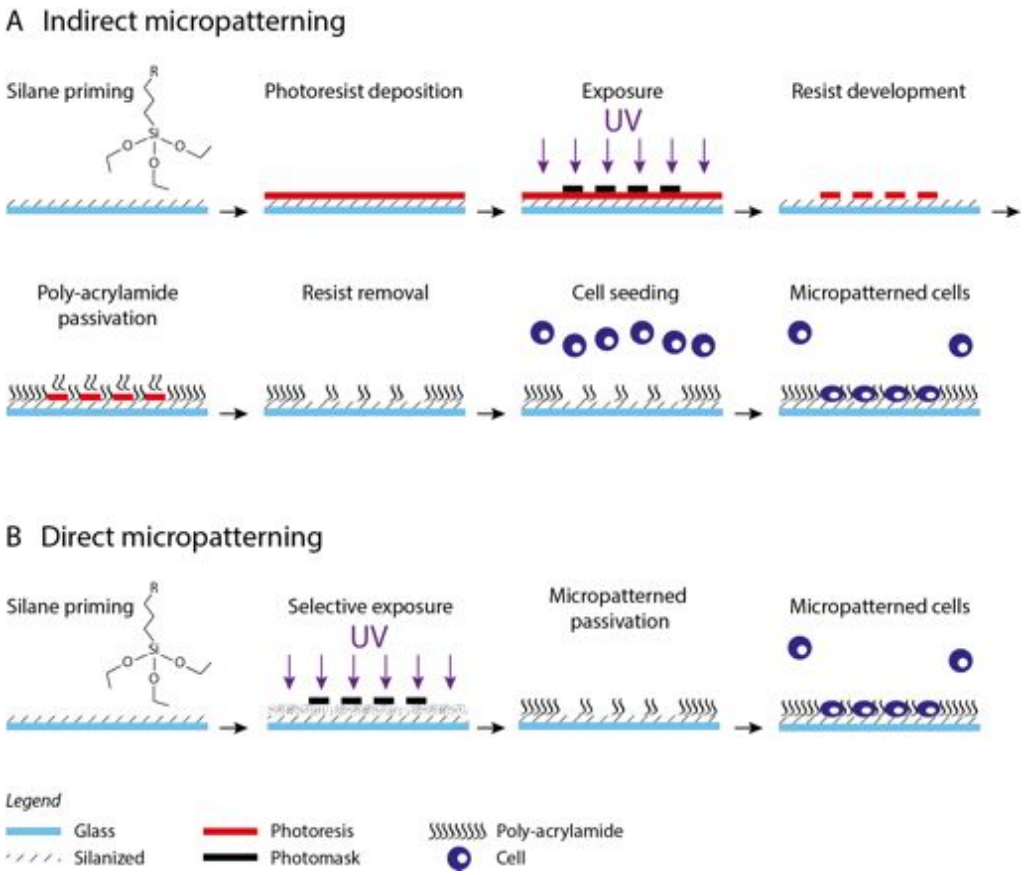

Figure 2.7.1 – Techniques for topological control of cell cultures. (A) Indirect micropatterning. Glass is functionalized with an methacrylic-terminated silane and thin film of positive photoresist is spinned on the entire surface. A defined pattern is transferred to the photoresist thanks to the UV light passing through a mask. Acrylamide is then polymerized passivating resist-free regions. Resist is then solubilized to unmask regions for cell adhesion. (B) Direct micropatterning. Silanized glass can be directly patterned using UV-activated polymerization of acrylamide. Non exposed areas are free of acrylamide and allow cell adhesion and patterned growth.

polymerization, while photomasks can exclude regions from light exposure and photo-polymerization. Techniques to topologically control cell cultures are reported in Figure 2.7.1. Geometric constrains down to the single-cell isolation were realized (Figure 2.7.2).

In Chapter 6, a concept of direct topological control inside finalized microfluidic platforms is presented. Thanks to this advantage, soluble environment, substrate

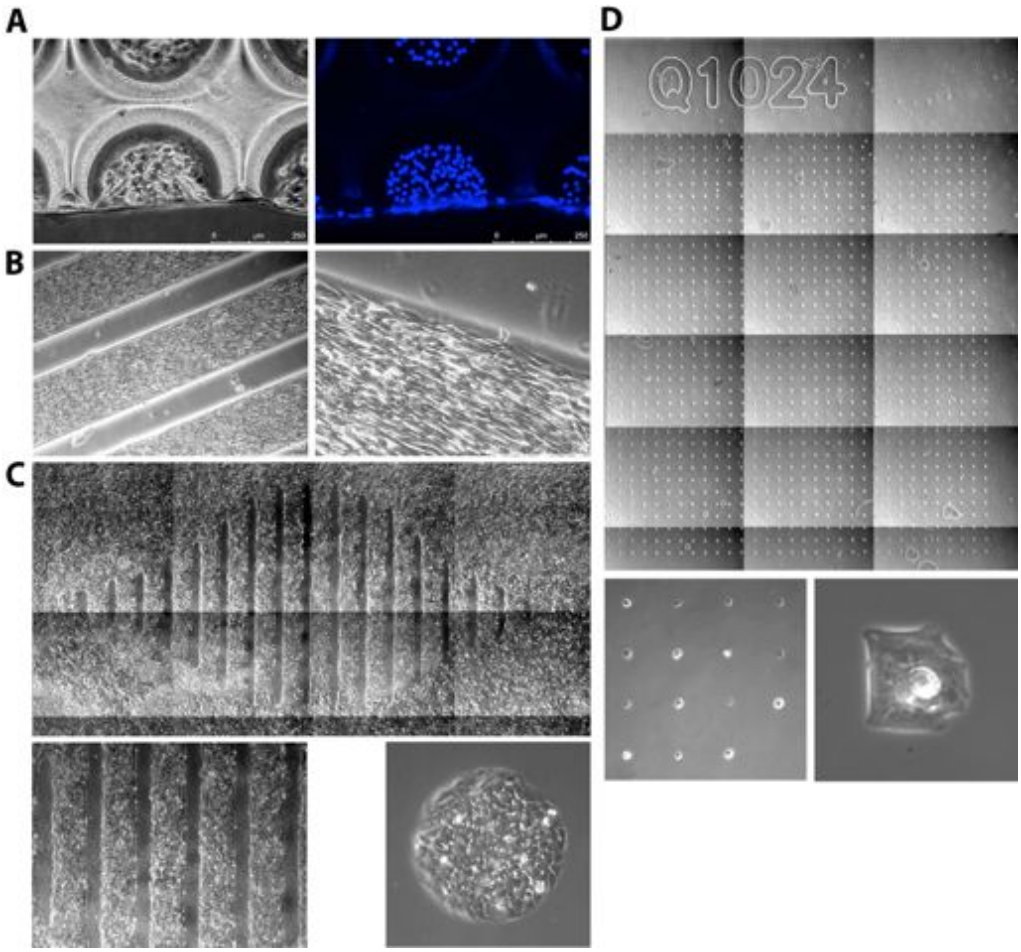

Figure 2.7.2 – Topologically controlled cell cultures. (A-C) Indirect patterning. (A) Crossilinked poly-acrylamide gels can be patterned on glass surfaces to obtain micrometric wells. Cells (here stained with blue nuclei) adhere at the bottom ad are confined by non-adhesive walls (100 height). (B) Linear poly-acrylamide has been used to pattern cells in different geometries. Adhesive lanes 500 μm wide are separated by 200 μm. Muscle pre-cursor cells align along the major axis, promoting cell fusion and myogenesis. (C) Large areas can be patterned with linear poly-acrylamide. Here a merged image shows a pattern obtained by after the removal of a spindle-shaped microfluidic stamp. Pre-polymer solution was injected ad exposed prior to the detatcment of the sticky rubber above. (D) Result of a high-resolution indirect patterning. Cells adhere on small adhesive areas aligned in a matrix. Two magnifications show how it is possible to have single-cell patterns. At higher magnification (bottom-right) it is possible to apprecciate the cell nucleus (bright spot at the center).

mechanics, chemistry and topology can be tailored and combined in an unique platform to mimic human physiology and pathology to improve research discovery and industrial valuable products.

2.8 Functionalization of PDMS based devices

Poly-dimethysiloxane (PDMS) is a commercially available silicon rubber mostly used for micro-engineering applications. Although the precise chemical composition is unknown, many aspects of PDMS are characterized [85, 139].

Cured blocks of the polymer can be activated *via* a plasma oxidation treatment and permanently sealed together or with glass [140]. However, an effective and stable functionalization of cured PDMS is hard to achieve: inertness and evolution of exposed polymer chains to water environment are the major obstacles [141].

In order to perform substrate development also on materials commonly used in microfluidic applications, we explored the possibility to integrate previously described techniques on PDMS. Compliant hydrogel films could cover stretchable PDMS membranes and acrylamide surface chemistry may reduce adsorption of hydrophobic molecules and topographically pattern silicone surface.

To provide an easy and stable functionalization, we thought of doping the base pre-polymer of PDMS before the curing process (Figure 2.8.1).

Since the monomeric unit is based on a dimethyl-silane we introduced a 2.5% v/v methacryl-terminated silane to co-polymerize with the PDMS backbone. Early trials, evidenced that direct acrylamide polymerization occurs on methacrylate-doped PDMS and geometric patterns can be realized. Further investigation will complete the implementation PDMS modification for comprehensive control of surfaces in micro-engineered devices.

2.9 Conclusions

Conventional culture substrates offer simple but chaotic cell distribution and grow, and are not able to fully reproduce defined peculiarities such a biological valuable stiffness, complex physical and biochemical architectures and geometric controlled

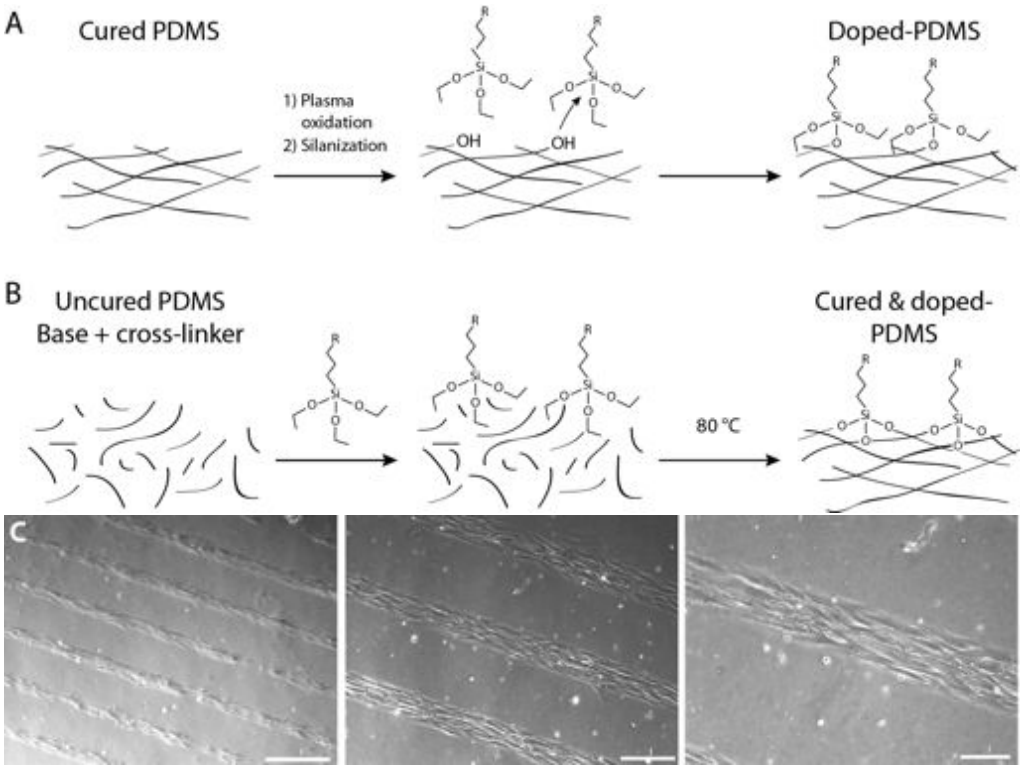

Figure 2.8.1 – Functionalization of PDMS. (A) Commercial PDMS can be thermally cured and oxidized through plasma activation. Oxidized species generated on the surface can be used to react with functional silanes. (B) Uncured PDMS is obtained by mixing a two-component kit. Since the monomeric unit is based on a siloxane, silanes can be included during the polymerization by heating the doped PDMS. (C) BJ fibroblasts seeded on functionalized PDMS with an array of adhesive lanes. Bars 500, 300, 100 μm from left to right

patterns. Emerging examples of body-on-a-chip studies underline the importance of controlling spatial, chemical and physical organization of cell culture environment in order to resemble *in vitro* architecture and functionality of human tissues.

In this chapter, the achievements obtained in substrate development at different levels were described. Starting from previously reported protocols, we extend the potential and applicability of substrate control for cell culture studies, achieving important research results and the possible scalability to commercialization.

The large adoption of synthetic biocompatible substrates with tunable stiffness evidence brand-new biological dynamics and implications in the biomedical field. Chemical activation and doping of hydrogels generated supports for long-term cell adhesion of contracting cells and compliant biosensors with the possibility of real-time measurements of metabolic activity. Looking at a clinical approach, we designed a 3D biodegradable hydrogel prototype for *in vitro* cell and tissue production and its straightforward delivery *in vivo* for muscular reconstruction and rehabilitation. Acrylamide chemistry was then redefined in order to provide topological control of cell culture down to the single-cell level and to modify PDMS rubber, a principal component of micro-scaled engineered devices.

The expertise gained with substrate development will be translated in microfluidics to provide substrates for long-term cultures, a key requirement for the reprogramming and programming of human cells at the microscale.

Chapter 3

Cell cultures in microfluidics

This chapter introduces to the cell culture in microfluidic systems. As a proof of concept, a first reversible integration of mammalian cell cultures with defined stimuli is proposed. A dissertation on the robust long-term cultivation in microfluics follows. Long-term cultivation will be evidenced as a fundamental prerequisite for reprogramming and programming studies at the microscale.

3.1 Motivation

Cells in our tissues are surrounded by an interstitial fluid that support the diffusion of metabolites and connects to the blood vessels network for their delivery throughout the body. Thanks to the low volume of these fluids, small changes in a solute secretion or withdrawal can result in fast and effective signals directed to cells of the local tissue or towards the periphery of our body [5].

In order to reproduce these advantages in an *in vitro* system, a miniaturized environment at the cell-level must be designed together with the use of semi-synthetic or synthetic media. Conventional culture systems based on plastic dishes result in macroscopic vessels that can be used when $10^5 - 10^6$ cells are required to grow as a monolayer in few milliliters of medium. When a massive production of cells is necessary, these culture surfaces can be extended in piles or cylindrical vessels requiring liters of growth medium.

Since the *in vivo* cellular dynamics are exerted in a tiny soluble environment, the previous examples can not provide a tool to screen and mimic biological processes

which can take down to seconds [5]. Reducing the working volumes down to the microscale, it is possible to perform a real-time control over the entire culture system and obtain reproducible conditions [25]. Second, the use of large amounts of media and of biochemical supplements needed for certain cellular activities dramatically increase the costs for the maintenance and the stimulation of the cell layer.

Microfluidics can potentially drive low amounts of compounds over a cell culture with high-efficiency and in an automated and parallelized manner [83, 91, 96, 142]. Moreover, microfluidics platforms can be designed as an open or closed system, with the latter one a key characteristic for Good Manufacturing Process (GMP) directives of Food and Drug Administration (FDA) [143].

All combined, these aspects are crucial for a next-generation cell culture platform that can permit the control of new variables and make feasible new studies at an affordable cost.

3.2 State of the art of microfluidic cell culture

Microfluidics is aimed at being utilized in various fields and for multiple purposes (e.g. chemical reactions, detection of biochemical species, cell sorting, etc.) [79, 144–146] and microfluidic components has also been used in commercial apparatuses (e.g. Agilent Technologies, Inc., USA; Affymetrix, Inc., USA; Fluidigm Corp., USA).

Working at the microscale, microfluidics has the potential to control the process in time and space in real-time [147]. Thanks to the laminar flow regime, the use of multiple inlets allow to perform multi-parametric analyses on the same sample, to create gradients of soluble species and the design of fluidic channel can significantly impact over the system behavior.

Cell cultures and living tissues have been integrated in microfluidics in the past decade, with the aim of controlling the microenvironment for higher reproducibility and higher throughput compared to conventional cell cultures [80, 82, 84, 142, 148]. Microfluidics has the potential to resemble the environmental conditions at the same scale of *in vivo* tissues and can be tailored both to 2D or 3D architectures for a better approximation of human organs.

Since microfluidic devices can be built in transparent materials (e.g. glass, plastic,

resins, rubbers, etc.) cull culture progression, real-time experimental behaviors or the analysis at a later stage are easy to monitor. Release of unwanted compounds and uptake of essential components for cell culture by any material can compromise the stability and healthy of cell cultures both at short and long term [85, 139]. In many cases, glass and poly-dimethylsiloxane (PDMS) were chosen as elective materials for their stability, low cytotoxicity, low price and easiness to assembly.

3.2.1 Materials for microfluidic cell cultures

In the development of microfluidic devices for cell cultures, some materials have raised among others for their superior biocompatibility. This aspect includes different issues referring the properties of a biomaterial. Any materials of the platform should not release toxic compounds into the cell culture environment:

- attention have to be placed not only to the surfaces where cells are directly growing but also to all materials exposed to the culture medium (i.e. upstream reservoirs, tubings, connectors, bulk and structural components of the device);

- the interaction between materials, cells and culture medium should not trigger any physical interaction or chemical reaction, leading to nutrients depletion or release of unwanted substances.

Oxidized poly-styrene plates have being used for decades as the elective culture surfaces in biology for *in vitro* cell and tissue cultures. Since microfluidic devices rely on the three-dimensional confinement of micrometric channels, gas-permeable materials have been adopted instead of plastic, which in turn can also result difficult to integrate with other materials.

Hybrid devices of glass and PDMS or PDMS alone have been extensively used in biological applications. While both show optimal optical properties and glass is totally inert, PDMS presents some issues that must be considered with cell cultures:

- different formulation of PDMS are commercialized (e.g. RTV-615, Sylgard 184, etc.), offer different approaches and may impact differently on cell culture quality;

- PDMS is a silicone rubber which is commonly polymerized through the catalysis of two-components (base and curing agent); uneven mixing can result in defects of chip fabrication and in monomers dispersion in the cell culture system. Additionally, a 5% of the initial monomer is estimated to always be uncured at the end of chip fabrication [85]; some solvents may be used to extract low molecular weight species, which are in part responsible for the unstable functionalization of PDMS surfaces [77].

- adsorption of lipophilic species and absorption of small non-polar molecules [139];

- while diffusivity of oxygen and carbon dioxide in PDMS is not a limiting factor, water evaporation from the tiny fluid circuit results in biased osmolarity that strongly affect cell culture healthy.

Glass slides are commonly used in standard cultures when a thin support is required for a later analysis. To improve the adhesion properties and the spreading capacity of seeded cells, the glass surface is often coated with extracellular matrix (ECM) proteins (e.g. fibronectin, lamin, collagen, gelatin, etc.) which normally support cell adhesion *in vivo*. The physical adsorption of these proteins to the glass surface can support cell culture for various days. Once cells have colonized the entire culture surface, cell-cell interaction can become prominent over the cell-substrate interaction. In this period, duplicating cells also rearrange the composition of the initial protein layer, synthesizing a more complex network which can eventually not interact with the glass surface [149]. For these reasons, a compact cell layer can laminate from the support compromising the sample.

Due to the particular characteristics of microfluidic chips, this and other issue must be addressed when culturing mammalian cells. A brief argumentation of current limititations follows.

3.2.2 Current limitations and perspectives

Despite various efforts, the integration of cell culture in microfluidics always revealed problematic since cells require multiple aspects to be solved at once [25]. Here are

reported some of the main challenges to culture mammalian cells in microfluidics:

- the biocompatibility of the materials directly or indirectly exposed to the cells;
- adsorption/absorption of crucial molecules;
- the adhesion properties of the substrate for cell culture and its long-term stability;
- sterility;
- culture medium management and evaporation;
- limited operability at 37 °C and permeability to oxygen and carbon dioxide.

In many studies, once the cells were integrated within microfluidic chambers they were not maintained for more than few hours or days and reflected abnormal phenotypes [68, 82, 86, 87]. Human cells can reveal more demanding compared to animal cells and specific cell type can be extremely sensitive to the variations of the microenvironment requiring *ad hoc* design and management of the microfluidic system [86].

Another important aspect is the simplicity in using microfluidic devices. Behind new built-in functionalities in a same chip, these devices must be both user-friendly and simple to integrate with delicate biological samples. The need of a complex apparatus and skilled operators in both biology and engineering limit the broadening of this technology [150].

The integration of miniaturized add-ons to the microfluidic core is a powerful feature that can not be straightforward and present with the same packaging in standard plastic culture plates. Biosensors upstream and downstream the culture chamber can reveal many biological processes in real-time (e.g. metabolites, secreted factors, etc.) [151]. At this time, no sensor has been successfully integrated in microfluidic devices.

Such fully integrated microfluidic chips would outperform existing biological and biomedical devices providing real high-throughput performance and un-precedented cost reduction and efficiency. Moreover, miniaturized accurate human *in vitro* models will substitute animal models that can not fulfill the entire human biology and

physiology [81]. Dangerous pre-clinical trials will be avoided for human testers, and personalized drug compounds would be easier to develop.

3.3 Culture approaches in microfluidics

In the following sections, the main issues of microfluidic cell culture referred in the 3.2.2 are addressed. The research and results achieved during this thesis are focused on various strategies to obtain a robust long-term cell culture platform over several weeks. The cultivation over this timespan will be fundamental in order to perform the reprogramming and programming processes at the microscale; a minimum of 2 weeks for each step is required in standard protocols.

The achievements obtained in this section have been obtained thanks to an interdisciplinary development across chemistry, biology and engineering. The long-term integration of cell cultures in microfluidics required a comprehensive knowledge spanning from chemical bonds in biomaterial development to the physics of the microfluidic liquid environment. Especially regarding complex and delicate cell cultures such hPSC, additional parameters fulfilling the biological requirements of these cells must be taken into account. The accumulation of secreted factors by the cells or the their washout with sustained exogenous stimuli carried by the medium can significantly alter the homeostasis of hPSC [86].

In the following sections we report the results obtained integrating cell cultures in microfluidic devices:

- in section 3.4, we report a first integration of conventional cell cultures in an *ad hoc* microfluidic platform.
- in section 3.5, we extend the knowledge gained with substrates development (Chapter 2) in microfluidic devices for long-term cell cultures.
- in section 3.6, we report the technical improvement for the definition a liquid handling platform serving microfluidic chips.
- in section 3.7, we report the study of optimal strategies for medium delivery on microfluidic cell cultures.

3.4 Conventional cell cultures integrated in microfluidics

An early step to respond to some of the issues in 3.2.2 was performed by integrating cells grown in a conventional culture system into a microfluidic platform. The work reported in Appendix D shows how starting from a conventional glass dish, we integrated a defined cell culture in a microfluidic device with reversible sealing.

Briefly, starting from the expertise in structured cell cultures gained in the lab, we integrated cells cultured in well defined static conditions in a fluidic chamber (Figure 3.4.1A,C). Three layers of PDMS were combined together: (i) at the bottom, a glass (75x50 mm) support with a thin silicone membrane carved to accommodate the cell culture glass slide; (ii) in the middle, a PDMS membrane permits the sealing on the chip with a vacuum ring system and the communication between the sample and the microfluidic layer above; (iii) at the top, the microfluidic channels provide inlet and outlet support to the common culture chamber. Middle and top layer were irreversibly bonded by plasma treatment (Figure 3.4.1A). After the prototyping of different geometries and flow operative conditions, we achieved a platform to perform multi-parametric experiments within a single sample with an accurate control of the delivered species (Figure 3.4.1B). Since the platform serves as a temporary solution for the selective delivery of factors above cells, the culture glass slides were transferred back in the conventional dishes after the infection process. This platform has proved that microfluidics, delivering a thin layer of viral suspension above the cell layer, can increase the efficiency of infection (Figure 3.4.1D-E). Experimental validations have also been confirmed by mathematical modeling in our laboratory. Moreover, defined area of cell culture subjected to viral exposition were also detectable in static condition 24 hours after the perfusion (data not shown), indicating that microfluidics can optimally regulate stimuli in time and space over a cell culture.

This work represented a first approach on microfluidic cell cultures aimed at understanding the limits and the potential of the technology when coupled to biologial systems. Since chip fabrication has been routinely adopted in our lab, we next focused on the permanent integration of cells directly in the fluidic circuits (section 3.5).

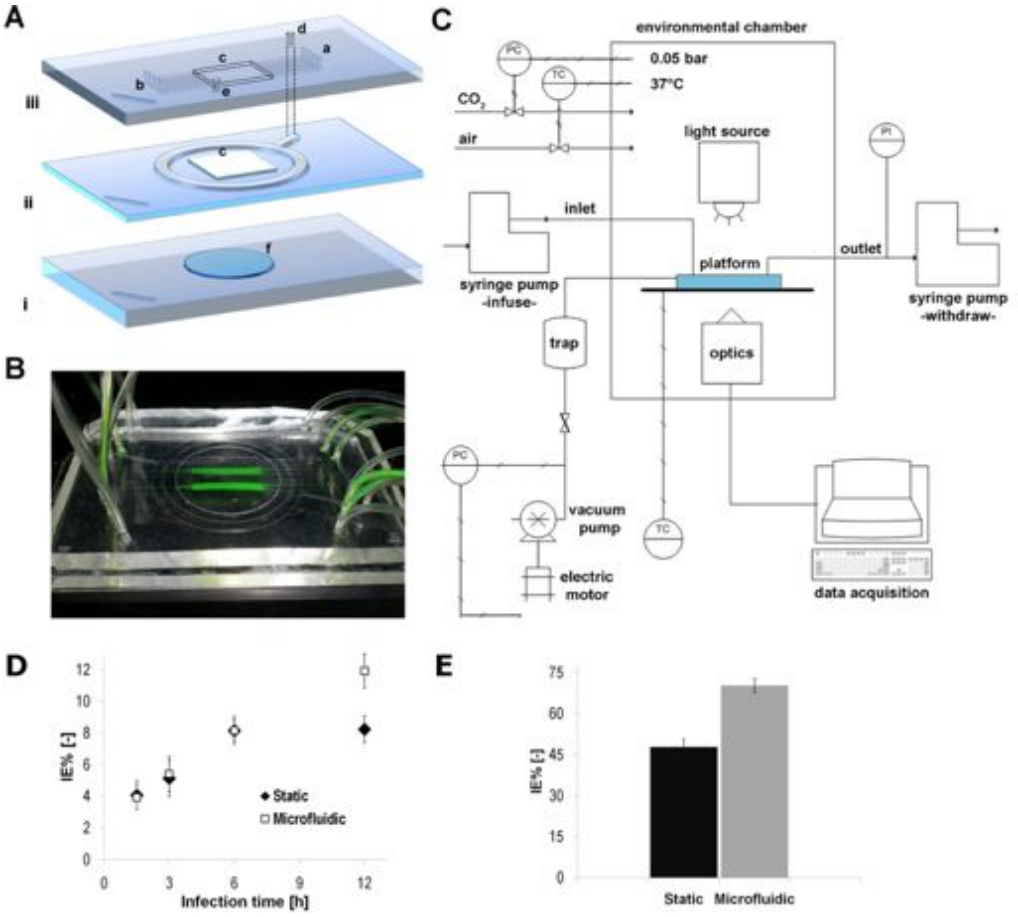

Figure 3.4.1 – Conventional cell culture integration in microfluidics. (A) Schematic representation of chip assembly, with (i) base for culture coverslip, (ii) sealing system with common chamber and (iii) microfluidic layer. (B) Assembled chip with inlets and outlets connected and perfusing either saline solution or fluorescein tracer. (C) Platform overview. The microfluidic chip is integrated in a climatic chamber with an automatized fluorescent microscope for data acquisition. Syringe pumps and a vacuum system serve the chip for liquid handling and temporary sealing. (D) Controlled viral infections in microfluidics. Once viral particles above cells have been internalized in the cells, the delivery of the same amount of virus per cell results in higher infection efficiency using the microfluidic integration with continuous perfusion (> 6 h). (E) Since infections performed in static vessels and microfluidics rely on extremely different amounts o media, infection efficiency was determined using the effective number of viral particles perfused over cells (effective MOI). Microfluidics results significantly more efficient that static infection. Detailed material is reported in Appendix D.

3.5 Substrate development in microfluidic devices for long-term cultures

The knowledge and practice achieved with the first platform were transferred in microfluidic chips where cell can be directly seeded and cultured. When glass and PDMS are permanently sealed together the chip offers inlet and outlet ports for the cell seeding and medium perfusion. This permit a stable and and more robust device compared to previous one (section (3.4)). On one side, this solution do not need any sealing control, a two-step process (seeding and culturing separated by the stimulus) is avoided and the chip is ready to use after the sterilization process; on the other side cell culture on the surfaces of microfluidic channels require the development of surfaces and protocols adapted to the micrometric scale.

Normally, PDMS layers are plasma bonded on mounting glass slides (1 mm thick) to support the rubber layer with a rigid one. Coverslips normally used in cell culturing ($\sim$100-130 μm thick) have a different composition based on borosilicate. This aspect can impact on cell culturing since one cell type can behave differently on naive surfaces with different compositions.

In order to understand how cell cultures behave in microfluidic channels, we first applied the standard coating procedures injecting each solution form the inlet. Before cell seeding, ECM proteins are adsorbed on the glass at the bottom of each channel. Cells start adhering to the ECM protein and spread in few hours. Lack of adhesion proteins results in lower and retarded attachment and can affect cell growth rate and overall behavior at a later stage.

Despite the hydrophobicity of PDMS, ECM proteins may also adsorb to its exposed surfaces in the channel. Proteins commonly have different aminoacids and oligomers that interact in different manners depending on the side group chain; apolar groups and aliphatic chains can weakly interact with PDMS, anchoring proteins to the surface; proteins themselves may also recruit others and stack together. Due to the tiny height of a microfluidic channel (e.g. 50-200 μm), the injected cells are preferentially dispersed at the mid-height of the channel with few cells at the roof and floor level; once the flow is interrupted, cells are subjected to gravity and concentrate

at the bottom of the channel, with almost no cells on the PDMS roof.

When cells reached confluence and cover the entire glass at the bottom, the cell-cell interaction becomes predominant. In particular:

- the initial provided substrate is dynamically rearranged during the culture period by the cells.
- each cell is surrounded and in direct contact with various cells;
- the more the culture area is crowed the more the cell reduce their spreading and contact area with the substrate;
- at confluence, cells stop growing and can than behave differently according to the cell type.
- microfluidic channels have a discontinuity of materials (i.e. glass/PDMS) and surfaces (i.e. edges) that can interfere with the homogeneity of the initial coating and forces exerted by the cell layer.

When cell cultures remain confluent for various days, a tight cell monolayer is formed and can eventually laminate where a discontinuity is present. In Figure 3.5.1, a typical case is presented on the left. Cell layer laminates at the edges of glass/PDMS interface and rolls for the cell-cell interaction with the progression of the culture until a complete detachment of the cell layer.

The concentration of ECM proteins and their interaction with the surface at the initial stage, thus, were found to be critical for the long-term stability of cell cultures. In order to provide a stable culture surface for long-term studies various functionalizations were explored, both absorption-based or with chemical immobilization (Table 3.5.1). The work on substrate development (Chapter 2) revealed particularly important and previous techniques were transferred inside microfluidic channels.

Glass surface can be easily activated for the generation of chemical groups that can stabilize the adsorbed proteins or can serve as bonding site for covalent immobilization of ECM proteins. We stabilized the internal surface of microfluidic channels by chemical bonding of ECM. Using previously functionalizations either based on

Table 3.5.1 – ECM protein functionalization of microfluidic channels. Conventional adsorption methods or cross-linking strategie are reported. Eventual cell layer lamination was reported at 25 days of culture within microfluidic channels. Silanes were used to functionalize the glass.

	method	cell layer lamination
gelatin 0.6% w/v	adsorption	yes, ∼7 days
gelatin 0.1% w/v	adsorption	yes, ∼10 days
fibronection 0.05 mg/ml	adsorption	yes, ∼15 days
gelatin 0.1% w/v + aminated silane	adsorption	yes, ∼10-15 days
fibronection 0.05 mg/ml + aminated silane	adsorption	yes, ∼15-20 days
gelatin + aminated silane + glutaraldehyde bridging	cross-link	no, not fully tested
methacrylated gelatin 0.1% w/v + methacrylic silane	cross-link	no
oxidized fibronectin + aminated silane	cross-link	no

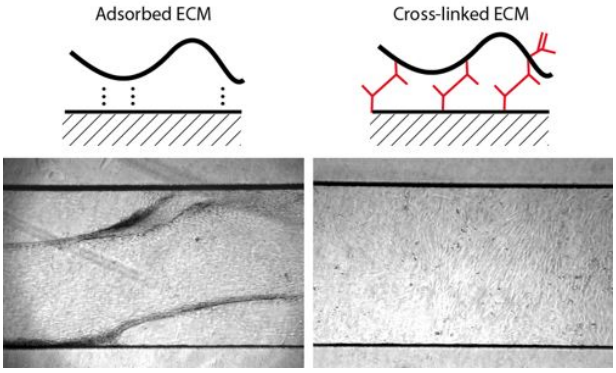

Figure 3.5.1 – Substrate development for microfluidic cell cultures. Adsorption of ECM molecules on the surfaces inside a channel (left) leads to the detachment of confluent cell layers, starting at the edges. When a covalent attachment of ECM proteins was performed (right), cultures resulted in stable cell layers for weeks.

methacrylation or oxidation (section 2.6 and 2.4, respectively), we bonded proteins on glass surfaces *via* methacrylic- or amine-terminated silanes. Cells were stably cultured for various weeks on chemically engineered surfaces (Figure 3.5.1).

Thanks to the know how acquired in Chapter 2, we were able to apport chemically enginered biomolecules at the microscale. Since reprogramming and programming procedures require various weeks of culture, the individuation of stable substrates that allow a prolonged cell culturing is a fundamental step.

3.6 Liquid handling

Once we stabilized the cell substrate for cell cultures at the microscale, we focused on the soluble microenvironment.

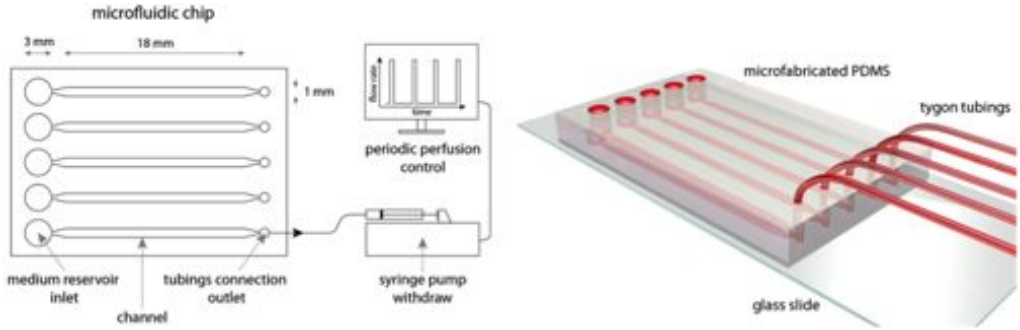

Figure 3.6.1 – Schematic representation of a microfluidic platform. A microfluidic chip composed by various parallel channels with indipendent reservoirs is connected with ta bundle of tubings to a syringe pump. Controlled withdrawal is actuated by a LabVIEW interface developed in the lab. A finalized chip with a glass as sealing and cell culture surface is modeled on the right.

Since each microfluidic channel relies on few microliters of liquid volume and cells need fresh nutrients before their depletion and waste products accumulation, new fresh culture medium must be supplemented in the microfluidic system with a refresh rate higher than conventional culture systems with lower culture surface/medium volume ratios.

Depending on the cell requirements and microfluidic design, refresh rates of culture medium may not be possible to perform by an operator. Especially when the number of similar operations is too frequent, a liquid handling automation is required and can reduce possible errors by a human being (e.g. vehicle of contamination, removal of chip from incubators and loss of temperature and gases, etc.).

Two liquid handling systems available in the laboratory were converted and interfaced with a software in order to perform scheduled operations of culture medium delivery. Syringe pumps and then step motor pumps (components of a previous-generation DNA sequencer) were connected *via* serial ports to a computer and two applications were written in LABVIEW software accommodating the machine own language. LABVIEW offers an intuitive graphical interface to build applications as a block diagram and basic templates serve a starting point to build your own application. For each pump type, instructions can be either sent as command string or by pressing a sequence of buttons. Further software implementation will be required if pumps, micro-valves inside the microfluidic chip and an external medium source have to work in synergy in a unique system.

3.7 Medium delivery strategies in microfluidics

Having developed a cell substrate for a durable integration of cell layers in microfluidics and a tool for automated medium delivery, we explored the best strategy of medium management to perform robust long-term microfluidic cell cultures and to maintain optimal phenotype and biological functions of cultured cells.

In our body, a few cell types are exposed to a continuous flow. Endothelial cells on the inner surface of blood vessels are continuously exposed to the flow at least on one side [5]. The rest of our cells exchange nutrients and waste products thanks a diffusion gradient between the tissue and the capillary bed. This gradient can be subjected to fluctuations: for example, during digestion, glucose is delivered throughout the circulating system to restore and support cell metabolism of tissues and organs after a resting period [115].

Many studies reported to sustain cell cultures in microfluidics for prolonged time [152] and either continuous or periodic medium delivery has been used [68, 82, 83, 87–93, 153]. Although the complexity of microfluidic architecture has been extensively explored, and the effect of some operative variables has been analyzed, the identification of an optimal strategy for medium delivery is still an open issue .

Microfluidics offers an efficient system in terms of medium consumption and delivery but showed some drawbacks when coupled with cell culture systems: due to the high surface/volume ratio, frequent accumulation or washout of extrinsic factors can result in a long-term toxicity effect [68, 82, 91]. Even using the same overall amount of medium in a time interval, it should be considered that different delivery strategies imply different spatio-temporal profiles of metabolites and growth factors, which may significantly influence overall cell behavior and long-term culture stability (Figure 3.7.1A-B).

In the publication reported in Appendix E we reported that a periodic flow, resulting in a fast perfusion pulse followed by a prolonged resting period is the best strategy to:

- avoid downstream effects due to upstream consumption and release of species (Figure 3.7.1C);

- sustain grow by the accumulation of cell-secreted species for sufficient time (Figure 3.7.1C and 3.7.1A-B);
- grow cells at normal rates and maintain their overall phenotype (Figure 3.7.2A-B);
- optimize medium consumption.

These results were obtained using either mouse or human cells, and different cell types and differentiation stages. Even though operative parameters of medium management may be defined for each cell type, a common strategy emerged when integrating cells in microfluidics channels. The model provided by E. Magrofuoco confirms that continuous perfusion favours heterogeneous conditions along the culture chamber and periodic pulses of fresh medium can restore optimal culture conditions (Figure 3.7.2C).

3.8 Conclusions

Microfluidics has the potential to improve current techniques in many fields thanks to unique properties of a high surface/volume ratio and a small amount of fluid at the microliter scale. Although this technology has been proposed in various studies coupled with cell cultures and has found some biology-related commercial applications, it has never been fully characterized for the integration of long-term cell cultures. Since the phenomena at the microscale are unique, the adoption of proper substrate and medium delivery strategy are key aspect for a successful cell culture.

In this chapter, substrate development *via* biochemistry and periodic medium management are reported as powerful tools for the integration of long-term cell culture in microfluidics. Conventional cultures have been first integrated in *ad hoc* microfluidic reversible chambers to evidence in our hand the potential and limits of microfluidics. The infection process perfomed on integrated conventional samples evidenced that microfluidics can efficiently and selectively deliver biochemical species at the cell layer. Substrate development was integrated in microfluidics in order to extend the lifespan of microscaled cell cultures. ECM cross-linking methods revealed as the most reliable for culturing cell for several weeks. Medium delivery strategies

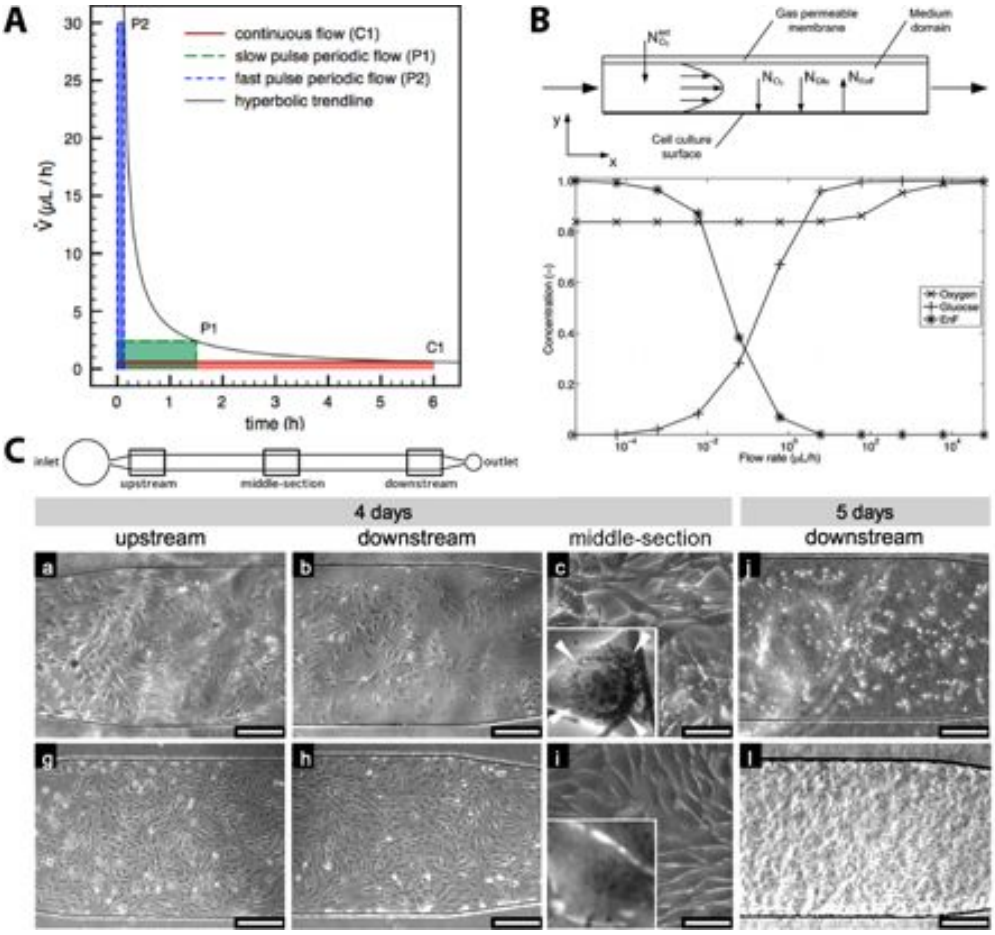

Figure 3.7.1 – Medium delivery strategies for cell cultures. (A) The same amount of medium can be perfused in a defined period with different strategies. Continuous or perdiodic perfusion with different flow rates can be applyied and the same total perfused medium equals to the rectangular area under a hyperbolic curve. (B) Transversal section of a microfluidic channel with fluxes of metabolites. Below, steady state behaviour of the system (i.e. metabolites concentration) as a function of medium flow rate (at 80% of cell culture confluence). (C) Microfluidic C2C12 cell line cultures at 4 days. Three different regions of microfluidic channel were analysed, the upstream, the middle-section, and the downstream. Upstream and downstream conditions are reported for continuous (up) and periodic perfusion (down). Continuous flow presented marked heterogeneous growth (a – b) and cellular death especially downstream. Altered morphologies resulted all along the channel with marked perinuclear vesiculation (c). Applying a fast pulse with a periodic flow of medium delivery, cells grew uniformly along the channel (g and h) and did not present alterations (i). Microfluidic C2C12 cultures at 5 days. Continuouslly perfused cultures reached confluence even with abnormalities but an antithetic situation followed downstream (j), compared to the downstream channel of periodic flow where the culture was over-confluent (l). Insets were taken at half-length of each channel.

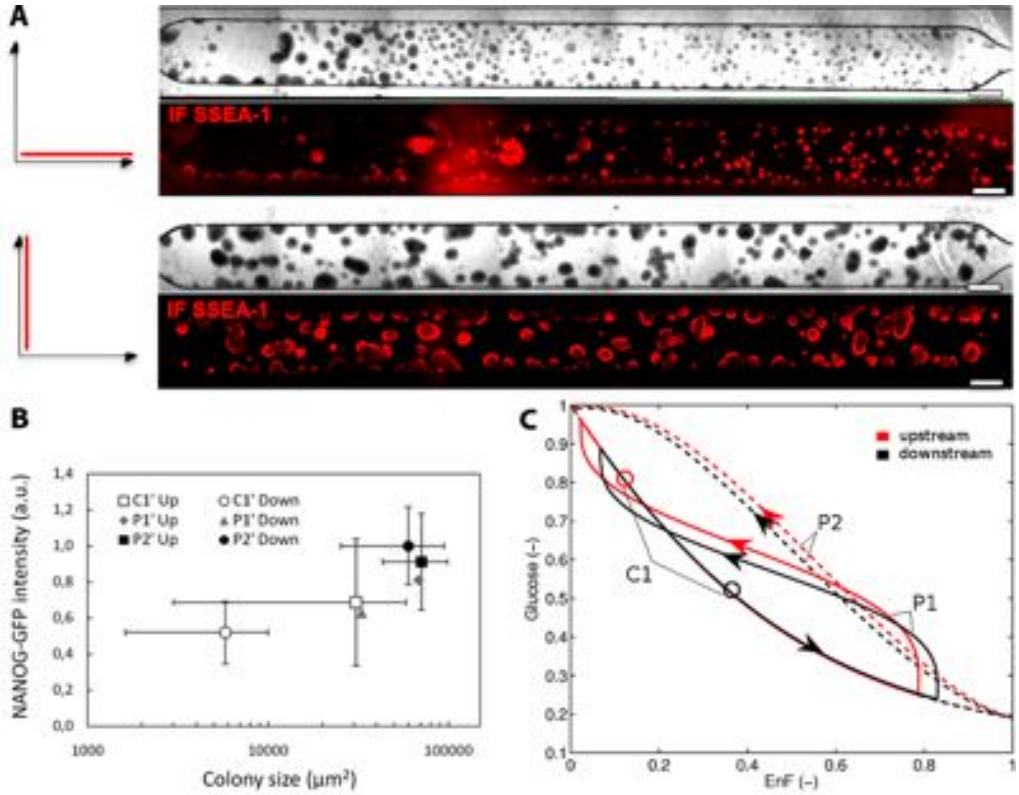

Figure 3.7.2 – Microfluidic mouse embryonic stem cell (mESC) cultures at 6 days. (A) Bright field and immunofluorescence (IF) analysis for pluripotency marker SSEA-1 are illustrated. Continuouslly perfused channel presented marked heterogeneous up-/downstream growth and marked differentiation with SSEA-1 negative flattened cells. Periodic condition resulted in homogeneous and pluripotent compact colonies. Scale bars 250 μm. The same amount of medium was used either in periodic or continuous regime. (B) Image analysis of the pluripotency marker *Nanog* indicate that a fast pulsed periodic flow (P2') is optimal for mESC cultures. (C) Model of concentration profiles of glucose in the medium and cell-produced factors (endogenous factors, EnF). Periodic perfusions result in oscillating concentration while continuous perfusion generates two different microenviroment up and downstream.

evidenced that the soluble control in microfluidic cell culture is a fundamental aspect for cell culture grow and long-term maintenance. Periodic flow was found as the best strategy to culture a variety of cell types.

A comprehensive, fine and tunable control of microfluidic environment for weeks is a fundamental prerequisite to maintain human PSC and direct human pluripotent stem cells fate *in vitro*. Achivements both on substrate development and microfluidic cell cultures were fundamental for the development of a reprogramming strategy at the microscale: cell behavior control, defined delivery of exogenous factors and reduced requirements and reagents will be evidenced in Chapter 4 as key components for a next generation reprogramming platform.

Chapter 4

Human reprogramming in a substrate-defined microfluidics

This chapter describes the technological integration of substrate and microfluidics development for the reprogramming of human cells at the microscale. The downscale of the reprogramming process would introduce a fundamental tool to substantially extend the actual capabilities and unleash the potential of human pluripotent stem cells for screening assays and drug development from a population scale to individual needs. Detailed methods of this chapter are available in Appendix F.

4.1 Introduction

Human pluripotent cells can provide insights on human development and generate differentiated cells of our body for *in vitro* investigations on biological processes, drug development and tissue regeneration [97]. Besides some limits of embryonic stem cells, mostly ethical and relative to abundance, induced pluripotent stem cells can be derived without these problems and expanded in large quantities.

The major limit regarding hiPSC is the generation phase: despite various available systems, these products still retain a considerable cost for every sample to be reprogrammed. When looking forward for a large number of patients with different clinical profiles, genetics, habits, etc., that reflects a population, the derivation of at least one single clone per person becomes unsustainable in terms of material expenses, skilled operators, facilities and required time [4].

Scaling down the cost for each reprogramming sample would make possible the realization of a platform for the reprogramming of a multitude of people and the screening of human biodiversity at various level. With the difficulty in developing new drugs for pharmaceutical industries, the scalability of reprogramming process would provide unlimited *in vitro* human cells of different tissues [81]. Improvements would span from the understanding of the variety of human biotypes to the *ad hoc* solutions for unique people and rare diseases.

Thanks to the new achievements on cell culture substrates and microfluidics gained in this thesis, it would be possible to generate a new platform for the microscaled and extended derivation of hiPSC. A significant cost and material reduction would also allow to avoid the expansion process of hiPSC, realizing a straightforward one-step process for derivation of human tissues on-a-chip.

4.2 Delivery of reprogramming factors at the microscale

In order to understand the practical aspects of the reprogramming process, we first tried available conventional reprogramming systems. Early efforts to introduce reprogramming factors inside cells in conventional and microfluidic environments focused on the adoption of viral constructs, the most used and efficient system known at that time.

Since we wanted a system that relies on a transient expression of exogenous reprogramming factors, we decided to adopt non-integrating viruses such as adenovectors and Sendai (data not shown). The use of repeated infections of transient adenovectors produced at the Dept. of Molecular Medicine resulted in a long-term toxicity and some of the vectors had also production issues. The commercially available Sendai virus (Life technolgies, USA) was adopted in conventional systems to understand the implications of delivering four different variants of the virus carrying OCT4, SOX2, KLF-4 and c-MYC human genes. As stated in the official protocol, a single series of viral transfections had a substantial toxicity on reprogramming cultures with a cell death up to 60% in the first 4 days. After 7 days cells were replated on non-replicating murine cells that support reprogramming process. Three samples of 10^5 cells each were cultivated for at least 5 weeks in hiPSC media and

10-cm-wide dishes, resulting in 0, 1, 13 stable clones. Efficiency is calculated as the number of hiPSC clones over the initial cell number (0, 0.001%, 0.013%, respectively). Transfection process performed in microfluidics resulted extremely cytotoxic with cell cultures collapsing before 5 days, even with a $^1/_{10}$ of the concentration used in standard systems.

Despite the various problems emerged with the previous techniques, the standard reprogramming revealed the importance of transition steps from adult cell to a pluripotent phenotype. Cell density, transfection efficiency, morphological changes were taken into account in order to design the microfluidic protocol.

Since these methods were not satisfactory in our hands we looked for new alternatives to be scaled in microfluidics. As proposed in the next paragraph 4.2.1, the emerging technology of modified mRNAs was studied and implemented.

4.2.1 Emerging modified-mRNAs technology

The 2011 International ISSCR conference on stem cells (Yokohama, Japan. 2011. isscr.org) offered the great opportunity to discover the emerging reprogramming technology based on modified RNA messengers (mmRNA) provided by Stemgent, Inc. (USA). mmRNAs directly encode encode proteins of reprogramming factors and by their nature are degraded in less then 48 hours from the delivery inside the cell [9, 14]. A subsequent partnership with Miltenyi biotec, GmbH (Germany) provided own-developed GMP-grade mmRNAs for reprogramming.

We first assessed the delivery of mmRNAs in microfluidics with a sequence promoting a nuclear-localizing fluorescent protein (nGFP). A cell fraction, 24 hours after transfection, evidenced fluorescent nuclei and, thus, the possibility of delivering reprogramming factors. We next explored how to increment the transfection efficiency by altering the ratio of mmRNAs, transfection complex necessary for the delivery inside cells medium and time of transfection, and by providing non-adsorbent surface in a microfluidic system (see section 2.8). Transfections are performed by incapsulating mmRNAs in solution within lipid vesicles that in turn are dispersed in an *ad hoc* medium for reprogramming (see Appendix F). In order to provide all the seven mmRNAs encoding the reprogramming factors in the provided kit in the 5 μl

Table 4.2.1 – Delivery efficiency of nGFP mmRNA reported for various conditions tested. Medium proportion was reduced from the conventional protocol (0% means pure transfection complex without PL). An incubation for 4 h revealed optimal for higher nGFP delivery. Average percentage of nGFP positive cells at 24 h from a single transfection are reported.

Conventional PL amount	1X mmRNA single transfection	Transfection time 1 h	Transfection time 2 h	Transfection time 4 h
100%	12%	-	-	-
50%	28%	6%	13%	28%
25%	31%	9%	24%	29%
0%	13%	-	-	-

volume of each microfluidic chamber, we had to reduce the proportion of medium (Pluriton, PL) of the transfection mix presented in the official protocol (Table 4.2.1). A 25%-50% of PL volume - compared to standard transfections performed in static vessels - resulted optimal for repeated delivery of mmRNAs. Starting from the first transfection, microfluidic was significantly more efficient than standard static procedures (Figure 4.2.1). Although the previous treatment of microfluidic surfaces with 2% w/v Pluronic F-127 for 1 hour gave an higher transfection efficiency, probably due to the lower adsorption of lipophilic vesicles on PDMS, at this stage, we maintained the platform the as simple as possible. Since mmRNAs have an expression peak after 18-24 hour from the transfection, daily subministration of reprogramming factors must be performed. Daily transfection a evidenced complete delivery over the cell population (Figure 4.2.1).

4.3 Strategies for reprogramming and programming at the microscale

Once verified that it is possible to deliver mmRNAs in microfluidics for days following a fluorescent reporter, we introduced in the transfection complex all the 7 available mmRNAs for reprogramming (OCT4, SOX2, KLF-4, c-MYC, LIN-28, NANOG, nGFP). A comprehensive scheme of the reprogramming apparatus is reported in Figure 4.3.1.

Standard procedures performed on static vessels follow the following pattern: (i) target cell isolation, (ii) expansion, (iii) reprogramming, (iv) hiPSC clone isolation, (v) clonal expansion, (vi) characterization and (vii) differentiation in defined

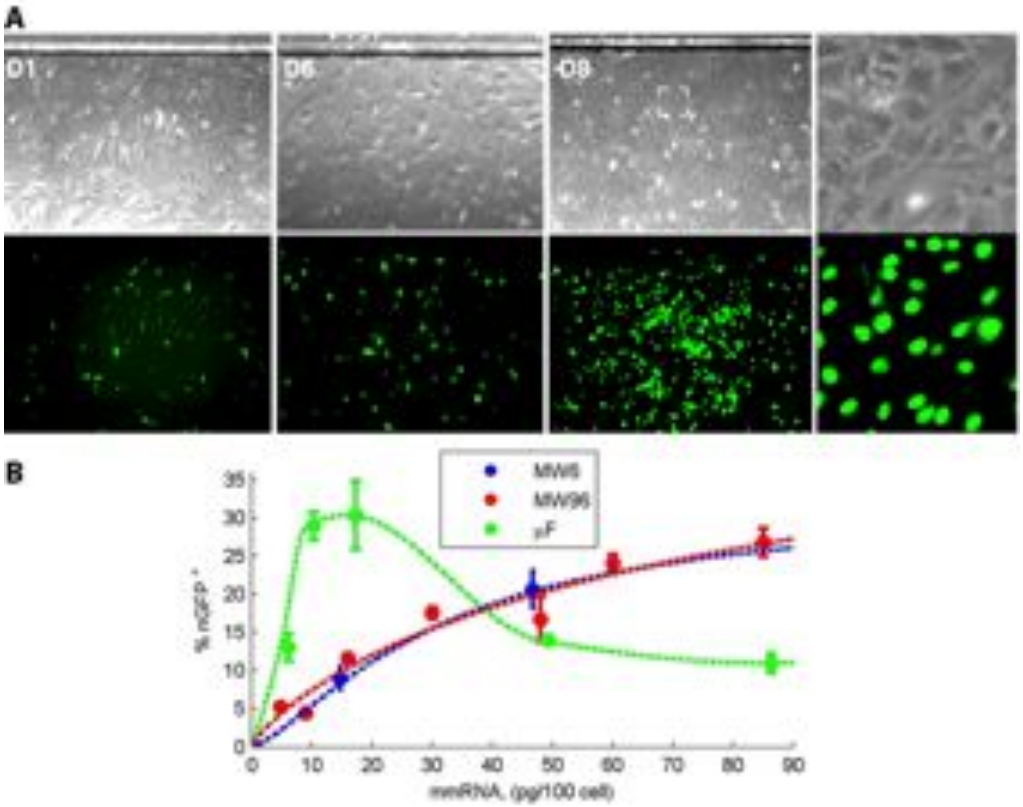

Figure 4.2.1 – (A) Daily complete reprogramming mmRNAs delivery on BJ cells in microfluidics with 25% PL. Acquisition was performed at 1, 5, 8 days after the first transfection. nGFP positive cells increased during culture and morphological changes occured on cells. (B) Even with a single transfection, microfluidics results more efficient with lower amounts of mmRNAs compared to medium (MW6) and small (MW96) conventional culture plates.

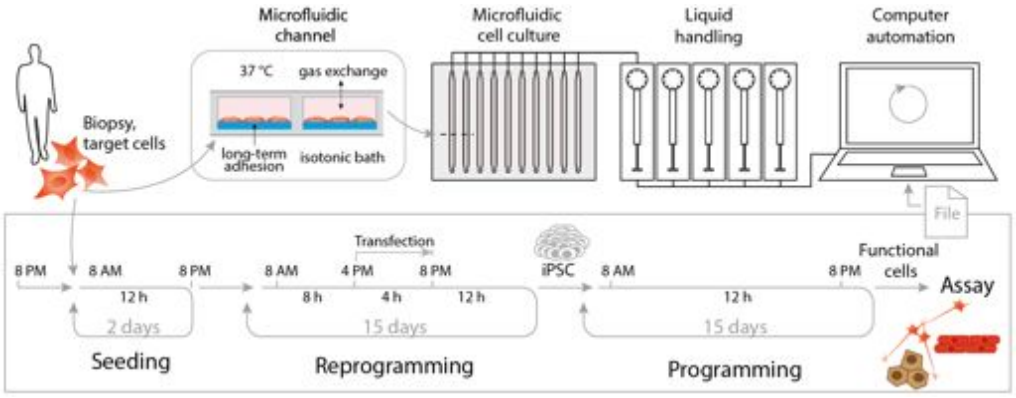

Figure 4.3.1 – Reprogramming apparatus. Cells are taken from biopsies or established cell lines and integrated in the microfluidic platform. Liquid handling pumps are controlled by a LabVIEW software. A reprogramming sequence is proposed on the panel below. After an initial seeding, repeated transfections were performed for 16 days followed by 15 days of differentiation.

cell types. Reducing the minimum requirements to perform a microfluidic reprogramming, it should be possible to reduce or eliminate expansion steps and perform one-shot experiments. In order to recapitulate the standard pattern in microfluidics and dissect and optimize procedures at the microscale, we planned three different strategies.

Strategy A: reprogramming in microfluidics, clone isolation and standard expansion and characterization, differentiation. This strategy would clarify the performance of microfluidics in the generation of hiPSC. Eventually, clones would be isolated from the chip and expanded with standard procedures to verify the stability of clones and the differentiation potential.

Strategy B: reprogramming in microfluidics, collection and clones plating on new chip for differentiation. This strategy avoid the need of clonal expansion. Different clones are pooled in new chips with free available space to grow and differentiated.

Strategy C: one-step reprogramming with differentiation. This strategy represent the best option to obtain new defined cell types from the cells of a patient. Patient cells are reprogrammed in microfluidics and directly differentiated toward desired cell types to perform assays.

In order to obtain the best performance from our microfluidic chip, we used the substrates developed in section 3.2.1 and the whole expertise detailed in Chapter 3. In the next section, the results of evaluated strategies are reported.

4.4 Strategy A: reprogramming at the microscale

Reprogramming. Starting from the basics of the Stemgent's reprogramming protocol (available at stemgent.com) we daily transfected cells inside microfluidic channels. Using the BJ fibroblast cell line model, we evaluated their reprogramming starting with different seeding densities. In the first five days, normally elongated cells evolved in more round shapes as seen in standard protocols. At day 12, we experienced the first *bona fide* hiPSC colony generated at the microscale (Figure 4.4.1).

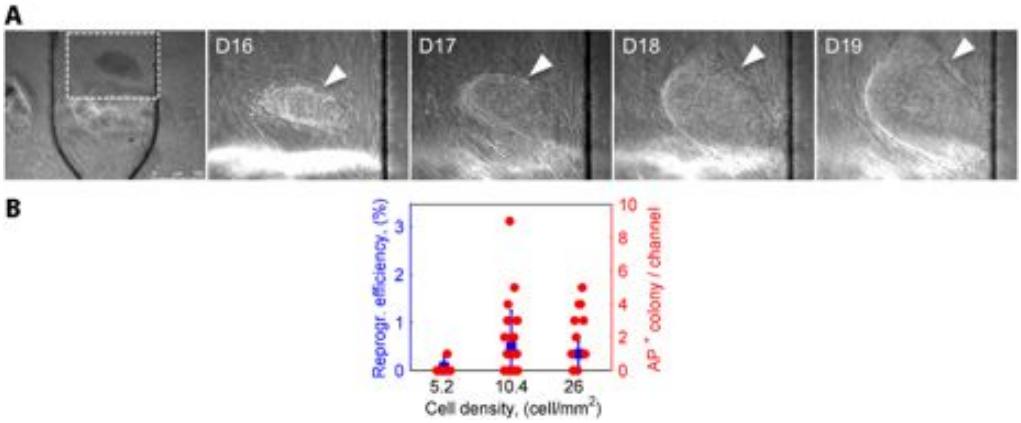

Figure 4.4.1 – hiPSC colony derived in microfluidics. (A) Colony present characteristic morphological markers such as compact cells, defined edges, well formed-nucleoli. Colony expanded progressively in 4 days before being processed. (B) Reprogramming efficiency of BJ cells. Average efficiency in a chip is displayed in blue. Total number of colonies per channel is displayed in red. Higher seeding densities of BJ cells were more efficient in producing hiPSC.

Due to the enormous importance of this hallmark, we continued following the evolution of reprogramming. Best results were obtained with higher cell density tested. In fact, different other colonies appeared the days later. As evidence by the plot in Figure 4.4.1, we obtained efficiencies up to 3.2%.

Isolation. We next evaluated how to isolate colonies from each microfluidic channel. Two strategies were adopted:

- using a biopsy punch, we generated a core through the PDMS rubber and exposed colonies were dissected and aspirated;
- based on the recent published method [154], we applied a high flow rate inside the channels. hiPSC colonies detached preferentially leaving the non-reprogrammed cell layer on the chip.

Expansion & characterization. hiPSC clones were expanded for several passages on conventional plates in the presence of non-proliferating murine fibroblasts. All molecular markers tested proved the effective pluripotency of each clone. Both random or specific differentiation protocols available in the lab were effective. It can be argued if microfluidic-derived clones have same characteristics of hiPSC obtained with conventional procedures.

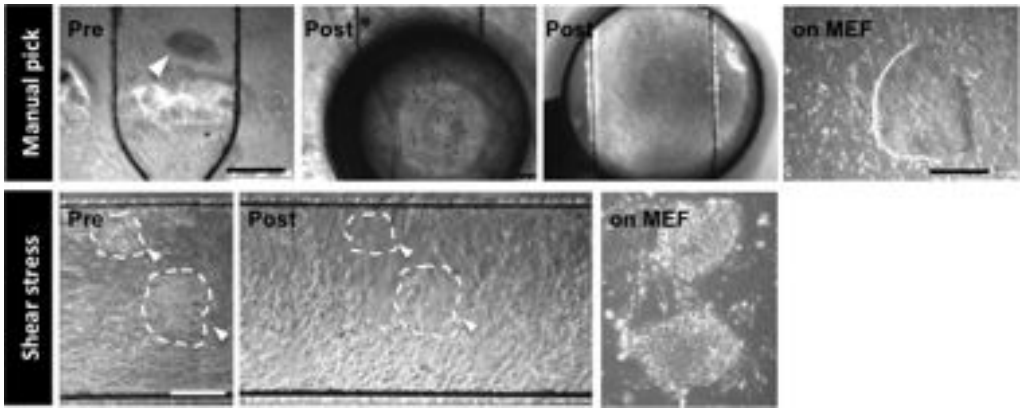

Figure 4.4.2 – Microfluidic-derived colonies extraction methods. PDMS rubber was cored in order to have access to the colony on bottom of the channel (top). Some colonies were also isolated by shear-stress leaving non reprogrammed cells on the channel (bottom).

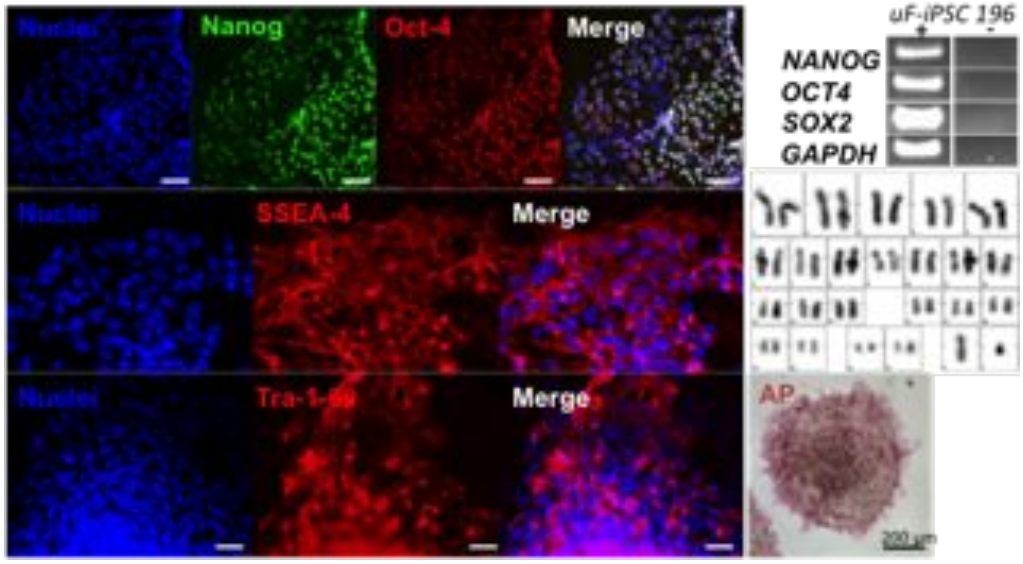

Figure 4.4.3 – Characterization of isolated colonies for pluripotency. Immunofluorescence analysis evidenced standard pluripotency markers (Oct-4, Nanog, SSEA-4, Tra-1-60). Additional analysis were performed via RT-PCR, karyotype stability and alkaline phosphatase assay (right).

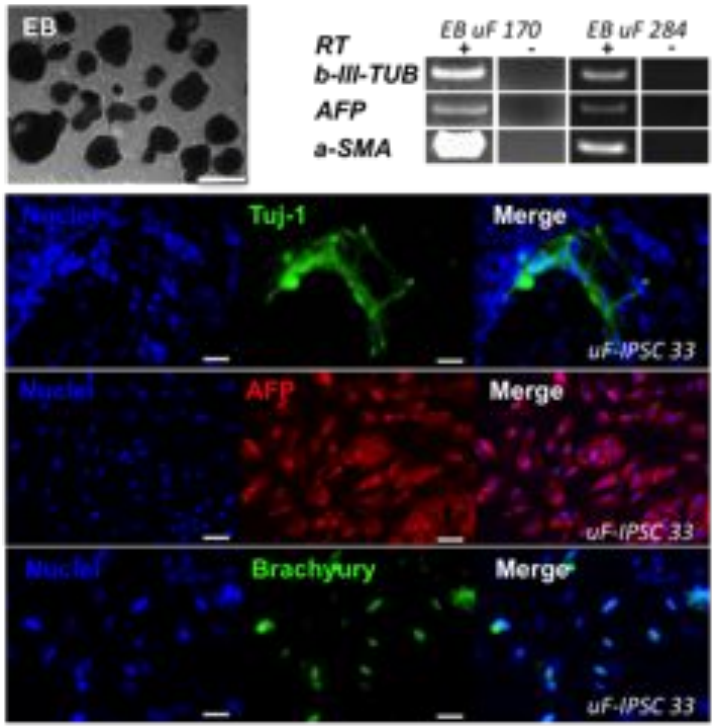

Figure 4.4.4 – Characterization of isolated colonies for differentiation potential. Colonies cultured on non adhesive wells formed spheroidal clusters that differentiate spontaneously in the three germ layers that form our body. RT-PCR analysis revealed typical markers (b-III-tubulin, AFP, aSMA). Immunofluorescence analysis evidenced markers for all germ layers ectoderm (Tuj-1), mesoderm (brachyury), endoderm (AFP).

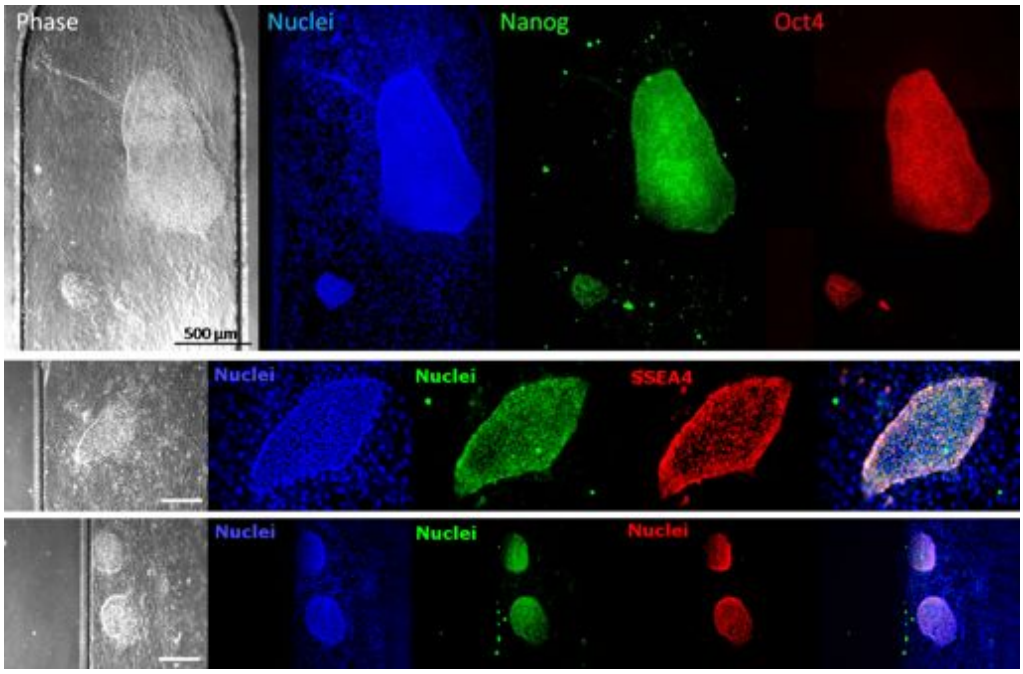

Figure 4.4.5 – HFF-derived hiPSC. Various *in situ* immunofluorescence assays reveal the expression of pluripotency markers NANOG, OCT4 an SSEA-4 within compact cell colonies.

4.4.1 Reprogramming of other cells types in microfluidics

HFF fibroblasts were tested to prove the reliability of the microfluidic system. It is worth to underline that HFF were used at higher passage (P18) compared to fresh BJ cells. In fact, fresh isolated cells are usually preferred since they are more prone to undergo a reprogramming process. Reprogramming of HFF in microfluidics gave clones with efficiencies similar to BJ. In situ characterization of HFF hiPSC clones is reported in Figure 4.4.5.

A step towards clinics. Since the goal of this thesis is the application of the developed platform on cells freshly-derived patient's cells, we studied a non-invasive way to obtain cells. To obtain fresh fibroblasts, an invasive skin biopsy is normally required. It has been shown that epithelial cells can be derived from patients by their isolation from urine and subsequently reprogrammed [36]. Regenerating renal epithelium normally lose few luminal cells that are washed out with urine. Collecting these cells we were able to introduce and cultivate them in the microfluidic environment (Figure 4.4.6A-B). Although these cells can be subdivided in two different categories and one resulted somehow refractory to repeated mmRNA transfections, we were

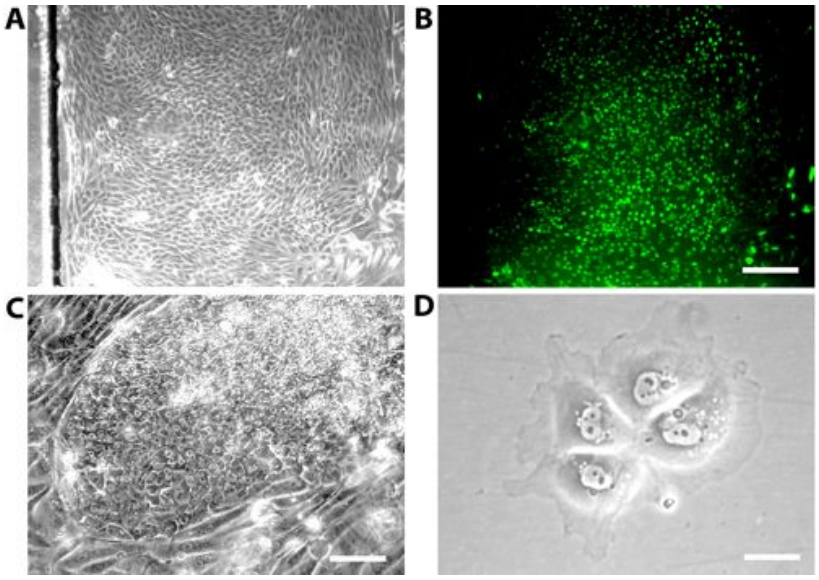

Figure 4.4.6 – hiPSC derived from urine cells. (A) Phase contrast of renal epithelial cell cultured in microfluidics under reprogramming. (B) Relative fluorescence image of nGFP positive cells carrying the other factors. (C) An emerging compact hiPSC colony from the epithelial cell layer. (D) A small colony of four hiPSC under expansion and derived from the dissection of the colony in panel C.

able to generate hiPSC clone freshly derived from a patient (Figure 4.4.6B-D).

The isolation of cells from urine in a totally non-invasive manner and their reprogramming in our microfluidic chip is a paramount milestone for the realization on an integrated platform for a large-scale screening based on hiPSC derived tissues.

Feeder-free. Since mmRNA protocol requires a co-culture of non-proliferating cells other than patient's cells to sustain reprogramming (feeder-cells), we evaluated the possibility to remove such external cells to simplify the system and to simulate a clinical-like approach. BJ fibroblasts were solely seeded at higher density in microfluidic platforms. With a dose-ramping of 100%-75%-50%-25% of conventional static medium in the first 4 days we allowed cells to sustain factors uptake with a tolerable stress before applying a full dose. Feeder-free hiPSC colonies were obtained and showed expression of pluripotency markers.

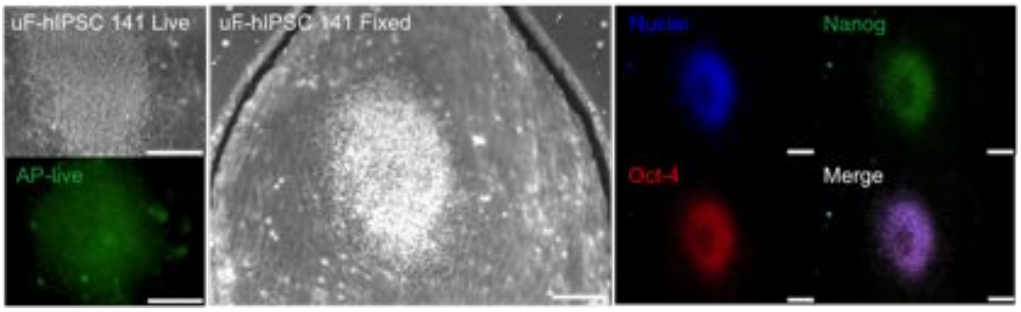

Figure 4.5.1 – In situ characterization of hiPSC. Fresh derived colonies inside each channel have been analyzed for the expression of pluripotency markers after three days from the latest transfection. A live staining for alkaline phosphatase (AP, Life technologies) was performed (left). Once AP signal disappeared, cells were fixed (center) and processed for immunofluorescent analysis (right). The colony in the middle of the channels is positive for NANOG and OCT-4, nuclei are stained with Hoechst 33342.

4.5 Strategy B: pooling colonies for optimal differentiation

***In situ* characterization.** Once verified that microfluidic-derived hiPSC resulted in stable pluripotent clones for various expansion passages (at least 12), we verified the presence of pluripotency factors in fresh derived colonies *in situ*. As reported in Figure 4.5.1, it is possible to perform assays directly in the reprogramming channels and freshly obtained hiPSC express characteristic markers.

Pooling. Since our hiPSC directly express the pluripotent genes, we next isolated and pooled freshly obtained colonies in new chips without a subclonal expansion process. This was an required steo since a minimum cell density is required by available protocols in order to properly induce defined differentiated cell types.

Differentiation. Since mmRNAs reprogramming technique relies on fast (24-48 hours) transient expression of exogenous factors, emerged clones have to express a stabilized endogenous hiPSC pattern (namely, *transcriptome*) to proliferate. With this strategy, we verified that non-expanded colonies are able to generate differentiated cell types. It is possible that the full transcriptome of the same fresh and expanded clone slightly varies due to the selection process made on the clonal expansion. We are analyzing the actual transcriptome of clones before and after expansion. If no significant chances are detected, expansion process could be considered if a cell

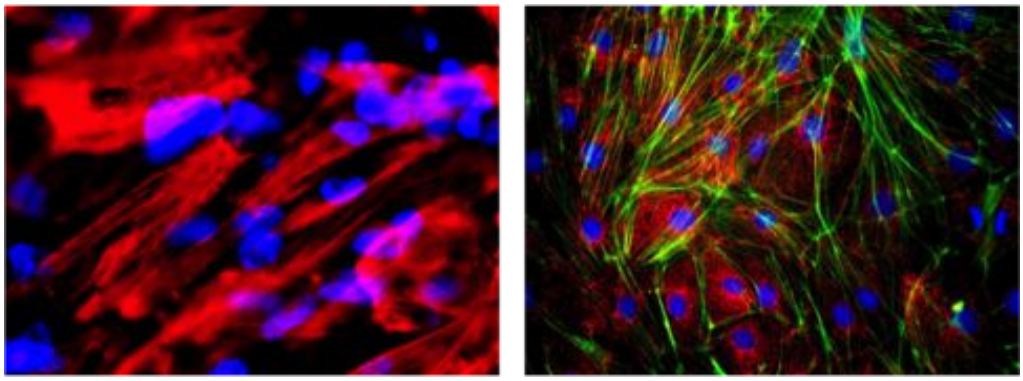

Figure 4.5.2 – Specific differentiation of freshly generated hiPSC. Immunofluorescence assay on chip with red-labeled proteins of terminally differentiated cells, nuclei are stained in blue. On the left, cardiomyocytes expressing functional troponin proteins, sarcomeric striatures are present evidencing contractile capabilities. On the right, functional hepatocite-like cells expressing cytokeratin CK18, actin fibers in green evidence characteristic poligonal shape of hepatocytes.

bank is required.

In hour hands, freshly derived hiPSC were able to differentiate as much as standard expanded clones.

4.6 Strategy C: one-step process for reprogramming and programming

Strategy B was required since the density of rising hiPSC was not enough to perform a differentiation protocol. We next investigated to increase the reprogramming efficiency and perform differentiation protocols without clonal isolation. This strategy would allow to obtain particular differentiated cells from a patient's starting cells in one-step without isolation or subculturing.

Substrate study. When microfluidic reprogramming was performed, we noticed that reprogramming efficiency was lower that experienced with a conventional protocol. Delivered liposomal vesicles used to deliver mmRNAs normally fall by gravity until they coalesce with cellular membranes. Due to an intrinsic toxic effect of transfections, efficient delivery performed by microfluidics resulted in a high selective pressure and stress on cells at the bottom. Since chemical functionalization of culture surface in microfluidics are performed in a finalized chip, adsorption of modified proteins occured on PDMS. Cells that were able to escape the glass surface tended to

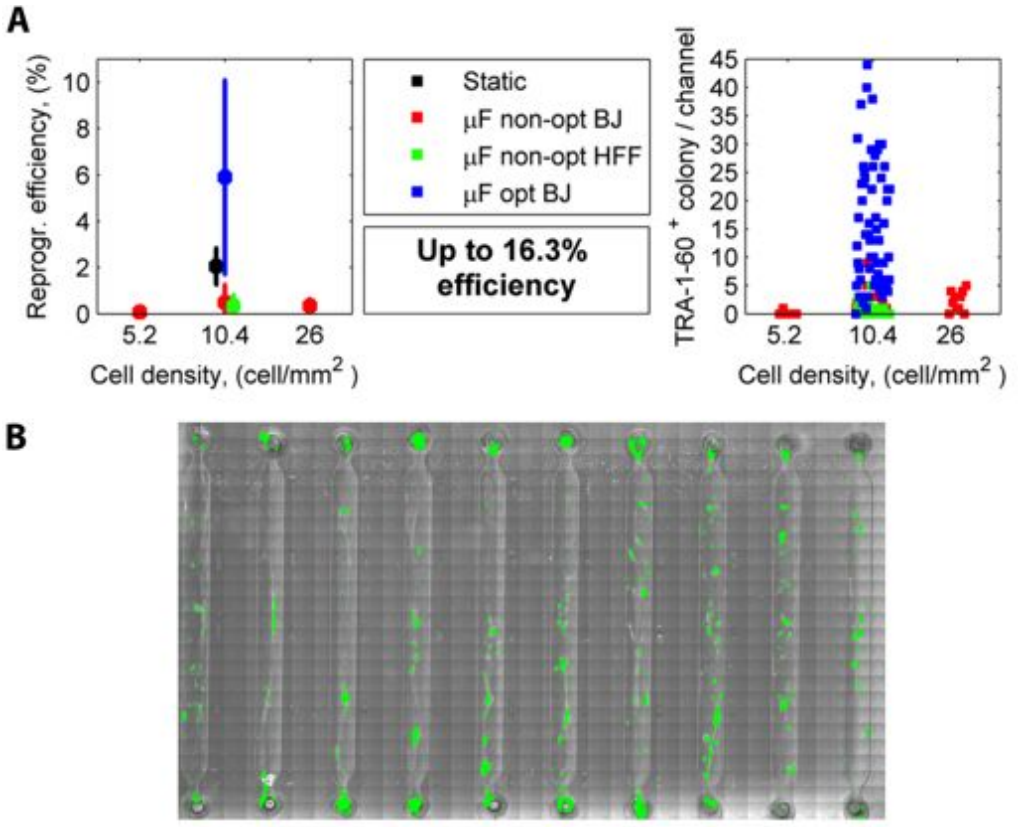

Figure 4.6.1 – Enhanced reprogramming efficiency in microfluidics. (A) Favoring the cell interaction with the glass against the PDMS surfaces, transfection efficiency was enhanced (blue data) and reprogramming yieled up to 44 hiPSC colonies per channel, that equals to a 16.3% (more than 5 times higher than the standard protocol). (B) Constrast phase image of a fixed chip after reprogramming. Overimposed image of immunofluorescence analysis for NANOG positive hiPSC (bynary image in green).

travel side walls and transfer on the roof where mild conditions and low transfection efficiency can be found. This resulted in a partial and continuous loss of cells that limited sustained delivery on cell at the bottom.

Substrate optimization/high reprogramming effciency. At this stage, we reduced the concentration of protein for the long-term functionalization in order to reduce the adsorption on PDMS and make this surface less appealable for cell growth. As a remarkable result, we generated up to 44 single colonies in a single channel, equivalent to a 16.3% of reprogramming efficiency (Figure 4.6.1). This efficiency was never obtained with the induction of only Yamanaka-like factors and is more than 5-times higher than commercially proposed values (up to 3%).

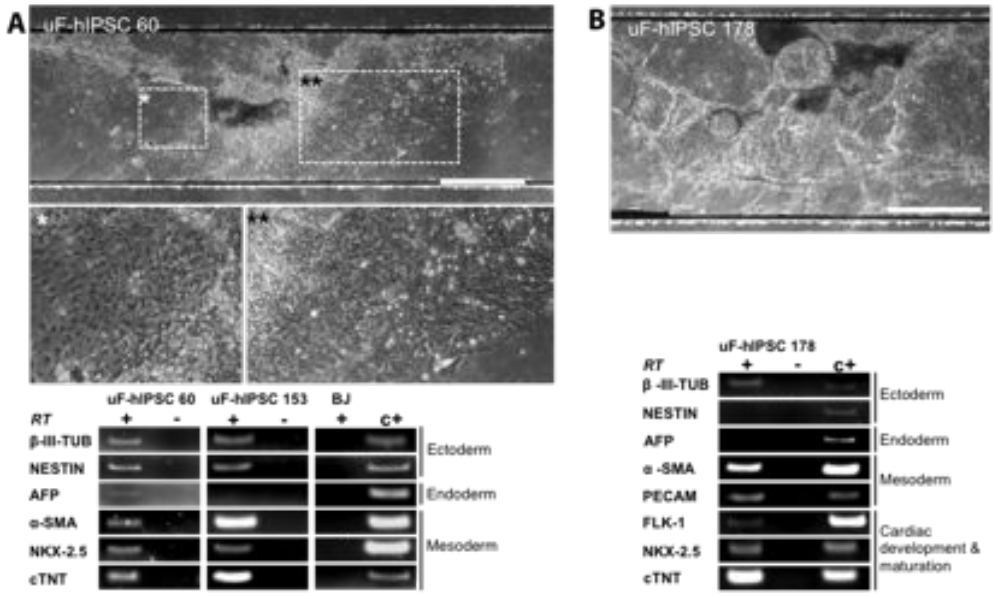

Figure 4.6.2 – One-step derivation of adult-like cells from patient's cells. (A) Random differentiation of fresh derived hiPSC with aspecific media and protocols. Different cell types with various morphologies are present in the field. At the bottom, biomolecular RT-PCR analysis revealed the presence of markers of the three germ layers, indicating the possibility to generate the entire cellular set of the adult body. (B) Specific cardiac differntiation at 15 days from the end of reprogramming. Dark and bright culture areas enriched in cardiomyocyte cells. RT-PCR reveald prominent differentiation in the cardiogenic pathway with the presence of FLK-1, NKX2.5, cTNT characteristic markers.

Differentiation. After canonical 16 days of daily transfection we cultured emerging clones for additional 3 days in order to growth against non reprogrammed cells. Applying differentiation procedures, hiPSC were able to generate the three germ layer in aspecific medium and matured in functional cardiac cells expressing troponin-T using a specific protocol (Figure 4.6.2).

4.7 Conclusions

Advantages in substrate development and long-term microfluidic cell culture were fundamental to approach the reprogramming of human cells at the microscale. The transition from viral vectors to mmRNA offered a safe and defined approach to deliver Yamanaka-like factors without the need of forced removal of exogenous material with a subclonal expansion.

To describe at best the work performed to obtain such result, a list of key features that has been implemented can be listed:

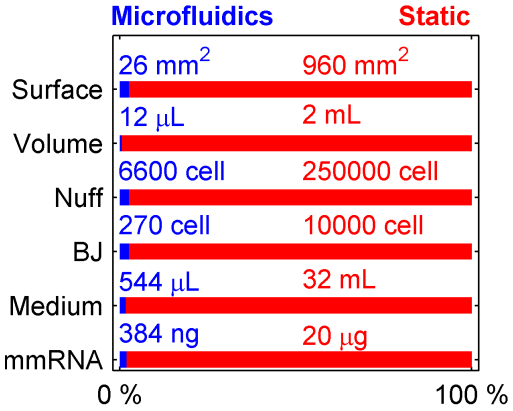

Figure 4.7.1 – Scale down of minimum requirements in microfludics. Device area, cells and reagents needed have been significantly reduced compared to standard procedures.

- defined substrates,
- robust microfluidics,
- clinical-grade mmRNA,
- patient's non-invasive isolation,
- feeder-free reprogramming,
- scale-down of minimum requirements (Figure 4.7.1),
- increased efficiency,
- one-step reprogramming-programming process,
- fulfilling integration.

Thanks to these a charateristic, our platform has the potential to serve as new tool for the extended reprogramming of cells derived from hundreds of patients. hiPSC derived at a population scale can serve the study of both common and rare diseases. Moreover, the cost reduction of the entire process (Figure 4.7.1) can attract the pharmaceutical industry in discovery and developing drugs with more cost effective procedures and avoid non fully predictive animal models before the clinical trials.

Chapter 5

Role of substrates on reprogramming and hPSC maintenance.

5.1 Mechanotransduction in reprogramming

In chapter 2, the interplay between cells and their substrate was described. Hydrogels were optimized for large studies, clinical applications and biosensoring. Moreover, in chapter 4, substrates and microfluidics were combined for the realization of a breakthrough reprogramming approach at the microscale.

When the research focus on the study or the production of large quantities of cells larger systems can be adopter such as the one realized in section 2.5. Since we are now able to produce hydrogel on large culture vessels the mechanical role of the matrix in the reprogramming process can be investigated at the larger scale. It have been evidenced that substrates can have a role in the reprogramming process[24] and may help in producing large quantities of hiPSC with a reduction of factors, transfections and time to complete the reprogramming. A matrix with soft stiffness has been demonstrated to sustain a pluripotent phenotype in mouse embryonic stem cells without the use of factors normally required on conventional culture system [22].

Since this research is at the beginning we report in this chapter the early results

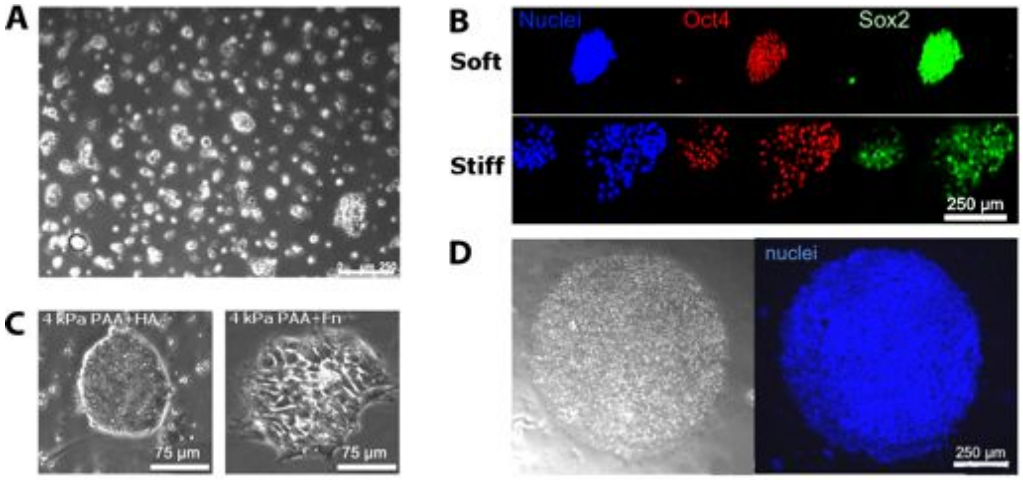

Figure 5.1.1 – Pluripotency and substrate stiffness. (A-C,E) Human PSC lines are cultured on hydrogels with various stiffness or compositions. (A) Functionalizzation of poly-acrylamide hydrogel allow proper attachment of PSCs. (B) Reducing the substrate stiffness (˜1 kPa), PSCs grow in more compact colonies compared to stiff substrates. (C) Poly-acrylamide hydrogel with same nominal stiffness are functionalized with hyaluronic acid (left) and fibronectin (right). HA leads to significantly more dense cell colonies optimal for PSCs maintenance. (D) Hydrogels of pure methacrylated hyaluronic acid allow isotropic grow of hPSC.

on mechanotransduction implications of pluripotency. Before performing a reprogramming on substrates, we investigated the main differences between adult cells and hPSC on soft substrates.

Mechanotransduction in hPSC. In order to assess any implication of mechanopathways on hPSC, we first seeded our hiPSC and hES on hydrogel at various stiffnesses (0.7-80 kPa) (Figure 5.1.1A). We did not not recognized any preferential stiffness for hPSC to maintain the expression of pluripotency marker OCT-4 in the presence of a poly-acrylamide substrate, a Matrigel coating and standard culture media for hPSC (Figure 5.1.1B). In each case, OCT-4 and SOX2 were expressed in the large majority (>95%) of cells after 6 days. Similar data were confirmed by Schaffer and colleagues [69]. However, within each colony, cell density was lower on stiff hydrogels (80 kPa) compared to softer ones (0.7 kPa) (Figure 5.1.1B). As evidenced in Chapter 1, compact colonies with defined edges are a key characteristics of hPSC.

Matrigel (BD biosciences) is an extracellular matrix mixture extracted from mice and therefore it is not defined and subjected to variability. Thus,we wanted to

understand the role of the ECM coating comparing the morphology of hPSC cultured on an poly-acrylamide substrate at 4 kPa. When we functionalized the gel with hyaluronic acid described in Chapter 2, we obtained compact colonies compared to the one cultured on fibronectin. Not surprisingly, when we adopted a hydrogel based on pure methacrylated hyaluronic acid used in a 3D application (2.6) with a *bona fide* stiffness of <10 kPa, we obtained well defined circular colonies with compact cells. This result recapitulate the previous findings present in literature [98, 123–125].

Biochemical composition of the ECM matrix is thus a key player of hPSC shaping. Despite matrix stiffness has not evidenced a role in the expression of characteristic pluripotency markers, it affects significantly the cell density within the colony. Since a tight contact of hPSC is essential for theit survival an expansion as pluripotent cells, matrix stiffness can have a role in pluripotency maintenance and reprogramming process. As reported in Appendix B and A, higher cell density also affects the single cell shape and its iternal architecture, leading to mechanotransduction pathways that can trigger certain biological functions normally repressed.

Mechanotransduction in reprogramming. It has been recently shown in a recent publicatio that substrate topology can affect the expression of certain DNA-binding proteins (histones) through mechanotransduction pathways [8]. Histone activity and the accessibilty of certain regions of the DNA are known fundamental barriers in the reprogramming process [51, 52, 155].

Since we had the evidence that topology, stiffness and chemical composition of the substrate can act in a common circuit acting on internal cellular components [156, 157], we wanted to perform a first experiment by reprogramming adult fibroblasts.

As shown in Figure 5.1.2A on the left, we recapitulated the mechano-associated transition in cell shape of adult fibroblast comparing the shape of adapted single-cell hES cultured in standard conditions. The normalized ratio between cell perimeter and area (circularity) was used as a shape descriptor of cells. Fibroblasts cultured on ∼1 kPa poly-acrylamide hydrogels evidenced a circularity similar to hPSC. We next performed a reprogramming experiment using poly-acrylamide hydrogels developed in standard poly-styrene culture vessels 2.5. We used a 1 kPa hydrogel, a 12 kPa (as a stiffness control) and murine fibroblasts (MEF) as standard support for

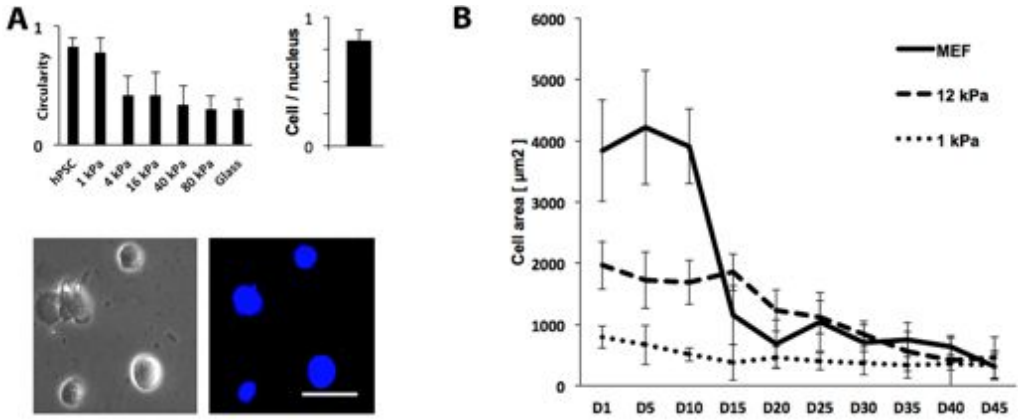

Figure 5.1.2 – Reprogramming and substrate stiffness. (A) BJ fibroblast cells progressively round on softer hydrogels (left image). Circularity is $4\pi(\pi r^2)/(2\pi r)^2$ with r the cell radius. Differentiated fibroblast on 1 kPa have a circularity similar to hPSC. Also, fibroblast evidenced an high cell area / nucleos area ratio, similar to hPSC. Single cells are presented at the bottom with nuclei stained in blue with Hoechst 33342. (B) BJ fibroblasts were infected with a Sendai virus to promote the reprogramming process and transferred either on conventional dishes (MEF) or on poly-acrylmaide hydrogels at different stiffness (1 and 12 kPa). Cell area was used as a shape descriptor and analyzed for 45 days. After 10 days, BJs on MEF undergo a remarked reduction in cell area, which is readily observable during the first days of culture on 1 kPa substrates.

reprogramming experiments with viral vectors. Yamanaka's factors were delivered using the commercially available Sendai virus. Cells on softer hydrogel evidenced high circularity and reduced cell area, with a prominent high ratio between cell area and nucleus area (Figure 5.1.2A-B). In particular cell area followed a common trend for the three samples (Figure 5.1.2B). As expected in conventional reprogramming, cells undergo a phenotypical and morphological transition (Mesenchymal-Epithelial Transition, MET) with rounded and smaller cells. Ten days after the transfection, cell reduce significantly their ashesion area. Cell cultured on 12 kPa hydrogels were less spread from the beginning and followed the same trend on MEF during the 45 days of reprogramming. Cells cultured on 1 kPa hydrogel maintained a reduce and round adhesion area throughout the whole experiment.

Although no hiPSCs were generated with soft hydrogels, it must be considered that the reprogramming on MEF was not efficient, generating only 1 single stable hiPSC clone (see also 4.2.1). Therfore, at this stage, we can not exclude that substrates may enhance the reprogramming efficiency. A recent report has evidenced that soft substrates can support the reprogramming process initiated by viral vectors [23].

Moreover, the maintenance of a high growth rate of adult stem cells on softer hydrogels (∼1 kPa or below) is still an open issue due to the inteference of newly discovered mechanotranduction pathways (Appendix A, B).

These evidences indicate that soft hydrogel can readily promote a cell shape that is required to complete the reprogramming process in standard conditions. Further experiments have been planned to reveal new insights on the mechano-associated reprogramming process. In order to improve the statistical analysis and experimental throughput, we will adopt the mmRNA reprogramming technology seen in Chapter 4.

5.2 Conclusions

Mechanotransduction behaviors have been extensively proved on adult cells especially when focusing on their differentiation and maturation process.

The role of mechano-associated phenomena in controlling hPSC biology is still poorly understood. In this chapter we have described the early studies we performed to understand the role of substrate mechanics on hPSC and especially on the reprogramming process. As evidendeced in Appendix A and B, since linage specific cells can activate mechanotransduction processes, we wanted to dissect the role of substrates in hPSC maintenance. Although ECM composition clearly proved to guide hPSC phenotype, substrate stiffness had an impact at least on hPSC conformation and colony organization. When we looked at the transition from an adult phenotype towards a pluripotent target on different substrates, cell morphological descriptors evidenced a common pattern compared to conventional reprogramming substrates. In particular, softer hydrogel can istantly guide single-cells under reprogramming to a defitive cell shape transition mimicking a late strandard reprogramming phase.

Since soft gels induce a mechano-responsive behavior reducing the replication activity, cells under reprogramming with a reduced hPSC-like shape will be stimulated in order to elicit an important reorganization of DNA activity in the early replication stages.

Chapter 6

Perspectives for a human body on a chip

The engineering of substrates for biological applications (Chapter 2) introduced to new insights of biological pathways and offered new tools for the *in vitro* and *in vivo* studies and applications. The development of cell culture in microfluidic channels (Chapter 3) has revealed that a comprehensive reorganization of current culture protocols is necessary in order to take an advantage on the phenomena occurring at the microscale. In order to accomplish sofisticated procedures for the reprogramming process at the microscale, a deep integration of the achievements obtained in substrate development and microfluidic cell cultures was fundamental.

Various groups are proposing micro-engineered systems that allow the realization of challenging *in vitro* tissues and organoids [158]. Due to the extreme complexity in reproducing organs on a chip, multidisciplinary knowledge and integration in biology, chemistry, physics and engineering is indispensable.

In this perspective, we aim at developing *in vitro* tools for a better description of biological phenomena and for the realization of biomimetic environments for functional physiological and pathological tissues and organoids.

In the following paragraph, we propose a proof on concept that integrates some of the techniques developed in this thesis for the development of an analytical device in diabetes studies. Muscles are a major tissue implicated in diabetes[115] and healthy and disease tissues can respond in different ways to physiological stimuli or drugs.

The generation of highly differentiated muscle fibers in a microfluidic chip can result in a platform with high temporal and spatial resolution for stimuli delivery. Since we demonstrated that optimal myotube differentiation occurs on aligned cell patterns [108], it is crucial to transfer topological feautures in finalized microfluidic platfrorms.

Here we propose an effective and simple method to promote the differentiation of muscle precursors in patterned areas within a microfluidic culture chamber.

In situ tolopological control of microfluidic environments. When cells are chaotically distributed, overall population is normally investigated to individuate a biological behavior and it can be extremely difficult to dissect different phenomena occurring in various sub-populations.

Topological control of cell cultures reported in section 2.7 can offer advantages to screen the biodiversity over a common cell line and distill biological analysis from biased phenomena. Open systems such as a glass coverslip or hydrogel film offer an easy access to physically print the surface with adhesive patterns or introduce repellent features. Sealed systems such microfluidic chips only allow an indirect access to the main chamber through inlet and outlet ports, making impossible any selective geometrical treatment.

Thanks to the optical transparency and limited thickness of of the platform it can be possible to selectively photo-activate the surface with UV-light and a photomask. Adjusting the dose of UV, we were able to selectively attach linear poly-acrylamide chains on the silanized glass. Cells adhered on non-exposed areas presenting the acryl terminus of the silane, eventually coated with ECM proteins.

Since defined geometries can alter cell behavior, we analyzed the efficacy of micropatterned aligned lanes in promoting myogenesis. When myoblasts were seeded in micropatterned chips, they distributed and adhered in non-repellent areas. When they reached confluence after few days, packed cells aligned along the major axis of each lane and differentiated in mature myotubes.

These system are being used to analyzed the expression profiles of engineered myotubes subjected to conditioned media from healthy and diabetic patients.

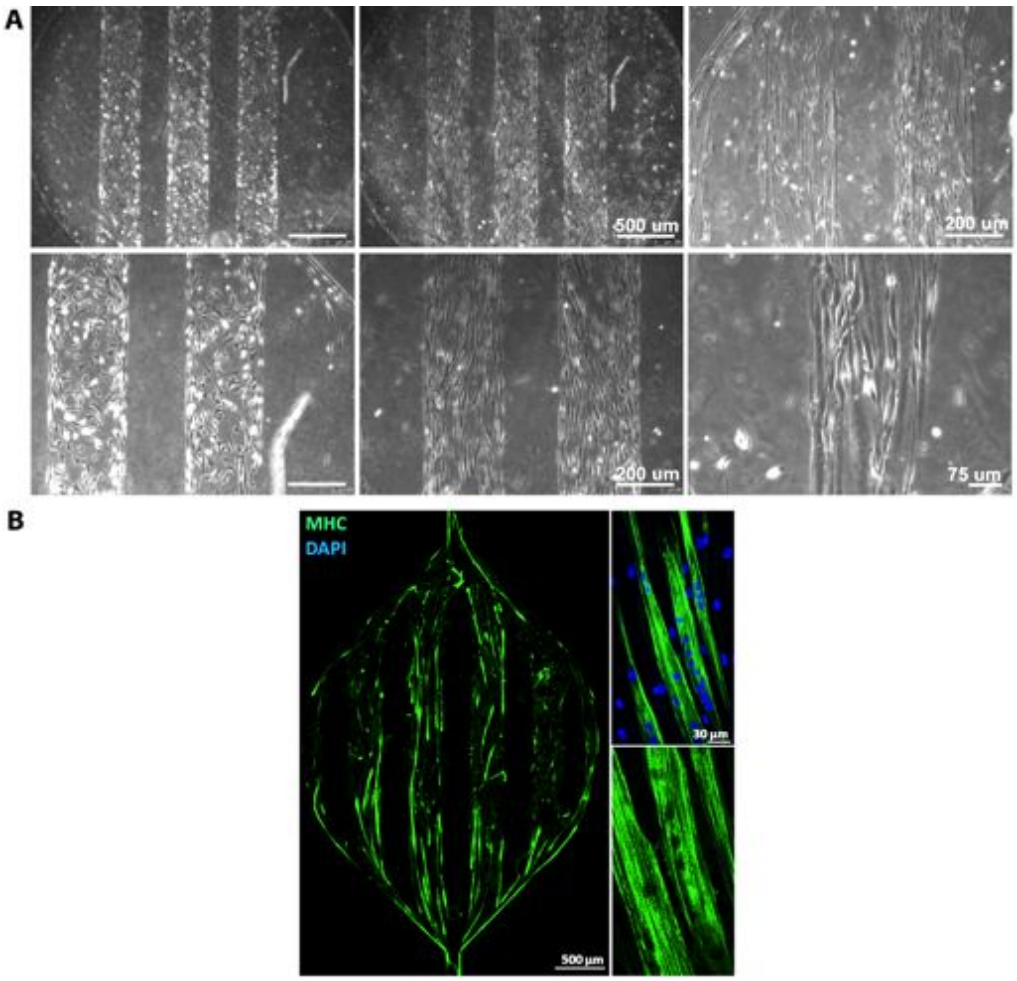

Figure 6.0.1 – Cell patterns inside a microfluidic chip. (A) Adhesive/repellent patterns were obtained through direct patterning technique reported in 2.7. Myoblast cells adhere on 300 µm wide lanes and progressively align along the major axis and differentiate in myotubes. (B) Each channel can be fixed and stained to perform assays. Here it is reported the expression of myosin protein (MHC), a major functional cytoskeletal component of the muscle. The immunofluorescent assay (left magnifications) reveals a defined sarcomeric architecture with repeated bands of MHC.

Conclusions

This work focused on the development of a reprogramming platform for the high-throughput derivation of human induced pluripotent stem cells (hiPSC).

Since hiPSC are highly sensitive cells and their derivation is subject to various intrinsic and extrinsic factors, the regulation of internal pathways and cell behavior, and the tight control of environmental culture conditions are crucial aspects. Substrates and microfluidic technology were used in order to provide a microscaled integrated solution for the reprogramming process.

Substrate development focused on the realization of cell culture supports with tunable properties such as stiffness, chemistry and topology. First, we optimized current available protocols to produce biocompatible hydrogels based on poly-acrylamide with a tunable stiffness mimicking the physiological range of *in vivo* tissues. Consistent large-scale experiments with over 5000 used samples served for the identification of new cell behaviors associated with the mechanical properties of the culture substrate. By changing the stiffness of the hydrogel, cell can dramatically change its shape and internal architecture. Crucial proliferation-associated factors YAP/TAZ were either blocked or activated overriding previously known biochemical pathways. The same high-throughput technology was applied to a subsequent study in order to investigate the mechano-associated players that transduce the environmental mechanical cues into internal biochemical regulations and cell behaviors. Structural and enzymatic mediators were found to be responsible of the mechanical checkpoint of YAP/TAZ. Altogether, these studies evidenced a fundamental role of the extracellular matrix in determining the cell behavior and fate.

Poly-acrylamide hydrogels have also been used to realized biosensors within a soft compliant cell culture substrate optimal for muscle cell differentiation. Chemical

functionalization of poly-styrene cell culture vessels was performed to integrate soft hydrogels for large-scale studies and analysis.

Biodegradable hydrogels based on hyaluronic acid were developed in order to provide a biomimetic environment for *in vivo* applications. Micro-engineered bundles of aligned muscle fibers were generated *in vitro* on functionalized gelatin surfaces. The hydrogel construct was integrated in ablated mice muscles to evaluate its regeneration capability. Although a faster degradation was necessary to allow the full viability and integration of engineered fibers, muscle regeneration was elicited by the biodegradable hydrogel construct and further improvements are being applied.

The knowledge on substrate development and control of cell behavior were transferred on microfluidic cell culture environments. First, cell cultures on standard supports were integrated in an *ad hoc* microfluidic platform to prove in our hand the potential of an efficient delivery of biological species inside cells. Second, cell cultures were directly integrated in microfluidic channels providing a stable adhesive surface treatment for long-term cell cultures.

In order to provide also a favorable soluble environment, a liquid handling management software was realized to allow automated delivery of culture medium over cells. The study of an optimal strategy to perform robust long-term microfluidic cultures revealed that a periodic fast pulse of fresh media followed by a prolonged pause allows the homogeneous culture of different cell types with correct phenotype.

Having developed a substrate-integrated microfluidic technology for long-term cell cultures, we delivered on human cells modified messenger RNAs (mmRNA) translating for the reprogramming factors. The delivery of a mRNA encoding a fluorescent protein revealed that microfluidic can efficiently introduce exogenous material in cells to be reprogrammed.

hiPSC were obtained at the microscale from different human biopsies and their characterization revealed the full potential to derive all somatic cell type present in our body. Since our platform dramatically reduces the minimum requirements for a single reprogramming, fresh hiPSC can be directly and effectively differentiated in a one-step process towards functional adult cell types valuable to perform *in vitro* screenings on human tissues. This results open new research perspectives extendible

at a hundreds of people. New drugs could be developed with a cost-effective approach for both common and rare diseases.

Concluding, the research on substrates and microfluidic cell culture technology led to the definition of an integrated platform to control the behavior of adult human cells. Passing through the efficient generation of hiPSC at the microscale, we generated new functional cell types in a one-step process usable for high-value human assays at the population scale.

Bibliography

[1] K. Takahashi and S. Yamanaka. "Induction of Pluripotent Stem Cells from Mouse Embryonic and Adult Fibroblast Cultures by Defined Factors". In: *Cell* 126 (2006), pp. 663–676.

[2] Kazutoshi Takahashi et al. "Induction of pluripotent stem cells from adult human fibroblasts by defined factors". eng. In: *Cell* 131.5 (Nov. 2007). PMID: 18035408, pp. 861–872.

[3] M. Wernig et al. "In vitro reporgramming of fibroblasts into a pluripotent ES-cell-like state". In: *Nature* 448.19 (2007), pp. 317–324.

[4] Saeed Abbasalizadeh and Hossein Baharvand. "Technological progress and challenges towards cGMP manufacturing of human pluripotent stem cells based therapeutic products for allogeneic and autologous cell therapies". In: *Biotechnology Advances* 31.8 (2013), pp. 1600–1623.

[5] Bruce Alberts et al. *Molecular Biology of the Cell*. 2002.

[6] Daniel D. De Carvalho, Jueng Soo You, and Peter A. Jones. "DNA methylation and cellular reprogramming". In: *Trends in Cell Biology* 20.10 (Oct. 2010), pp. 609–617.

[7] Zhonghui Zhang et al. "Efficient Generation of Fully Reprogrammed Human iPS Cells via Polycistronic Retroviral Vector and a New Cocktail of Chemical Compounds". In: *PLoS ONE* 6.10 (Oct. 2011), e26592.

[8] Timothy L. Downing et al. "Biophysical regulation of epigenetic state and cell reprogramming". In: *Nature Materials* (Oct. 2013).

[9] Pankaj K Mandal and Derrick J Rossi. "Reprogramming human fibroblasts to pluripotency using modified mRNA". In: *Nature Protocols* 8.3 (Feb. 2013), pp. 568–582.

[10] E.P. Papapetrou et al. "Stoichiometric and temporal requirements of Oct4, Sox2, Klf4, and c-Myc expression for efficient human iPSC induction and differentiation". In: *Proceedings of the National Academy of Sciences* 106.31 (2009), pp. 12759–12764.

[11] X. Gaeta, Y. Xie, and W. E. Lowry. "Sequential addition of reprogramming factors improves efficiency". en. In: *Nature Cell Biology* 15.7 (July 2013), pp. 725–727.

[12] "A chemical approach to stem-cell biology and regenerative medicine". In: *Nature* 453.7193 (2008), pp. 338–44.

[13] Aniruddh Solanki and Ki Bum Lee. "A Step Closer to Complete Chemical Reprogramming for Generating iPS Cells". en. In: *ChemBioChem* 11.6 (2010), pp. 755–757.

[14] Luigi Warren et al. "Feeder-Free Derivation of Human Induced Pluripotent Stem Cells with Messenger RNA". In: *Scientific Reports* 2 (Sept. 2012). PMID: 22984641 PMCID: PMC3442198.

[15] J. Hanna et al. "Direct cell reprogramming is a stochastic process amenable to acceleration". In: *Nature* 462.3 (2009), pp. 595–603.

[16] Z.D. Smith et al. "Dynamic single-cell imaging of direct reprogramming reveals an early specifying event". In: *Nature biotechnology* 28.5 (2010), pp. 521–526.

[17] Yoach Rais et al. "Deterministic direct reprogramming of somatic cells to pluripotency". In: *Nature* 502.7469 (Sept. 2013), pp. 65–70.

[18] Matthias P. Lutolf, Penney M. Gilbert, and Helen M. Blau. "Designing materials to direct stem-cell fate". en. In: *Nature* 462.7272 (Nov. 2009), pp. 433–441.

[19] A. J. Engler. "Myotubes differentiate optimally on substrates with tissue-like stiffness: pathological implications for soft or stiff microenvironments". In: *The Journal of Cell Biology* 166.6 (Sept. 2004), pp. 877–887.

[20] Matthew Raab et al. "Crawling from soft to stiff matrix polarizes the cytoskeleton and phosphoregulates myosin-II heavy chain". en. In: *The Journal of Cell Biology* 199.4 (Dec. 2012). PMID: 23128239, pp. 669–683.

[21] C. S. Chen. "Geometric Control of Cell Life and Death". In: *Science* 276.5317 (May 1997), pp. 1425–1428.

[22] Farhan Chowdhury et al. "Soft substrates promote homogeneous self-renewal of embryonic stem cells via downregulating cell-matrix tractions". eng. In: *PloS one* 5.12 (2010). PMID: 21179449, e15655.

[23] Sayaka Higuchi et al. "Culturing of mouse and human cells on soft substrates promote the expression of stem cell markers". In: *Journal of Bioscience and Bioengineering* ().

[24] Jiao Jiao et al. "Promoting Reprogramming by FGF2 Reveals that the Extracellular Matrix Is a Barrier for Reprogramming Fibroblasts to Pluripotency". en. In: *STEM CELLS* 31.4 (2013), pp. 729–740.

[25] Edmond W K Young and David J Beebe. "Fundamentals of microfluidic cell culture in controlled microenvironments". In: *Chem Soc Rev* 39.3 (2010), pp. 1036–48.

[26] *Centre for Commercialization of Regenerative Medicine*. Jan. 2014. URL: `www.ccrm.ca` (visited on 2014).

[27] Bahram Valamehr et al. "A novel platform to enable the high-throughput derivation and characterization of feeder-free human iPSCs". In: *Scientific Reports* 2 (Jan. 2012).

[28] Ulf Tiemann et al. "Optimal reprogramming factor stoichiometry increases colony numbers and affects molecular characteristics of murine induced pluripotent stem cells". In: *Cytometry A* 79.6 (2011), pp. 426–35.

[29] Bryce W Carey et al. “Reprogramming factor stoichiometry influences the epigenetic state and biological properties of induced pluripotent stem cells”. In: *Cell stem cell* 9.6 (Dec. 2, 2011). PMID: 22136932, pp. 588–598.

[30] Thorold W. Theunissen et al. “Nanog overcomes reprogramming barriers and induces pluripotency in minimal conditions”. In: *Current Biology* 21.1 (2011), pp. 65–71.

[31] Ludovic Vallier et al. “Activin/Nodal signalling maintains pluripotency by controlling Nanog expression”. eng. In: *Development (Cambridge, England)* 136.8 (Apr. 2009). PMID: 19279133, pp. 1339–1349.

[32] Matthias Stadtfeld and Konrad Hochedlinger. “Induced pluripotency: history, mechanisms, and applications”. In: *Genes & development* 24.20 (Oct. 15, 2010). PMID: 20952534 PMCID: PMC2956203, pp. 2239–2263.

[33] Jieun Lee et al. “Activation of innate immunity is required for efficient nuclear reprogramming”. In: *Cell* 151.3 (Oct. 26, 2012). PMID: 23101625 PMCID: PMC3506423, pp. 547–558.

[34] Sergio Menendez, Suzanne Camus, and Juan Carlos Izpisua Belmonte. “p53: guardian of reprogramming”. In: *Cell Cycle* 9.19 (2010), pp. 3917–3921.

[35] Han Qin et al. “Transcriptional analysis of pluripotency reveals the Hippo pathway as a barrier to reprogramming”. In: *Human molecular genetics* 21.9 (2012), pp. 2054–2067.

[36] Ting Zhou et al. “Generation of human induced pluripotent stem cells from urine samples”. In: *Nature Protocols* 7.12 (Nov. 2012), pp. 2080–2089.

[37] Matthias Stadtfeld et al. “Induced Pluripotent Stem Cells Generated Without Viral Integration”. In: *Science* 322.5903 (July 11, 2008). PMID: 18818365, pp. 945–949.

[38] Hiroshi Ban et al. “Efficient generation of transgene-free human induced pluripotent stem cells (iPSCs) by temperature-sensitive Sendai virus vectors”. In: *Proceedings of the National Academy of Sciences of the United States of America* 108.34 (Aug. 23, 2011). PMID: 21821793 PMCID: PMC3161531, pp. 14234–14239.

[39] S. M. Choi et al. “Reprogramming of EBV-immortalized B-lymphocyte cell lines into induced pluripotent stem cells”. In: *Blood* 118.7 (May 31, 2011), pp. 1801–1805.

[40] Hongyan Zhou et al. “Generation of Induced Pluripotent Stem Cells Using Recombinant Proteins”. In: *Cell Stem Cell* 4.5 (May 2009), pp. 381–384.

[41] Yang Yang et al. “Proteins Reprogramming: Present and Future”. In: *The Scientific World Journal* 2012 (Nov. 22, 2012).

[42] Stemgent. *Stemgent mRNA reprogragramming protocol available at Stemgent.com.*

[43] Pingping Hou et al. “Pluripotent Stem Cells Induced from Mouse Somatic Cells by Small-Molecule Compounds”. en. In: *Science* (July 2013). PMID: 23868920.

[44] Wenyu Zhou et al. “HIF1-alpha induced switch from bivalent to exclusively glycolytic metabolism during ESC-to-EpiSC/hESC transition”. eng. In: *The EMBO journal* 31.9 (May 2012). PMID: 22446391, pp. 2103–2116.

[45] Brooke N. Mason, Joseph P. Califano, and Cynthia A. Reinhart-King. “Matrix Stiffness: A Regulator of Cellular Behavior and Tissue Formation”. In: *Engineering Biomaterials for Regenerative Medicine*. Ed. by Sujata K. Bhatia. New York, NY: Springer New York, 2012, pp. 19–37.

[46] Kshitiz et al. “Matrix rigidity controls endothelial differentiation and morphogenesis of cardiac precursors”. eng. In: *Science signaling* 5.227 (June 2012). PMID: 22669846, ra41.

[47] Harald C Ott et al. “Perfusion-decellularized matrix: using nature’s platform to engineer a bioartificial heart”. In: *Nature Medicine* 14.2 (Jan. 2008), pp. 213–221.

[48] Robert W. Tilghman et al. “Matrix Rigidity Regulates Cancer Cell Growth and Cellular Phenotype”. In: *PLoS ONE* 5.9 (Sept. 2010), e12905.

[49] Adam Engler et al. “Substrate compliance versus ligand density in cell on gel responses”. In: *Biophysical journal* 86.1 (2004), pp. 617–628.

[50] Dennis E. Discher, Paul Janmey, and Yu-li Wang. "Tissue cells feel and respond to the stiffness of their substrate". In: *Science* 310.5751 (2005), pp. 1139–1143.

[51] Diana E. Jaalouk and Jan Lammerding. "Mechanotransduction gone awry". In: *Nature Reviews Molecular Cell Biology* 10.1 (Jan. 2009), pp. 63–73.

[52] Ning Wang, Jessica D. Tytell, and Donald E. Ingber. "Mechanotransduction at a distance: mechanically coupling the extracellular matrix with the nucleus". In: *Nature Reviews Molecular Cell Biology* 10.1 (Jan. 2009), pp. 75–82.

[53] J. Fu and et al. "Mechanical regulation of cell function with geometrically modulated elastomeric substrates". In: *Nature* (2010).

[54] Francesco D'Angelo et al. "Mechanotransduction: Tuning Stem Cells Fate". In: *Journal of Functional Biomaterials* 2.4 (June 2011), pp. 67–87.

[55] Wolfgang H. Goldmann. "Mechanotransduction and focal adhesions". In: *Cell Biology International* 36.7 (July 2012), pp. 649–652.

[56] Anant Chopra et al. "Augmentation of integrin-mediated mechanotransduction by hyaluronic acid". In: *Biomaterials* 35.1 (Jan. 2014), pp. 71–82.

[57] Benjamin Kim Kiat Teo et al. "Nanotopography Modulates Mechanotransduction of Stem Cells and Induces Differentiation through Focal Adhesion Kinase". In: *ACS Nano* 7.6 (June 2013), pp. 4785–4798.

[58] Kai Lu, Tong Cao, and Richard Gordon. "A cell state splitter and differentiation wave working-model for embryonic stem cell development and somatic cell epigenetic reprogramming". In: *Biosystems* 109.3 (Sept. 2012), pp. 390–396.

[59] Shyam B. Khatau et al. "The Differential Formation of the LINC-Mediated Perinuclear Actin Cap in Pluripotent and Somatic Cells". In: *PLoS ONE* 7.5 (May 2012), e36689.

[60] Kyle E. Hammerick et al. "Elastic Properties of Induced Pluripotent Stem Cells". In: *Tissue Engineering. Part A* 17.3-4 (Feb. 2011). PMID: 20807017 PMCID: PMC3052278, pp. 495–502.

[61] A. Pillarisetti et al. "Mechanical characterization of mouse embryonic stem cells". In: *Engineering in Medicine and Biology Society, 2009. EMBC 2009. Annual International Conference of the IEEE*. Sept. 2009, pp. 1176 –1179.

[62] Anand Pillarisetti et al. "Mechanical phenotyping of mouse embryonic stem cells: increase in stiffness with differentiation". In: *Cellular reprogramming* 13.4 (Aug. 2011). PMID: 21728815, pp. 371–380.

[63] Robert Kiss et al. "Elasticity of human embryonic stem cells as determined by atomic force microscopy". In: *Journal of biomechanical engineering* 133.10 (Oct. 2011). PMID: 22070334, p. 101009.

[64] Brian R. Daniels et al. "Differences in the Microrheology of Human Embryonic Stem Cells and Human Induced Pluripotent Stem Cells". In: *Biophysical Journal* 99.11 (Dec. 2010). PMID: 21112280 PMCID: PMC2998615, pp. 3563–3570.

[65] Ying J Li et al. "Hydrogels as artificial matrices for human embryonic stem cell self-renewal". eng. In: *Journal of biomedical materials research. Part A* 79.1 (Oct. 2006). PMID: 16741988, pp. 1–5.

[66] Samira Musah et al. "Glycosaminoglycan-Binding Hydrogels Enable Mechanical Control of Human Pluripotent Stem Cell Self-Renewal". In: *ACS Nano* 6.11 (Nov. 2012), pp. 10168–10177.

[67] Yubing Sun et al. "Mechanics Regulates Fate Decisions of Human Embryonic Stem Cells". In: *PLoS ONE* 7.5 (May 2012), e37178.

[68] Laralynne M Przybyla and Joel Voldman. "Attenuation of extrinsic signaling reveals the importance of matrix remodeling on maintenance of embryonic stem cell self-renewal". In: *Proc Natl Acad Sci U S A* (2012).

[69] Albert J. Keung et al. "Soft microenvironments promote the early neurogenic differentiation but not self-renewal of human pluripotent stem cells". In: *Integrative Biology* 4.9 (2012), p. 1049.

[70] Dong Li et al. "Integrated biochemical and mechanical signals regulate multifaceted human embryonic stem cell functions". en. In: *The Journal of Cell Biology* 191.3 (Jan. 2010), pp. 631–644.

[71] Dong Li et al. “Role of mechanical factors in fate decisions of stem cells”. In: *Regenerative medicine* 6.2 (Mar. 2011). PMID: 21391856 PMCID: PMC3128460, pp. 229–240.

[72] Farhan Chowdhury et al. “Material properties of the cell dictate stress-induced spreading and differentiation in embryonic stem cells”. In: *Nature Materials* 9.1 (Oct. 2009), pp. 82–88.

[73] Yeh-Chuin Poh et al. “Embryonic Stem Cells Do Not Stiffen on Rigid Substrates”. In: *Biophysical Journal* 99.2 (July 2010), pp. L19–L21.

[74] Schaffer. “Engineering microenvironments to control stem cell fate and function”. In: *StemBook* (2008).

[75] Imbisaat Geti et al. “A Practical and Efficient Cellular Substrate for the Generation of Induced Pluripotent Stem Cells from Adults: Blood-Derived Endothelial Progenitor Cells”. en. In: *Stem Cells Translational Medicine* 1.12 (Jan. 2012). PMID: 23283547, pp. 855–865.

[76] Jonathan K. Earls, Sha Jin, and Kaiming Ye. “Mechanobiology of Human Pluripotent Stem Cells”. In: *Tissue Engineering Part B: Reviews* (2013).

[77] Jessamine Ng Lee, Cheolmin Park, and George M. Whitesides. “Solvent Compatibility of Poly(dimethylsiloxane)-Based Microfluidic Devices”. In: *Analitical Chemistry* 75 (2003), pp. 6544–6554.

[78] D. Xiao, T. Van Le, and M.J. Wirth. “Surface Modification of the Channels of Poly(dimethylsiloxane) Microfluidic Chips with Polyacrylamide for Fast Electrophoretic Separations of Proteins”. In: *Anal. Chem.* 76 (2004).

[79] W.C. Sung et al. “Functionalized 3D-Hydrogel Plugs Covalently Patterned Inside Hydrophilic Poly(dimethylsiloxane) Microchannels for Flow-Through Immunoassays”. In: *Anal. Chem.* (2009).

[80] Min-Hsien Wu, Song-Bin Huang, and Gwo-Bin Lee. “Microfluidic cell culture systems for drug research”. In: *Lab on a Chip* 10.8 (2010), pp. 939–56.

[81] Pavel Neuži et al. “Revisiting lab-on-a-chip technology for drug discovery”. en. In: *Nature Reviews Drug Discovery* 11.8 (Aug. 2012), pp. 620–632.

[82] Wei Gu et al. "Computerized microfluidic cell culture using elastomeric channels and Braille displays". In: *Proceedings of the National Academy of Sciences of the United States of America* 101.45 (2004), pp. 15861–15866.

[83] Paul J Hung et al. "Continuous perfusion microfluidic cell culture array for high-throughput cell-based assays". In: *Biotechnol Bioeng* 89.1 (2005), pp. 1–8.

[84] Hun Ju Yeon and Je-Kyun Park. "Microfluidic Cell Culture System for Cellular Analysis". In: *Biochip Journal* 1 (2007), pp. 17–27.

[85] Keil J. Regehr et al. "Biological implications of polydimethylsiloxane-based microfluidic cell culture". In: *Lab on a Chip* 9.15 (2009), p. 2132.

[86] Laralynne Przybyla and Joel Voldman. "Probing Embryonic Stem Cell Autocrine and Paracrine Signaling Using Microfluidics". In: *Annual Review of Analytical Chemistry* 5.1 (July 2012), pp. 293–315.

[87] Samuel P Forry and Laurie E Locascio. "On-chip CO2 control for microfluidic cell culture". In: *Lab on a Chip* 11.23 (2011), pp. 4041–6.

[88] Elisa Cimetta et al. "Microfluidic device generating stable concentration gradients for long term cell culture: application to Wnt3a regulation of beta-catenin signaling". eng. In: *Lab on a chip* 10.23 (Dec. 2010). PMID: 20936235, pp. 3277–3283.

[89] Anna Tourovskaia, Xavier Figueroa-Masot, and Albert Folch. "Differentiation-on-a-chip: a microfluidic platform for long-term cell culture studies". In: *Lab on a Chip* 5.1 (2005), pp. 14–9.

[90] Faisal Moledina et al. "Predictive microfluidic control of regulatory ligand trajectories in individual pluripotent cells". In: *Proc Natl Acad Sci U S A* 109.9 (2012), pp. 3264–9.

[91] Huaying Chen et al. "Microwell perfusion array for high-throughput, long-term imaging of clonal growth". In: *Biomicrofluidics* 5.4 (2011), pp. 44117–4411713.

[92] Wang Li LM et al. "Integrated Microdevice for Long-Term Automated Perfusion Culture without Shear Stress and Real-Time Electrochemical Monitoring of Cells". In: *Analytical chemistry* 83.24 (2011), pp. 9524–9530.

[93] Natanel Korin et al. "Periodic "flow-stop" perfusion microchannel bioreactors for mammalian and human embryonic stem cell long-term culture". In: *Biomedical Microdevices* 11.1 (Sept. 2008), pp. 87–94.

[94] Jamil El-Ali, Peter K Sorger, and Klavs F Jensen. "Cells on chips". eng. In: *Nature* 442.7101 (July 2006). PMID: 16871208, pp. 403–411.

[95] Sébastien Degot et al. "Improved Visualization and Quantitative Analysis of Drug Effects Using Micropatterned Cells". In: *Journal of Visualized Experiments* 46 (Dec. 2010).

[96] Ru Zang et al. "Cell-based assays in high-throughput screening for drug discovery". In: *Int. J. Biotechnol. for Wellness Industries* 1 (2012), pp. 31–51.

[97] Phillip E. Woolwine. "hiPSCs: Reprogramming towards cell-based therapies". In: (2013).

[98] "The effects of covalently immobilized hyaluronic acid substrates on the adhesion, expansion, and differentiation of embryonic stem cells for in vitro tissue engineering". In: *Biomaterials* 32.33 (Nov. 2011), pp. 8404–8415.

[99] Dennis E. Discher, David J. Mooney, and Peter W. Zandstra. "Growth Factors, Matrices, and Forces Combine and Control Stem Cells". en. In: *Science* 324.5935 (June 2009), pp. 1673–1677.

[100] AS Curtis et al. "Adhesion of cells to polystyrene surfaces." In: *The Journal of cell biology* 97.5 (1983), pp. 1500–1506.

[101] Stella H North et al. "Plasma-based surface modification of polystyrene microtiter plates for covalent immobilization of biomolecules". In: *ACS applied materials & interfaces* 2.10 (2010), pp. 2884–2891.

[102] Kevin S. Kolahi. "Effect of Substrate stiffness on early mouse embryo development". In: *PloS one* (2012).

[103] Eleonora Carletti, Antonella Motta, and Claudio Migliaresi. "Scaffolds for tissue engineering and 3D cell culture". In: *Methods in molecular biology (Clifton, N.J.)* 695 (2011). PMID: 21042963, pp. 17–39.

[104] Brahatheeswaran Dhandayuthapani et al. "Polymeric Scaffolds in Tissue Engineering Application: A Review". In: *International Journal of Polymer Science* 2011 (Sept. 11, 2011).

[105] Jeffrey G. Jacot, Andrew D. McCulloch, and Jeffrey H. Omens. "Substrate Stiffness Affects the Functional Maturation of Neonatal Rat Ventricular Myocytes". In: *Biophysical Journal* 95.7 (Oct. 2008), pp. 3479–3487.

[106] Andrew S Rowlands, Peter A George, and Justin J Cooper-White. "Directing osteogenic and myogenic differentiation of MSCs: interplay of stiffness and adhesive ligand presentation". In: *Am J Physiol Cell Physiol* 295.4 (2008), pp. C1037–44.

[107] Aleksandar Marinković et al. "Improved throughput traction microscopy reveals pivotal role for matrix stiffness in fibroblast contractility and TGF-beta responsiveness". en. In: *American Journal of Physiology - Lung Cellular and Molecular Physiology* 303.3 (Jan. 2012), pp. L169–L180.

[108] Susi Zatti et al. "Micropatterning topology on soft substrates affects myoblast proliferation and differentiation". eng. In: *Langmuir: the ACS journal of surfaces and colloids* 28.5 (Feb. 2012). PMID: 22217143, pp. 2718–2726.

[109] Ruth Freitag. *Synthetic polymers for biotechnology and medicine*. Landes Bioscience, 2003. 180 pp.

[110] Robert J. Pelham and Yu-li Wang. "Cell locomotion and focal adhesions are regulated by substrate flexibility". en. In: *Proceedings of the National Academy of Sciences* 94.25 (Sept. 1997). PMID: 9391082, pp. 13661–13665.

[111] JR Tse and AJ Engler. "Preparation of Hydrogel Substrates with Tunable Mechanical Properties". In: *Current Protocols in Cell Biology* 10.16 (2010), pp. 1–16.

[112] P. Moshayedi et al. “Mechanosensitivity of astrocytes on optimized polyacrylamide gels analyzed by quantitative morphometry”. In: *Journal of Physics: Condensed Matter* 22 (2010), p. 194114.

[113] Hans-Jürgen Butt, Brunero Cappella, and Michael Kappl. “Force measurements with the atomic force microscope: Technique, interpretation and applications”. In: *Surface Science Reports* 59.1-6 (Oct. 2005), pp. 1–152.

[114] Amnon Buxboim et al. “How deeply cells feel: methods for thin gels”. In: *Journal of Physics: Condensed Matter* 22.19 (May 2010), p. 194116.

[115] Ralph A. DeFronzo, Riccardd C. Bonadonna, and Eleuterio Ferrannini. “Pathogenesis of NIDDM: A Balanced Overview”. en. In: *Diabetes Care* 15.3 (Jan. 1992). PMID: 1532777, pp. 318–368.

[116] J. N. Coleman et al. “Percolation-dominated conductivity in a conjugated-polymer-carbon-nanotube composite”. In: *Physical Review B* 58.12 (Sept. 1998), R7492–R7495.

[117] Vesna Damljanovic, Christoffer Lagerholm, and Ken Jacobson. “Bulk and micropatterned conjugation of extracellular matrix proteins to characterized polyacrylamide substrates for cell mechanotransduction assays”. In: *BioTechniques* 39 (2005), pp. 847–851.

[118] Paul Menter. *Acrylamide Polymerization — A Practical Approach*. Tech. rep. Bio-Rad Laboratories, 2000.

[119] Elena Serena et al. “Soft substrates drive optimal differentiation of human healthy and dystrophic myotubes”. In: *Integrative Biology* 2.4 (2010), p. 193.

[120] Elena Serena et al. “Micro-Arrayed Human Embryonic Stem Cells-Derived Cardiomyocytes for In Vitro Functional Assay”. In: *PLoS ONE* 7.11 (Nov. 2012), e48483.

[121] Robert Stern. “Hyaluronan catabolism: a new metabolic pathway”. In: *European Journal of Cell Biology* 83.7 (2004), pp. 317–325.

[122] Xian Xu et al. “Hyaluronic acid-based hydrogels: from a natural polysaccharide to complex networks”. In: *Soft Matter* 8.12 (Feb. 29, 2012), pp. 3280–3294.

[123] Yongxing Liu et al. "Modified hyaluronan hydrogels support the maintenance of mouse embryonic stem cells and human induced pluripotent stem cells". eng. In: *Macromolecular bioscience* 12.8 (Aug. 2012). PMID: 22730306, pp. 1034–1042.

[124] Sharon Gerecht-Nir et al. "Propagation of undifferentiated embryonic stem cells in hyaluronic acid hydrogel". U.S. Classification: 424/93.21; 435/325; 435/366; 435/404.

[125] Sharon Gerecht et al. "Hyaluronic acid hydrogel for controlled self-renewal and differentiation of human embryonic stem cells". en. In: *Proceedings of the National Academy of Sciences* 104.27 (Mar. 2007), pp. 11298–11303.

[126] Jan. 2014. URL: `http://www.glycosan.com/`.

[127] Jason A. Burdick and Glenn D. Prestwich. "Hyarulonic Acid Hydrogels for Biomediacal Applications". In: *Advanced Materials* 23 (2011), H41–H56.

[128] Sei Kwang Hahn et al. "Synthesis and degradation test of hyaluronic acid hydrogels". eng. In: *International journal of biological macromolecules* 40.4 (Mar. 2007). PMID: 17101173, pp. 374–380.

[129] Christopher S. Chen et al. "Using Self-Assembled Monolayers to Pattern ECM Proteins and Cells on Subtrates". In: *Extracellular Matrix Protocols*. Springer, 2000, pp. 209–219.

[130] Mary Rose Burnham et al. "Biological functionalization and surface micropatterning of polyacrylamide hydrogels". In: *Biomaterials* 27.35 (2006), pp. 5883–91.

[131] J. Fink et al. "Comparative study and improvement of current cell micropatterning techniques". In: *Lab on a Chip* 7.6 (2007), p. 672.

[132] Ammar Azioune et al. "Simple and rapid process for single cell micro-patterning". In: *Lab on a chip* 9.11 (June 2009). PMID: 19458875, pp. 1640–1642.

[133] Ammar Azioune et al. "Protein Micropatterns". In: *Methods in Cell Biology*. Vol. 97. Elsevier, 2010, pp. 133–146.

[134] Michael J Poellmann et al. “Geometric microenvironment directs cell morphology on topographically patterned hydrogel substrates”. In: *Acta Biomater* (2010).

[135] A.M. Leclair, S.S.G. Ferguson, and F. Lagugné-Labarthet. “Surface patterning using plasma-deposited fluorocarbon thin films for single-cell positioning and neural circuit arrangement”. In: *Biomaterials* (2010).

[136] Nicolas Carpi et al. “Micropatterning on glass with deep UV”. In: *Protocol Exchange* (July 2011).

[137] Ilaria E. Palamà et al. “Cell self-patterning on uniform PDMS-surfaces with controlled mechanical cues”. In: *Integrative Biology* (2011).

[138] Nikhil Jain et al. “Cell geometric constraints induce modular gene-expression patterns via redistribution of HDAC3 regulated by actomyosin contractility”. In: *Proceedings of the National Academy of Sciences* 110.28 (2013), pp. 11349–11354.

[139] Michael W Toepke and David J Beebe. “PDMS absorption of small molecules and consequences in microfluidic applications”. In: *Lab on a chip* 6.12 (Dec. 2006). PMID: 17203151, pp. 1484–1486.

[140] Dong Qin, Younan Xia, and George M Whitesides. “Soft lithography for micro- and nanoscale patterning”. In: *Nature Protocols* 5.3 (Feb. 2010), pp. 491–502.

[141] Dhananjay Bodas and Chantal Khan-Malek. “Hydrophilization and hydrophobic recovery of PDMS by oxygen plasma and chemical treatment—An SEM investigation”. In: *Sensors and Actuators B: Chemical* 123.1 (Apr. 10, 2007), pp. 368–373.

[142] Anna Tourovskaia, Xavier Figueroa-Masot, and Albert Folch. “Long-term microfluidic cultures of myotube microarrays for high-throughput focal stimulation”. In: *Nat Protoc* 1.3 (2006), pp. 1092–104.

[143] *Food and Drug Administration*. Jan. 2014. URL: `www.fda.gov`.

[144] Andrew J. deMello. “Control and detection of chemical reactions in microfluidic systems”. In: *Nature* 442.7101 (July 27, 2006), pp. 394–402.

[145] Federica Rusmini, Zhiyuan Zhong, and Jan Feijen. "Protein Immobilization Strategies for Protein Biochips". In: *Biomacromolecules* 8 (2007), pp. 1775–1789.

[146] Chun H Chen et al. "Microfluidic cell sorter with integrated piezoelectric actuator". In: *Biomedical microdevices* 11.6 (Dec. 2009). PMID: 19649710 PMCID: PMC2776170, pp. 1223–1231.

[147] Todd M. Squires and Stephen R. Quake. "Microfluidics: Fluid physics at the nanoliter scale". In: *Reviews of modern physics* 77.3 (2005), p. 977.

[148] Atsushi Takano et al. "On-chip Incubation System for Long-term Microfluidic Cell Culture". In: 2011.

[149] P. Sivakumar. "New insights into extracellular matrix assembly and reorganization from dynamic imaging of extracellular matrix proteins in living osteoblasts". In: *Journal of Cell Science* 119.7 (Apr. 1, 2006), pp. 1350–1360.

[150] George M. Whitesides. "The origins and the future of microfluidics". In: *Nature* 442.7101 (July 27, 2006), pp. 368–373.

[151] Suveen Kumar et al. "Microfluidic-integrated biosensors: Prospects for point-of-care diagnostics". In: *Biotechnology journal* (Sept. 6, 2013). PMID: 24019250.

[152] Monica L Moya and Steven C George. "Integrating in vitro organ-specific function with the microcirculation". In: *Current Opinion in Chemical Engineering* 3 (Feb. 2014), pp. 102–111.

[153] Hiroshi Kimura et al. "An integrated microfluidic system for long-term perfusion culture and on-line monitoring of intestinal tissue models". In: *Lab on a Chip* 8.5 (2008), pp. 741–6.

[154] Ankur Singh et al. "Adhesion strength–based, label-free isolation of human pluripotent stem cells". In: *Nature Methods* (Apr. 2013).

[155] Susan C Wu and Yi Zhang. "Active DNA demethylation: many roads lead to Rome". eng. In: *Nature reviews. Molecular cell biology* 11.9 (Sept. 2010). PMID: 20683471, pp. 607–620.

[156] Sirio Dupont et al. "Role of YAP/TAZ in mechanotransduction". In: *Nature* 474.7350 (June 2011), pp. 179–183.

[157] Mariaceleste Aragona et al. “A Mechanical Checkpoint Controls Multicellular Growth through YAP/TAZ Regulation by Actin-Processing Factors”. In: *Cell* (2013).

[158] Adam Williamson et al. “The future of the patient-specific Body-on-a-chip”. In: *Lab on a Chip* (2013).

[159] Francesco Lamberti et al. “Surface Functionalization of Fluorine-Doped Tin Oxide Samples through Electrochemical Grafting”. In: *ACS applied materials & interfaces* 5.24 (2013), 12887–12894.

Appendix A

Role of YAP/TAZ in mechanotransduction

Sirio Dupont[1], Leonardo Morsut[1], Mariaceleste Aragona[1], Elena Enzo[1], Stefano Giulitti[2], Michelangelo Cordenonsi[1], Francesca Zanconato[1], Jimmy Le Digabel[3], Mattia Forcato[4], Silvio Bicciato[4], Nicola Elvassore[2] and Stefano Piccolo[1]

1. Department of Histology, Microbiology and Medical Biotechnologies, University of Padua School of Medicine, viale Colombo 3, 35131 Padua, Italy.
2. Department of Chemical Engineering (DIPIC), University of Padua, via Marzolo 9, 35131 Padua, Italy.
3. Laboratoire Matière et Systèmes Complexes (MSC), Université Paris Diderot, and CNRS, UMR 7057, Paris, France.
4. Center for Genome Research, Department of Biomedical Sciences, University of Modena and Reggio Emilia, via G. Campi 287, 41100 Modena, Italy.

Nature

Volume 474(7350): 179–183

10.1038/nature10137

A.1 Summary

Cells perceive their microenvironment not only through soluble signals but also in term of physical and mechanical cues, such as extracellular matrix (ECM) stiffness or confined adhesiveness. By mechanotransduction systems, cells translate these stimuli into biochemical signals controlling multiple aspects of cell behavior, including growth, differentiation and cancer malignant progression; but how rigidity mechanosensing is ultimately linked to activity of nuclear transcription factors remains poorly understood. Here we report the identification of the Yorkie-homologues YAP and TAZ as nuclear relays of mechanical signals exerted by ECM rigidity and cell-shape. This regulation requires Rho activity and tension of the acto-myosin cytoskeleton but is independent from the Hippo/LATS cascade. Crucially, YAP/TAZ are functionally required for differentiation of mesenchymal stem cells induced by ECM stiffness and for survival of endothelial cells regulated by cell geometry; conversely, expression of activated YAP overrules physical constraints in dictating cell behavior. These findings identify YAP/TAZ as sensors and mediators of mechanical cues instructed by the cellular microenvironment.

A.2 Introduction

Physical properties of the extracellular matrix (ECM) and mechanical forces are integral to morphogenetic processes in embryonic development, defining tissue architecture and driving specific cell differentiation programs [1]. In adulthood, tissue homeostasis remains dependent on physical cues, such that perturbations of ECM stiffness - or mutations affecting its perception - are causal to pathological conditions of multiple organs, contributes to aging and cancer malignant progression [2]. Mechanotransduction enables cells to sense and adapt to external forces and physical constraints [3,4]; these mechanoresponses involve the rapid remodeling of the cytoskeleton, but also require the activation of specific genetic programs. In particular, variations of ECM stiffness or changes in cell shape caused by confining the cell's adhesive area have profound impact on cell behavior across multiple cell types, such as mesenchymal stem cells [5,6], muscle stem cells [7] and endothelial cells [8].

The nuclear factors mediating the biological response to these physical inputs remain incompletely understood.

A.3 Results

A.3.1 ECM stiffness regulates YAP/TAZ activity

To gain insight into these issues, we asked if physical/mechanical stimuli conveyed by ECM stiffness actually signal through known signaling pathways. For this, we performed a bioinformatic analysis on genes differentially expressed in mammary epithelial cells (MEC) cultivated on ECM of high vs. low stiffness [9]. Specifically, we searched for statistical associations between genes regulated by stiffness and gene signatures denoting the activation of specific signaling pathways (Supplementary Fig. 2, Supplementary Table 1 and see Methods). We included signatures of MAL/SRF and NF-kB as these factors translocate in the nucleus in response to changes in F-actin polymerization and cell stretching [10]. Strikingly, only signatures revealing activation of YAP/TAZ transcriptional regulators emerged as significantly overrepresented in the set of genes regulated by high stiffness (Supplementary Fig. 2). To test if YAP (Yes-associated protein) and TAZ (transcriptional coactivator with PDZ-binding motif, also known as WWTR1) activity is regulated by ECM stiffness, we monitored YAP/TAZ transcriptional activity in human MEC cultured on fibronectin-coated acrylamide hydrogels of varying stiffness (elastic modulus ranging from 0.7 to 40 kPa, matching the physiological elasticities of natural tissues6). For this, we assayed by real-time PCR two of the best YAP/TAZ regulated genes from our signature, CTGF and ANKRD1. The activity of YAP/TAZ in cells cultured on stiff hydrogels (15-40 kPa) was comparable to that of cells grown on plastics, whereas culturing cells on soft matrices (in the range of 0.7-1 kPa) inhibited YAP/TAZ activity, to levels comparable to siRNA-mediated YAP/TAZ depletion (Fig.1a and data not shown). We confirmed this finding in other cellular systems, such as MDA-MB-231 and HeLa cells, where we used a synthetic YAP/TAZ-responsive luciferase reporter (4xGTIIC-lux) as direct read-out of their activity (Fig. 1a and Supplementary Fig. 4). Next, we assayed endogenous YAP/TAZ subcellular localization; indeed, their cytoplas-

mic relocalization has been extensively used as primary read-out of their inhibition by the Hippo pathway or by cell-cell contact (Supplementary Fig. 5 and Ref [11]). By immunofluorescence on MEC and human mesenchymal stem cells (hMSC, an established non-epithelial cellular model for mechanoresponses5,6), YAP/TAZ were clearly nuclear on hard substrates but became predominantly cytoplasmic on softer substrates (Fig. 1b, Supplementary Fig. 6 and 7). Collectively, these data indicate that YAP/TAZ activity and subcellular localization are regulated by ECM stiffness.

A.3.2 YAP/TAZ are regulated by cell geometry

It is recognized that changes in ECM stiffness impose different degrees of cell spreading [6,12]. We thus asked whether cell spreading is sufficient to regulate YAP/TAZ. To this end, we used micropatterned fibronectin islands of defined size, on which cells can spread to different degrees depending on the available adhesive area8. On these micropatterns, the localization of YAP/TAZ changed from predominantly nuclear in spread hMSC cells, to predominantly cytoplasmic in cells on smaller islands (Fig. 1c). Of note, the use of single-cell adhesive islands rules out the possibility that cell-cell contacts could be involved in YAP/TAZ relocalization. We confirmed these results using human lung microvascular endothelial cells (HMVEC, Fig. 1d), that are well known to regulate their growth according to cell shape8. Cells seeded on stiff hydrogels or large islands display an increased cell spreading but, at the same time, experience a broader cell-ECM contact area. To test if YAP/TAZ are regulated by cell spreading irrespectively of the total amount of ECM, we visualized YAP/TAZ localization in hMSC grown on the tip of closely arrayed fibronectin-coated micropillars [12]: on these arrays, cells stretch from one micropillar to another, and assume a projected cell area comparable to cells plated on big islands (3200 μm^2 on average, Fig. 1e); however, in these conditions, the actual area available for cell/ECM interaction is only about 10% of their projected area (300 μm^2 on average, corresponding to the smallest islands used in Fig. 1c). YAP/TAZ remained nuclear on micropillars (Fig. 1e), indicating that YAP/TAZ are primarily regulated by cell spreading imposed by the ECM.

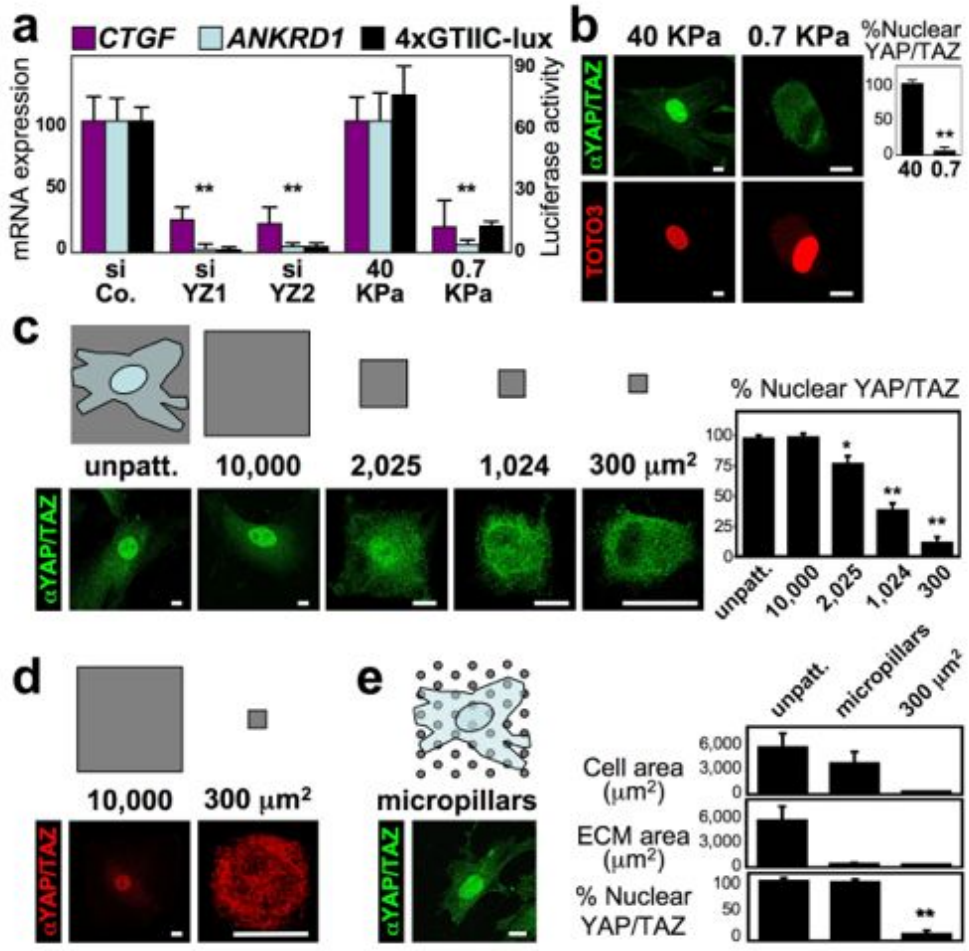

Figure A.3.1 – YAP/TAZ are regulated by ECM stiffness and cell shape. a, Real-time PCR analysis in MCF10A cells (CTGF and ANKRD1, coloured bars) and luciferase reporter assay in MDA-MB-231 cells (43GTIIC-lux, black bars) to measure YAP/TAZ transcriptional activity. Cells were transfected with the indicated siRNAs (siCo., control siRNA; siYZ1 and siYZ2, two YAP/TAZ siRNAs; see Supplementary Fig. 3) and grown on plastic, or plated on stiff (elastic modulus of 40 kPa) and soft (0.7 kPa) fibronectin-coated hydrogels. Data are normalized to lane 1. n = 4. **b**, Confocal immunofluorescence images of YAP/TAZ and nuclei (TOTO3) in human mesenchymal stem cells (MSC) plated on hydrogels. Scale bars, 15 μm. Graphs indicate the percentage of cells with nuclear YAP/TAZ. (n = 3). **c**, On top: grey patterns show the relative size of microprinted fibronectin islands on which cells were plated. Outline of a cell is shown superimposed to the leftmost unpatterned area (Unpatt.). Below: confocal immunofluorescence images of MSC plated on fibronectin islands of decreasing sizes (mm^2). Scale bars, 15 μm. Graph provides quantifications. (n = 8). See also Supplementary Fig. 8. **d**, Confocal immunofluorescence images of YAP/TAZ in HMVEC plated as in c. Scale bars, 15μm. See also Supplementary Fig. 9. **e**, On top: grey dots exemplify the distribution of fibronectin on micropillar arrays, shown superimposed with the outline of a cell. Below: representative immunofluorescence of YAP/TAZ in MSC plated on rigid micropillars. Scale bars, 15μm. Graphs, quantification of the projected cell area, total ECM contact area, and nuclear YAP/TAZ in MSC plated on unpatterned fibronectin, micropillars and 300 mm^2 islands. (n = 4). All error bars are s.d. (*P $<$ 0.05; **P $<$ 0.01; Student's t-test is used throughout). Experiments were repeated n times with duplicate biological replicates.

A.3.3 YAP/TAZ sense cytoskeletal tension

We then considered that cell spreading entails activation of the small GTPase Rho that, in turn, regulates the formation of actin bundles, stress fibers and tensile actomyosin structures [2,3]. Indeed, cells on stiff ECM or big islands displayed more prominent stress fibers compared to those plated on soft ECM or small islands (Supplementary Fig. 9 and 10). As shown in Figure 2a, we found that Rho and the actin cytoskeleton are required to maintain nuclear YAP/TAZ in hMSC. As a control, inhibition of Rac1-GEFs, or disruption of microtubules, did not alter YAP/TAZ localization (Fig. 2a). Similar results were obtained also in HMVEC and MEC (not shown). Crucially, inhibition of Rho and of the actin cytoskeleton also inhibited YAP/TAZ transcriptional activity, as assayed by expression of endogenous target genes (Fig. 2b) and by luciferase reporter assays (Fig. 2c). Conversely, triggering F-actin polymerization and stress fibers formation by overexpression of activated Diaphanous promoted YAP/TAZ activity (Supplementary Fig. 12). We then asked whether YAP/TAZ are regulated by the ratio of monomeric/filamentous actin, as others observed for MAL/SRF13. To increase monomeric G-actin, we overexpressed the R62D mutant actin13, but this was insufficient to inhibit YAP/TAZ (Fig. 2c). Moreover, increasing the amount of F-actin either by overexpressing the F-actin stabilizing V159N actin mutant or by serum stimulation [13] had no effect on YAP/TAZ activity (Supplementary Fig. 13) or nuclear localization (data not shown). As a control, in the same experimental set-up, MAL/SRF activity was instead clearly modulated (Supplementary Fig. 14). Taken altogether, these data indicate that Rho and stress fibers, but not F-actin polymerization per se, are required for YAP/TAZ activity. Cells respond to the rigidity of the ECM by adjusting the tension and organization of their stress fibers, such that cell spreading is accompanied by increased pulling forces against the ECM3,6,12. By inhibition of ROCK and non-muscle myosin (NMM-II)4,6, we found that cytoskeletal tension is required for YAP/TAZ nuclear localization (Fig. 2d) and activity (Fig. 2e and Supplementary Fig. 16). Of note, YAP/TAZ exclusion caused by these inhibitions is an early event (occurring within 2 hours) that can be uncoupled from destabilization of stress fibers (see Supplementary Fig. 17). By comparison, the activity of MAL/SRF was only

marginally affected by the same treatments (Supplementary Fig. 18). To address more directly the relevance of cell-generated mechanical force without using small-molecule inhibitors and irrespectively of the surface properties of the hydrogels, we compared rigid vs highly elastic micropillars [12]; on the elastic substrate, cytoplasmic localization of YAP/TAZ was clearly increased (Fig. 2f). Collectively, the data indicate that YAP/TAZ respond to cytoskeletal tension. We also tested if inhibition of YAP/TAZ occurs by entrapping YAP/TAZ in the cytoplasm or by promoting their nuclear exclusion. As shown in Supplementary Fig. 20a, blockade of nuclear export with LeptomycinB rescued nuclear localization of YAP/TAZ in hMSC treated with cytoskeletal inhibitors, suggesting that YAP/TAZ keeps shuttling between cytoplasm and nucleus irrespectively of cell tension, and that the presence of a tense cytoskeleton promotes their nuclear retention. Moreover, YAP/TAZ relocalization was rapid (occurring in as little as 30 min with LatrunculinA), reversible after small-molecule washout (Supplementary Fig. 20b), and insensitive to inhibition of protein synthesis with cycloheximide (data not shown), suggesting a direct biochemical mechanism.

A.3.4 Mechanical cues act independently from Hippo

YAP and TAZ are the nuclear transducers of the Hippo pathway [14]. In several organisms and cellular set-ups, activation of the Hippo pathway leads to YAP/TAZ phosphorylation on specific serine residues; in turn, these phosphorylations inhibit YAP/TAZ activity through multiple mechanisms, including proteasomal degradation [14]. Intriguingly, similar to Hippo activation by cell-cell contacts (Fig. 3a), TAZ protein was also degraded by culturing MEC cells on soft matrices (Fig. 3b) or by treatment with inhibitors of Rho, F-actin and actomyosin tension (Fig. 3c and Supplementary Fig. 21). Similar results were obtained with hMSC and HMVEC (Supplementary Fig. 22 and data not shown). Is then the Hippo cascade responsible for YAP/TAZ inhibition by mechanical cues? Several evidences indicate this is not the case. First, we noted that phosphorylation of YAP on serine 127, a key target of the LATS kinase downstream of the Hippo pathway [15], was not increased upon treatment of hMEC and hMSC with cytoskeletal inhibitors (Fig. 3c and Supplementary Fig. 22), at difference with its regulation by high confluence (see Fig. 3a).

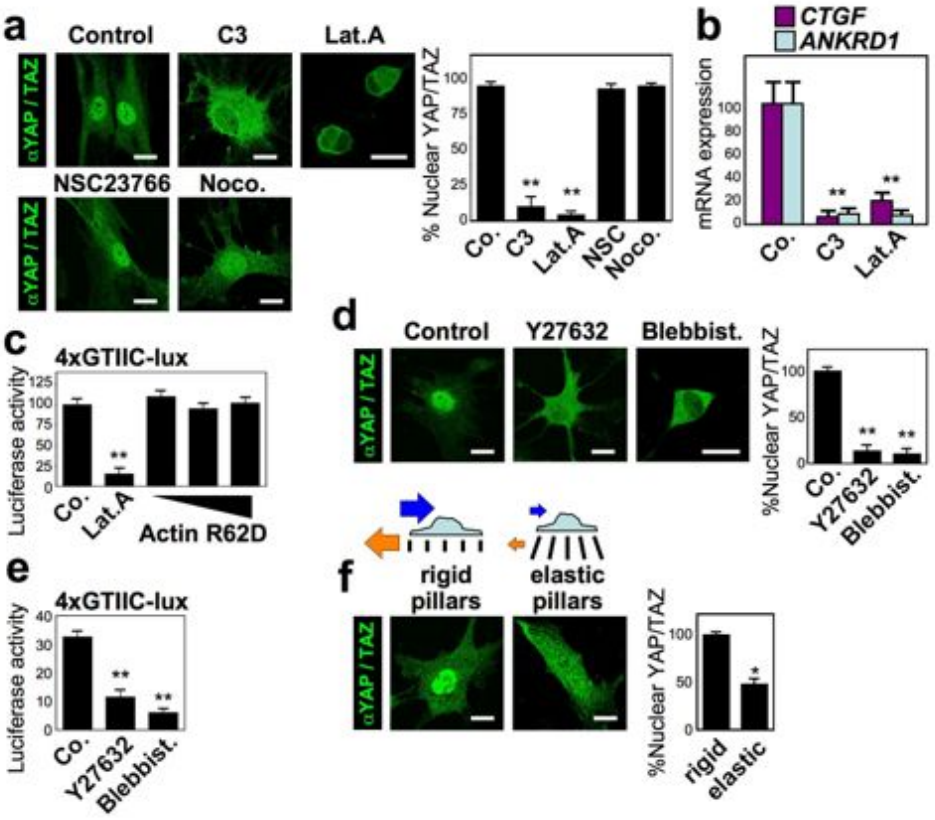

Figure A.3.2 – YAP/TAZ activity requires Rho and tension of the actin cytoskeleton. **a**, Confocal immunofluorescence images of YAP/TAZ in MSC treated with the Rho inhibitor C3 (3 $\mu g\,ml^{-1}$), the F-actin inhibitor latrunculin A (Lat.A, 0.5 $\mu g\,ml^{-1}$), the Rac1-GEFs inhibitor NSC23766 (100 $\mu g\,ml^{-1}$) or the microtubule inhibitor nocodazole (Noco., 30 $\mu g\,ml^{-1}$). Scale bars, 15 mm. Graph provides quantifications (n = 10). See also Supplementary Fig. 11. **b**, Real-time PCR of MCF10A treated with cytoskeletal inhibitors as in a. Data are normalized to untreated cells (Co.) (n = 4). **c**, Luciferase assay for YAP/TAZ activity in HeLa cells transfected with the indicated expression plasmids (Co. is empty vector, actin R62D encodes for a mutant unable to polymerize into F-actin) and treated with latrunculin A (n = 4). Similar effects were observed in MDA-MB-231 (not shown). **d**, Confocal immunofluorescence images of MSC treated with the ROCK inhibitor Y27632 (50 $\mu g\,ml^{-1}$), or the non-muscle myosin inhibitor blebbistatin (Blebbist., 50 $\mu g\,ml^{-1}$). Scale bars, 15 μm. Graph provides quantifications (n = 9). See also Supplementary Fig. 15. **e**, Luciferase activity of the YAP/TAZ reporter in HeLa treated as in d. (n = 4). **f**, Confocal immunofluorescence images of MSC plated on arrays of micropillars of different rigidities. On rigid micropillars (black lines) cells develop cytoskeletal tension (blue arrow) by pulling against the ECM (orange arrow); cells bend elastic micropillars and develop reduced tension exemplified by reduced size of the arrows. Scale bars, 15 μm. Graph provides quantifications (n = 2). See also Supplementary Fig. 19. All error bars are s.d. (*P $<$ 0.05; **P $<$ 0.01). Experiments were repeated n times with duplicate biological replicates.

Second, depletion of LATS1 and LATS2 (see Fig. 3f and Supplementary Fig. 23 for positive controls) had marginal effect on YAP/TAZ inactivation by mechanical cues, as judged by: i) YAP/TAZ nuclear exit induced by micropatterns or cytoskeletal inhibition in hMEC, hMSC or HMVEC (Fig. 3d, Supplementary Fig. 24, 25 and data not shown); ii) TAZ degradation (Fig. 3e); iii) endogenous target gene expression in cells plated on soft hydrogels (Fig. 3f) or treated with LatrunculinA (Supplementary Fig. 26). Finally, we compared wild-type or LATS-insensitive 4SA [16] TAZ in MDA-MB-231 depleted of endogenous YAP/TAZ and reconstituted at near-to-endogenous YAP/TAZ activity levels with siRNA-insensitive mouse TAZ (mTAZ) vectors. As shown in Fig. 3g, both wild-type (WT) and 4SA mTAZ remain sensitive to mechanical cues. Further supporting these results, we found that MDA-MB-231 cells are homozygous mutant for NF2/merlin (Supplementary Fig. 27), an essential component of the Hippo cascade [14]. Collectively, these data suggest that LATS phosphorylation downstream of the Hippo cascade is not the primary mediator of mechanical/physical cues in regulating YAP/TAZ activity. We then asked if mechanical cues regulate YAP/TAZ not only in isolated cells, but also in confluent monolayers, when cells reorganize their shape and structure and engage in cell-cell contacts, leading to activation of Hippo/LATS signaling11. We first explored the effects of cell confluence in a simplified experimental set-up, namely in MCF10A cells rendered insensitive to Hippo activation by depletion of LATS1/2; in these conditions, Rho and the cytoskeleton remain relevant inputs to support TAZ stability (Supplementary Fig. 28). Moreover, in parental MCF10A, plating cells at high confluence cooperate with soft hydrogels in inhibiting YAP/TAZ activity (Fig. 3h). Thus, mechanical cues and Hippo signaling represent two parallel inputs converging on YAP/TAZ regulation.

A.3.5 YAP/TAZ mediate cellular mechanoresponses

Data presented so far indicate YAP and TAZ as molecular “readers” of ECM elasticity and cell geometry; but are YAP/TAZ relevant to mediate the biological responses to these mechanical inputs? An appropriate cellular model to address this question are hMSC, that can differentiate into osteoblasts when cultured on stiff ECM, mimicking

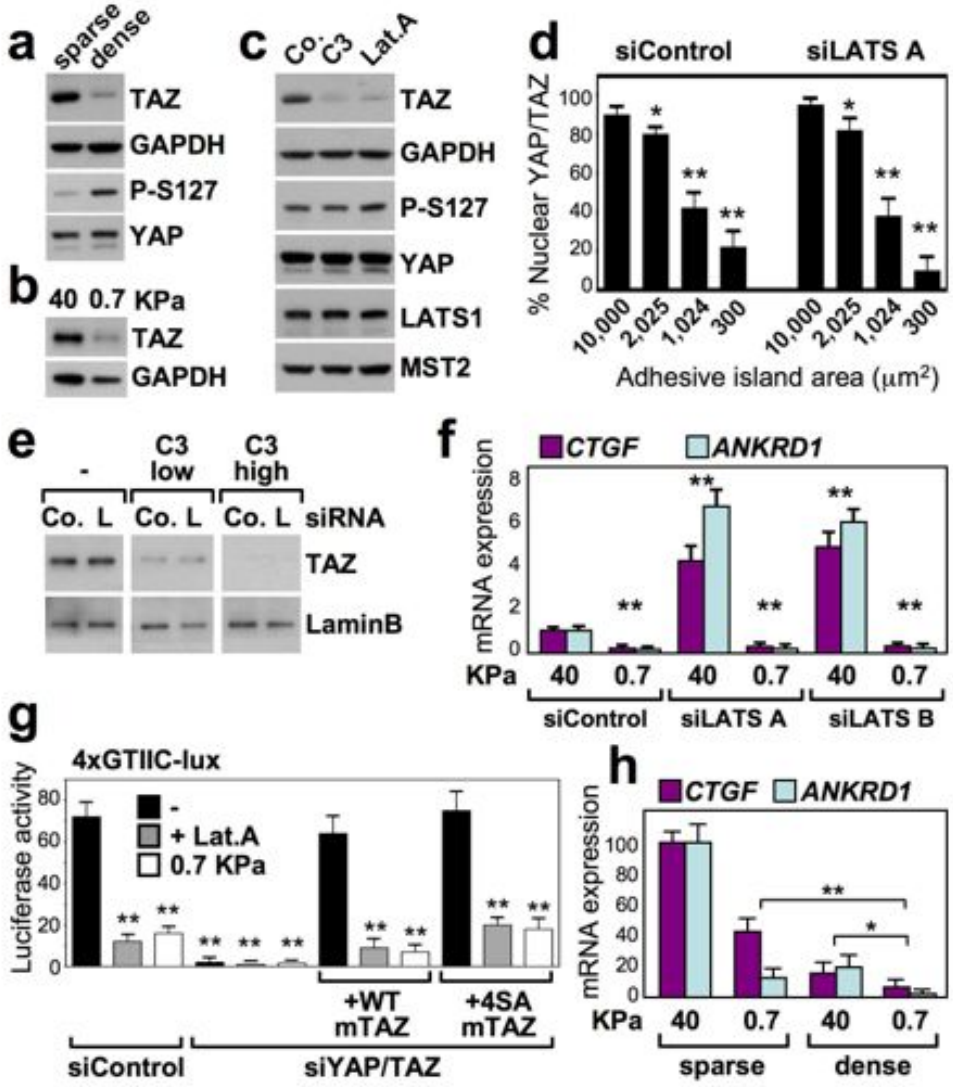

Figure A.3.3 – ECM stiffness and cell spreading regulate YAP/TAZ independently of the Hippo pathway. **a–c**, Immunoblotting for the indicated proteins in MCF10A under the following conditions: a, plating on plastic at low (sparse) or high (dense) confluence; **b**, plating on stiff (40 kPa) or soft (0.7 kPa) hydrogels; **c**, untreated (Co.) or treated with C3 and latrunculin A (Lat.A). P-S127 is phospho-YAP. **d**, Quantification of nuclear YAP/TAZ in MSC transfected with control or LATS1/2 siRNA A (siLATS A) and plated on microprinted islands of different size (n = 4). Similar results were obtained with HMVEC (not shown). e, Immunoblotting from MSC cells transfected with the indicated siRNAs (Co., control siRNA; L, LATS1/2 siRNA A), plated on plastic and treated with C3 (0.5 or 3 $\mu g\, ml^{-1}$). Similar results were obtained by using blebbistatin or latrunculin A, or by treating HMVEC and MCF10A (not shown). **f**, Real-time PCR analysis of MCF10A transfected with the indicated siRNAs and cultured on hydrogels. Data are normalized to the first lane (n = 3). g, Luciferase assay in MDA-MB-231 transfected as indicated and treated with latrunculin A (Lat.A) or replated on soft hydrogels. (n = 8). h, RT– PCR of MCF10A grown under sparse or confluent (dense) conditions on the indicated hydrogels. Data are normalized to the first lane (n = 2). All error bars are s.d. (*P $<$ 0.05; **P $<$ 0.01). Experiments were repeated n times with duplicate biological replicates.

the natural bone environment, while on soft ECM - or small islands - they differentiate into other lineages, such as adipocytes [5,6]. A similar case applies to endothelial cells, that respond differently to the same soluble growth factor by proliferating, differentiating or involuting according to the degree of cell spreading against the surrounding ECM8. We hypothesized that cell fates induced by stiff ECM and large islands (i.e. where YAP/TAZ are active) should require YAP/TAZ function and, conversely, cell fates associated to soft ECM and small islands (where YAP/TAZ are inhibited) should require their inactivation. In line with this hypothesis, osteogenic differentiation induced in hMSC on stiff ECM was inhibited upon depletion of YAP and TAZ, and a similar inhibition was achieved either by culturing cells on soft ECM or by incubation with C3 (Fig. 4a, b). We also monitored adipogenic differentiation, a fate normally not allowed on stiff ECM; strikingly, YAP/TAZ knockdown enabled adipogenic differentiation on stiff substrates, thus mimicking a soft environment (Fig. 4c and Supplementary Fig. 30). In the case of HMVEC, cells plated on small islands undergo apoptosis, while cells on bigger islands proliferate, as assayed by TUNEL staining and BrdU incorporation, respectively8. Upon YAP/TAZ depletion, cells on bigger islands behaved as if they were on small islands; this is overlapping with the biological effects of Rho inhibition (Fig. 4d). In line with the Hippo independency of this regulation, knockdown of LATS1/2 was not sufficient to rescue osteogenesis upon C3 treatment, or endothelial cell proliferation on small islands (Supplementary Fig. 32). Collectively, these data suggest that YAP/TAZ are required for cell differentiation triggered by changes in ECM stiffness and for geometric control of cell survival. We next tested if the sole YAP/TAZ activity can re-direct the biological responses elicited by soft/confined ECM. Overexpression of activated 5SA-YAP with lentiviral infection (to at least ten fold the endogenous levels, data not shown) remarkably overruled the geometric control over proliferation and apoptosis in HMVEC (Fig. 4e), and rescued osteogenic differentiation of hMSC treated with C3 or plated on soft ECM (Fig. 4f, g). Thus, cells on soft matrices or on small adhesive areas can be tricked to behave as if they were adhering on harder/larger substrates by sustaining YAP/TAZ function.

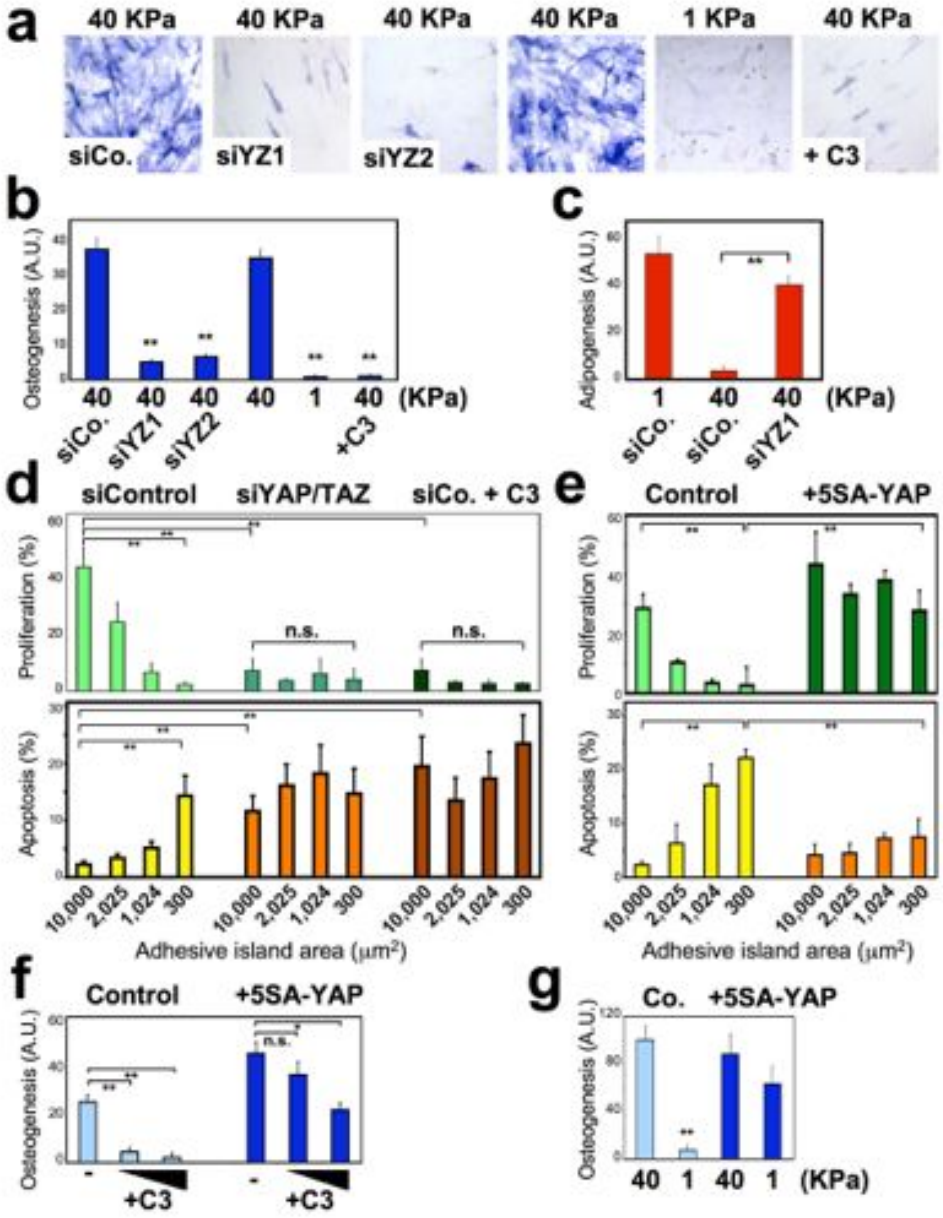

Figure A.3.4 – YAP/TAZ are required mediators of the biological effects controlled by ECM elasticity and cell geometry. **a–c**, MSC were transfected with the indicated siRNA (control, siCo.; YAP/TAZ, siYZ1 and siYZ2), plated on stiff (40 kPa) or soft (1 kPa) substrates and induced to differentiate into osteoblasts **(a, b)** or adipocytes **(c)**. C3 (0.5 mg ml21) was added and renewed with differentiation medium. a, Representative alkaline phosphatase stainings and b, quantifications of osteogenic differentiation (n = 4). **c**, Quantification of adipogenesis based on oil-red stainings (n = 2) (A.U., arbitrary units, see methods). See Supplementary Figs 29 and 30 for controls. These results are consistent with ref. 23. **d**, Proliferation (BrdU, upper panel) and apoptosis (TUNEL, lower panel) of HMVEC plated on adhesive islands of different size; where indicated, cells were treated overnight with C3 (2.5 $\mu g\, ml^{-1}$), or transfected with the indicated siRNAs (n = 5). Similar results were obtained with siYZ2 (not shown). Representative stainings in Supplementary Fig. 31. e, Proliferation (upper panel) and apoptosis (lower panel) of control and 5SA-YAP-expressing HMVEC, plated on adhesive islands. **f, g**, Quantifications of osteogenesis in MSC transduced with 5SA-YAP, and treated with C3 (50 and 150 $ng\, ml^{-1}$) (n = 3) (f) or plated on hydrogels (n = 2) (**g**). Representative stainings in Supplementary Fig. 33. All error bars are s.d. (*P < 0.05; **P < 0.01; n.s., not significant). Experiments were repeated n times with duplicate biological replicates.

A.4 Discussion

In sum, our findings indicate a fundamental role of the transcriptional regulators YAP and TAZ as downstream elements in how cells perceive their physical microenvironment (Supplementary Fig. 1). Our data define an unprecedented modality of YAP/TAZ regulation, that acts in parallel to the NF2/Hippo/LATS pathway and instead requires Rho activity and the acto-myosin cytoskeleton. Interestingly, this recapitulates aspects of MAL/SRF regulation13, but also entails profound differences: YAP/TAZ activity requires stress fibers and cytoskeletal tension induced by ECM stiffness and cell spreading, but is not directly regulated by G-actin levels. The detailed biochemical mechanisms by which cytoskeletal tension regulates YAP/TAZ awaits further characterization, but it is tempting to speculate that stress-fibers inhibit an unidentified YAP/TAZ-interacting molecule that, when released, would promote their inactivation. Functionally, we showed that different cellular models read ECM elasticity, cell shape and cytoskeletal forces as levels of YAP/TAZ activity, such that experimental manipulations of YAP/TAZ levels can dictate cell behavior, overruling mechanical inputs. This identifies a new widespread transcriptional mechanism by which the mechanical properties of the ECM and cell geometry instruct cell behavior. This may now shed light on how physical forces shape tissue morphogenesis and homeostasis, for example in tissues undergoing constant remodeling upon variation of their mechanical environmnent; indeed, alterations of YAP/TAZ signaling have been genetically linked in animal models to the emergence of cystic kidney, pulmonary emphysema, heart and vascular defects [17-20]. In cancer, changes in the ECM composition and mechanical properties is the focus of intense interest, as these have been correlated with progression and build-up of the metastatic niche [2]; in light of their powerful oncogenic activities [14], YAP/TAZ might serve as executers of these malignant programs. Genetically, YAP and TAZ have been linked to a universal system that control organ size14. The current view implicates Hippo signaling as the sole determinant of YAP/TAZ regulation in tissues. However, our results suggest physical/mechanical inputs as alternative determinant of YAP/TAZ activity. Supporting our model, it has been observed that growth of epithelial tissues entails the build-up of mechanical stresses at tissue boundaries21, and theoretical work pro-

posed that these serve as positive feedback to homogenize cell growth, compensating for uneven activity of soluble growth factors [22]. It is tempting to speculate that proliferative tissue homeostasis may be achieved by a combination of growth factor signaling and localized control of YAP/TAZ activation by cell-cell contacts and mechanical cues.

References

[1] Mammoto, T. & Ingber, D.E. Mechanical control of tissue and organ development. Development 137, 1407–1420 (2010).

[2] Jaalouk, D.E. & Lammerding, J. Mechanotransduction gone awry. Nature Rev. Mol. Cell Biol. 10, 63–73 (2009).

[3] Schwartz, M. A. Integrins and extracellular matrix in mechanotransduction. Cold Spring Harb. Perspect. Biol. 2, a005066 (2010).

[4] Vogel, V. & Sheetz, M. Local force and geometry sensing regulate cell functions. Nature Rev. Mol. Cell Biol. 7, 265–275 (2006).

[5] McBeath, R., Pirone, D. M., Nelson, C. M., Bhadriraju, K. & Chen, C. S. Cell shape, cytoskeletal tension, and RhoA regulate stem cell lineage commitment. Dev. Cell 6, 483–495 (2004).

[6] Engler, A.J., Sen, S., Sweeney, H.L. & Discher, D.E. Matrix elasticity directs stem cell lineage specification. Cell 126, 677–689 (2006).

[7] Gilbert, P. M. et al. Substrate elasticity regulates skeletal muscle stem cell self-renewal in culture. Science 329, 1078–1081 (2010).

[8] Chen, C. S., Mrksich, M., Huang, S., Whitesides, G. M. & Ingber, D. E. Geometric control of cell life and death. Science 276, 1425–1428 (1997).

[9] Provenzano, P. P., Inman, D. R., Eliceiri, K. W. & Keely, P. J. Matrix density-induced mechanoregulation of breast cell phenotype, signaling and gene expression through a FAK-ERK linkage. Oncogene 28, 4326–4343 (2009).

[10] Olson, E.N. & Nordheim, A. Linking actin dynamics and gene transcription to drive cellular motile functions. Nature Rev. Mol. Cell Biol. 11, 353–365 (2010).

[11] Zhao, B. et al. Inactivation of YAP oncoprotein by the Hippo pathway is involved in cell contact inhibition and tissue growth control. Genes Dev. 21, 2747–2761(2007).

[12] Fu, J. et al. Mechanical regulation of cell function with geometrically modulated elastomeric substrates. Nature Methods 7, 733–736 (2010).

[13] Miralles, F., Posern, G., Zaromytidou, A. I. & Treisman, R. Actin dynamics control SRF activity by regulation of its coactivator MAL. Cell 113, 329–342 (2003).

[14] Pan, D. The hippo signaling pathway in development and cancer. Dev. Cell 19, 491–505 (2010).

[15] Oka, T., Mazack, V. & Sudol, M. Mst2 and Lats kinases regulate apoptotic function of Yes kinase-associated protein (YAP). J. Biol. Chem. 283, 27534–27546 (2008).

[16] Lei, Q. Y. et al. TAZ promotes cell proliferation and epithelial-mesenchymal transition and is inhibited by the hippo pathway. Mol. Cell. Biol. 28, 2426–2436 (2008).

[17] Chen, Z., Friedrich, G.A. & Soriano, P. Transcriptional enhancer factor 1 disruption by a retroviral gene trap leads to heart defects and embryonic lethality in mice. Genes Dev. 8, 2293–2301 (1994).

[18] Makita, R. et al. Multiple renal cysts, urinary concentration defects, and pulmonary emphysematous changes in mice lacking TAZ. Am. J. Physiol. Renal Physiol. 294, F542–F553 (2008).

[19] Morin-Kensicki, E. M. et al. Defects in yolk sac vasculogenesis, chorioallantoic fusion, and embryonic axis elongation in mice with targeted disruption of Yap65 . Mol. Cell. Biol. 26, 77–87 (2006).

[20] Skouloudaki, K. et al. Scribble participates in Hippo signaling and is required for normal zebrafish pronephros development. Proc. Natl Acad. Sci. USA 106, 8579–8584 (2009).

[21] Nienhaus, U., Aegerter-Wilmsen, T. & Aegerter, C.M. Determination of mechanical stress distribution in Drosophila wing discs using photoelasticity. Mech. Dev. 126, 942–949 (2009).

[22] Schwank, G. & Basler, K. Regulation of organ growth by morphogen gradients. Cold Spring Harb. Perspect. Biol. 2, a001669 (2010).

[23]. Hong, J. H. et al. TAZ, a transcriptional modulator of mesenchymal stem cell differentiation. Science 309, 1074–1078 (2005).

[24] Tse, J.R. & Engler, A.J. Preparation of hydrogel substrates with tunable mechanical properties. Curr. Protoc. Cell Biol. 47, 10.16.1–10.16.16 (2010).

[25] duRoure, O. et al. Force mapping in epithelial cell migration. Proc. Natl Acad. Sci. USA 102, 2390–2395 (2005).

[26] Mahoney, W.M. Jr, Hong, J.H., Yaffe, M.B. & Farrance, I.K. The transcriptional co-activator TAZ interacts differentially with transcriptional enhancer factor-1 (TEF-1) family members. Biochem. J. 388, 217–225 (2005).

[27] Martello, G. et al. A Micro RNA targeting Dicer for metastasis control. Cell 141, 1195–1207 (2010).

[28] Dupont, S. et al. FAM/USP9x, a deubiquitinatin genzyme essential for TGFb signaling, controls Smad4 monoubiquitination. Cell 136, 123–135 (2009).

[29] Morsut, L. et al. Negative control of Smad activity by ectodermin/Tif1cpatternsthe mammalian embryo. Development 137, 2571–2578 (2010).

[30] Galbraith, C.G., Yamada, K.M. & Sheetz, M.P. The relationship between force and focal complex development. J. Cell Biol. 159, 695–705 (2002).

[31] Giannone, G., Jiang, G., Sutton, D.H., Critchley, D.R. & Sheetz, M.P. Talin1 is critical for force-dependent reinforcement of initial integrin-cytoskeleton bonds but not tyrosine kinase activation. J. Cell Biol. 163, 409–419 (2003).

[32] Padua, D. et al. TGFb primes breast tumors for lung metastasis seeding through angiopoietin-like 4. Cell 133, 66–77 (2008).

[33] Adorno, M. et al. A mutant-p53/Smad complex opposes p63 to empower TGFb-induced metastasis. Cell 137, 87–98 (2009).

[34] Bild, A. H. et al. Oncogenic pathway signatures in human cancers as a guide to targeted therapies. Nature 439, 353–357 (2006).

[35] Mackay, A. et al. cDNA microarray analysis of genes associated with ERBB2 (HER2/ neu) overexpression in human mammary luminal epithelial cells. Oncogene 22, 2680–2688 (2003).

[36] Zhao, B. et al. TEAD mediates YAP-dependent gene induction and growth control. Genes Dev. 22, 1962–1971 (2008).

[37] Dong, J. et al. Elucidation of a universal size-control mechanism in Drosophila and mammals. Cell 130, 1120–1133 (2007).

[38] Ota, M. & Sasaki, H. Mammalian Tead proteins regulate cell proliferation and contact inhibition as transcriptional mediators of Hippo signaling. Development 135, 4059–4069 (2008).

[39] Zhang, H. et al. TEAD transcription factors mediate the function of TAZ in cell growth and epithelial-mesenchymal transition. J. Biol. Chem. 284, 13355–13362 (2009).

[40] DiMeo, T. A. et al. A novel lung metastasis signature links Wnt signaling with cancer cell self-renewal and epithelial-mesenchymal transition in basal-like breast cancer. Cancer Res. 69, 5364–5373 (2009).

[41] Mazzone, M. et al. Dose-dependent induction of distinct phenotypic responses to Notch pathway activation in mammary epithelial cells. Proc. Natl Acad. Sci. USA 107, 5012–5017 (2010).

[42] Descot, A. et al. Negative regulation of the EGFR-MAPK cascade by actin-MAL- mediated Mig6/Errfi-1 induction. Mol. Cell 35, 291–304 (2009).

[43] Selvaraj, A. & Prywes, R. Expression profiling of serum inducible genes identifies a subset of SRF target genes that are MKL dependent. BMC Mol. Biol. 5, 13 (2004).

[44] Park, B. K. et al. NF-kB in breast cancer cells promotes osteolytic bone metastasis by inducing osteoclastogenesis via GM-CSF. Nature Med. 13, 62–69 (2006).

Appendix B

A mechanical checkpoint controls multicellular growth through YAP/TAZ regulation by actin capping/severing factors

Mariaceleste Aragona[1], Tito Pancera[1], Andrea Manfrin[1], Stefano Giulitti[2], Federica Michielin[2], Nicola Elvassore[2] and Sirio Dupont[1], Stefano Piccolo[1].

1. Department of Molecular Medicine, University of Padua School of Medicine, viale Colombo 3, 35131 Padua, Italy

2. Department of Industrial Engineering (DII), University of Padua, via Marzolo 9, 35131 Padua, Italy.

Cell

Volume 154(5):1047-1059

10.1016/j.cell.2013.07.042

B.1 Summary

Key cellular decisions, such as proliferation or growth arrest, typically occur at spatially-defined locations within tissues. Loss of this spatial control is a hallmark of many diseases, including cancer. Yet, how these patterns are established is incompletely understood. Here we report that physical and architectural features of a multicellular sheet inform cells about their proliferative capacity through mechanical regulation of YAP and TAZ, known mediators of Hippo signaling and organ growth. YAP/TAZ activity is confined to cells exposed to mechanical stresses, such as stretching, location at edges/curvatures contouring an epithelial sheet, or stiffness of the surrounding extracellular matrix. We identify the F-actin capping/severing proteins Cofilin, CapZ and Gelsolin as essential gatekeepers that limit YAP/TAZ activity in cells experiencing low mechanical stresses, including contact inhibition of proliferation. We propose that mechanical forces are overarching regulators of YAP/TAZ in multicellular contexts, setting responsiveness to Hippo, WNT and GPCR signaling.

B.2 Introduction

Spatially restricted patterns of cell proliferation shape embryonic development and maintain adult epithelial tissues. How these local growth patterns are established remains unclear. In the past decades, major emphasis has been placed on graded distribution of soluble growth factors or their restricted activity in "niches". This view, however, does not fully explain how the microenvironment can robustly template cell behavior in time and space, with micrometer accuracy [1,2]. Moreover, soluble factors alone can hardly account for some remarkable examples of ordered proliferation, differentiation and self-organization of entire organs emerging in vitro from naïve cells cultured in media saturated of mitogens and growth factors [3]. This suggests that tissues are somehow endowed with the capacity to inform individual cells on their proliferative competence, likely including the responsiveness to soluble cues. Although the molecular nature of these informational systems is uncertain, an intriguing model is that the architectural form of the tissue - its shape and three-dimensional geometry - serves as template to initiate and self-sustain asymmetric patterns of cell prolifer-

ation [4,5]. Key elements of such architectural signal are cell shape, cell geometry and deformation generated by the pulling forces of the extracellular matrix (ECM) and of neighboring cells, and the associated changes in cytoskeletal organization and tension [6-9]. In this model, a specific tissue conformation would translate into a pattern of mechanical forces potentially targeting individual cells with exquisite detail. Supporting this "biomechanical" perspective, the physical properties of the microenvironment are increasingly recognized as potent and pervasive regulators of cell behavior, such as proliferation and differentiation [10]. A critical step forward in understanding these processes has been the discovery that mechanical signals are transduced by two related transcriptional coactivators, YAP and TAZ [11]. These are powerful regulators of cell proliferation and survival, playing critical roles in organ growth [12,13]. A number of human cancers hijack these properties to foster their own growth, including induction of cancer stem cells and metastatic colonization [14,15]. YAP and TAZ shuttle between the cytoplasm and the nucleus, where they interact with TEAD transcription factors to regulate transcription. Classically, the Hippo cascade has been regarded as the major regulatory input upstream of YAP/TAZ [12]. Very recently, WNT and GPCR signaling pathways have also been recognized as important regulators of YAP/TAZ [16,17]. Thinking along the connections between tissue architecture, cell mechanics and YAP/TAZ biology, we asked: is the mechanical regulation of YAP and TAZ translating spatial force distribution into patterned growth within multicellular layers? If so, how is positional information transmitted to YAP/TAZ? Are the different inputs feeding on YAP/TAZ (e.g. mechanical stimulation, Hippo, WNT or GPCR signaling) parallel or interdependent regulations? Here we started to shed light on these issues by discovering that cell proliferation in an epithelial monolayer is profoundly influenced by a mechanical and cytoskeletal checkpoint that regulates YAP and TAZ. This tissue-level checkpoint is enforced by the F-actin capping and severing proteins CapZ, Cofilin and Gelsolin. These factors inhibit YAP and TAZ in cells that, within a monolayer, are located at sites of low mechanical stress. Conversely, YAP/TAZ-mediated proliferative competence occurs in cells that exhibit higher contractility in response to stretching forces, depending on the shape of the epithelial sheet or on the rigidity of the surrounding

ECM. We propose that mechanical stresses are overarching regulators of YAP/TAZ in multicellular contexts, also setting cell responsiveness to Hippo, WNT and GPCR signaling.

B.3 Results

Mechanical regulation of cell proliferation through YAP/TAZ A classic paradigm on the control of proliferation in multicellular aggregates is contact inhibition of proliferation (CIP), a process by which cultured cells stop dividing when they become confluent occupying the entire space allotted to them. This behavior recapitulates the proliferative arrest of most epithelia typically leading to cell differentiation or death. Interestingly, loss of CIP is considered a hallmark of cancer [18,13]. In CIP, a unifying theme is the regulation of YAP and TAZ, that tend to remain nuclear in cells growing at low density and relocate in the cytoplasm in confluent cultures [19]. CIP is associated with phosphorylation of YAP and TAZ, indicating the activation of the Hippo pathway kinases [19]. However, the regulation of YAP/TAZ by contact inhibition appears more complex. For example, recent data show that, at least in MEFs or keratinocytes, the mammalian Hippo homologue MST1/2 and LATS1/2 are dispensable for CIP [20]. Here we decided to explore a different scenario, in which CIP incorporates a mechanical regulation of YAP and TAZ. To test this, we compared immortalized human mammary epithelial cells (MEC) plated at different densities (3000, 15000, 75000 $cells/cm^2$) (Figure 1A). At the lowest plating density (hereafter called "sparse"), cells exhibited no or minimal contact between neighboring cells. At the intermediate plating density ("confluent"), cells were confluent with all-around cell-cell contacts, while, at the highest density ("dense"), space constraints caused cells to form a densely packed monolayer. Using anti-E-Cadherin immunofluorescence to identify cell borders, we quantified that the projected cell area dropped more than ten folds with increasing density, from 1400 μm^2 in sparse cells, to 700 μm^2 in confluent cells and down to 130 μm^2 in dense cells (Figure 1A). As measured by BrdU incorporation, confluent cultures displayed about a 30% reduction of S-phase entry when compared to sparse cultures (Figure 1B). This degree of proliferative inhibition is in agreement with the expected contribution of cell-cell contact and

E-Cadherin engagement to CIP [21], and was paralleled by a partial YAP/TAZ cytoplasmic relocalization (Figure 1C). That said, both nuclear YAP/TAZ levels and proliferation remained clearly evident in confluent cultures (Figures 1B and 1C), with YAP/TAZ activity being causal for S-phase entry (Figure 1B). This suggests that cell-cell contact per se is not sufficient to induce either post-confluence inhibition of proliferation, or robust YAP/TAZ inactivation. This is in contrast to the cells seeded at high density (dense), which are overtly growth arrested and exhibit largely cytoplasmic, transcriptionally inactive YAP/TAZ (Figures 1B, 1C, S1A). CIP is reversible, as inducing a "wound" in the monolayer by scraping away a stripe of cells caused the cells lying within a few cell diameters from the edge of the wound to stretch without losing cell-cell contacts, re-localize YAP/TAZ to the nuclei and proliferate (Figure S1B and data not shown). Similar results were observed by using immortalized human HaCaT keratinocytes (Figures S1C-F and data not shown). YAP/TAZ inactivation in the course of CIP has been associated with activation of cell-cell adhesion machinery and activation of the Hippo pathway (Zhao et al., 2007). We thus asked if the distinct degrees of YAP/TAZ inactivation observed in confluent and dense cultures, were dependent on catenins and LATS. Consistently with previous reports [21,20], knockdown of α-catenin, p120-catenin or LATS1/2 rescued YAP/TAZ transcriptional activity in confluent cultures, as measured by the expression of YAP/TAZ target genes CTGF, CYR61 and ANKRD1 (Figures S1G-I and data not shown). Surprisingly, however, the same depletions had marginal effects on YAP/TAZ signaling in dense cultures (Figures S1G-I). The above results suggest that, beside cell-cell contacts, the main determinant for YAP/TAZ inhibition and post-confluent growth arrest is actually to attain a small cell size - intended as adhesion to a small ECM substrate area (Figure 1A). Indeed, cells attaching to a small area are known to experience low mechanical stresses, as they display decreased integrin-mediated focal adhesions, reduced actin stress fibers, and blunted cell contractility [22,8,9]. Importantly, these mechanical cues have recently been shown to be essential for YAP/TAZ nuclear localization and activity [11,23]. In this perspective, CIP would represent the response to a mechanical constraint: as cell crowding progressively boxes individual cells into smaller areas, these would

be subjected to the same YAP/TAZ-regulating mechanotransduction pathways that affect isolated cells plated on small ECM islands. In line with this view, MEC plated as single cells on micropatterned fibronectin islands of defined areas displayed strong inhibition of YAP/TAZ nuclear levels and BrdU incorporation when individual cell-size dropped below 300 μm^2 (Figures 1D and 1E), independently of cell-cell contacts. Similarly, decreasing mechanical cues by culturing cells on soft substrates (i.e., fibronectin-coated acrylamide hydrogels) also caused cell rounding, YAP/TAZ nuclear exclusion and proliferative inhibition (Figures 1F, 1G and S1J).

The remarkable phenotypic similarities between cells cultured in small, soft or dense conditions clearly suggest that these apparently different modalities to regulate YAP/TAZ may actually all correspond to the control of YAP/TAZ by mechanical cues. To address more directly the notion that in a multicellular layer the control of YAP/TAZ activity and cell proliferation occurs through mechanical cues, we developed a microdevice that reproduces some of the mechanical challenges experienced by tissues, such as stretching (Figure 2A and S2A-C). This microdevice was built by fabricating into polydimethylsiloxane silicone (PDMS) a microfluidic network of hollow channels connecting larger "chambers" filled with saline solution. The surface of PDMS was coated with ECM (fibronectin) to allow cell attachment. MECs were seeded on this surface at high cell density causing cells to exclude YAP/TAZ from nuclei and undergo CIP. Next, we slowly applied computer-controlled pressure to the system, imposing cells to radially stretch as the PDMS membrane overlaying each chamber inflated (Figure 2A). This applied strain increased the cell adhesive surface to 150%, as quantified from measurements of the cell-projected area (Figure 2B). This was associated to a remodeling of the F-actin cytoskeleton with appearance of phalloidin-positive actin bundles in stretched cells (Figure S2D). Remarkably, stretched cells rapidly reactivated YAP/TAZ, as monitored by nuclear localization, and re-entered S-phase (Figure 2C and 2D). Based on these experiments we conclude that mechanical forces acting on specific areas of an epithelial sheet reflect into changes of shape and mechanics of the individual cells, and act as spatially localized determinants of cell proliferation through YAP/TAZ regulation.

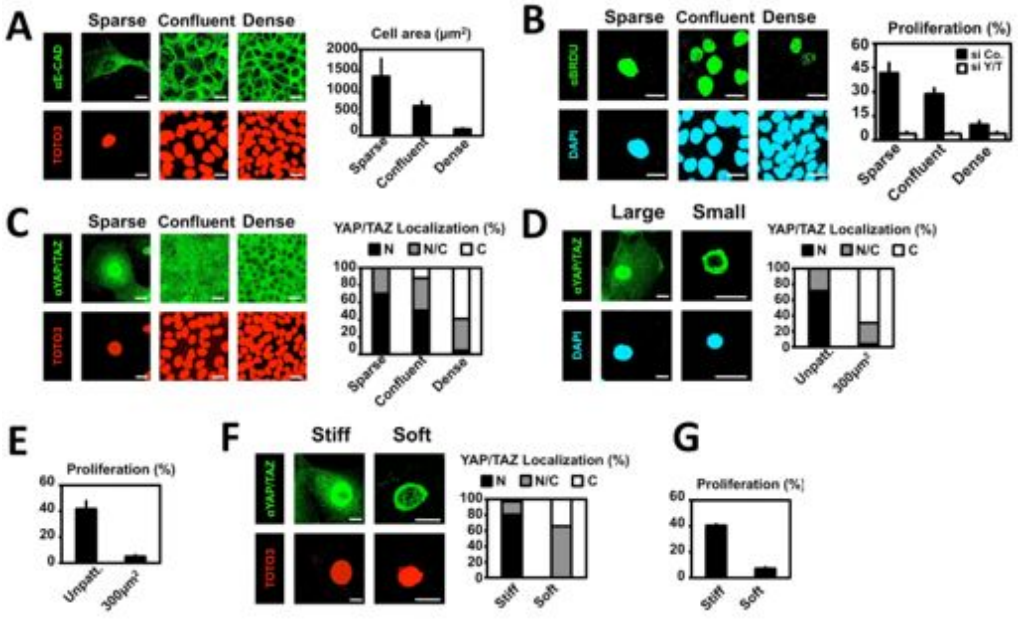

Figure B.3.1 – High Cell Density, Small Cell Geometry, and Soft ECM All Lead to Restriction of Cell Area, YAP/TAZ Relocalization, and Growth Arrest (A) Cells plated at different densities display increasingly smaller cell-substrate adhesion areas. MECs were seeded to obtain sparse cells and confluent or dense monolayers. After 2 days, cells were fixed for immunofluorescence with anti- E-cadherin antibody (anti-E-CAD) to visualize formation of cell-cell contacts by confocal microscopy. TOTO3 is a nuclear counterstain. Scale bar, 20 mm. (Right) Average cell area in the three seeding conditions. Similar results were obtained with HaCaT keratinocytes (Figure S1C). (B) MECs were plated as in (A); after 2 days, cells were incubated for 1 hr with a pulse of BrdU to label cells undergoing DNA duplication. Cells were fixed and processed for anti-BrdU immuno- fluorescence (aBRDU). (Right) Quantitation of proliferation measured as the percentage of BrdU-positive cells. Similar results were obtained with HaCaT keratinocytes (Figure S1D). Note minimal residual proliferation in dense cells, even after YAP/TAZ depletion, suggesting that cell proliferation in culture may not be totally dependent on YAP/TAZ. (C) MECs were plated as in (A) and stained for immunofluorescence with anti-YAP/TAZ antibody (aYAP/TAZ). TOTO3 is a nuclear counterstain. Scale bar, 20 μm. (Right) Proportion of cells dis- playing preferential nuclear YAP/TAZ localization (N, black), even distribution of YAP/TAZ in nucleus and cytoplasm (N/C, gray), or cytoplasmic YAP/ TAZ (C, white). Similar results were obtained with HaCaT keratinocytes (Figure S1E) and with an in- dependent anti-YAP antibody (not shown). (D and E). Restricting cell-substrate adhesion area to levels comparable to those of dense cells is sufficient to cause YAP/TAZ nuclear exclusion and inhibition of proliferation. MECs were seeded as individual cells plated on fibronectin-coated glass (large) or on square microprinted fibronectin islands of 300 mm^2 (small). In (D), cells were fixed after 1 day for immunofluorescence with anti-YAP/ TAZ antibody (aYAP/TAZ). DAPI is a nuclear counterstain. Scale bar, 20 μm. (Right) YAP/TAZ nucleo/cytoplasmic localization was scored as in (C). In (E), cells were processed for BrdU incorporation as in (B). (F and G) Effects of a soft ECM substrate on epithelial proliferation. Confocal immunofluorescence images of YAP/TAZ of MECs plated on fibronectin-coated stiff (plastic) and soft (acrylamide hydrogels of 0.7 kPa) substrates. TOTO3 is a nuclear counterstain. Scale bar, 20 mm. On the right: YAP/TAZ nucleo/cytoplasmic localization was scored as in (C). In (G) cells were processed for BrdU incorporation as in (B). Similar results were obtained using acrylamide hydrogels of 40 kPa or plastics (Dupont et al., 2011 and data not shown). Data are mean and SD. Experiments were per- formed at least three times with three biological replicates each time. Quantitations were carried out by scoring at least 2,000 cells for each sample. Pictures show representative results. See also Table S1 for siRNA sequences and Figure S1.

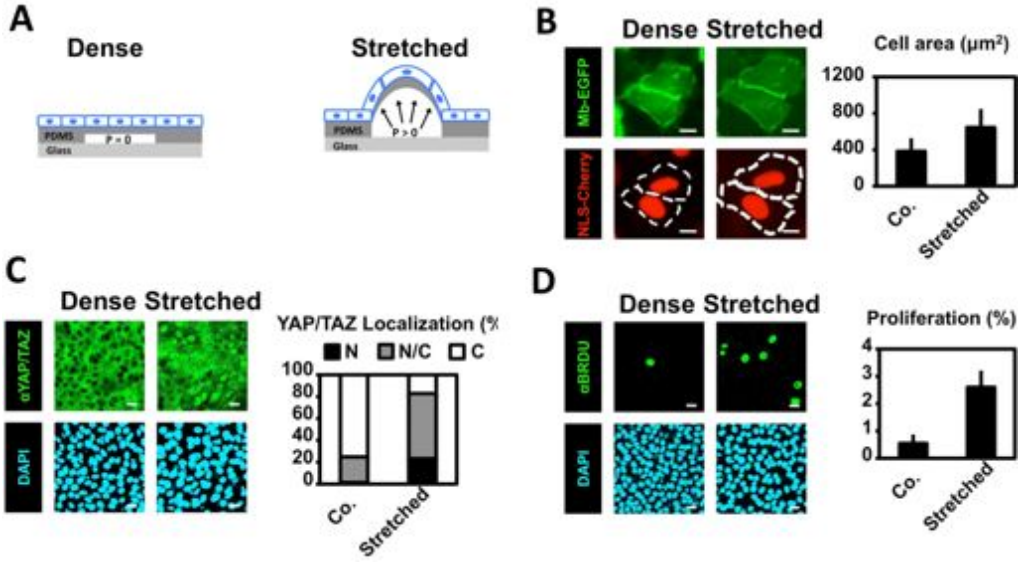

Figure B.3.2 – Stretching of an Epithelial Mono- layer Overcomes YAP/TAZ Inhibition and Growth Arrest in Contact-Inhibited Cells (A) A monolayer stretching device. Cells were seeded on the upper surface of a PDMS substrate to obtain a dense monolayer (see also Figure S2A). Underneath the PDMS is a chamber filled of fluid (white space between the PDMS and glass). At atmospheric pressure (dense, p = 0), the cell monolayer remains flat; when pressure is applied to the fluid inside the chamber (stretched, p > 0), the increase of the chamber volume causes a corresponding increase of the surface to which the monolayer is attached. (B) MECs stably expressing membrane-bound EGFP (Mb-EGFP) and nuclear-localized mCherry (NLS-Cherry) were seeded at dense conditions as in Figure 1A on top of the stretching device. After 2 days, cells were imaged under the epifluorescent microscope before (Co.) and immediately after stretching. Pressure was then maintained constant during observation. Projected cell area was measured in the two conditions (dashed lines in the lower pictures indicate the cell boundaries before and after stretching). The graph shows the average quantitation of cell area. The ramping of pressure increase was set in order to avoid destruction of cell-cell contacts (as monitored with Mb-EGFP; data not shown). Scale bar, 20 mm. (C) MECs were plated on the stretching device as in (B). After 2 days, cells were subjected to 6 hr of static stretching, fixed with the device still under pressure, and then processed for immunofluorescence with anti-YAP/TAZ antibody (aYAP/TAZ). DAPI is a nuclear counterstain. Scale bar, 20 mm. (Right) Proportion of cells displaying preferential nuclear YAP/TAZ localization (N, black), even distribution of YAP/TAZ between the nucleus and the cytoplasm (N/C, gray), or prevalently cytoplasmic YAP/TAZ (C, white). Similar results were obtained after 3 hr of stretching (not shown). (D) MECs were plated on the stretching device as described in (B). After 2 days, cells were subjected to 6 hr of static stretching in the presence of BrdU to label cells undergoing DNA duplication. Scale bar, 20 mm. (Right) Quantitation of proliferation measured as the percentage of BrdU-positive cells. Throughout the panels, data are mean and SD. Experiments were performed at least three times with at least three biological replicates each time. Quantitations were carried out by scoring at least 2,000 cells for each sample. Pictures show representative results. See also Figure S2.

B.3.1 F-actin capping and severing proteins are YAP/TAZ inhibitors

We next sought to identify molecular players involved in YAP/TAZ regulation by mechanical cues. F-actin regulatory proteins appeared as ideal candidates: treatments that disrupt F-actin or cytoskeletal contractility oppose YAP/TAZ function [11,23,19]; then, it is recognized that cells respond to external mechanical cues by adjusting the tension and overall organization of their actin cytoskeleton by engaging a plethora of actin-binding proteins [22]. Finally, cells plated on small ECM islands, on soft ECM or in a dense monolayer are characterized by similar F-actin organization, as they retain cortical F-actin, but all display reduced or absent F-actin bundles (Figure S2D and data not shown). We thus reasoned that knockdown of endogenous negative regulators of F-actin should restore cytoskeletal structures required for YAP/TAZ activity in inhibitory mechanical conditions. We selected a total of 62 genes identified as F-actin inhibitors in a genome-wide screen [24]. In order to specifically identify genes relevant for YAP/TAZ regulation by mechanical cues, we screened them using an unambiguous mechanotransduction assay, that is, the rescue of YAP/TAZ-dependent transcription on soft ECM substrates. MECs were transfected with two pairs of siRNAs for each F-actin inhibitor and seeded on soft hydrogels (approximating an elastic modulus of 0.7 kPa). Cells were harvested after 48 hours and analysed by qPCR for CTGF mRNA expression as read-out of YAP/TAZ activity (Figure 3A). Although most siRNAs were ineffective, few siRNAs reactivated CTGF expression to levels comparable to, or higher than, those of cells growing on a stiff matrix (Figure 3B). These candidates were then validated by using individual siRNAs and testing their effectiveness at activating multiple YAP/TAZ endogenous targets (CTGF, ANKRD1, CYR61); among the candidates, Cofilin1/2, Capzb and Gelsolin, well-established organizers of F-actin distribution and dynamics [25], stood out as potent YAP/TAZ inhibitors (Figure 3C and S3A and data not shown). Cofilin and Gelsolin (also known as Actin Depolymerizing Factors) increase the turnover of F-actin by severing microfilaments; after severing, Gelsolin remains attached to the newly formed barbed end, preventing filament annealing and polymerization. CapZ (also known as β-actinin or Capping Protein) shares with Gelsolin such actin-capping function [25]. Most of what we know about Cofilin, Gelsolin

and CapZ in mammalian cells is based on cell migration studies, particularly in the context of dynamic cell protrusions, or from in vitro studies [25], while little data is available on their role in other relevant biological processes. In sparse MECs, depletion of Cofilin, CapZ and Gelsolin caused a general increase in F-actin staining, with particularly thickened stress-fibers, and increased peripheral protrusions resembling filopodia and lamellipodia (Figure 3D and S3B). Supporting the notion that F-actin capping and severing proteins do work through F-actin modification to regulate YAP/TAZ, we found that CapZ depletion could not increase YAP/TAZ activity in cells treated with LatrunculinA, an F-actin inhibitory drug (Figure S3C). To further dissect which subset of the F-actin networks is relevant for YAP/TAZ activity we treated cells with chemical inhibitors of formins (SMIFH2) or ARP2/3 (CK666; CK869; see Supplemental Information for details): these compounds preferentially inhibit formation of F-actin bundles (formin-dependent), or of F-actin branched networks that sustain lamellipodia formation (ARP-dependent). qPCR for CTGF indicated that YAP/TAZ activity mostly depends on F-actin bundles (Figure 3E). Taken together, the results link mechanical regulation of YAP/TAZ activity to F-actin capping/severing proteins and formation of stress fibers. We next used F-actin capping/severing proteins as tools to further query the nature of YAP/TAZ inhibition by cell density. Depletion of Cofilin, CapZ or Gelsolin rescued formation of stress fibers as well as YAP/TAZ nuclear localization, TAZ protein stability and YAP/TAZ-dependent gene expression in dense cells (Figures 4A-C, S4A and S4B). These findings support the notion that control of YAP/TAZ by high cell density entails a mechanical and cytoskeletal regulation.

B.3.2 Role of YAP/TAZ and F-actin inhibitors in mechanical patterning of cell proliferation

Next, we wondered whether YAP/TAZ reactivation by depletion of F-actin capping and severing proteins is also paralleled by a rescue of CIP. To address this question, we employed microfabrication methods to stamp fibronectin-coated substrates of defined shape and area. This set-up allows studying how patterns of mechanical forces generate patterned growth within a monolayer: cells located at the borders

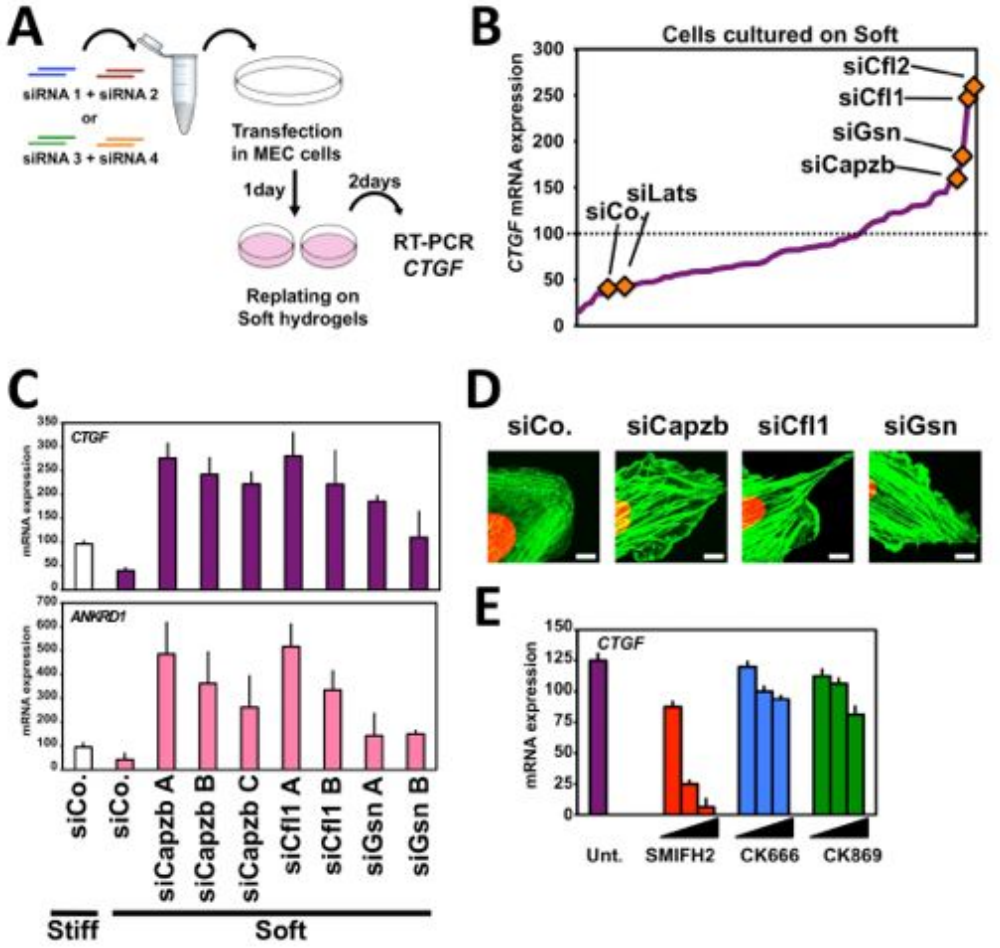

Figure B.3.3 – CapZ, Cofilin, and Gelsolin Inhibit YAP/TAZ Activity (A and B) siRNA screen for negative regulators of the F-actin cytoskeleton impinging on YAP/TAZ activity. (A) Schematic overview of the screening procedure. MECs were transfected with two independent couples of siRNAs against each gene (siRNA 1+2 or siRNA 3+4). The day after transfection, cells were replated as single cells on a soft ECM hydrogel (0.7 kPa) and harvested after 2 more days for qPCR analysis. (B) Results of the screening, where each point of the purple line corresponds to a single siRNA/gene. The orange diamonds indicate the effects of controls and of selected siRNAs that were further validated (see text). Cfl, Cofilin; Gsn, Gelsolin. The dotted line represents CTGF levels in cells transfected with siControl (siCo.) but plated on a stiff ECM substrate. Here and throughout the figures, CTGF levels are relative to GAPDH expression. (C) Loss of capping and severing proteins rescues YAP/TAZ inhibition on soft ECM. CTGF (purple) and ANKRD1 (violet) expression in MECs are independent readouts of YAP/TAZ transcriptional activity. Cells were transfected with single siRNA against each gene (A, B, or C). Stiff (white column) is a stiff ECM substrate; soft (colored columns) is a 0.7 kPa ECM hydrogel. See Figure S3A for knockdown efficiencies on endogenous proteins. (D) Loss of Capzb, Cfl1, and Gsn induces formation of thicker actin bundles. Close-up confocal immunofluorescence of MECs transfected with the indicated siRNA and stained for F-actin with phalloidin (green) and nuclei (TOTO3, red). Scale bar, 20 μm. See Figure S3B for increased filopodia and lamellipodia after Capzb, Cfl1, and Gsn knockdown. Consistent results were obtained with independent siRNAs (not shown). (E) Regulation of F-actin dynamic and assembly by formin proteins is required for YAP/TAZ activity. MECs were plated on a stiff ECM substrate and treated for 24 hr with increasing doses of the inhibitor of formin-homology 2 domains SMIFH2 (used at 5, 15, 30 μM) or of the Arp2/3 inhibitors CK666 (5, 10, 50 mM) and CK869 (5, 10, 50 μM). Data are mean and SD. Experiments were performed three times with at least three biological replicates each time. See also Figure S3 and Tables S1 and S2.

of the island experience higher mechanical stress than cells located in the center [26]. MECs were uniformly seeded at high density on circular islands and, after 48 hours, cell proliferation rate was assayed by BrdU incorporation (Figure S4C). As shown in Figure 4D, the number of cells in S-phase greatly decreased in the center of the island but persisted at the border, matching the distribution of physical forces [26]. Knockdown of YAP and TAZ revealed that proliferation at the border was YAP/TAZ dependent (Figure 4D). This growth pattern - as previously noticed [26] - was driven by tensional forces, since inhibition of non-muscle myosin II with blebbistatin, or of myosin light chain kinase with ML-7, greatly reduced proliferation at the culture borders, phenocopying attenuation of YAP/TAZ (Figure 4D). Strikingly, depletion of CapZ and Cofilin clearly prevented CIP in center cells. Importantly, this occurred without increasing the growth of cells at the border, thus partially leveling the growth differentials within the epithelial sheet (Figure 4D). The restoration of proliferation by depletion of capping and severing proteins was dependent on YAP and TAZ (Figure 4D). We obtained similar results by seeding cells on square-shaped islands, where YAP/TAZ-dependent proliferation was concentrated at corners and edges (Figures S4D, S4E and data not shown). The above results suggest that the form of an epithelial monolayer generates patterns of tensional forces that translate into differentials of YAP/TAZ activity, whose establishment requires F-actin inhibitors. Yet, in vivo, distinct tissues not only exhibit specific shapes, but also their ECM composition varies greatly, due to the content, crosslinking and topology of collagen fibers [27]. To mimic such integration, we investigated the roles of YAP/TAZ, and F-actin capping and severing proteins, on the behavior of MECs growing in three dimensions (3D). For this, we used reconstituted ECM containing a mix of basement membrane (BM; Matrigel) and collagenI (COL), whose concentration can be changed to obtain soft and stiff BM/COL gels (COL 1.2 mg/ml or 3 mg/ml, respectively) [28] (see Figure S5A for validation of these gel compositions as mechano-regulators of YAP/TAZ). After 8 days in culture, MECs growing embedded in soft BM/COL gels formed growth-arrested acini (Figure 5A). When collagen concentration was increased, we observed the formation of larger spheroids, actively growing tubules and organoid-like structures (Figure 5A). By immunofluorescence,

YAP/TAZ were predominantly evenly distributed in cells cultured in soft ECMs, but were clearly nuclear in cells embedded in the stiffer ECM (Figure 5B). Transcriptional activation of YAP/TAZ by increased ECM stiffness in 3D cultures was confirmed by induction of endogenous markers, such as CTGF, CYR61 and ANKRD1 mRNAs (Figure S5B). siRNA-mediated knockdown of YAP and TAZ caused severe reduction of the overall number and size of the 3D colonies, that in no case expanded beyond small aggregates, regardless of substrate rigidity (data not shown). We next sustained endogenous YAP/TAZ activity in cells embedded in the soft ECM through siRNA-mediated knockdown of Cofilin or Gelsolin. Strikingly, this induced the formation of bigger acini and caused the appearance of elongated or branched structures (Figure 5C) and was paralleled by YAP/TAZ-dependent induction of CTGF and CYR61 mRNAs (Figure 5D). Using phospho-histone-3 as proliferation marker, acini transfected with control-siRNA were mainly growth arrested, while Cofilin or Gelsolin-depleted spheroids retained proliferative activity (Figure 5E). We conclude that YAP/TAZ regulation by F-actin capping and severing proteins plays a critical role in regulating the growth of epithelial cells in a 3D reconstituted ECM.

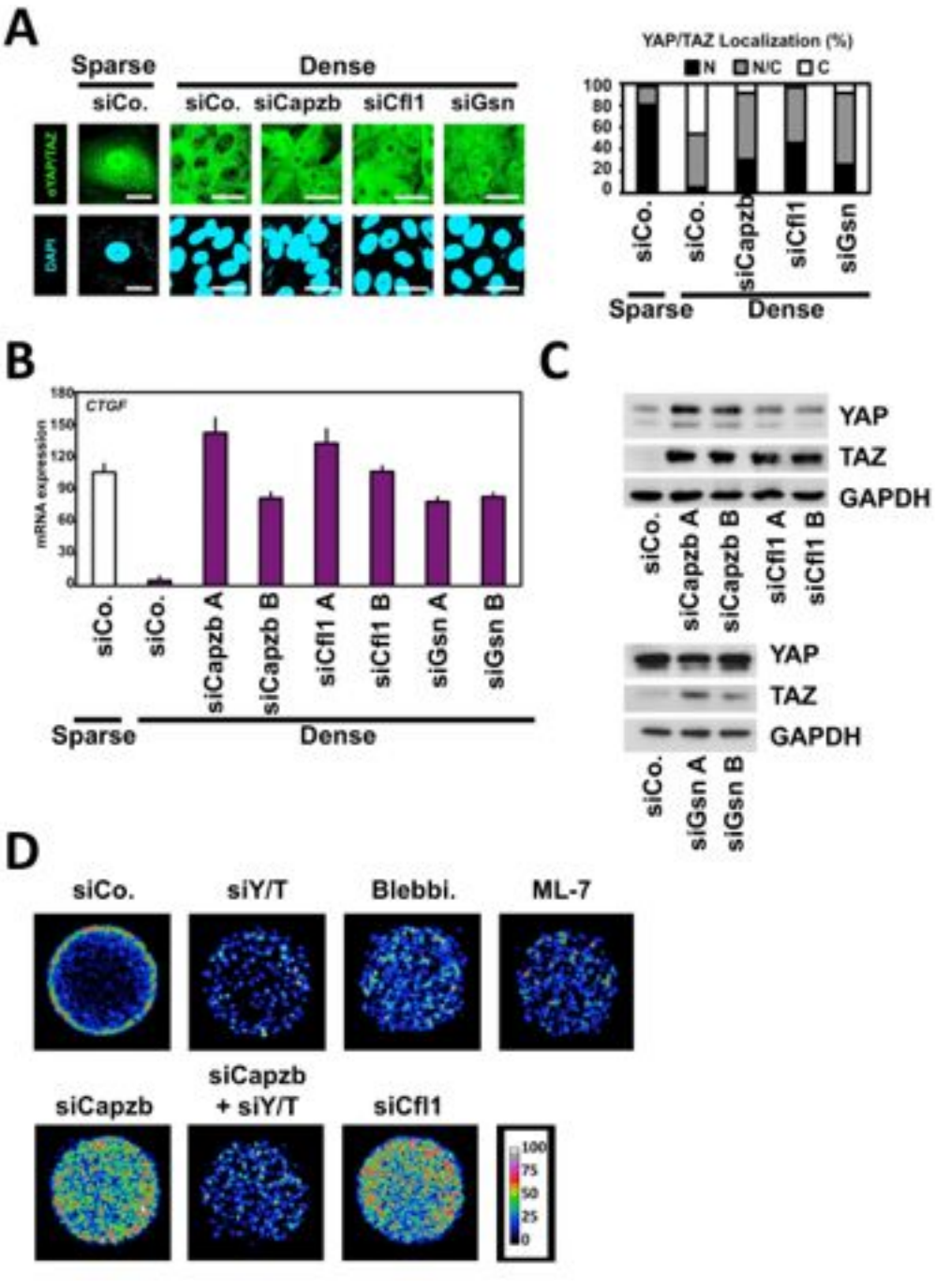
A
Sparse
Dense
siCo.
siCo.
siCapzb
siCfl1
siGsn
αYAP/TAZ
DAPI
YAP/TAZ Localization (%)
N
N/C
C
100
80
60
40
20
0
siCo.
siCo.
siCapzb
siCfl1
siGsn
Sparse
Dense
B
CTGF
mRNA expression
180
150
120
90
60
30
0
siCo.
siCo.
siCapzb A
siCapzb B
siCfl1 A
siCfl1 B
siGsn A
siGsn B
Sparse
Dense
C
YAP
TAZ
GAPDH
siCo.
siCapzb A
siCapzb B
siCfl1 A
siCfl1 B
YAP
TAZ
GAPDH
siCo.
siGsn A
siGsn B
D
siCo.
siY/T
Blebbi.
ML-7
siCapzb
siCapzb
+ siY/T
siCfl1
100
75
50
25
0

Figure B.3.4 – Knockdown of F-Actin-Capping and -Severing Factors Rescues Contact Inhibition of Proliferation (A) Loss of Capzb, Cfl1, or Gsn rescues YAP/TAZ nuclear localization in dense monolayers. MECs were transfected with the indicated siRNA and were seeded to obtain sparse cells or a dense mono- layer. After 2 days, cells were fixed for immunofluorescence with anti-YAP/TAZ antibody (aYAP/ TAZ). DAPI is a nuclear counterstain. Scale bar, 20 μm. (Right) Proportion of cells displaying preferential nuclear YAP/TAZ localization (N, black); even distribution of YAP/TAZ between the nucleus and the cytoplasm (N/C, gray); or cytoplasmic YAP/ TAZ (C, white). Consistent results were obtained with independent siRNAs (not shown). (B) CTGF expression in MECs transfected and seeded as in (A). Loss of Capzb, Cfl1, and Gsn rescues YAP/TAZ transcriptional activity in dense monolayers. (C) Western blotting for TAZ and YAP in MECs transfected and seeded as in (A). GAPDH is a loading control. (D) Panels show colorimetric stacked images of BrdU incorporation, used to visualize spatial variations of proliferation in cell monolayers of defined shape and dimensions. MECs were plated as monolayers on large microprinted fibronectin islands (diameter, 350 μm) and processed as described in the text and as in the Figure S4C legend. The color scale indicates the extent of cell proliferation in a given position of the monolayers. The proliferation rate decreases to nearly undetectable levels at the center of the circle due to CIP (black/blue color), whereas cells continue proliferating along the border of the cellular sheet (green/ red color). Cultures were treated with blebbistatin (Blebbi, 50 μM) or myosin light-chain kinase inhibitor (ML-7, 10 μM) overnight before the BrdU pulse. For experiments with siRNAs, cells were first transfected with the indicated siRNA and were re- plated after 1 day. Similar results were obtained on islands of square shape (Figures S4D and S4E). Data are mean and SD. Experiments were per- formed at least twice with biological replicates each time. Quantitations were carried out by scoring at least 2,000 cells for each sample. Pictures show representative results. See also Figure S4 and Table S1.

B.3.3 Cytoskeletal regulation of YAP/TAZ dominates over Hippo signaling

We next sought to investigate the intersections between the control of YAP/TAZ activity by cytoskeletal cues and the classical Hippo cascade, centered on the activity of two kinases, MST1/2 (Hippo in Drosophila) and LATS1/2, the latter directly phosphorylating YAP/TAZ and causing their inhibition [12]. CIP has been associated to increased YAP/TAZ phosphorylation mediated by LATS1/2 [19]; similar phosphorylation occurs in cells rounded after placing them in suspension, or upon disruption of the F-actin cytoskeleton [29,23,19]. Fully confirming these associations, we also found increased YAP/TAZ phosphorylation in cells treated with LatrunculinA, an F-actin inhibitory drug (Figure 6A). YAP/TAZ phosphorylation, however, may not automatically surrogate for biological function, and no previous studies supported this biochemical observation with functional evidence [10]. To investigate the functional role of LATS, we used independent pairs of validated siRNAs targeting both LATS1 and LATS2. We first controlled the efficacy of LATS-depletion by reconstituting

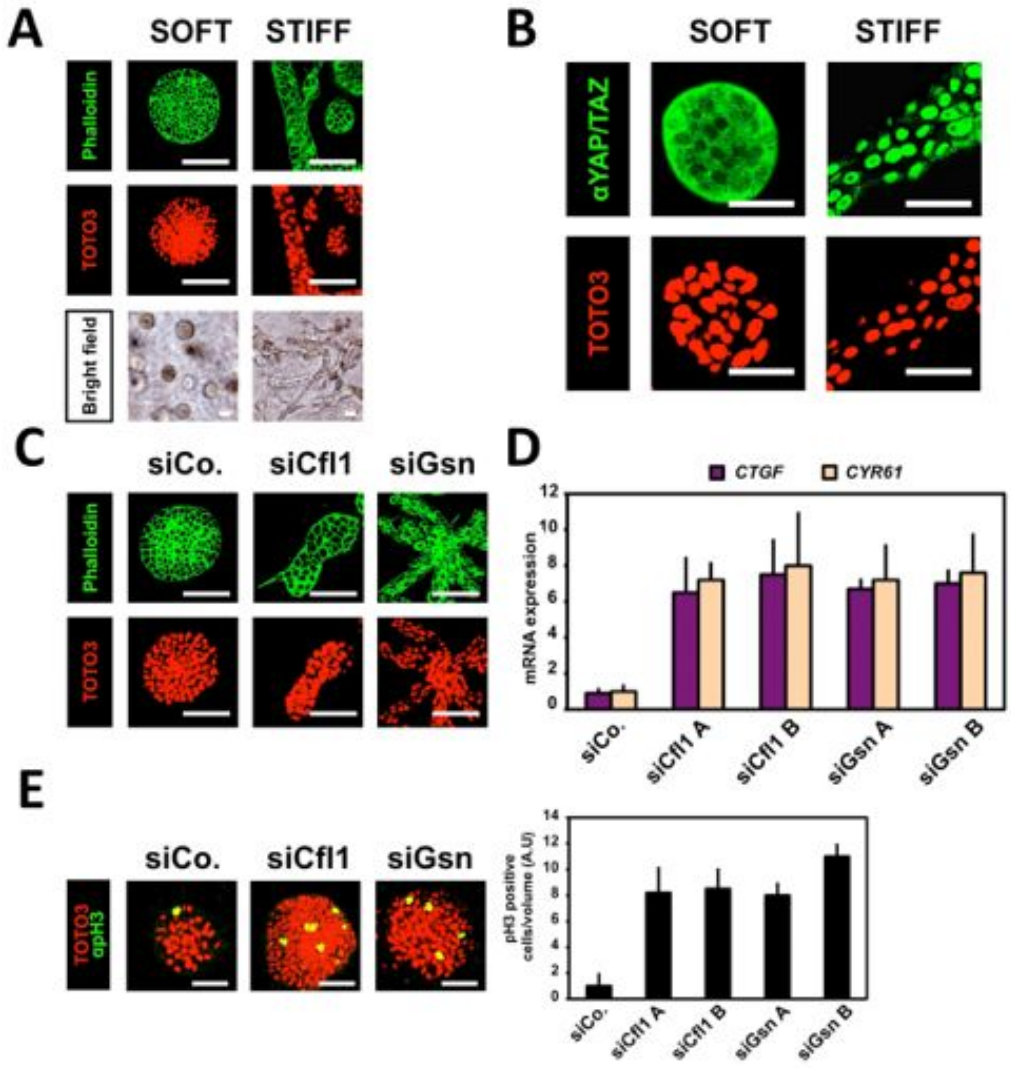

Figure B.3.5 – 3D Matrix Stiffness Regulates Growth and Morphogenesis of Mammary Epithelial Cells through YAP/TAZ (A) Mammary epithelial cells (MECs) were embedded as a single cell in a matrix formed of a different mixture of Matrigel and CollagenI (see Experimental Procedures). Soft matrix contained 1.2 mg/ml CollagenI, whereas stiff matrix contained 3 mg/ml CollagenI [36]. After 8 days, cells were fixed and stained for phalloidin to help visualize the morphology of multicellular structures. TOTO3 is a nuclear counterstain. Scale bar, 100 μm. Bottom panels show bright fields at lower magnification. (B) 3D matrix density regulates YAP/TAZ localization, as assayed by confocal immunofluorescence with anti-YAP/TAZ antibody (aYAP/TAZ). MECs were plated as in (A) and were fixed after 6 days. TOTO3 is a nuclear counterstain. Scale bar, 100 μm. (C) Loss of Cfl1 and Gsn promotes the formation of tubule-like structures in soft 3D matrix. MECs were transfected with the indicated siRNAs and then embedded in soft matrix as in (A). After 8 days, acini were fixed and stained for phalloidin. TOTO3 is a nuclear counterstain. Scale bar, 100 μm. (D) Loss of Cfl1 and Gsn increases YAP/TAZ transcriptional activity in soft 3D matrix. MECs were treated as in (C) and were harvested for qPCR of the YAP/TAZ target genes CTGF and CYR61. (E) Loss of Cfl1 and Gsn promotes proliferation of cells embedded in 3D soft matrix. MECs were treated as in (C) and were stained with anti-pH3 antibody to mark mitotic cells. pH3 signal is shown merged with the TOTO3 nuclear counterstaining. Scale bar, 100 μm. (Right) Quantitation of cell mitosis normalized to the volume of the multicellular structures, as calculated from 3D z stacks reconstructions. Data are mean and SD obtained from at least 20 structures per condition. Data are mean and SD. Experiments were performed at least twice with biological replicates each time. Pictures show representative results. See also Figure S5 and Table S1.

NF2 expression, a bona fide upstream regulator of the Hippo cascade, in the NF2-null breast cancer cell line MDA-MB-231 [11]. NF2 re-expression caused a dramatic inhibition of TEAD luciferase reporter and LATS1/2 inactivation completely abolished this effect, confirming the efficacy of our siRNAs (Figure 6B). Similarly, NF2 re-expression was completely ineffective in cells expressing only a LATS-insensitive, phosphorylation mutant form of YAP or TAZ (Figure S6A and data not shown). Next, we wondered if LATS1/2 were downstream of mechanical cues. If this were the case, as in the above NF2 paradigm, loss-of-LATS1/2, or loss-of-YAP/TAZ phosphorylation, should also rescue YAP/TAZ activity in cells on soft ECM or dense cultures. In stark contrast to this hypothesis, the results for mechanical regulation were different: depletion of LATS1/2 could not rescue YAP/TAZ inhibition by a soft environment (Figures 6C), indicating that F-actin and mechanical regulation affect YAP/TAZ activity independently from their phosphorylation by LATS. In line, cells expressing only LATS-insensitive YAP or TAZ mutants (5SA-YAP, 4SA-TAZ) did not escape mechanical inhibition when cultured on soft hydrogels (Figure S6B and S6C). Using CapZ inactivation as paradigm of cytoskeletal remodeling, we also found that cells expressing 4SA-TAZ were still responding to depletion of CapZ (Figure S6D). Finally, knockdown of CapZ left the YAP/TAZ phosphorylation levels completely unchanged, as shown by Phos-TAG analysis (Figure 6D); collectively, the results strongly suggest that YAP/TAZ control by the F-actin cytoskeleton and Hippo signaling represent formally distinct regulations. An unexpected discovery came when we simultaneously inactivated CapZ together with LATS1/2 in MECs cultured in soft or dense conditions. The results actually showed that LATS1/2 are effective inhibitors of YAP/TAZ only in the context of a mechanically competent F-actin cytoskeleton. Several results support this conclusion: (i) combined depletion of CapZ and LATS1/2 cooperated to fully induce nuclear localization of YAP and TAZ in cells seeded on soft hydrogels and dense conditions (Figure 6E and 6F); (ii) LATS1/2 depletion in either soft or dense MEC cultures was inconsequential per se but potently synergized with CapZ depletion to maximize YAP/TAZ transcriptional activity (Figure 6G and 6H); (iii) in large square (or round) fibronectin-coated islands, LATS1/2 depletion alone could not rescue CIP (Figure 6I, S6E, S6F), and

left proliferation of cells at the border still sensitive to inhibitors of cytoskeletal tension (Figure S6E). However, combined depletion of CapZ and LATS1/2 fully rescued the blockade of S-phase entry in cells located at the center of the epithelial sheets triggering unabated proliferation evenly throughout the island (Figure 6I and S6F). We next tested how loss of YAP/TAZ regulation by the Hippo kinases impacted on MECs growing in 3D within a soft or stiff ECM. To this end, we compared MECs stably expressing near to endogenous levels of wild-type TAZ, and LATS phosphorylation-insensitive 4SA-TAZ. As shown in Figure 6J, wild-type TAZ expressing cells behaved similarly to their parental counterparts. 4SA-TAZ expressing cells displayed increased protrusive activity in soft ECM, yet retained a spheroid structure. Notably, in the more rigid ECM, 4SA-TAZ expressing cells did not form tubular structures and invaded the matrix as single cells. As TAZ overexpression has been shown to induce Epithelial-to-Mesenchymal Transition in cells cultured on plastic in 2D [30], this 3D phenotype likely reflects fully unleashed TAZ activity. Finally, we asked if the permissive effect of the cytoskeleton is specific for the Hippo pathway or also applies to other regulatory inputs. To this end, we used two inducers of YAP/TAZ, WNT and GPCR signaling [16,17], and monitored their efficacy in soft vs. stiff extracellular conditions. As shown in Figure 6K, knockdown of APC (mimicking WNT signaling by inactivation of the APC/Axin/GSK3 TAZ destruction complex [16]) caused robust upregulation of YAP/TAZ-dependent transcription in cells cultured on stiff substrates, but had minimal effect in cells seeded on a soft matrix. Similarly, addition of TRAP6, a positive inducer of YAP/TAZ activity through GPCR-signaling, could operate only in cells cultured on stiff, but not on soft matrices (Figure 6L). Remarkably, depletion of capping and severing proteins re-empowered YAP/TAZ activation by WNT and GPCR signaling (Figures 6K, 6L and data not shown). Collectively, the results suggest that mechanical and physical properties of the environment control not just Hippo signaling but also YAP/TAZ responsiveness to signaling cascades initiated by soluble growth factors.

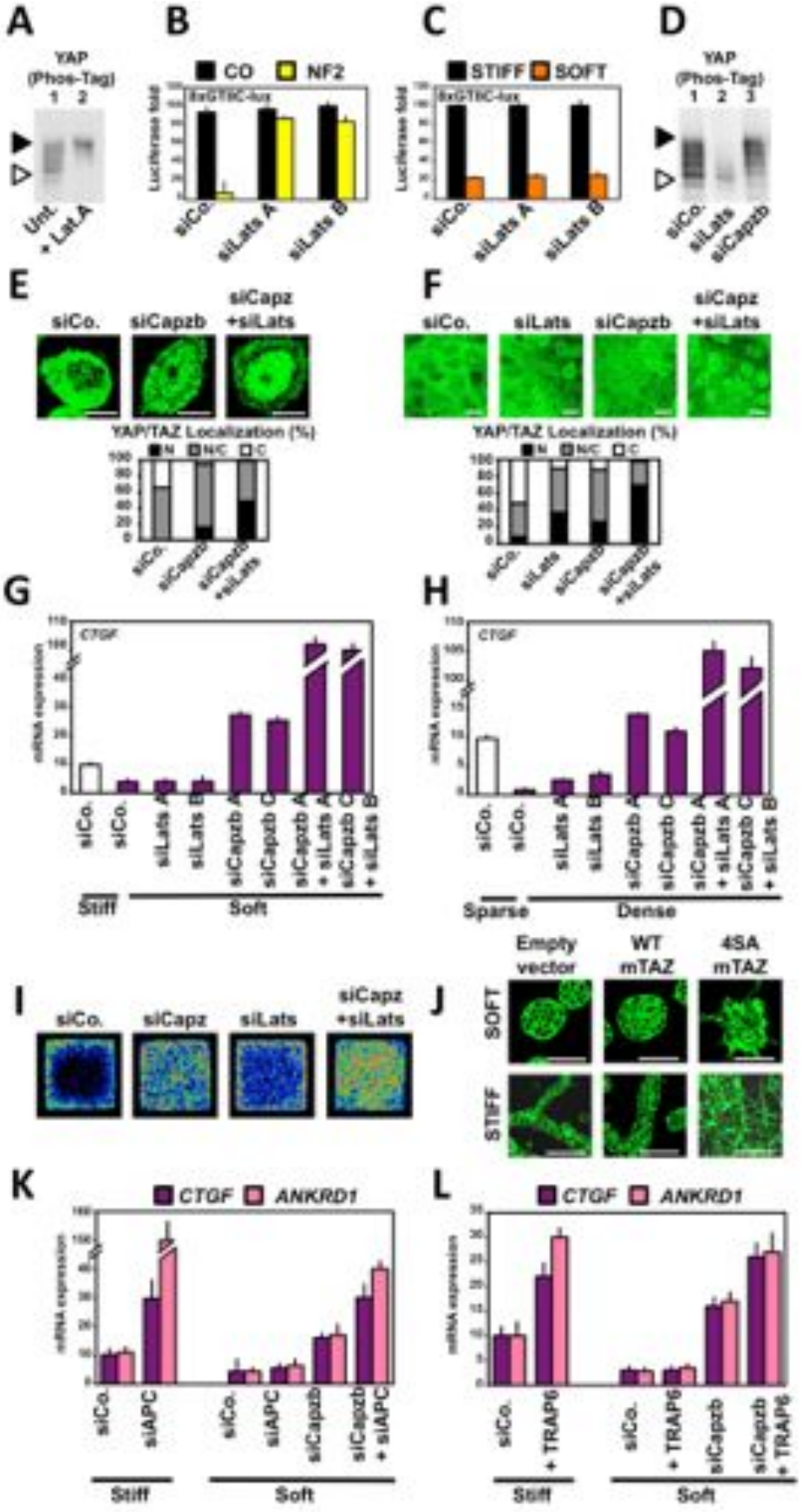
A
YAP
(Phos-Tag)
1 2
Unt.
+ LatA
B
CO
NF2
8xGTIIC-lux
Luciferase fold
siCo.
siLats A
siLats B
C
STIFF
SOFT
8xGTIIC-lux
Luciferase fold
siCo.
siLats A
siLats B
D
YAP
(Phos-Tag)
1 2 3
siCo.
siLats
siCapzb
E
siCo.
siCapzb
siCapz
+siLats
YAP/TAZ Localization (%)
N
N/C
C
siCo.
siCapzb
siCapz
+siLats
F
siCo.
siLats
siCapzb
siCapz
+siLats
YAP/TAZ Localization (%)
N
N/C
C
siCo.
siLats
siCapzb
siCapz
+siLats
G
CTGF
mRNA expression
siCo.
siCo.
siLats A
siLats B
siCapzb A
siCapzb C
siCapzb A
+ siLats A
siCapzb C
+ siLats B
Stiff
Soft
H
CTGF
mRNA expression
siCo.
siCo.
siLats A
siLats B
siCapzb A
siCapzb C
siCapzb A
+ siLats A
siCapzb C
+ siLats B
Sparse
Dense
I
siCo.
siCapz
siLats
siCapz
+siLats
J
Empty
vector
WT
mTAZ
4SA
mTAZ
SOFT
STIFF
K
CTGF
ANKRD1
mRNA expression
siCo.
siAPC
siCo.
siAPC
siCapzb
siCapzb
+ siAPC
Stiff
Soft
L
CTGF
ANKRD1
mRNA expression
siCo.
+ TRAP6
siCo.
+ TRAP6
siCapzb
siCapzb
+ TRAP6
Stiff
Soft

Figure B.3.6 – Cytoskeletal Mechanics Is a Dominant Input for YAP/TAZ Activity. (A) Disruption of the F-actin cytoskeleton induces YAP phosphorylation. Phos-TAG SDS-PAGE analysis of MECs plated as confluent monolayer and treated with LatrunculinA (Lat.A, 100 μM) for 3 hr. Black and white arrowheads indicate hyperphosphorylated or nonphosphorylated YAP, respectively. Identity of YAP isoforms was defined based on extracts from cells transfected with YAP siRNA and on l-phosphatase treatment (not shown). (B) LATS1/2 knockdown completely rescues YAP/ TAZ inhibition by NF2/Merlin. Luciferase reporter assay (8XGTIIC) in MDA-MB-231 transfected with the indicated siRNA and without (Co.) or with NF2 expression plasmid. See Figure S6A for similar results obtained with LATS-insensitive 5SA-YAP mutant. Similar results were obtained in HeLa cells (not shown). (C) LATS1/2 knockdown does not rescue YAP/ TAZ inhibition by soft ECM. Luciferase reporter assay (8XGTIIC) in MDA-MB-231 cells transfected with the indicated siRNA and replated on stiff or soft ECM substrates. See Figure S6B for similar results obtained with LATS-insensitive 5SA-YAP mutant. Similar results were obtained in HeLa cells (not shown). Of note, inhibition of LATS by constitutive-activation of PI3K or AKT (Fan et al., 2013), known for being downstream of integrin signaling, could not rescue YAP/TAZ inhibition by soft ECM; and inhibition of PI3K, AKT, and mTOR by small-molecule inhibitors had no effect on a stiff ECM (data not shown). (D) Capzb knockdown does not result in a decrease of YAP phosphorylation. Phos-TAG SDS-PAGE analysis of MECs transfected with the indicated siRNAs and plated as confluent mono- layers. Black and white arrowheads indicate hyperphosphorylated or nonphosphorylated YAP, respectively. (E) MECs were transfected with the indicated siRNAs and were plated on soft ECM substrates. After 2 days, cells were fixed for immunofluorescence with anti-YAP/TAZ antibody. Scale bar, 10 μm. (Below the pictures) Proportion of cells displaying preferential nuclear YAP/TAZ localization (N, black), even distribution of YAP/TAZ between the nucleus and the cytoplasm (N/C, gray), or prevalently cytoplasmic YAP/TAZ (C, white). Transfection of LATS1/2 siRNA alone had no significant effects on YAP localization (not shown). Consistent results were obtained with independent siRNAs (not shown). (F) MECs were transfected with the indicated siRNAs and were seeded to obtain a dense monolayer. After 2 days, cells were fixed for immunofluorescence with anti-YAP/TAZ antibody. Scale bar, 20 μm. (Below the pictures) Proportion of cells displaying preferential nuclear YAP/TAZ localization (N, black), even distribution of YAP/ TAZ between the nucleus and the cytoplasm (N/C, gray), or prevalently cytoplasmic YAP/TAZ (C, white). (G) MECs were transfected with the indicated siRNAs and were plated on stiff (white column) or soft (colored columns) ECM substrates. After 2 days, cells were harvested for qPCR analysis. LATS knockdown has no effects on a soft ECM but potently enhances CTGF transcription upon combined depletion of Capzb. Similar results were obtained with ANKRD1 and CYR61. (H) MECs were transfected with the indicated siRNAs and plated as sparse cells (white column) or dense monolayers (colored columns). After 2 days, cells were harvested for qPCR analysis. Similar results were obtained with ANKRD1 and CYR61.

(J) MECs were transfected with YAP/TAZ siRNA (to avoid interference from endogenous proteins) and reconstituted with siRNA-insensitive mouse TAZ (mTAZ). TAZ add-back was carried out with both WT and LATS-insensitive 4SA mTAZ. Cells expressing empty vector and transfected with control siRNA serve as controls. Cells were embedded as a single cell in a matrix formed of a different mixture of Matrigel and CollagenI to obtain softer and stiffer gels (see legend to Figure 5A and Experimental Procedures). After 6 days, cells were fixed and stained for phalloidin to help visualize the morphology of multicellular structures. Scale bar, 100 μm. (K and L) WNT and GPRC signaling efficiently promote YAP/TAZ-dependent transcription on soft substrates only after Capzb depletion. (K) MECs were transfected with control siRNA (siCo.), APC siRNA (siAPC) to activate WNT signaling, or with Capzb siRNA (siCapzb). Cells were plated on stiff or soft ECM substrates and were harvested after 2 days for qPCR of YAP/TAZ target genes (CTGF and ANKRD1). (L) MECs were transfected with the indicated siRNAs and were plated on stiff or soft ECM substrates. After 1 day, cells were serum starved overnight and were subsequently left untreated or treated with 2 μM TRAP6 for 3 hr. Data are mean and SD. Experiments were performed at least twice with biological replicates each time. Quantitations were carried out by scoring at least 2,000 cells for each sample. Pictures show representative results. See also Figure S6 and Table S1.

B.4 Discussion

How cell shape and tissue form connect with tissue function, growth and patterning is one of the most fascinating and least understood aspects of biology. Here we provide evidence that tissue shape and three-dimensional ECM compliance pattern the proliferative competence of an epithelial sheet. These inputs localize YAP/TAZ activity at sites of high mechanical stresses, and inhibit it where mechanical forces are minimal. Thus, YAP and TAZ regulation serves as link between tissue architecture and a key cellular function, that is, proliferation. YAP/TAZ inhibition entails a remodeling of the F-actin cytoskeleton mediated by F-actin capping and severing proteins, for which we reveal an essential role as proliferative checkpoints in mammalian epithelial sheets through YAP/TAZ regulation. The presently described connections appear to hold a number of implications for the biology of epithelial cells. For organ size control, tissue regeneration and homeostasis cells must be constantly informed of the size and shape of the whole organ (Discher et al., 2009; Huang and Ingber, 1999; Nelson and Bissell, 2006). This suggests that cells are able to perceive what happens many cell diameters away and respond to it with great spatial accuracy. Mechanical forces are ideally suited to serve as messenger of this global control, as it has been recently shown that forces display long-range and broad scale effects (Halder et al., 2012; Guo et al., 2012). Using monolayers of defined shape and size, here we show that patterns of mechanical stresses locally control YAP/TAZ

activity. At sites of low mechanical forces, that is, in contact-inhibited center cells, YAP/TAZ are inhibited by F-actin capping and severing proteins, as loss-of-CapZ or Cofilin potently rescues YAP/TAZ nuclear localization, transcriptional activity and proliferation. In contrast, cells at edges and corners of the same multicellular sheets display YAP/TAZ dependent proliferation induced by cytoskeletal contractility and, here, loss-of-CapZ or Cofilin has marginal effects.

Inactivation of capping and severing proteins is accompanied by reappearance of F-actin stress fibers. Conversely, YAP/TAZ inactivation is phenocopied by inhibiting formin and myosin, which by themselves are essential for stress fibers formation and cellular contractility. These data collectively suggest that mechanical forces promote YAP/TAZ activity at least in part by inhibiting capping and severing proteins. However, this does not exclude a different scenario, one in which YAP/TAZ are regulated independently by mechanical forces and capping/severing proteins; the latters may operate to unbalance the distribution of microfilaments to different, perhaps competing, F-actin pools (e.g. cortical F-actin, stress fibers and nuclear actin) endowed with different YAP/TAZ activating capacities. In other words, while this study unambiguously identifies endogenous F-actin capping and severing proteins as YAP/TAZ inhibitors, a more detailed picture of their function will necessarily require the unraveling of the precise mechanisms by which F-actin affects YAP/TAZ-dependent transcription as well as a more comprehensive understanding of cellular rigidity sensing. Classical experiments using transformed mammary epithelial cells grown as spheroids in three-dimensional ECM of distinct rigidities and compositions unequivocally showed that the physical properties of the matrix could lead to tumor cells "reversion" to a near normal phenotype, overriding oncogenic aberrations [5]. Conversely, ECM stiffening, and ensuing cytoskeletal tension, cooperate with oncogenes, and may even initiate aberrant proliferation [27]. Yet, how the microenvironment intercepts the malignant phenotype at the level of gene-expression is a major question in cancer biology. Here we show that transformed mammary epithelial cells grown in low-collagen 3D environments display low levels of YAP/TAZ activity, while collagen-rich matrices induce YAP/TAZ nuclear localization, YAP/TAZ target genes and YAP/TAZ dependent proliferation. These observations are consis-

tent with the positive correlations between collagen content and tissue stiffness (as determined by mammographic density) with breast cancer risk and metastasis [27]. Here we show that F-actin capping and severing proteins are instrumental for the effects of a soft ECM, as their depletion induces YAP/TAZ activation and proliferation, phenocopying the attributes of a more rigid ECM environment. This work also provides a unifying principle for how contact inhibition of proliferation is realized. We propose a two-step model of this classic phenomenon [18]. As cells engage in cell-cell adhesion - starting from a situation of unrestricted adhesive areas with fully nuclear YAP/TAZ - the E-cadherin/catenins system triggers LATS activation and YAP/TAZ phosphorylation, as previously reported [21,32], but this is insufficient for overt growth arrest. Then, as proliferation continues, cell crowding causes reduction of cell size and low mechanical stress, now leading to a more effective contact inhibition. We show that the regulation of YAP/TAZ by cell mechanics is not only distinct from Hippo pathway-induced YAP/TAZ phosphorylation and inhibition, but in fact dominates over it. Remarkably, LATS1/2 inactivation is per se inconsequential in cells experiencing a low mechanical stress. Moreover, depletion of F-actin capping/severing proteins sustains YAP/TAZ activity without affecting their phosphorylation. In fact, LATS-mediated inhibition of YAP/TAZ requires a mechanically competent cytoskeleton, as the effect of LATS knockdown becomes manifest only in the absence of F-actin capping/severing proteins. Our finding that LATS and F-actin organization act independently to regulate YAP/TAZ is also supported by genetic evidence in Drosophila [33,34]. In fly wing development, inactivation of the CapZ homologue induces organ overgrowth similarly to Hippo mutations, and the extent of this phenotype can be either counteracted or amplified, respectively by overexpression or inactivation of LATS, altogether making unlikely an epistatic relationship between the two inputs. Our data further suggest that the scale of activation of YAP/TAZ may be particularly broad, depending on the relative intensity and duration of cytoskeletal and Hippo controls. There is ample genetic evidence for the Hippo pathway as an intrinsic regulator of organ size; for example, inactivation of the upstream Hippo kinase MST1/2, or of its cofactor Salvador/WW45, causes remarkable tissue overgrowth in several organs, including liver, intestine and skin [35].

According to our findings, the effect of a Hippo pathway mutation should not indiscriminately affect all cells, but preferentially expand the cell populations experiencing a mechanical stress. The existence of a second control layer for YAP/TAZ activity overseeing the effects of an Hippo mutation is supported by in vivo observations: in the liver, YAP/TAZ hyperactivation by Hippo deficiencies generates a functional and histologically well-organized organ [35], a finding incompatible with global and uncontrolled cell proliferation. Similarly, in the α-catenin knockout mouse model, YAP activation remains spatially restricted to the basal layer of the skin, where YAP protein is normally confined [20], suggesting that cell attachment to the appropriate ECM is instrumental to locally sustain normal as well as aberrant YAP activation. Finally, the idea that the cytoskeleton is a key input for YAP/TAZ in vivo is supported by recent genetic evidence: kidney development requires YAP activation by the CDC42 Rho-GTPase, well known promoter of F-actin polymerization.

Besides the Hippo pathway, mechanical cues also dominate the cellular response to soluble cues positively affecting YAP and TAZ activity. We show that YAP/TAZ activation by WNT or GPCR signaling requires a mechanically stressed cytoskeleton, or, in cells experiencing a soft ECM, inactivation of F-actin capping and severing proteins. In the same line of thought, the fact that YAP/TAZ are stabilized and act in stem and progenitor cells, typically lodged in specific tissue-niches [35], is an enticing argument that the status of the ECM, the cell's cytoskeletal organization and tension may impart a "physical" competence for stemness and differentiation.

B.5 Experimental procedures

Details are provided in the Extended Experimental Procedures

Plasmids siRNA-insensitive FLAG-hYAP1 WT and 5SA were generated by PCR and subcloned in pcDNA3. pXJ40-HA-Merlin/NF2 S518A is Addgene# 19701. 8xGTIIC-lux [11] is Addgene# 34615.

Cell cultures and Transfections MCF10A and MII cells were used with equal results, except for experiments shown in Figure 3 and 5 where we used only MII cells. Micropatterned glass slides were from Cytoo. Fibronectin-coated hydrogels were as previously described [11]. The monolayer stretching-device was fabricated by using

standard soft-lithography techniques. For 3D assays, cells were embedded into mixes of Growth Factor Reduced Matrigel (BD Biosciences) and CollagenI (TREVIGEN CULTUREX 3D Culture Matrix Rat CollagenI). For assays on large square and circular fibronectin-coated islands, 1.000.000 cells were plated in a 35mm dish containing a single Cytoo glass slide. siRNA transfections were done with Lipofectamine RNAi-MAX (Life technologies). Sequences of siRNA are provided in Table S1 and S2. DNA transfections were done with TransitLT1 (Mirus Bio). siRNA and DNA transfection were performed on sparse cells plated on tissue culture plastics before replating on the various ECM substrates and islands. For Retroviral infections see (Azzolin et al., 2012).

Antibodies and Bioassays Antibodies: anti-YAP/TAZ (sc101199), anti-CAPZB (sc81804), anti-COFILIN1 (Epitomics 6663-1), anti-GELSOLIN (sc57509), anti-GAPDH (Millipore mAb374), anti-LATS1 (CST) and anti-LATS2 (Abcam), anti-E-Cadherin (BD Biosciences). For microscopy, luciferase, proliferation and real-time PCR assays see Extended Experimental Procedures.

SUPPLEMENTAL INFORMATION Supplemental Information includes Extended Experimental Procedures, Supplemental References, six Figures, two Tables.

ACKNOWLEDGEMENTS We thank Michelangelo Cordenonsi, Francesca Zanconato, Elena Enzo and Oliver Wessely for thoughtful discussion. This work is supported by AIRC-PI and PRIN-Miur, and University of Padua grant to SD; and by AIRC Special Program Molecular Clinical Oncology “5 per mille”, HSFP, Excellence-IIT, and Epigenetics Flagship project CNR-Miur grants to S.P.

References

[1] Discher, D.E., Mooney, D.J., and Zandstra, P.W. (2009). Growth factors, matrices, and forces combine and control stem cells. Science 324 , 1673– 1677.

[2] Huang, S., and Ingber, D.E. (1999). The structural and mechanical complexity of cell-growth control. Nat. Cell Biol. 1 , E131–E138.

[3] Sasai, Y. (2013). Cytosystems dynamics in self-organization of tissue architecture. Nature 493 , 318–326.

[4] Nelson, C.M., Jean, R.P., Tan, J.L., Liu, W.F., Sniadecki, N.J., Spector, A.A.,

and Chen, C.S. (2005). Emergent patterns of growth controlled by multicellular form and mechanics. Proc. Natl. Acad. Sci. USA 102 , 11594–11599.

[5] Nelson, C.M., and Bissell, M.J. (2006). Of extracellular matrix, scaffolds, and signaling: tissue architecture regulates development, homeostasis, and cancer. Annu. Rev. Cell Dev. Biol. 22 , 287–309.

[6] Berrier, A.L., and Yamada, K.M. (2007). Cell-matrix adhesion. J. Cell. Physiol. 213 , 565–573.

[7] Miranti, C.K., and Brugge, J.S. (2002). Sensing the environment: a historical perspective on integrin signal transduction. Nat. Cell Biol. 4 , E83–E90.

[8] Schwartz, M.A. (2010). Integrins and extracellular matrix in mechanotransduction. Cold Spring Harb. Perspect. Biol. 2 , a005066.

[9] Vogel, V., and Sheetz, M. (2006). Local force and geometry sensing regulate cell functions. Nat. Rev. Mol. Cell Biol. 7 , 265–275.

[10] Halder, G., Dupont, S., and Piccolo, S. (2012). Transduction of mechanical and cytoskeletal cues by YAP and TAZ. Nat. Rev. Mol. Cell Biol. 13 , 591–600.

[11] Dupont, S., Morsut, L., Aragona, M., Enzo, E., Giulitti, S., Cordenonsi, M., Zan- conato, F., Le Digabel, J., Forcato, M., Bicciato, S., et al. (2011). Role of YAP/ TAZ in mechanotransduction. Nature 474 , 179–183.

[12] Pan, D. (2010). The hippo signaling pathway in development and cancer. Dev. Cell 19 , 491–505.

[13] Zeng, Q., and Hong, W. (2008). The emerging role of the hippo pathway in cell contact inhibition, organ size control, and cancer development in mammals. Cancer Cell 13 , 188–192.

[14] Cordenonsi, M., Zanconato, F., Azzolin, L., Forcato, M., Rosato, A., Frasson, C., Inui, M., Montagner, M., Parenti, A.R., Poletti, A., et al. (2011). The Hippo transducer TAZ confers cancer stem cell-related traits on breast cancer cells. Cell 147 , 759–772.

[15] Harvey, K.F., Zhang, X., and Thomas, D.M. (2013). The Hippo pathway and human cancer. Nat. Rev. Cancer 13 , 246–257.

[16] Azzolin, L., Zanconato, F., Bresolin, S., Forcato, M., Basso, G., Bicciato, S., Cordenonsi, M., and Piccolo, S. (2012). Role of TAZ as mediator of Wnt signaling.

Cell 151 , 1443–1456.

[17] Yu, F.-X., Zhao, B., Panupinthu, N., Jewell, J.L., Lian, I., Wang, L.H., Zhao, J., Yuan, H., Tumaneng, K., Li, H., et al. (2012). Regulation of the Hippo-YAP pathway by G-protein-coupled receptor signaling. Cell 150 , 780–791.

[18] McClatchey, A.I., and Yap, A.S. (2012). Contact inhibition (of proliferation) redux. Curr. Opin. Cell Biol. 24 , 685–694.Zeng, Q., and Hong, W. (2008). The emerging role of the hippo pathway in cell contact inhibition, organ size control, and cancer development in mammals. Cancer Cell 13 , 188–192.

[19] Zhao, B., Li, L., Wang, L., Wang, C.-Y., Yu, J., and Guan, K.-L. (2012). Cell detachment activates the Hippo pathway via cytoskeleton reorganization to induce anoikis. Genes Dev. 26 , 54–68.

[20] Schlegelmilch, K., Mohseni, M., Kirak, O., Pruszak, J., Rodriguez, J.R., Zhou, D., Kreger, B.T., Vasioukhin, V., Avruch, J., Brummelkamp, T.R., and Camargo, F.D. (2011). Yap1 acts downstream of a -catenin to control epidermal proliferation. Cell 144 , 782–795.

[21] Kim, N.-G., Koh, E., Chen, X., and Gumbiner, B.M. (2011). E-cadherin mediates contact inhibition of proliferation through Hippo signaling-pathway com- ponents. Proc. Natl. Acad. Sci. USA 108 , 11930–11935.

[22] Berrier, A.L., and Yamada, K.M. (2007). Cell-matrix adhesion. J. Cell. Physiol. 213 , 565–573.

[23] Wada, K.-I., Itoga, K., Okano, T., Yonemura, S., and Sasaki, H. (2011). Hippo pathway regulation by cell morphology and stress fibers. Development 138 , 3907–3914.

[24] Rohn, J.L., Sims, D., Liu, T., Fedorova, M., Scho¨ ck, F., Dopie, J., Vartiainen, M.K., Kiger, A.A., Perrimon, N., and Baum, B. (2011). Comparative RNAi screening identifies a conserved core metazoan actinome by phenotype. J. Cell Biol. 194 , 789–805.

[25] Pollard, T.D., and Cooper, J.A. (2009). Actin, a central player in cell shape and movement. Science 326 , 1208–1212.

[26] Nelson, C.M., Jean, R.P., Tan, J.L., Liu, W.F., Sniadecki, N.J., Spector, A.A., and Chen, C.S. (2005). Emergent patterns of growth controlled by multicellular form and mechanics. Proc. Natl. Acad. Sci. USA 102 , 11594–11599.

[27] Butcher, D.T., Alliston, T., and Weaver, V.M. (2009). A tense situation: forcing tumour progression. Nat. Rev. Cancer 9 , 108–122.

[28] Paszek, M.J., Zahir, N., Johnson, K.R., Lakins, J.N., Rozenberg, G.I., Gefen, A., Reinhart-King, C.A., Margulies, S.S., Dembo, M., Boettiger, D., et al. (2005). Tensional homeostasis and the malignant phenotype. Cancer Cell 8 , 241–254.

[29] Kim, M., Kim, M., Lee, S., Kuninaka, S., Saya, H., Lee, H., Lee, S., and Lim, D.-S. (2013). cAMP/PKA signalling reinforces the LATS-YAP pathway to fully suppress YAP in response to actin cytoskeletal changes. EMBO J. 32 , 1543–1555.

[30] Lei, Q.-Y., Zhang, H., Zhao, B., Zha, Z.-Y., Bai, F., Pei, X.-H., Zhao, S., Xiong, Y., and Guan, K.-L. (2008). TAZ promotes cell proliferation and epithelial-mesenchymal transition and is inhibited by the hippo pathway. Mol. Cell. Biol. 28 , 2426–2436

[31] Guo, C.-L., Ouyang, M., Yu, J.-Y., Maslov, J., Price, A., and Shen, C.-Y. (2012). Long-range mechanical force enables self-assembly of epithelial tubular pat- terns. Proc. Natl. Acad. Sci. USA 109 , 5576–5582.

[32] Zeng, Q., and Hong, W. (2008). The emerging role of the hippo pathway in cell contact inhibition, organ size control, and cancer development in mammals. Cancer Cell 13 , 188–192.

[33] Fernandez, B.G., Gaspar, P., Bra´ s-Pereira, C., Jezowska, B., Rebelo, S.R., and Janody, F. (2011). Actin-Capping Protein and the Hippo pathway regulate F-actin and tissue growth in Drosophila. Development 138 , 2337–2346.

[34] Sansores-Garcia, L., Bossuyt, W., Wada, K.-I., Yonemura, S., Tao, C., Sasaki, H., and Halder, G. (2011). Modulating F-actin organization induces organ growth by affecting the Hippo pathway. EMBO J. 30 , 2325–2335.

[35] Ramos, A., and Camargo, F.D. (2012). The Hippo signaling pathway and stem cell biology. Trends Cell Biol. 22 , 339–346.

[36] Paszek, M.J., Zahir, N., Johnson, K.R., Lakins, J.N., Rozenberg, G.I., Gefen, A., Reinhart-King, C.A., Margulies, S.S., Dembo, M., Boettiger, D., et al. (2005). Tensional homeostasis and the malignant phenotype. Cancer Cell 8 , 241–254.

Appendix C

Biosensing with electroconductive biomimetic soft materials

Francesco Lamberti[1,2], Stefano Giulitti[1,2], Monica Giomo[1] and Nicola Elvassore[1,2]

1. Department of Industrial Engineering (DII), University of Padua, via Marzolo 9, 35131 Padua, Italy.

2. Venetian Institute of Molecular Medicine, University of Padua, via Orus 2, 35129 Padua, Italy

Journal of Material Chemistry B

Volume 1:5083-5091

10.1039/C3TB20666A

C.1 Summary

The development of smart biomaterials able to quantitatively analyse the dynamic of biological systems with high temporal resolution in biomimetic environments is of paramount importance in biophysics, biology and medicine. In this context, we develop a biosensing water-based soft biomaterial with tunable mechanical properties through the generation of an electro-conductive nano-element network. As a proof of concept, in order to detect glucose concentration, we fabricate an electroconductive poly-acrylamide glucose-oxidase loaded hydrogel modified with a low amount of Single-Walled Carbon Nanotubes (SWNTs) (up to 0.85 wt%). Micro-Raman maps and optical analysis show nanotube distribution in the samples at different mass fraction. Electrochemical impedance spectra and their fitting with equivalent circuit models reveal an electron conduction in charged hydrogels in addition to ionic conductivity. The effective resulting resistance of the nanostructured network is comparable to the gold electrode one. These findings are also confirmed by cyclic voltammetries. Interestingly, heterogeneous clustering of SWNTs shows double electric mechanisms and efficiencies. GOx-SWNT doped hydrogels show a glucose-concentration linear response in the range between 0.1 mM to 1.6 mM; all together these results show high detection limits for glucose (down to 15 μM) and a sensitivity of 0.63 μA/mM. In the perspective of monitoring cell dynamics, hydrogel functionalization allows cell adhesion and long-term cell culture whereas atomic force microscope is used for mapping the doped hydrogel stiffness. Myoblasts, cell sensitive to mechanical substrate properties, show proper differentiation and phenotype in SWNT-HYs with nominal physiological stiffness.

C.2 Introduction

Soft biomaterials are nowadays of great interest in various field such as biophysics, biotechnology, biology and medicine [1-4]. Among different biomaterials, their soft nature provides an artificial bi-dimensional and tri-dimensional environment which closely resembles both biochemical and biomechanical cues found in cell and tissue interactions in vivo [5, 6]. These features are achieved by latest progresses in the

development of biomimetic substrates that require a deep integration of material and biological sciences. In this context, polymeric hydrogels (HYs) have already reached a prominent position among the other water-based biomaterials because of their peculiar chemical and physical properties, which can be easily tuned by adjusting HY composition and crosslinking. Among other properties like biocompatibility, biodegradability, high permeability and smart chemistry, mechanical ones are very important because make HYs ideal to provide structural and biological support to cells and tissues, controlling the delivery of medium components and enrichment of autocrine and paracrine factors [7]. For this reason, HYs have been relevant for mechanotransduction applications,[8] specific topological targeting of cell adhesion and proliferation and biomimetic scaffold development for in vitro tissues [9-14]. Several works report the possibility of promoting a proper tissue specification and functional properties by tuning mechanical properties of substrate [15-18]. In this perspective, even if soft materials have been successfully applied to induce biological or biophysical responses related to their mechanical or chemical properties, there are no evidence about the possibility of recording biological activities through soft substrates. However, continuous analysis of living system has been recently exploited through the use of stiff materials. For instance, metallic nanowires [19, 20] and nanoparticle arrays [21] were used for metabolic biosensing as conductive supports for bioelectronic applications [22]. Moreover, examples in which glass or metallic multi-electrode arrays were used for electrophysiological studies have been reported [23-25]. This experimental effort underlines the importance of developing biomaterial capable of continuously and quantitatively analyzing cell activity. The possibility of combining compliant substrates with no-invasive continuous detection is extremely relevant to develop biological studies without affecting cell functionality. For instance, electrophysiological studies on contractile cell (such as, skeletal muscle cells or cardiomyocytes) on stiff substrates could be difficult to perform because of cell easily detach from the substrate. Thus, we aim at developing a biosensor integrated into a biomimetic soft material in order to quantitatively analyze the cell dynamics with high temporal resolution. In particular, as a proof of concept, we aim at targeting a metabolite, glucose that is important for cellular activity. Among different

mechanisms of detection, we used electrochemical methodologies because of the high sensitivity and specificity of electrochemical based devices. In fact, the specificity can be achieved using enzyme mediated biosensors: several works have been published on electrochemical biosensing devices using catalytic enzymes [26-28]. The major challenge that needs to be solved is to obtain an electronic flow within the biomaterial without affecting the biophysical and biological properties of HY. Although HYs are ionic conductors, due to the strong ion permeability in aqueous media, electron flow is actually forbidden and no electric charge can be collected when using HY-based electrodes. There are a lot of electron carriers usually used as dopants in polymeric biomaterials: particular attention may be given to noble metallic nanoparticles (NPs), such as Au, Ag, Pd and Pt [29-33] but strong limitations occur when used in biological systems due to the toxic effect induced by the large amount of NPs needed to obtain an effective electron current [34, 35]. Carbonaceous particles are also used, such as graphite, fullerenes and single-walled carbon nanotubes (SWNTs) [36-38]. The latter are very interesting due to their intrinsic peculiar electronic properties: high conductivities can be achieved with very low additions of particles (down to 4% with respect to 50% for metallic NPs) thus allowing the realization of quasi unmodified doped materials [39, 40]. In our knowledge, only a few works concerning the bulk modification of HYs are reported [41-44], however, works reporting the effect of dopant loading on mechanical properties of soft-materials together with biocompatibility and cell behaviour (in terms of both proliferation and differentiation) are never been reported yet. It would be extremely relevant for biological, physiological and pathophysiological studies to develop a soft-biosensor with minimal amount of dopant in order to preserve biomechanical and biochemical properties of the soft-materials and the cell biocompatibility while performing physiological measurements of metabolites in the physiological range (for instance, glucose concentration between 1-5 mM). For these reasons, we realized an electroconductive biomimetic HY in which the electroconductivity was achieved by the creation of a SWNT electronic network that could allow an electroconductive percolation across the biomaterial. The wiring effect of nanotubes would promote the electron jumps between the enzymatic core where the reaction takes place to the underlying collecting electrode. The biophys-

ical properties of the modified HYs are not altered because very low concentrations (less than 1% in weight) were used, whereas the catalytic behavior was tested by glucose detection, as a case of study, by specific loading of Glucose Oxidase (GOx). Doping uniformity and distribution were characterized by optic microscopy and Raman spectroscopy, whereas electronic conductivity was verified by electrochemical impedance spectroscopy (EIS) and cyclic voltammetry (CV). Biophysical and biological properties were verified by AFM force-distance curve on doped and undoped materials and by measuring the viability and the phenotype maintenance of cultured cells on the HY surface.

C.3 Results and discussion

C.3.1 Developing the sensor

In Fig. 1 it is shown a schematic representation of the steps involved in the preparation of the glucose bionsensor. A gold electrode fabricated as referred in Experimental Section is modified with an in situ polymerized polyacrylamide SWNT doped HY. SWNT-sodium cholate aqueous suspensions at different concentrations are used for doping HYs (Fig. 1A-1B). Then GOx is loaded into doped and undoped HYs biasing the working electrode in three electrochemical cell configurations (Fig. 1C): the charged enzyme can be drifted into the HY. Glucose is oxidized by the enzyme and indirectly detected potentiostatically in the cell as in Fig. 1D; the byproduct of the reaction is the hydrogen peroxide that oxidizes when a potential of +0.7V ref. Ag/AgCl is applied as reported elsewhere [45].

C.3.2 Hydrogel characterization

Raman spectroscopy is often used for characterizing carbon nanotube through SWNT scattering upon laser excitations in the near-IR range [46]. Fig. 2 shows histograms related to the G-band Raman intensity (about 1600 cm-1) of samples at different SWNT mass fractions. Qualitative increasing trend in the doping level was found. More detailed description about Raman measurements are reported in the Supporting Information (Fig. S5).

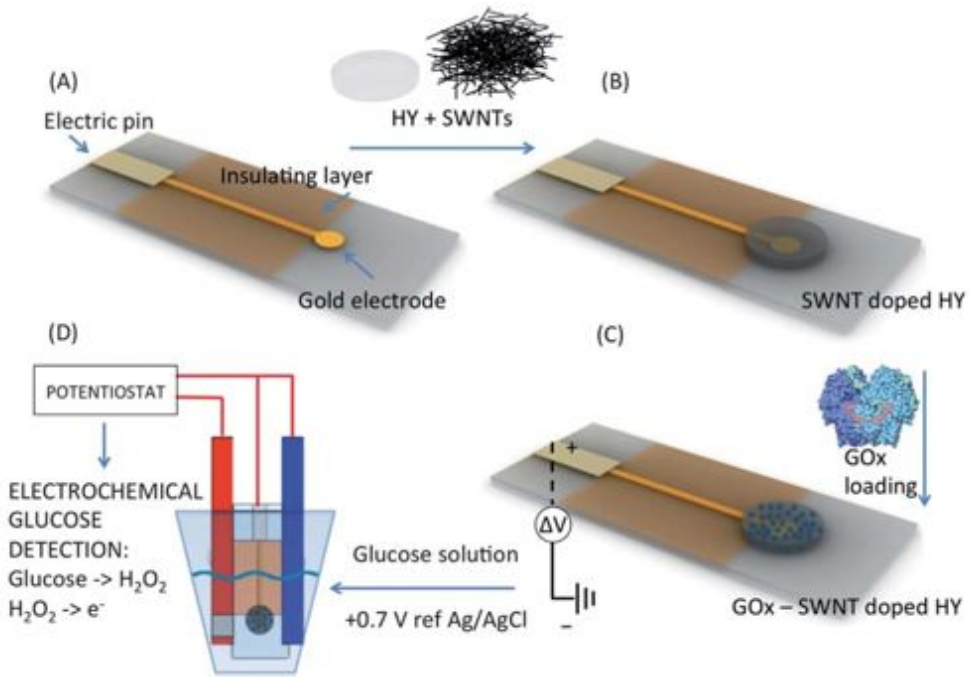

Figure C.3.1 – Schematic representation of the steps involved in the preparation of the biomimetic glucose biosensor. A clean, insulated gold electrode (A) is modified with an in situ polymerized SWNT doped HY at different SWNT concentrations (SWNT HYs) (B); then the electrode is biased with a positive voltage and the enzyme is loaded into the HY, forming a GOx-SWNT doped HY (GOx-SWNT HYs) (C). By means of a potentiostatic measurement, glucose is converted by the enzyme into hydrogen peroxide which can be electrochemically discharged by GOx-SWNT HYs (D).

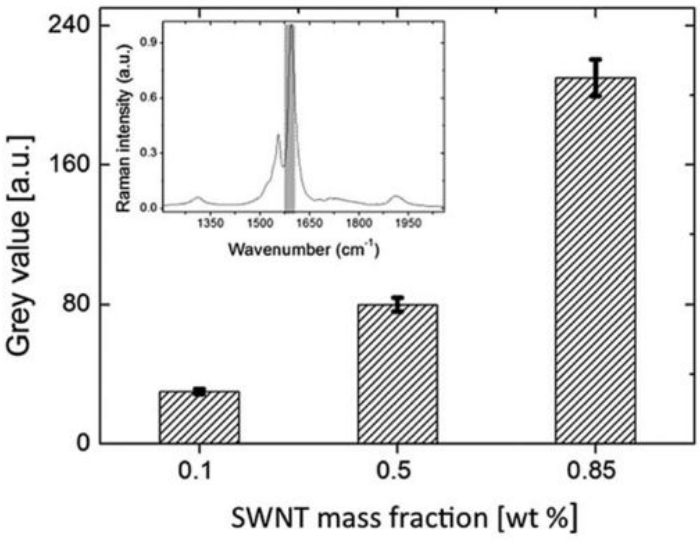

Figure C.3.2 – The carbon nanotube distribution within the samples at different concentrations. The histogram refers to the SWNT Raman G-band intensity. Error bars are described in the ESI. The inset graph represents an example of Raman scattering for a SWNT HY sample used in the paper.

In order to collect information about the resistivity of the SWNT doped material, electrochemical impedance spectroscopy (EIS) was used. Conventional 4-probe conductivity measurements did not lead to reproducible analysis because weak electric contact on soft substrate. EIS gives information about the electric behavior of the interface of an electrodic system by fitting the experimental data with specific equivalent circuit models; polarization resistance for the interface can be derived. A Randles cell was used for modeling equivalent circuits as reported in literature for organic electrodic interfaces [47]. A constant phase element (CPE) was used for replacing the ideal double layer capacitance (C). Fig. 3 summarizes EIS results. In Fig. 3A-C Bode phase plot for the samples at different SWNT mass fraction are shown, whereas, in Fig. 3D the polarization resistances obtained by fitting are reported as a function of SWNT mass fraction. Fig. 3A and Fig. 3C show a maximum in the frequency spectrum. On the other hand, two principal time constants for the electrodic system (i.e. two maxima in the spectrum) are shown for samples in Fig. 3B. For this reason, two different equivalent circuit models (with one or two RC systems) are required to fit all the data; Rs is the unsupported resistance solution, RPij is the polarization resistance indexed by i and j related to equivalent circuit I or II. Numerical outcomes for fitting and a more detailed description of circuits used are provided in the Supporting Information (Fig. S7). The resulting resistances are reported as a function of SWNT mass fraction in Fig. 3D-i, Fig. 3D-iii and Fig. 3D-v; for higher dopant concentration, lower RP value was observed only for lowest and at highest SWNT mass fraction samples ($\leq$0.25 wt% and $\geq$0.64 wt%). Interestingly, at intermediate mass fraction range, RP1II shows similar behavior to RP1I whereas RP2II is almost constant. The additional RP2II in intermediate SWNT mass fraction samples suggests the existence of a double electric behavior with peculiar electroconductive properties; this behavior could be associated to dopant phase separation and non uniform SWNT dispersion within the HY as shown in Fig. 3E, (black areas are likely to represent clustering zones of material). Uniform dispersion of SWNT within HY are associated with simple Randles cell (sample in the range of $\leq$0.25 wt%-Fig3D and $\geq$0.64 wt%-Fig.3F). The existence of a peak at low frequency value in the electrodic system may alter the time of response and the sensitivity of

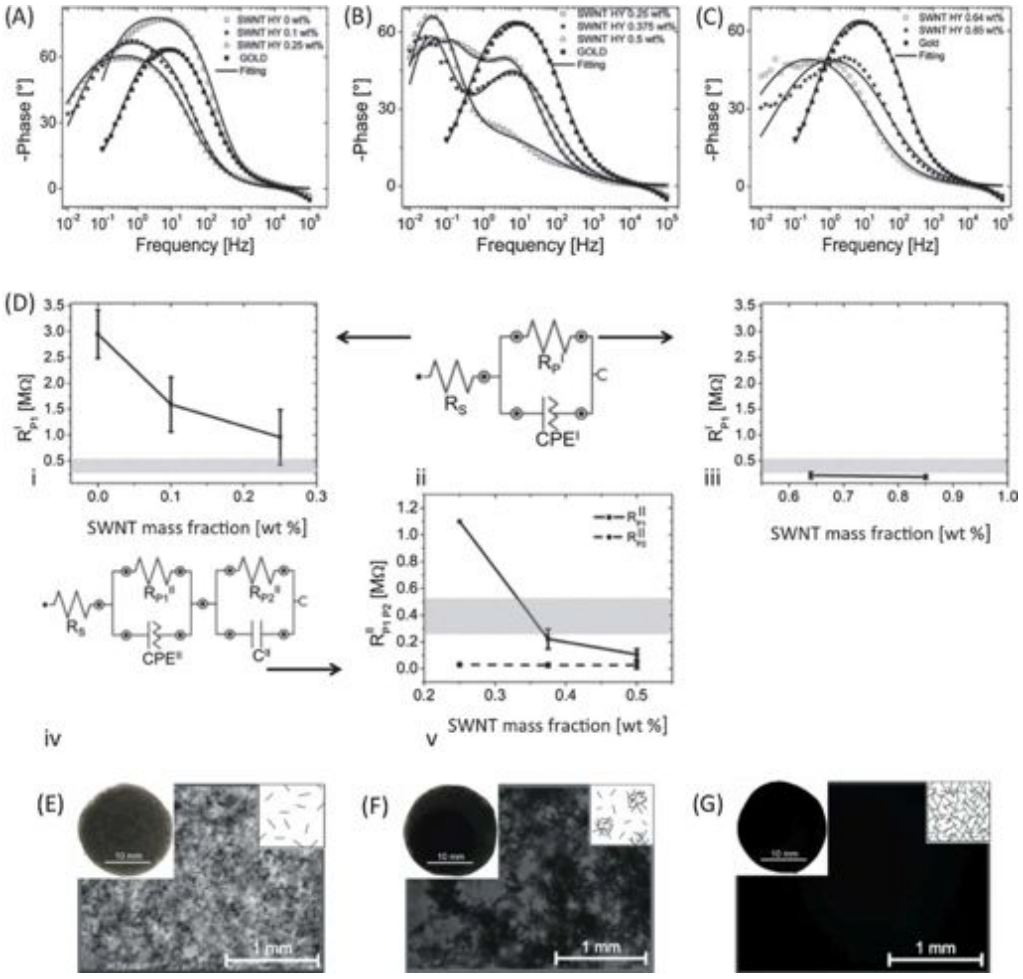

Figure C.3.3 – Electrochemical impedance spectroscopy and optical analysis of SWNT doped HYs. (A)-(C) Bode phase plots for doped HYs at different dopant concentrations; circles are experimental values, whereas the solid line is the fitting using the circuits in scheme (D)ii for (A) and (C) and the circuit in scheme (D)iv for (B). (D)i, (D)iii and (D)v show the fitted resistance versus SWNT doping percentage. Error bars and numerical values are available in the ESI. Symbols are noted in the manuscript. (E)-(G) show different optical images related to the three different regimes identified by varying the dopant concentration.

a SWNT-HY based biosensor.

A deeper analysis on electrochemical faradic response was required to identify the optimal dopant mass fraction for realizing electroconductive nanotube based biosensors. Cyclic voltammetry (CV) is a simple strategy for detecting faradic current from the electrode immersed into a redox probe solution (0.5 mM ferrocenemethanol in PBS 1x solution) for a specific time (Fig. 4). Fig. 4A shows faradic peak current of several CVs as a function of redox loading time. In all samples, the peak current increases reaching a plateau after few hours. Interestingly, the largest peak current value has been observed for sample with 0.85 wt% and 0.1 wt% SWNT mass fraction;

these samples also show an immediate increasing in the peak current. On the other hand, the sample at 0.5 wt% shows a delay in peak current increasing, reaching a plateau value lower than all other samples, including the control (SWNT HY 0 wt%). Fig. 4B show two different time points, at 6 min (left) and 150 min (right), respectively: the ohmic response and the high capacitive current of SWNT HY 0.5 wt% with respect to other samples confirms the sensor low-conductive behavior. On the other hand, SWNT HY 0.85 wt% provides highest currents. These data confirm that SWNT dispersed in the HY form an effective network of conductive materials that support electron flow. Redox probe detection in control HY without SWNT was only possible after diffusion of the probe within the hydrogel on the underneath electrode surface. Similar effect was observed for intermediate SWNT mass fraction samples. It seems that phase separation and clustering of SWNT previously observed, could limit the diffusion of redox probe leading to lower faradic current detection. This outcome highlights the goodness of EIS analysis by confirming the high catalytic feature for charge transfer reactions previously found (Fig. 3D-iii) for highly doped samples.

Mechanical and biocompatibility measurements

Surface stiffness is one of the most important parameters in determining cell-substrate interaction [49-51]. For this reason, we aim at studying the effect of SWNT doping on mechanical properties of HY samples. AFM distance-curve technique was used for characterizing the stiffness of the samples as reported in literature for low elastic modulus substrates [52-54]. Three HY samples without SWNT with defined Young's modulus (4.5 kPa (A), 17 kPa (B) and 40 kPa (C)) were fabricated in order to be used as reference [10]. The hydrogel that are mostly used in physiological study of soft tissues (stiffness ranging from 4.5 to 17 kPa) were doped with SWNT at 0.85 wt% (Aβ and Bβ samples respectively). Due to the uncertainty of Poisson's coefficient for such substrates and due to the difficulty of choosing the correct force-distance curve fitting model [54], stiffness was established as the phenomenological parameter for determining HY mechanical properties. In Fig. 5, force-distance curves are shown. Sample stiffness, i.e. the slope of the curve in the contact region, linearly increases

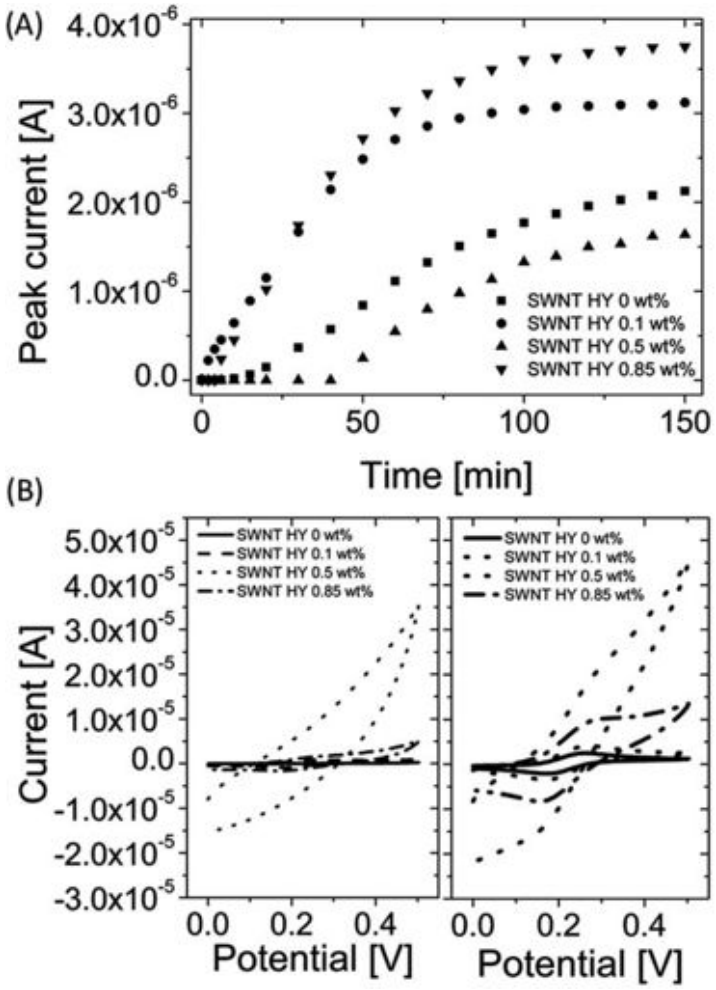

Figure C.3.4 – Cyclic voltammetry analysis of SWNT HYs. (A) Time dependence of faradic peak current in ferrocene methanol redox probe at different SWNT loadings. (B) Cyclic voltammograms at 6 minutes (left) and 150 minutes (right). All potentials are referenced to the Ag/AgCl reference electrode.

	Nominal Young's modulus ratio	Measured stiffness ratio
A to B	3.5	4
B to C	2.5	2.6
A to Aβ	-	2.4
B to Bβ	-	2

Table C.3.1 – Force distance curve analysis results.

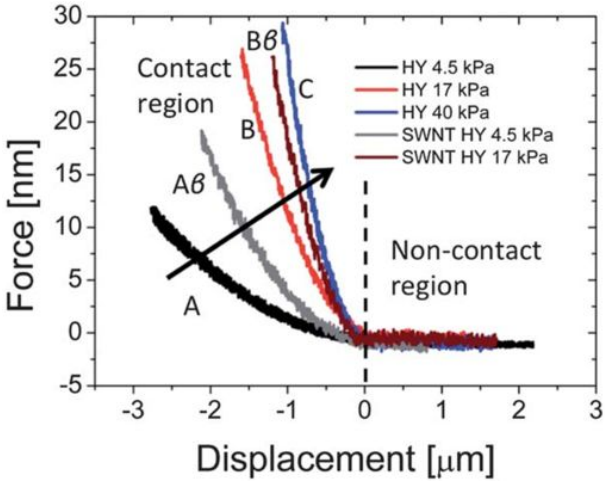

Figure C.3.5 – Force-distance curves for HY and SWNT-HY samples at different nominal Young's moduli. Stiffness is represented by the slope in the contact region.

with the nominal Young's modulus as reported in tab. 1. Comparison between control and doped hydrogel show that the hydrogels without SWNT show a reduction of stiffness of about 50%.

From these findings the SWNT network within the hydrogel leads to stiffer materials even at low SWNT mass fraction. However, even if this variation is quite significant, it is negligible if compared to stiffness variation required to elect any biological responses [8,9]; for instance, one order of magnitude variation from 15 kPa is required in order to depress functional maturation of skeletal muscle precursor cells [9]. These results are very relevant for the development of effective biosensors that fully recapitulates biomechanical properties of in vivo tissues. Other fundamental aspects required for interfacing biosensor with living biological systems are the biocompatibility and the maintenance of proper phenotype during proliferation and differentiation process. For this purpose, murine muscle cell line, C2C12, were cultured on doped HYs; skeletal muscle cell line could provide information not only to viability but also to cell response to mechanical substrate as we previously demonstrated [9]. Polyacrylamide hydrogels doped with SWNTs with 0 wt%, 0.1 wt% and 0.85 wt% were tested. Cell adhesion was complete within 4 hours after seeding,

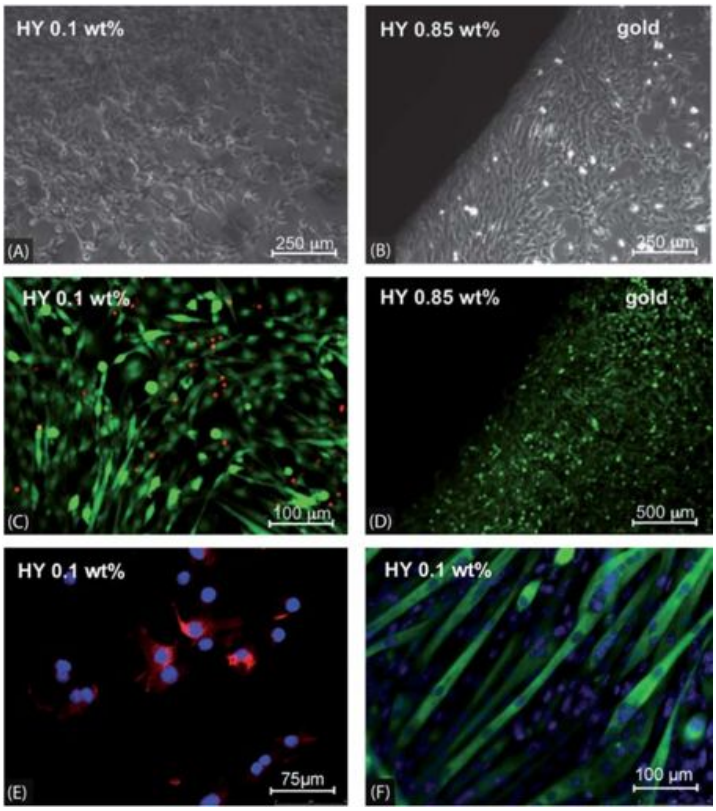

Figure C.3.6 – C2C12 live and dead viability test. (A) and (C) Cells are deposited on SWNT-HY 0.1 wt%; (B) and (D) Cells cultured on SWNT-HY 0.85 wt%. (E) C2C12 on SWNT-HY 0.1 wt% retained the proper expression of desmin, marked with a red-labelled antibody. (F) Confluent cells spontaneously differentiated into myotubes which expressed myosin-II, in green. Nuclei are stained with Hoechst dye (blue).

both in non-doped and doped HYs. Cells on doped HYs evidenced the same morphology and behavior compared to unmodified HYs. After three days of culture, a LIVE/DEAD assay was performed to evaluate the percentage of live and dead cells (Fig. 6). The green fluorescent dye calcein evidenced viable cells and red nuclei showed damaged and dead cells with the membrane-impermeant dye Eth-D1. Cell viability and proliferation were not altered on 0.1 and 0.85 wt% SWNT HYs. Cell proliferated reaching confluence, confirming that the SWNTs embedded in the gel did not altered cell behaviour. Moreover, on SWNT doped HYs, cells maintained proper expression of desmin, a typical skeletal muscle marker (Fig. 6e) and spontaneously differentiated into mature myotubes, the functional unit of muscle fibers expressing myosin-II (Fig. 6f).

C.3.3 Glucose monitoring

In order to give the proof of concept that metabolite concentration can be measured under cell culture in biomimetic stiffness, a glucose biosensor was developed for analysing glucose in physiological range between 1 and 5 mM. The realization

	Results
V_{max}	4.0 ± 0.2 µA
K_M	2.0 ± 0.4 mM
Sensitivity	0.63 µA mM^{-1}
Detection limit	15 mM

Table C.3.2 – Fitting outcomes for the GOx–SWNT–HY 0.85 wt% biosensor. V_{max} represents the maximum current produced by the biosensor for high glucose additions, whereas KM represents the concentration for which the current is $V_{max}/2$. The detection limit is calculated following the considerations outlined in ref. 57

of the biosensor is achieved by GOx loading as described in Experimental section. First of all we show that GOx-doped HYs without SWNT do not exhibit any detectable electrical signal increasing the glucose concentration up to 160 mM (Fig. S9 of Supporting Information). Fig. 7A shows potentiostatic measurement of glucose concentration using GOx-SWNT HY 0.85 wt%; sequential glucose additions are highlighted with vertical arrows in the figure. Fig. 7B shows quantification of plateau current values for each glucose addition as function of glucose concentration. Michaelis-Menten enzymatic kinetic model can be used to fit these experimental data (tab. 2); linearity is achieved in the range between 0.1 mM to 1.6 mM (inset graph).

All together, these data show that an effective glucose potentiostatic detection can be achieved through SWNT doped hydrogel at 0.85 wt% mass fraction. Moreover, the detection limit of 15 μM and the sensitivity of 0.63 μA/mM. The detection limit value is in total agreement with other biosensors fabricated for blood glucose detection which values vary in mM concentration range [27, 56-58]. These findings show that the enzyme bioactivity is well preserved within the three-dimensional hydrogel environment. The production of hydrogen peroxide, as mediator in glucose oxidation, can be easily and quantitatively detected by the three-dimensional network of SWNT within the biomaterial. This behavior suggests that the percolative pattern through SWNT clusters allows electron flow from hydrogel bulk to gold surface electrode. In addition, the lower dopant concentration (compared to those reported previously for other materials) and the choice of starting material (polyacrylamide HY) allows the biomaterial to preserve biophysical and biological properties letting the SWNT doped HY a reliable biomimetic soft material.

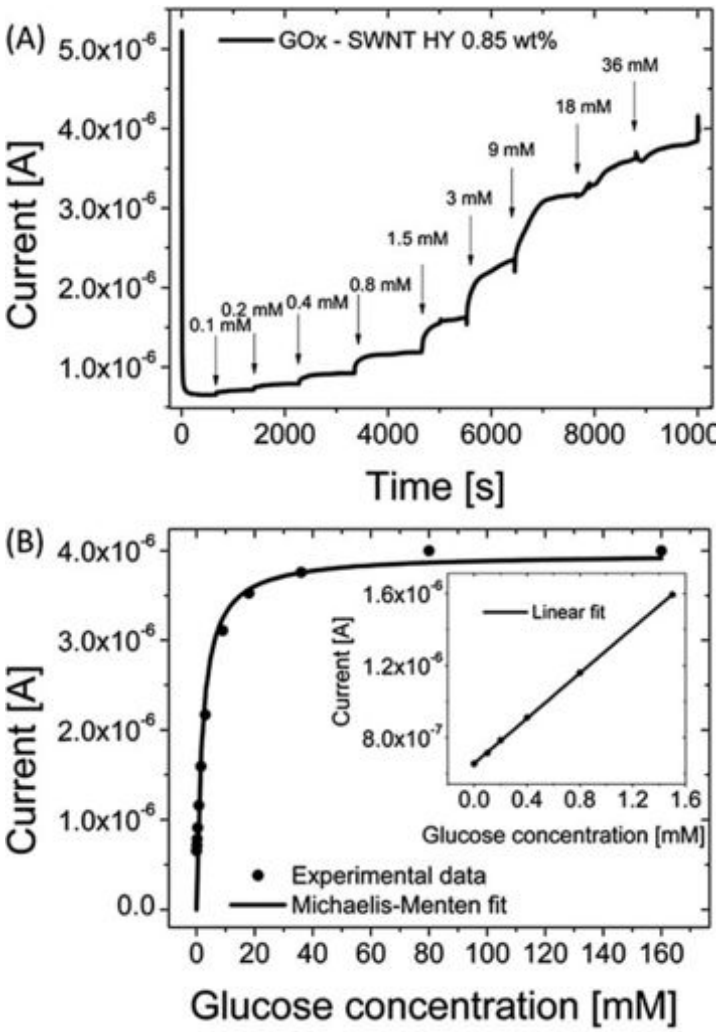

Figure C.3.7 – Glucose detection and biosensor calibration. (A) Potentiostatic measurements of GOx-SWNT-HY 0.85 wt% in PBS 1 solution. The arrows represent points of glucose addition; (B) plateau current values versus glucose concentration. Circles are experimental values of the measurements given in panel (A), and the solid line represents the fitting of the data with the enzymatic Michaelis-Menten kinetic equation. Outcomes of the fitting are shown in Table 1. The inset graph shows that linearity is achieved in the range between 0.1 mM and 1.6 mM.

Experimental

Chip preparation: Working electrode was realized by the patterned deposition of Au nanometric thin film on clean glass slides through PECVD using a photosensitive epoxidic mask (SU8, MicroChem, USA) that would be removed by Remover PG (MicroChem, USA) after metallic deposition. In order to enhance gold adhesion, a Ti nanometric seed layer was deposited before gold deposition. In order to ensure a uniform and prolonged adhesion of hydrogel to glass, a specific functionalization of the glass surface is necessary. The treatment protocol developed consists of glass surface chemical modification with silane and glutaraldehyde (Sigma-Aldrich, Italy) as reported in [48]. Supporting Methods are available. Electrochemical cleaning procedure was used by performing repetitive scans to the working electrode from 0 V to 1.5 V vs Ag/AgCl in HSO at 0.1 V/s. Measurement was stopped when reproducible scans have been obtained.

C.3.4 Water suspension of carbon nanotubes

100mg of CoMoCat SWCNTs (Sigma Aldrich, Italy) were added as received to 10mL of milliQ water to form 1 wt% suspension of SWCNTs. Also 20mg/mL of Sodium Cholate (SC, 99% Sigma-Aldrich, Italy) as surfactant agent were added to the mixture. The suspension was then ultrasonicated for 30 min in ice bath and filtered to remove clusters obtaining a dark black solution. The suspension was concentrated by heating until a 1.33 wt% final concentration were reached.

C.3.5 HY Preparation

To realize SWNT HYs, acrylamide/Metilen-bis-acrylamide 29:1 solution (AA/BIS) was used in addition to carbon nanotubes water mixtures at different final concentrations as reported in tab. 3.

C.3.6 Chemical polymerization

1/100 v/v Ammonium Persulfate, 5% solution (APS, Sigma-Aldrich, Italy) and 1/1000 v/v N,N,N,N-Tetramethylethylenediamine (TEMED, Sigma-Aldrich, Italy), were added to the prepolymer solution. APS in water produces SO radicals that

SWNT-HY (wt%)	1.33 wt% SWNT in H_2O (µL)	AA-bis 100 wt% (µL)	H_2O (µL)
0.0	0.0	100	400.0
0.1	37.6	100	362.4
0.25	93.9	100	306.1
0.375	141.0	100	259.0
0.5	188.0	100	212.0
0.64	240.0	100	160.0
0.85	320.0	100	80.0

Table C.3.3 – Chemical compositions of SWNT–HY samples used in this work

start the reaction. TEMED catalyzes the reaction because it exists as free radical in solution. The higher is the concentration of TEMED, the faster will be the polymerization. The pre-polymer solution was degassed because oxygen could inhibit the initiator. So the prepared solution was rapidly transferred to a silicon mold and then covered with a coverslip. It takes about 15 min to reach the complete polymerization of 0.5 mm tall cylindrical HY at room temperature.

C.3.7 Optical and Raman characterization

HY micrographs were taken with an inverted stereomicroscope (Olympus, Italy) coupled with a photo camera, at a magnification of 10X. A Raman/SNOM confocal spectrometer (Alpha 300S, WITec, Germany) equipped with a He-Ne laser (λ = 633 nm) and a 10X lens was used to perform scans over a 15x15 μm area on three humid hydrogels at three different SWNT concentrations (0.1 wt%, 0.5 wt% and 0.85 wt%). Spectra were integrated 10 times for each point in the G-band peak interval (between 1585 cm^{-1} and 1597 cm^{-1}). Then data were normalized on the maximum peak intensity collected throughout the three HYs and plotted as a function of x-y spatial coordinates obtaining three comparable microRaman maps of the surface of the HYs. The measurement was repeated four times to obtain statistical analysis.

C.3.8 Electrochemical characterization

Electrochemical impedance spectroscopy measurements were performed using a potentiostat/galvanostat (Autolab PGSTAT302N, Metrohm, EcoChemie, The Netherlands) managed by software NOVA 1.8 and equipped with a FRA2 module for frequency analyzer. The classic three electrodes cell scheme was used: gold electrode

acts as working electrode, a Ag/AgCl electrode (Amel Instruments, Italy) as the reference electrode and a Mettler Toledo Pt cylindrical electrode is used as counter electrode. Frequency scan range was established between 0.1 Hz to 100 kHz. Fitting of data were performed using NOVA 1.8 software. Cyclic voltammetries were conducted between 0 V and 0.5 V referred to the reference. Redox probe used was ferrocene methanol (Sigma-Aldrich, Italy) at 0.5 mM concentration. Electrolytic supporting solution was KNO 10 mM (Sigma-Aldrich, Italy). Potentiostatic measurements were performed at +0.7 V vs Ag/AgCl electrode in PBS 1x (Invitrogen, Italy). Concentrations from 0.1 mM to 160 mM of commercial sterilized glucose (Glucosata solution) were used.

C.3.9 Biocompatibility tests - Seeding and Culture of C2C12 cells

Biocompatibility tests were done. Live/Dead and immunochemical assays were conducted to assess viability and proper functionality of cell culture on doped HYs. (see Supporting Information for further details). Polyacrylamide hydrogels doped with SWNTs with 0 wt%, 0.1 wt% and 0.85 wt% were tested. To promote cell adhesion, the surface was coated with a 0.1 mg/ml solution of laminin-collagen. Cells were seeded at a density of 3x10 cell/mm and monitored with a phase-contrast microscope for three days.

C.3.10 AFM analysis

AFM studies were performed with a commercial SPM (XE-Bio, Park Systems Corp., Suwon, Korea). The instrument has AFM and SICM systems on the stage of an inverted optical microscope (Eclipse Ti, Nikon Corp., Tokyo, Japan). Manipulating Park XEP data acquisition software, force-distance spectroscopy was performed on HYs. The cantilever used for the force-distance spectroscopy was Biotools PNP-TR (triangle cantilevers with a spring constant of 0.32 N/m and resonance frequency of about 67 kHz, Nanotools, Germany). The cantilever was calibrated by measuring the thermally induced motion of the sample free cantilever in Park XEP software.

Conclusions

An electron conductive network is required to allow electron flow within soft biomaterial because of the insulating nature of polymeric hydrogels. In our work, we show that a proper electron network could be successfully used to acquire electrons from a redox enzymatic reaction that takes place within soft biomaterial. Loading of highly conductive species like carbonaceous nanoparticles within soft hydrogel is the easiest and the most effective approach to induce the formation of electron conductive percolative patterns. In particular, we developed an electrochemical biosensor with good quality using single-walled carbon nanotubes as dopants. We also optimize dopant percentage mass (up to 0.85 wt%) for high detecting efficiency (glucose detection limit of 15 μM, linearity in the range between 0.1 mM to 1.6 mM and a sensitivity of 0.63 μM/mM), consequently opening the range of potential interesting applications as quantitative analysis on cell dynamics through the non invasive direct measurement of metabolites. However, heterogeneous clustering of SWCNT, which compromise overall biosensor quality, was observed within the material when the mass fraction is varied in the intermediate range ($0.25 \leq \text{wt\%} \geq 0.5$) by optical imaging and verified by EI spectra. It is worth to underline that, since optical images and Raman spectroscopy can give qualitative and quantitative information about the homogeneity of the doping, electrochemical impedance spectroscopy can be used to monitor the efficiency of nanotube doping in terms of interface resistance by fitting experimental data with simple equivalent circuit models. This strategy is compatible with samples varying in size, compositions and structure and thus greatly extends the range of potential applications that soft materials based devices could be used. In the perspective of integrating the soft biosensor within cell culture technology for dynamically monitoring metabolic activity of living systems under physiological conditions, we show the biomechanical properties and the biocompatibility of doped and undoped materials.

Acknowledgments We thank University of Padova for financial support and Brian Choi (Park systems corp., Suwon, Korea) for precious help in AFM distance-curve measurements and analysis.

References

[1] P. M. Gilbert, K. L. Havenstrite, K. E. G. Magnusson, A. Sacco, N. A. Leonardi, P. Kraft, N. K. Nguyen, S. Thrun, M. P. Lutolf and H. M. Blau, Science, 2010, 329(5995), 1078-1081.

[2] J. Kim, J. Yoon and R. C. Hayward, Nat. Mater., 2010, 9(2), 159-164.

[3] M. S. Shoichet, Macromolecules, 2010, 43(2), 581-591.

[4] A. R. Parker and H. E. Townley, Nat. Nanotechnol., 2007, 2(6), 347-353.

[5] Y. Aizawa, S. C. Owen and M. S. Shoichet, Prog. Polym. Sci., 2012, 37(5), 645-658.

[6] F. Pampaloni, E. G. Reynaud and E. H. K. Stelzer, Nat. Rev. Mol. Cell Biol., 2007, 8(10), 839-845.

[7] S. Zatti, A. Zoso, E. Serena, C. Luni, E. Cimetta and N. Elvassore, Langmuir, 2012, 28(5), 2718-2726.

[8] S. Dupont, L. Morsut, M. Aragona, E. Enzo, S. Giulitti, M. Cordenonsi, F. Zanconato, J. Le Digabel, M. Forcato, S. Bicciato, N. Elvassore and S. Piccolo, Nature, 2011, 474(7350), 179.

[9] E. Serena, S. Zatti, E. Reghelin, A. Pasut, E. Cimetta and N. Elvassore, Integr. Biol., 2010, 2(4), 193-201.

[10] E. Cimetta, S. Pizzato, S. Bollini, E. Serena, P. De Coppi and N. Elvassore, Biomed. Microdevices, 2009, 11(2), 389-400.

[11] S. Mitragotri and J. Lahann, Nat. Mater., 2009, 8(1), 15-23.

[12] M. C. Cushing and K. S. Anseth, Science, 2007, 316(5828), 1133-1134.

[13] J. L. Drury and D. J. Mooney, Biomaterials, 2003, 24(24), 4337-4351.

[14] S. J. Hollister, Nat. Mater., 2005, 4(7), 518-524.

[15] J.C. Culver, J.C. Hoffmann, R.A. Poche, J.H. Slater, J. L. West and M. E. Dickinson, Adv. Mater., 2012, 24(17), 2344-2348.

[16] J. L. Young and A. J. Engler, Biomaterials, 2011, 32(4), 1002- 1009.

[17] F. Brandl, F. Sommer and A. Goepferich, Biomaterials, 2007, 28(2), 134-146.

[18] M. P. Lutolf and J. A. Hubbell, Nat. Biotechnol., 2005, 23(1), 47-55.

[19] M. Yang, F. Qu, Y. Lu, Y. He, G. Shen and R. Yu, Biomaterials, 2006, 27(35), 5944-5950.

[20] M. Delvaux and S. Demoustier-Champagne, Biosens. Bioelectron., 2003, 18(7), 943-951.

[21] Z. Wen, S. Ci and J. Li, J. Phys. Chem. C, 2009, 113(31), 13482- 13487.

[22] I. Willner and E. Katz, Angew. Chem., Int. Ed., 2000, 39(7), 1180-1218.

[23] S. M. Potter and T. B. DeMarse, J. Neurosci. Methods, 2001, 110(1-2), 17-24.

[24] M. O. Heuschkel, M. Fejtl, M. Raggenbass, D. Bertrand and P. Renaud, J. Neurosci. Methods, 2002, 114(2), 135-148.

[25] I. Suzuki, Y. Sugio, Y. Jimbo and K. Yasuda, Lab Chip, 2005, 5(3), 241-247.

[26] Y. Fu, P. Li, L. Bu, T. Wang, Q. Xie, J. Chen and S. Yao, Anal. Chem., 2011, 83(17), 6511-6517.

[27] Y. Wang, L. Liu, M. Li, S. Xu and F. Gao, Biosens. Bioelectron., 2011, 30(1), 107-111.

[28] L. M. C. Silva, A. M. Salgado and M. A. Z. Coelho, Environ. Technol., 2011, 32(5-6), 493-497.

[29] L. Janovak and I. Dekany, Appl. Surf. Sci., 2010, 256(9), 2809- 2817.

[30] J. M. Pringle, C. Lynam, G. G. Wallace, M. Forsyth and D. R. MacFarlane, Adv. Funct. Mater., 2008, 18(14), 2031-2040.

[31] Y. Leroux, E. Eang, C. Fave, G. Trippe and J. C. Lacroix, Electrochem. Commun., 2007, 9(6), 1258-1262.

[32] S. E. Moulton, P. C. Innis, L. A. P. Kane-Maguire, O. Ngamna and G. G. Wallace, Curr. Appl. Phys., 2004, 4(2), 402-406.

[33] G. G. Wallace and P. C. Innis, J. Nanosci. Nanotechnol., 2002, 2(5), 441-451.

[34] R. J. Griffitt, J. Luo, J. Gao, J. C. Bonzongo and D. S. Barber, Environ. Toxicol. Chem., 2008, 27(9), 1972-1978.

[35] R. Duffin, L. Tran, D. Brown, V. Stone and K. Donaldson, Inhalation Toxicol., 2007, 19(10), 849-856.

[36] Q. Tang, J. Lin and J. Wu, J. Appl. Polym. Sci., 2008, 108(3), 1490-1495.

[37] R. A. MacDonald, C. M. Voge, M. Kariolis and J. P. Stegemann, Acta Biomater., 2008, 4(6), 1583-1592.

[38] H. Dai, Acc. Chem. Res., 2002, 35(12), 1035-1044.

[39] J. N. Coleman, S. Curran, A. B. Dalton, A. P. Davey, B. McCarthy, W. Blau

and R. C. Barklie, Phys. Rev. B: Condens. Matter Mater. Phys., 1998, 58(12), 7492-7495.

[40] O. Meincke, D. Kaempfer, H. Weickmann, C. Friedrich, M. Vathauer and H. Warth, Polymer, 2004, 45(3), 739-748.

[41] C. Dispenza, C. L. Presti, C. Belflore, G. Spadaro and S. Piazza, Polymer, 2006, 47(4), 961-971.

[42] C. Dispenza, G. Fiandaca, C. Lo Presti, S. Piazza and G. Spadaro, Radiat. Phys. Chem., 2007, 76(8-9), 1371-1375.

[43] A. K. Bajpai, J. Bajpai and S. N. Soni, eXPRESS Polym. Lett., 2008, 2, 26-39.

[44] T. Dai, X. Qing, J. Wang, C. Shen and Y. Lu, Compos. Sci. Technol., 2010, 70(3), 498-503.

[45] F. Lamberti, C. Luni, A. Zambon, P. A. Serra, M. Giomo and N. Elvassore, Biomicrofluidics, 2012, 6(2), 024114.

[46] A. M. Rao, E. Richter, S. Bandow, B. Chase, P. C. Eklund, K. A. Williams, S. Fang, K. R. Subbaswamy, M. Menon, A. Thess, R. E. Smalley, G. Dresselhaus and M. S. Dresselhaus, Science, 1997, 275(5297), 187-191.

[47] D. Loveday, P. Peterson and B. R. G. Instruments, J. Coat. Technol., 2004, 1(88), 46-52.

[48] M. Thompson and S. L. R. Ellison, Accredit. Qual. Assur., 2005, 10, 82-97. 49 C. N. Grover, J. H. Gwynne, N. Pugh, S. Hamaia, R. W. Farndale, S. M. Best and R. E. Cameron, Acta Biomater., 2012, 8(8), 3080-3090.

[50] H. D. Kim and S. R. Peyton, Integr. Biol., 2012, 4(1), 37-52.

[51] B. Chen, R. R. Jones, S. Mi, J. Foster, S. G. Alcock, I. W. Hamley and C. J. Connon, Soft Matter, 2012, 8, 8379- 8387.

[52] C. A. Siedlecki and R. E. Marchant, Biomaterials, 1998, 19(4-5), 441-454.

[53] K. D. Jandt, Surf. Sci., 2001, 491(3), 303-332.

[54] J. J. Roa, G. Oncins, J. Diaz, F. Sanz and M. Segarra, Recent Pat. Nanotechnol., 2011, 5(1), 27-36.

[55] J. Wang and M. Musameh, Anal. Chim. Acta, 2005, 539(1-2), 209-213.

[56] Y. Yao and K. K. Shiu, Anal. Bioanal. Chem., 2007, 387(1), 303-309.

[57] B. Liang, L. Fang, G. Yang, Y. Hu, X. Guo and X. Ye, Biosens. Bioelectron.,

2013, 43, 131-136.

Appendix D

Microfluidic driven viral infection on cell cultures: theoretical and experimental study

Elisa Cimetta[1], Mauro Franzoso[2], Marta Trevisan[3], Elena Serena[1,2], Alessandro Zambon[1,2], Stefano Giulitti[1,2], Luisa Barzon[3], and Nicola Elvassore[1,2].

1. Department of Chemical Engineering, University of Padova, via Marzolo 9, I-35131 Padova, Italy.
2. Venetian Institute of Molecular Medicine, Padova, Italy.
3. Department of Histology, Microbiology and Medical Biotechnologies, University of Padova, via Gabelli 63, I-35131 Padova, Italy.

Biomicrofluidcs

Volume 6, 024127 (2012);

10.1063/1.4723853

D.1 Abstract

Advanced cell culture systems creating a controlled and predictable microenvironment together with computational modeling may be useful tools to optimize the efficiency of cell infections. In this paper, we will present a phenomenological study of a virus- host infection system, and the development of a multilayered microfluidic platform used to accurately tune the virus delivery from a diffusive-limited regime to a convective- dominated regime. Mathematical models predicted the convective-diffusive regimes developed within the system itself and determined the dominating mass transport phenomena. Adenoviral vectors carrying the enhanced green fluorescent protein (EGFP) transgene were used at different multiplicities of infection (MOI) to infect multiple cell types, both in standard static and in perfused conditions. Our results validate the mathematical models and demonstrate how the infection processes through perfusion via microfluidic platform led to an enhancement of adenoviral infection efficiency even at low MOIs. This was particularly evident at the longer time points, since the establishment of steady-state condition guaranteed a constant viral concentration close to cells, thus strengthening the efficiency of infection. Finally, we introduced the concept of effective MOI, a more appropriate variable for microfluidic infections that considers the number of adenoviruses in solution per cells for a certain time.

D.2 Introduction

The importance of performing efficient and controlled viral infections on mammalian cell cultures has long been crucial to optimize the gene transfer procedures for basic research and gene therapy [1-4]. The common denominator is the necessity of increasing viral infection efficiency while preserving viability and biological processes of the cultured cells. The use of adenoviruses, non-integrating viruses, preserve genomic integrity and offer reduced risks for human safety. Moreover, process automatization, low volumes of reagents, and reduced costs are desirable. Standard procedures for culture infection involve virus dilution in the media to defined concentrations, usually quantified by the multiplicities of infection (MOI), representing the number

of viral particles per cell. Efficiency of transfection of some cell types may be low, thus requiring high MOIs potentially resulting in toxic side effects on the cells. In parallel, the advent and ever-increasing use of microscaled technologies and microfluidic devices for lab-on- a-chip applications has led to relevant improvements in the study of complex biological systems [5-10]. Examples of applications of microfluidic platforms have been extensively reviewed [11,12] and point at the advantages deriving from the miniaturization, integration, and automation of biochemical assays. Recent literature reflects increased interest in adopting microfluidic devices in drug discovery process [13,14], molecular detection [15], and in clinical and medical research [16]. In order to efficaciously control and exploit their potential, it is fundamental to understand the physics of mass- transport phenomena and of fluid flows at the microscale [17,18] and the fabrication processes, and properties of typically used materials [19-21] Despite the advantages and versatile applications deriving from microfluidic platforms, only few studies combining these devices and viral infections of cultured cells can be found in the literature. Examples include some applications of microfluidic bioreactors for the continuous production of retroviral vectors [22], or the dielectrophoretic capture and imaging of viral particles on microelectrodes [23]. A microscale platform was developed to detect and quantify virus growth and spread [24] and micropatterning has been used to characterize the in vitro propagation of viruses in cell arrays [25] Cells were infected using virus gradients [26], but the biological readout showed a low number of cells within the microchannels, and virus replication studies were performed on hepatocytes seeded within micro cell-culture chambers [27]. However, neither rational studies on the influence of perfusion nor a screening of the infection parameters were performed. Finally, most of these systems suffered some of the major limitations deriving from culturing cells within standard microfluidic channels such as lower growth rates, and the need for frequent changes of media during the preliminary phases. Here, we develop a microfluidic platform that can be easily and reversibly coupled to cell cultures, that allows performing multiparametric experiments and exerting a precise control over the soluble extracellular microenvironment, thus increasing the efficiency of infection. Our microfluidic device is used for the optimization of the process of cell infection through an approach

that combines mathematical modeling with the experimental validation. On one hand, mathematical models evaluate the transport phenomena and the dominating regimes within a defined system, while experiments, on the other, analyze static and perfused microfluidic-driven infection processes, validating the modeled conditions and demonstrating that our microfluidic platform allows increasing the infection efficiency when compared to static conditions, even at the lowest MOIs. Infections are usually carried out in standard culture plates at defined MOIs and since the efficiency of infection is proportional to the virus adsorbed on the cellular membrane, the minimization of the total volume of viral suspension is crucial to favor the contact between viral particles and adhering cells. Viral particles are uniformly dispersed in the solvent, and their transport from the bulk of the liquid to the cell surface is purely driven by brownian-like diffusion. However, in microfluidic experimental setup, mass transport of particles is driven by both diffusion and convection phenomena. In particular, diffusion has a driving force represented by a difference in concentration (Δc), while convection results from a bulk velocity of the fluid. Consequently, convection gives an additional contribution enhancing the transport of viral particles to the cells, thus increasing the efficiency of infection. It will be crucial to define a method to compare the results of static and microfluidicperfused conditions in terms of infection efficiency. In order to have fair comparison between static and perfused conditions, a proper experimental design has been proposed to maintain the same concentration, MOI, and total volume of medium. This experimental design will allow to highlight the influence of different intrinsic properties of the hydrodynamic regimes (static and perfused) on infection efficiency. Mathematical modeling will allow to analyze the theoretical variations of the ratio of virus fluxes in static and perfused conditions and derives the optimal operative variables such as flow rates and infection times.

D.3 Materials and Methods

D.3.1 Cell culture

Mouse embryonic fibroblasts (MEFs) were purchased from Chemicon and were cultured in 79% Iscove's modified Dulbecco's medium (IMDM, Invitrogen), 20% foetal bovine serume (FBS, Invitrogen), and 1% penicillin/streptomycin (Invitrogen). Human foreskin fibroblasts (HFFs) were supplied by Dr. L. Barzon from the University of Padova and were cultured in 89% Dulbecco's modified eagles medium (DMEM, Sigma-Aldrich), 10% FBS (Invitrogen), and 1% penicillin/streptomycin (Invitrogen). Passaging of both cultures was performed with Trypsin 0.025%-EDTA (Invitrogen) and cells were either re -plated on culture flasks for further expansion or seeded on glass coverslips, both coated with 0.66% A-type pork gelatin (Sigma-Aldrich).

D.3.2 Microfluidic platform

The multilayered microfluidic platform (overall dimensions: 75 x50 mm) was designed for an easy interface with the cell system, and fabricated using lithographic techniques and molded in poly-dimethylsiloxane (PDMS)[28].The platform (Figure 1(A)) comprised: (i) a supporting glass slide with a PDMS slab carved to accommodate the cell culture coverslip, (ii) a membrane-based vacuum system for its reversible sealing, and (iii) the microfluidic channels (width x height 0.2 x 0.1 mm) delivering fluids to the cultured cells. The circular channel creating the suction sealing the two layers, faces the PDMS slab in (i) and is thermally (and irreversibly) bonded to the upper microfluidic layer (iii). The assembled platform formed a 16x16mm culture chamber, area in which the cultured cells were exposed to the fluid streams from the microfluidic channels. The height of the chamber could be varied as needed; for all the experiments presented here we used 0.5mm high membranes. The platform was entirely optically transparent, allowing in-line observations of the cultures by easy interface with standard microscopes (Figure 1(B)). The micro-perfusion apparatus (Figure 1(C)) was composed of the multilayered microfluidic platform, two syringe pumps (PHD, Harvard Apparatus, Holliston, MA), and a vacuum control system (membrane pump H35M and digital vacuum sensor, Vuototecnica, Italy). All con-

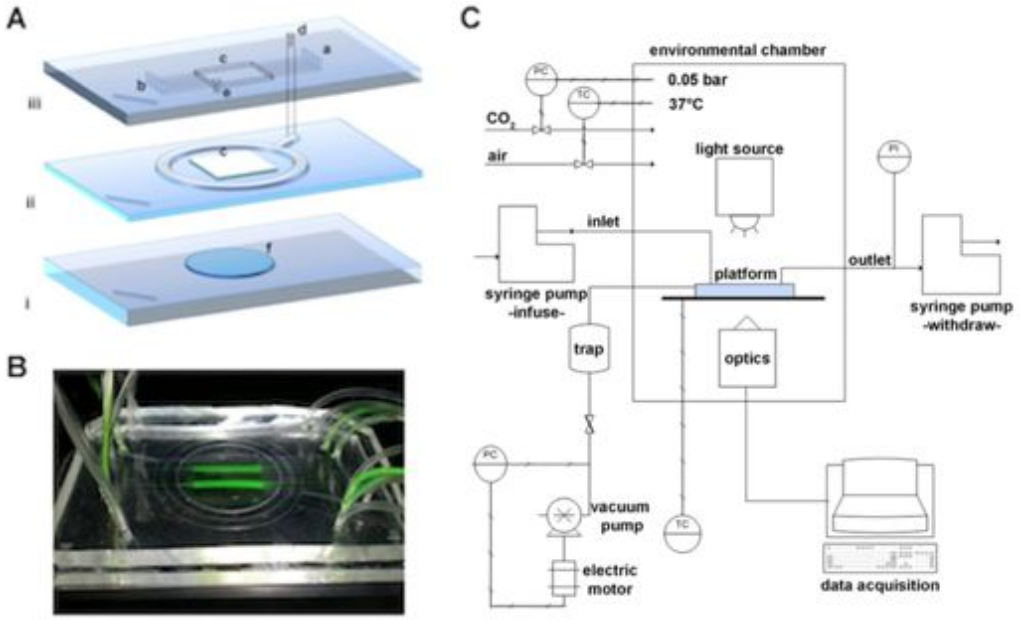

Figure D.3.1 – Platform design and experimental setup. Panel A. The platform comprised: i) a supporting glass slide with a PDMS slab carved to accommodate the cell culture coverslip (f), ii) a membrane-based vacuum system for the reversible sealing of i, and iii) the microfluidic channels delivering flu- ids to the cultured cells (inlets in (a) and exits in (b)). The assembled platform formed a 12x12 mm culture chamber (c) where cells were exposed to the fluid streams. The top layer embedded connections to the vacuum system (d) and to a pressure-monitoring auxiliary service (e). Panel B reports an image of the assembled platform, which was entirely optically transparent, operated flowing a color tracer (fluorescein) in 2 of the 8 channels. Panel C. The micro-perfusion appara- tus was essentially composed by the multilayered microfluidic platform, two syringe pumps, and a vacuum control system. The interface with a fluorescence microscope equipped with an environmental chamber is shown.

nections between components were made using Tygon tubings (0.5mm ID, 1.5mm OD, Cole Palmer, USA).

A brief description of the experimental procedures follows. Before assembling and coupling to the cell cultures, all components, connections, and tubings were rinsed with water and then sterilized via autoclave treatment. Tubings were then rinsed with sterile culture medium and incubated for at least 1 h prior to the platform assembly. This preconditioning of the tubings' walls reduced the potential loss of viral particles due to undesired adsorption. Sterile 3 ml syringes to be connected to the platforms outlets were filled with 500 μl of sterile PBS, to avoid the elastic effect of air, and connected to the microtubes exiting the platform. Sterile 3 ml syringes to be connected to the platforms inlets were filled with culture medium. The open cell chamber was covered with 1 ml of culture medium and the syringe-pumps activated to

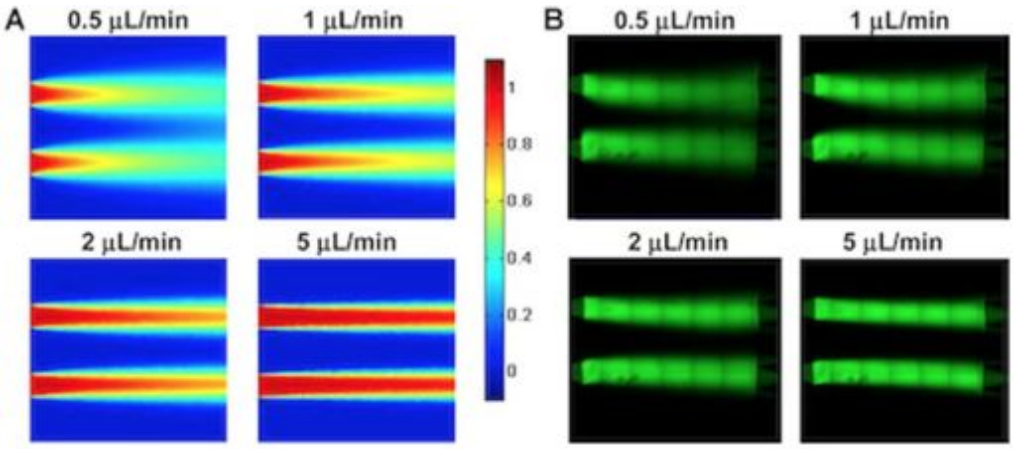

Figure D.3.2 – Model validation. Panel A reports representative results of the mathematical modeling showing concentration maps within the culture chamber. For a defined molecular species with its diffusion coefficient and fixed systems geo- metrical specifications, increases in the fluid flow rate change the shape of the compartment. Transport phenomena span from diffusion- to convection-dominated regimes following increases in flow rate. Panel B shows merged fluorescent images reconstructing the entire culture chamber, acquired during the experimental runs performed using parameters equal to the modeled ones.

stabilize the fluid flow and eliminate any residual bubble. Finally, the glass coverslip with the cultured cells was coupled to the lower layer, the entire platform assembled and the vacuum system ensuring hydraulic sealing activated. The multiple inlet and outlet channels allowed creating highly compartmentalized fluid regions within the culture chamber, thus increasing the throughput of the system potentially consenting to test several levels for a variable (i.e., virus MOIs) at a single time (Figure 2).

D.3.3 Fluid dynamics modeling

The Navier-Stokes equations for incompressible fluids were numerically solved using the finite elements method implemented in COMSOL Multiphysics (Burlington, MA). The 2D domain of the culture chamber was geometrically modeled and a non-structured mesh was automatically generated with triangular elements. Subsequent grid refinements were required to ensure independency of the solution from the spatial discretization. No-slip boundary conditions were used for the chamber and microfluidic conduits walls, a fixed velocity for the inlet channel and finally zero pressure for the outlet. The fluid properties viscosity and density were taken from the literature [29]. To obtain concentration profiles within the chambers, the mass balance equations for a convective-diffusive regime were solved again using COMSOL Multi-

physics software (Burlington, MA, USA). Fluid velocity profiles were obtained from the Navier-Stokes solutions. Defined concentrations were used as boundary conditions at the different inlets, convective flux at the outlets and insulation/symmetry elsewhere. The diffusion coefficient for the adenoviral vector (AdV) was calculated from the Stokes-Einstein equation [30]. The diffusion coefficient of a virus particle, approximated by a 90 nm hydrodinamic diameter, was assumed to be $6{\cdot}10^{-12}\ m^2 s^{-1}$. Fundamental assumptions of our modeling approach follows. Focusing on the resistances within the media compartment, we assumed that the virus adsorption was much faster (steady state assumption) than the mass transport. We also assumed that all intracellular phenomena related to viral protein expression such as virus internalization, virus decay, and protein production, were not affected by the velocity profile in the media compartment. Within these assumptions, the calculated virus molar flux at cell membrane could be considered directly related to the efficiency of infection. The ratio between virus molar fluxes of dynamic and static conditions is defined as the theoretical relative efficiency, \phi_r. In this work, we compared ϕ_r as a function of different parameters such as MOI, time of infection, and hydrodynamic regime. In particular, hydrodynamic regime was described through the dimensional Peclet number defined as Pe = νH/D, where ν is the velocity, H is a characteristic length (chamber height in our case), and D is the diffusion coefficient. This dimensionless variable identifies flow rate conditions at defined geometrical constraints into specific diffusional or convective transport regimes. Empirical calculations were also performed (fluxes were evaluated as a function of time, diffusion coefficient, volumes) and used as a comparison to validate the mathematical modeling (data not shown). Cell densities, MOIs, viral concentrations, and infection times were kept constant at their optimized values. In addition, during the preliminary design and development phases, experimental validation of the modeled fluid compartmentalization in multichannel platform was performed using fluorescein dye as a tracer. Figure 2 shows the good agreement between model prediction and experimental analysis allowing model prediction of small diffusing particles. Supplementary Figure AS1 reports additional data quantifying the fluorescence levels of the experimental images (directly correlated to concentration values) [31]. These plots can be compared to the analogous

concentration curves obtained by the modeled concentration maps.

D.3.4 Infection protocols

D.3.4.1 Static condition

AdVs carrying the EGFP transgene were used at different MOI to infect multiple cell lines, both in static or in perfused conditions. Briefly, AdV is based on the Ad5 genome and lacking the E1 and E3 regions was constructed by homologous recombination in E. coli using AdEasy vector system (Qbiogene, Carlsbad, CA). In this vector, human cytomegalovirus promoter was used to drive expression of green fluorescent protein. AdEGFP was propagated in E1- complementing HEK 293 cells, purified by cesium chloride density centrifugation, and titrated by TC_{ID50} endpoint assay according to the AdEasy production protocol. Viral vector stocks were stored at $5.0 \cdot 10^9$ pfu/ml concentration in 10% glycerol at -80 °C until use. The infection efficiency was evaluated at different time-points post-infection quantifying the EGFP expression on the live samples via image analysis. Cells were seeded on gelatin coated coverslips 24 h before infection; the volume of the viral high-titer stock solution to be used was calculated for any given cell density and experimental MOIs. The viral stock solution was thawed and aliquots prepared and diluted to the final volume with the required culture medium. Cell cultures were then incubated (37 °C, 5% CO_2, 95% humidity) with the viral solutions for defined times. Cells were rinsed with warm PBS without Ca^{2+}/Mg^{2+} (Gibco) and reincubated with culture medium. Post-infection incubation time varied depending on the experiment. In time-course runs, cells were re-incubated for up to 3 days. Images were acquired 48 h post infection.

D.3.4.2 Microfluidic perfused conditions

All of the above described procedures were followed, with the sole difference that the viral suspension was loaded in 3ml syringes and connected to the assigned inlet channels. Particular attention had to be paid at calculating the exact viral particles number which would ensure correspondence between the static and perfused infections.

D.3.4.3 Measurement of the infection efficiency

At the established time points, cell cultures were incubated with Hoechst 33342 (Invitrogen) nuclear dye. After this assay, images of randomly chosen positions were acquired (microscope Leica DMI 6000-B) on both fluorescence channels: blue for Hoechst marking all cell nuclei and green for the cytoplasmic EGFP signal expressed by the infected cells only. In order to obtain comparable set of data, the exposure, gain, and intensity values should be the same in every image. Quantification of these results was performed via image analysis on paired fluorescence pictures (blue and green channels). A custom developed script listing the command lines was implemented and run in MATLAB. Briefly, this script organized images in pairs, converted them in grayscale, enhanced contrast and finally converted them in binary format. Further processing allowed removing cell-debris, a potential source of quantification errors. The binary image of the nuclei was used to automatically count the total number of cells. After that, a pixel by pixel subtraction between the two binary images produced a new matrix creating the final image showing only the nuclei of successfully infected cells. Automated counting led to the obtainment of the number of infected cells and of the global efficiency of infection (number of infected cells over total number of cells).

D.4 Results

D.4.1 Model validation

The capability of the platform to generate well-defined concentration compartments was first modeled and then validated using fluorescein as a dye tracer. The results of the mathematical modeling are shown in Figure 2(a), where the sole culture chamber is represented for ease of visualization. The shape of the compartment can be precisely defined by simply tuning the fluid flow rate. At the lowest flow rates, transport by diffusion and convection competes determining a feather-like shaped concentration pattern. For increasing flow rates, convection becomes the dominant transport phenomena and leads to the formation of sharp compartments. Figure 2(b) reports the results of the experimental validation, performed using the same coefficients and

geometrical specifications applied for the mathematical modeling. The extremely close resemblance between the experimental concentration patterns and the modeled ones validated the model predictions and the systems performance. A quantification of this observation is available in supplementary Fig. AS1 [31].

D.4.2 Modeling of the cell infection process

Figure A3 summarizes representative results of the computational modeling of the infection process. Again, is the theoretical relative efficiency of microfluidic perfused versus static infection. The curves in panel A3(a) are parametric in Pe and reported as a function of the square root of time. The horizontal line at ϕ_r =1 highlights the threshold at which molar fluxes (and thus infection efficiencies) of perfused and static processes are equal, thus allowing to identify the parameters characterizing the variables-space where perfused-microfluidic ($\phi_r > 1$) or standard static ($\phi_r < 1$) infection conditions are favored. For example, given the systems geometrical constraints and the duration of the infection process, increases in fluid flow rate (which directly translate into increases in Pe number), will favor perfused-microfluidic processes, which will result in higher infection efficiencies. Vice versa, at the lowest flow rates where convection gives no significant contribution to the overall transport of viral particles from the bulk of the liquid to the cell surface, standard static infections prove to be more efficient. Panel 3(b) plots the values of ϕ_r as a function of Pe for a fixed time (t = 90 min) of infection. Again, it is evident how for increasing flow rates, perfused-microfluidic infections lead to higher yields with a trend plateauing for Pe higher than 200 (corresponding to a 1 $\mu l/min$ flow rate and 8 μm/s linear velocity). Finally, panel 3(c) plots the times at which $\phi_r = 1$ for Pe ≥ 100, showing again how for increasing Pe perfused-microfluidic infections could lead to higher yields than standard static processes exposing the cells to potentially harmful viruses for shorter times.

D.4.3 Cell infection

Several experiments have been performed in order to optimize the procedures and parameters characterizing the infection process, both in static and microfluidic cul-

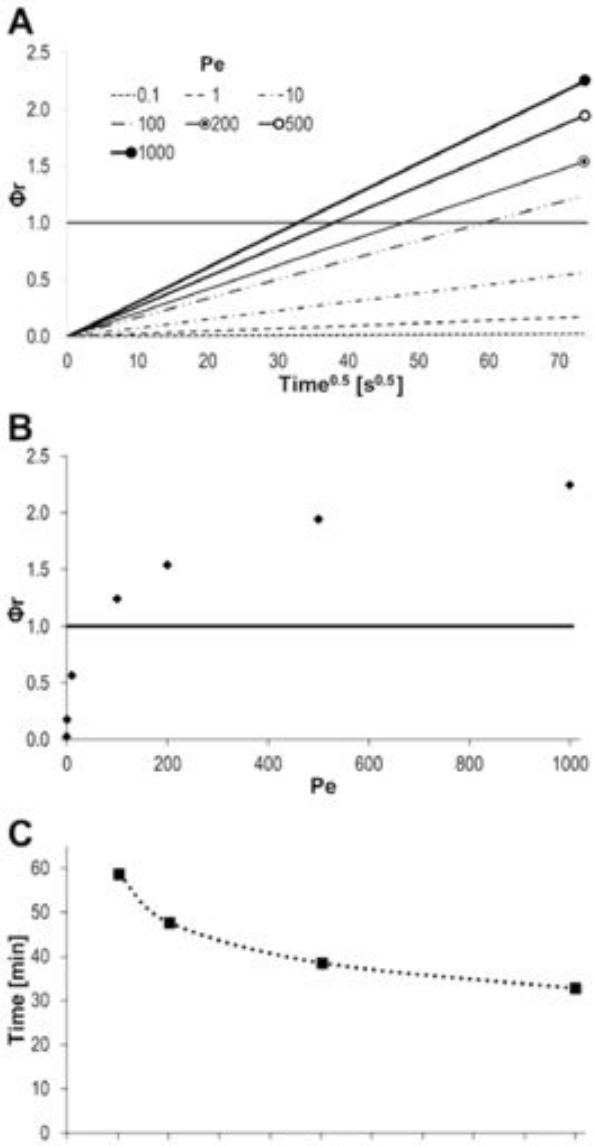

Figure D.4.1 – Computational modeling of the infection process. ϕ_r is the theoretical relative efficiency of microfluidic perfused versus static infection. Panel A reports ϕ_r curves parametric in Pe and as a function of the square root of time. The horizontal line at $\phi_r = 1$ (equality of perfused and static molar fluxes) separates the variables space where perfused-microfluidic ($\phi_r > 1$) or standard static ($\phi_r < 1$) infection conditions are favored. Panel B plots ϕ_r as a function of Pe at a defined time (t=90 min) of infection. Finally, panel C plots the times at wich $\phi_r = 1$ for P > 100.

ture. Cell line, cell density, cell passage, virus MOI, duration of the exposure to the viral solution (incubation time), and Pe number, were among the screened variables. From these preliminary experiments, we established optimal values and ranges: cell seeding density was kept constant at 100 cells/mm^2, MOI was varied from 10 to 100, Pe levels for microfluidic cultures were 10 and 100, and infection times spanned from 90 min to 12 h. In reporting some of the most significant findings on HFF cells, we highlight how: (a) increases in the incubation time led to increases in the infection efficiency (Figure A4(a)) (further discussion will be presented in the following sections). (b) An inverse-relationship correlation was established between viral suspension volume (at a given MOI) and infection efficiency: increases in the first led to decreases in the latter (Figure A4(b)); however, no changes in infection efficiencies were measured for increases in the viral suspension volume at constant viral particles concentration (Figure A4(c)). (c) For a given infection time, observation of the cell cultures over 3 days demonstrated how the efficiency increased over the first two days and reached a plateau by day 3 (data not shown). Additional material is presented in supplementary FigureA S2 [31]. Fundamental relations were established between variables, to allow comparisons between the different culture and infection conditions. In particular, to ensure constant virus concentration in static and microfluidic infections, MOIs must be translated into concentrations as follows:

$$c_v = \frac{MOI \cdot NCells_{Stat}}{Vol_{Stat}} = \frac{MOI \cdot MCells_{\mu Fl}}{Vol_{\mu Fl}} \tag{D.4.1}$$

and

$$Vol_{\mu Fl} = Q \cdot t \tag{D.4.2}$$

where c_v is the virus concentration in culture medium, MOI is the number of viral particles per cell, *NCells* is the total number of cells exposed to the viruses, and *Vol* is the total volume of fluid used in the experiment. Q is the fluid flow rate and t is the duration of the infection process. Subscripts *Stat* and *Fl* refer to static and perfused-microfluidic infections, respectively. It is important to underline how the possibility of compartmentalizing fluids within the microfluidic platform would

divide the culture area in 4 sections, each containing 1/4 of the total number of cells and exposing them to different MOIs; this thus need to be taken into account in evaluating virus concentrations and other variables.

Rearranging the above equations, we can calculate the volume of the viral suspension to be used in standard conditions as a function of the fluid flow rate, corresponding to the chosen Pe value, of the microfluidic process:

$$Vol_{Stat} = \frac{NCell_{Stat}}{NCell_{\mu Fl}} \cdot Q \cdot t \tag{D.4.3}$$

We planned the experimental runs following these variables constraints and obtained the results shown in Figure 5. Cell seeding density was constant at 100 cells/mm2. Experiments were performed at Pe=10 and Pe=100. Panels 5(a) and 5(c) refer to HFF cultures, 5(b) and 5(d) to MEF. Image acquisition was performed 48 h post infections on cells treated at MOI 100 for 90 min. At lower Peclet, static infections led to significantly higher infection efficiencies when compared to the corresponding microfluidic perfused ones for both cell lines, while differences were strongly reduced at the highest Pe value. This is an expected trend described by our model, as can be seen in the bottom graphs of Figure 5 (panels C and D), where the relative efficiency of microfluidic perfused versus static infection is reported as a function of the square root of time. Here, ϕ_r resulted in significant higher values at Pe=100 when compared to the ones at Pe=10 for both cell lines. In particular, the highest ϕ_r values were detected on MEFs, a result that led us to the use of MEFs for the following experiments. The relative infection efficiencies are in very good agreement with the theoretical ones. Higher Pe always led to higher infection efficiencies (measured by the theoretical relative efficiency factor) and, under the same conditions, MEFs showed higher infection efficiencies if compared to HFF. Regarding HFF, the value at higher Pe is overestimated by the model. It is worth to remind that the model describes the ideal case in which the delivery of viral particle is mainly limited by the transport phenomena within the liquid domain. If our hypothesis fails, an additional step normally faster than transport phenomena, such as virus adsorption or internalization, could negatively affect the overall infection efficiency.

To further explore this issue we performed additional experiments, whose results

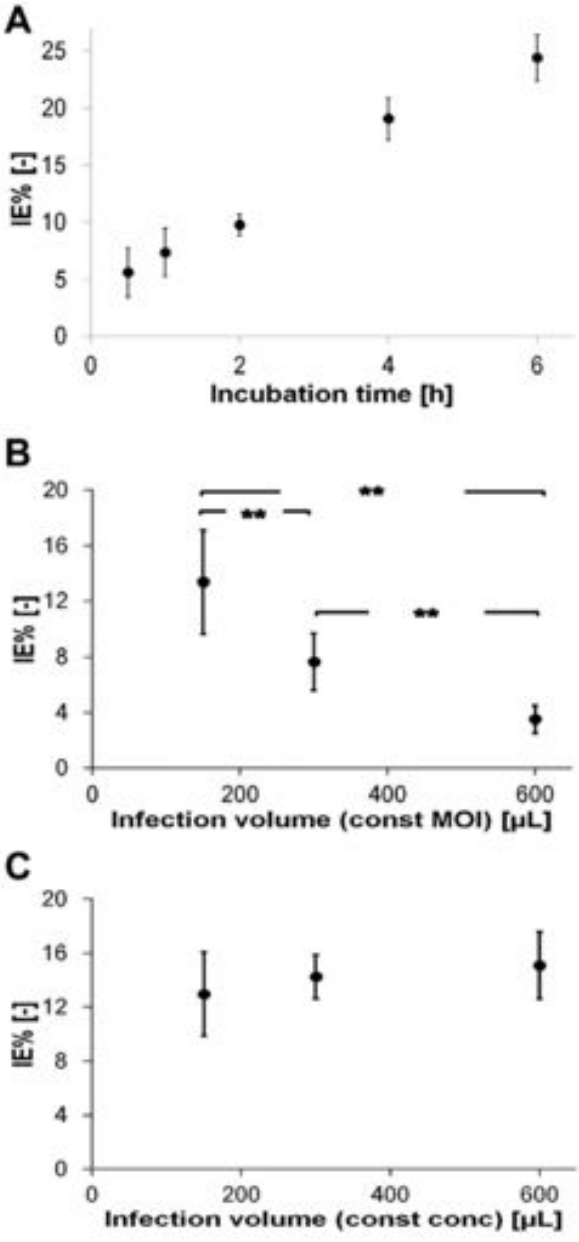

Figure D.4.2 – Static infections on HFF cultures. HFF were plated at a 100 cells/mm2 density, and all infections started 24 h after seeding. MOIs were: 50 in panel A, 100 in panel B, and 100, 200, 400 respectively for the data points in panel C. In panel A, the plotted data points demonstrate how longer incubation times of cell cultures with the viral suspension led to increases in the infection efficiency. In panel B, increases in the viral suspension volume (at a given MOI) led to reduced infection efficiencies; in parallel, panel C demonstrates that no significant changes in infection efficiencies were measured for increases in the viral suspension volume at constant viral particles concentration.

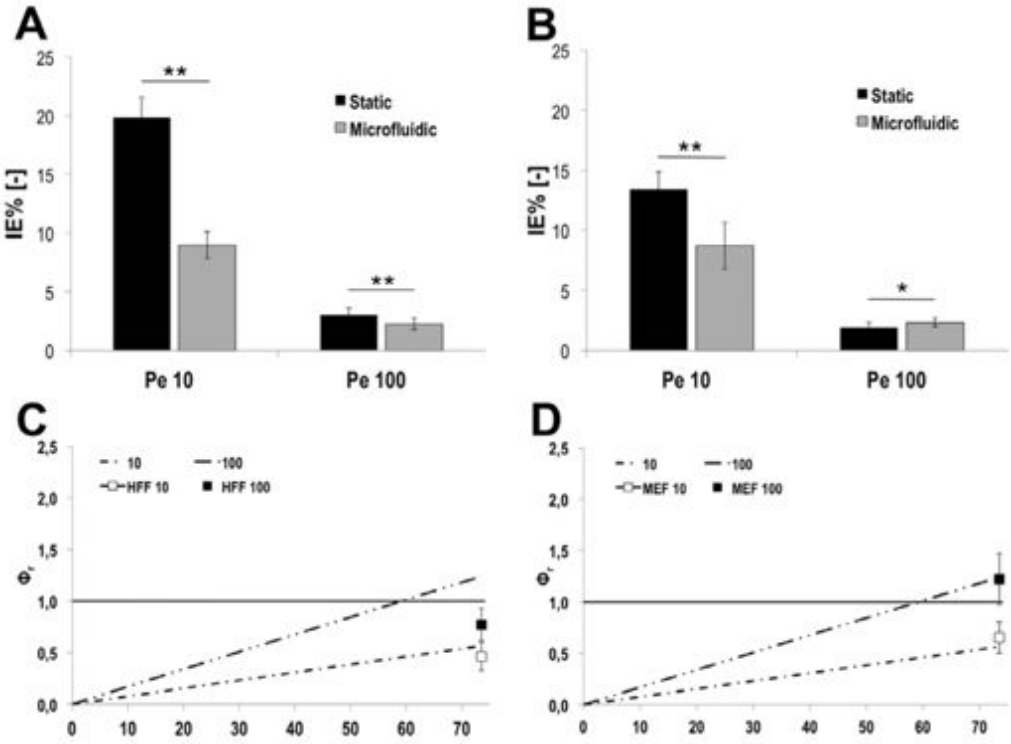

Figure D.4.3 – Comparison between static and microfluidic infec- tions at different Peclet numbers for two cell types. Cell density was kept constant at 100 cells/mm^2; MOI was 100, and infection time 90 min. Experiments were performed at Pe = 10 and Pe = 100. Panels A and C refers to HFF cultures, B and D to MEF. Data were obtained via image analysis of cell cul- tures 48 hours post infection. Panels C and D graph the mod- eled profiles for ϕ_r (the theoretical relative efficiency of microfluidic perfused versus static infection) and allow comparison with representative experimental results. Empty markers are for Pe = 10 and filled markers for Pe = 100.

are presented in Figure 6. First of all, we analyzed the effect of increasing infection times at low MOIs. Panel 6A shows infection efficiencies measured following exposure of cell cultures (MEFs) to adenoviruses at MOI 10 for times ranging from 90 min to 12 h, both in static and microfluidic perfused culture. Additional material is available in Figure S3 [31]. The results highlighted how the use of microfluidics allowed obtaining higher efficiencies for longer incubation times. This is due to the fact that, while in static infections the concentration of viral particles surrounding a cell decreased with time, resulting in plateauing efficiencies, the steady state that was established perfusing the cultures ensured the maintenance of a constant concentration of viruses around cells and further increases in the infection efficiency. Finally, we introduced the new concept of "effective MOI": as the standard MOI is the total number of viral particles per cell which varies with time as viruses are transported to cells, the effective MOI was defined as the number of viral particles surrounding a cell at a certain time. This value is considered constant in perfused conditions, according to the establishment of the steady state. Now, the two MOIs are related through the fluid volumes used for the experiment (in turn determined by the chosen Pe number):

$$MOI_{total} = MOI_{effective}\frac{V_i}{V_{ch}} \tag{D.4.4}$$

where V_i is the viral suspension volume used for cell infection during a single experiment and V_{ch} is the volume of the cell chamber. The total and effective MOI are equal in static conditions, where V_i corresponds to V_{ch}, and different in experiments with perfusion, where $V_i V_{ch}$. Experiments performed using the effective MOI produced the results shown in Figure 6(b). Exposing cells to the viral suspension at an effective MOI of 100 for 12 h led to favored efficiencies for the microfluidic perfused processes, resulting in significantly higher infection efficiencies than those reached in static conditions.

D.5 Discussion and conclusions

In this study, we present a rational approach to the issue of viral infection of cell cultures, comparing theoretical modeling and experimental evidence. An accurate

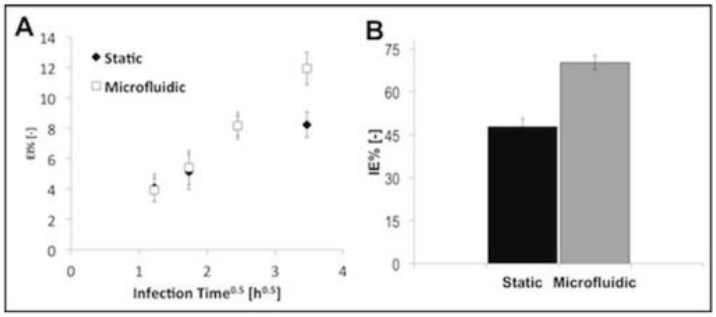

Figure D.4.4 – Comparison between static and microfluidic infec- tions for different infection times and at effective MOI. In Panel A the cells were exposed to the viral suspension at MOI 10 for times ranging from 90 minutes to 12 hours, both in static and microfluidic perfused culture. The use of mi- crofluidics allowed obtaining higher efficiencies for longer in- cubation times. In Panel B, infections were performed at an effective MOI of 100 for 12 hours and led to significantly higher efficiencies in microfluidic infections compared with those reached in static conditions.

analysis of the phenomenological behavior of an infection process on a cell culture, explored the effects of transport (diffusional and convective) in static and microfluidic-perfused conditions. Rationalization of the infection steps and limiting phenomena acting on the system highlighted the pros and cons of both conditions. Static conditions, for example, represent the standard procedure and are thus routinely performed with well established techniques; however, they tend to utilize high MOIs in order to ensure high infection efficiencies, are diffusion-dependent and regulated by unpredictable and continuously varying kinetics (since virus concentration in the cells surroundings decreases uncontrollably due to virus degradation, consumption, and internalization by the cells). Perfused infections, on the contrary, can be precisely controlled and the persistence of a steady state renders the system more stable and predictable. At the steady state, the virus concentration at the cell membrane is constant and maintained at the established optimal level, thus allowing the use of lower MOIs to obtain higher infection efficiencies while reducing the risk of exposing cultures to a hostile environment. In addition, we developed a relationship between molar fluxes of viral particles and infection efficiencies, with molar fluxes determined by the systems parameters and variables (geometry, flow rates, etc.). Such variables have been translated into correlation terms that take into account the necessity of having comparable entities for static and perfused conditions. Dimensionless forms, where applicable, were favored. This approach led us to a more accurate experimental plan, where only one variable at a time was varied in parallel

static and perfused infections; the obtained results were thus directly comparable. Our static controls were performed using standard multiwell plates, fitting the glass coverslips used as culture substrates. We want to point out how this choice, over that of statically operating the microfluidic platforms, allowed us to use the same total volumes reached in the perfused experiments; this is of paramount importance in sight of obtaining infection efficiency data that could be compared between the two conditions. Flow rate choices in the microfluidic experiments were translated in corresponding infection volumes in static controls ($V = Q * t$), and a variable such as MOI could then be independently changed. All together, these results show how the microfluidic technology can be used for rational designing an infection process with high intrinsic efficiency without the risk of viral associated-cytotoxic derived by high MOI static treatment.

ACKNOWLEDGMENTS

We thank Ca.Ri.Pa.Ro., F.S.E., and Ministero della Salute for funding.

D.6 References

[1] B. Kaspar, J. Llado´, N. Sherkat, J. Rothstein, and F. Gage, Science 301, 839 (2003).

[2] J. Luo, M. Kaplitt, H. Fitzsimons, D. Zuzga, Y. Liu, M. Oshinsky, and M. During, Science 298, 425 (2002).

[3] F. C. Marini, Q. Yu, T. Wickham, I. Kovesdi, and M. Andreeff, Cancer Gene Ther. 7, 816 (2000).

[4] S. Vorburger and K. Hunt, Oncologist 7, 46 (2002).

[5] H. Andersson and A. van den Berg, Lab Chip 4, 98 (2004).

[6] E. Cimetta, C. Cannizzaro, R. James, T. Biechele, R. T. Moon, N. Elvassore, and G. Vunjak-Novakovic, Lab Chip 10,3277 (2010).

[7] E. Cimetta, E. Figallo, C. Cannizzaro, N. Elvassore, and G. Vunjak-Novakovic, Methods 47, 81 (2009).

[8] N. Jeon, S. Dertinger, D. Chiu, I. Choi, A. Stroock, and G. Whitesides, Langmuir 16, 8311 (2000).

[9] T. Keenan and A. Folch, Lab Chip 8, 34 (2007).

[10] G. M. Whitesides, Nature (London) 442, 368 (2006).

[11] D. Breslauer, P. Lee, and L. Lee, Mol. BioSyst. 2, 97 (2006).

[12] S. Haeberle and R. Zengerle, Lab Chip 7, 1094 (2007).

[13] P. S. Dittrich and A. Manz, Nat. Rev. Drug Discovery 5, 210 (2006).

[14] Y. Wen and S.-T. Yang, Expert Opin. Drug Discovery 3, 1237 (2008).

[15] B. D. Piorek, S. J. Lee, J. G. Santiago, M. Moskovits, S. Banerjee, and C. D. Meinhart, Proc. Natl. Acad. Sci. U.S.A 104, 18898 (2007).

[16] M. Toner and D. Irimia, Annu. Rev. Biomed. Eng. 7, 77 (2005). 96 A. Microfluidic driven viral infection on cell culture: theoretical and experimental study

[17] D. J. Beebe, G. A. Mensing, and G. M. Walker, Annu. Rev. Biomed. Eng. 4, 261 (2002).

[18] T. Squires and S. Quake, Rev. Mod. Phys. 77, 977 (2005).

[19] J. C. McDonald, D. C. Duffy, J. R. Anderson, D. T. Chiu, H. Wu, O. J. Schueller, and G. M. Whitesides, Electrophoresis 21, 27 (2000).

[20] S. K. Sia and G. M. Whitesides, Electrophoresis 24, 3563 (2003).

[21] G. M. Whitesides, E. Ostuni, S. Takayama, X. Jiang, and D. E. Ingber, Annu. Rev. Biomed. Eng. 3, 335 (2001).

[22] H. N. Vu, Y. Li, M. Casali, D. Irimia, Z. Megeed, and M. L. Yarmush, Lab Chip 8, 75 (2008).

[23] D. Akin, H. Li, and R. Bashir, Nano Lett. 4, 257 (2004).

[24] Y. Zhu, J. W. Warrick, K. Haubert, D. J. Beebe, and J. Yin, Biomed. Microdevices 11, 565 (2009).

[25] E. E. Endler, K. A. Duca, P. F. Nealey, G. M. Whitesides, and J. Yin, Biotechnol. Bioeng. 81, 719 (2003).

[26] G. Walker, M. Ozers, and D. Beebe, Sens. Actuators B 98, 347 (2004).

[27] T. R. Sodunke, M. J. Bouchard, and H. M. Noh, Biomed. Microdevices 10, 393 (2008).

[28] Y. Xia and G. Whitesides, Annu. Rev. Mater. Sci. 28, 153 (1998).

[29] E. Cimetta, M. Flaibani, M. Mella, E. Serena, L. Boldrin, P. De Coppi, and N. Elvassore, Int. J. Artif. Organs 30, 415 (2007).

[30] R. Bird, W. Stewart, and E. Lightfoot, Transport Phenomena (Wiley, 1960).

[31] See supplementary material at 10.1063/1.4723853 for images of infected cells.

Appendix E

Optimal perfusion strategy for robust long-term cell culture in microfluidics

Stefano Giulitti[1,2], Enrico Magrofuoco[1,2], Lia Prevedello[1,2], and Nicola Elvassore[1,2]

1. Department of Industrial Engineering (DII), University of Padua, via Marzolo 9, 35131 Padua, Italy.

2. Venetian Institute of Molecular Medicine (VIMM), via Orus 2, 35129 Padova, Italy.

Lab on a Chip

Volume 13(22):4430-41

10.1039/c3lc50643f

E.1 Summary

Long-term cell culture in microfluidic devices is an essential prerequisite for "on a chip" based biological and physiological studies. We investigated how medium delivery, from continuous to periodic perfusion, affects long-term cell cultures in a microfluidic platform. Computational simulations suggested that different delivery strategies result in different temporal profiles of accumulation and washing out of endogenous (EnF) and exogenous (ExF) factors, respectively. Thus, cultures exposed to the same overall amount of medium with different temporal profiles were analysed in terms of homogeneity, cell morphology and phenotype. Murine and human cell lines (C2C12 and HFF) and mouse embryonic stem cells (mESC) were cultured in microfluidic channels. Ad hoc experimental setup was developed to perform continuous and periodic medium delivery into the chip, tuning the flow rate, the perfusion time, and the interval of perfusion while using the same amount of medium volume. Periodic medium delivery with a short perfusion pulse ensured cell homogeneity compared to standard cell culture. Conversely, a continuous flow resulted in cell heterogeneity, with abnormal morphology and vesiculation. Only dramatic and unfeasible increasing of perfused medium volume in the continuous configuration could rescue normal cell behaviour. Consistent results were obtained for C2C12 and HFF. In order to extend these results to highly sensitive cells, mESC were cultured for 6 days in the microfluidic channels. Our analysis demonstrates that a periodic medium delivery with fast pulses (with frequency of 4 times per day) resulted in a homogeneous cell culture in terms of cell viability, colony morphology and maintenance of pluripotency markers. According to experimental observations, the computational model provided a rational description of the perfusion strategies and of how they deeply shape cell microenvironment in microfluidic cell cultures. These results provide new insight to define optimal strategies for homogeneous and robust long-term cell culture in microfluidic systems, an essential prerequisite for lab on chip cell-based applications.

E.2 Introduction

The demand of tightly controlled cell microenvironments, high reproducibility and high-throughput processing for multi-parametric analyses is undoubtedly increasing. The exploding field of microfluidics offers attractive technologies, which can fulfil these requests and extend conventional cell culture experiments for the study of biological systems, for a better insight of the physiology and for the development of in vitro models. Hence, robust long-term microfluidic cell cultures are of paramount importance to fully establish a highly controlled integrated system. Microfluidic devices have become extremely relevant for cellular bioassays and tissue engineering [1]. Their reduced system dimensions allow an accurate control of the spatial and temporal local system properties [2,3], a fast stimulation and detectable cell response, and high-throughput arrays for multi-parametric analysis while reducing the operating costs [4]. Various examples of long-term microfluidic cell culture are reported in the literature [5–13]. Either continuous [6–10] or periodic [11–14] medium delivery has been used to maintain cell cultures for prolonged time. Although the complexity of microfluidic architecture has been extensively explored, and the effect of some operative variables has been analysed, the identification of an optimal strategy for medium delivery is still an open issue. Despite being a fascinating tool to tightly control medium composition, microfluidics showed some drawbacks when coupled with cell culture systems. Even using the same overall amount of medium in a time interval, it should be considered that different delivery strategies imply different spatio-temporal profiles of metabolites and growth factors, which may significantly influence overall cell behaviour and long-term culture stability. Due to the high surface/volume ratio in microfluidics, frequent accumulation or washout of extrinsic factors has been reported to end up with a long-term toxicity effect [11]. Especially for high demanding cells, nutrient supply and waste removal should be finely balanced with the requirement of growth factors secreted by the cells. When a continuous perfusion is applied, soluble factors can be depleted9 resulting in a culture failure [11]. Additionally, the culture media flowing from the upstream region (inlet) of a microfluidic chamber can accumulate or be deprived of various substances resulting in a different soluble environment affecting downstream cell culture behaviour [9,

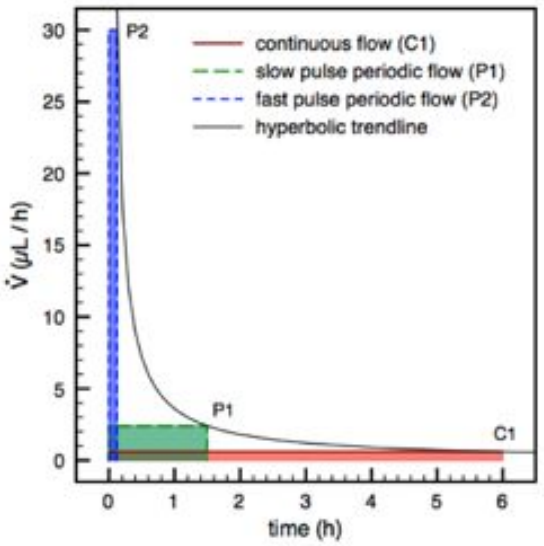

Figure E.2.1 – Microfluidics offers an unlimited set of flow rate values within a low shear stress range for cell cultures. The same amount of medium (given by the product between the flow rate and the time of perfusion, and represented by a rectangular area under a hyperbolic trend line) can be managed by varying the flow rate and the perfusion interval. Three different operative conditions with the same experimental perfused medium volume are represented. Each condition in the plot results in the same area (e.g. same volume). Assuming a 6-hour cycle, C1 results in a continuous flow regime, P1 and P2 result in discontinuous flow regime.

15]. In this article, we aim at studying the effect of different strategies in medium delivery on long-term cell culture. In particular, we used an approach, both experimental and theoretical, to rationally understand how the spatio-temporal evolution of extrinsic factors, both secreted by the cell or delivered from the media (referred in this paper as endogenous factors and exogenous factors, respectively), is affected by different isovolumetric conditions of medium delivery. In order to compare cell responses, we analysed the effect of the delivery of the same amount of medium according to different temporal profiles, as reported in Figure 1: continuous medium flow (C1) and periodic delivery of either fast (P2) or slow (P1) pulses were applied in a defined time interval. Moreover, we designed a multiple channel microfluidic chip with a high length/width ratio to investigate upstream and downstream heterogeneity of microfluidic cell cultures.

E.3 Materials and Methods

E.3.1 Cell culture

C2C12 (ATCC) were cultured in 89% DMEM (1 g/L glucose) (Sigma-Aldrich), 10% FBS (Life Technologies) and 1% penicillin/streptomycin (Life Technologies) at 37 °C and humidified 5% CO_2. Passaging of both cultures was performed with 0.025% trypsin-EDTA (Life Technologies) and cells were either re-plated on culture flasks for further expansion or seeded inside microfluidic chambers, both coated with 0.6%

A-type pork gelatin (Sigma-Aldrich). Nanog-GFP reporter mouse embryonic stem cells (mESC, Millipore) were cultured in MilliTrace cell expansion medium on 0.1% A-type pork gelatine according to the manufacturer's guidelines. mESC colonies were passaged and dissociated in single cells with Accutase (Millipore) for 3 minutes. Culture channels were fed injecting cell suspension via the outlet avoiding cells in the medium reservoir. Regarding C2C12 and HFF, initial cell density within the chip was 15 cell/mm^2 and cultures were monitored during perfusion experiments until confluence was reached. mESC were seeded at 100 cells/mm^2 in order to promote aggregation and formation of small colonies. Tubings were connected to the chip 12 hours after seeding to allow complete adhesion and spreading of cells. The NANOG-GFP fluorescent construct was monitored in live mESC cultures. mESC were fixed at day 6 in 4% paraformaldehyde and directly characterized within the channel by immunofluorescence for SSEA-1 surface pluripotency marker (Santa-Cruz) in 3% bovine serum albumin. An Alexa-594 conjugated secondary antibody (Life technologies) was used for SSEA-1 fluorescent labelling. Image analysis for quantification of mESC colony size and marker fluorescence intensity was performed with ImageJ analysis tools.

E.3.2 Microfluidic platform

The microfluidic platform was designed to accommodate five independent parallel channels for cell culture (18 x 1 x 0.1 mm) with well-shaped reservoirs for fresh medium upstream and tubing connection downstream (Fig. 2). The microfluidic layer was fabricated using standard lithographic techniques16 and molded in PDMS with a 10:1 base/curing agent ratio (Dow Corning). A supporting borosilicate glass slide (Menzel-Glaser) was used to seal each channel after plasma treatment of surfaces. The micro-perfusion apparatus (Fig. 2) was composed of the microfluidic platform, a set of PHD2000 syringe pumps in withdraw mode (Harvard Apparatus) and glass syringes (Hamilton). All connections between components were made using Tygon tubings (0.5 mm ID, 1.5 mm OD, Cole Parmer). A brief description of the experimental procedures follows. Before assembling and coupling to the cell cultures, all components were extensively rinsed with milliQ water (Millipore) and then

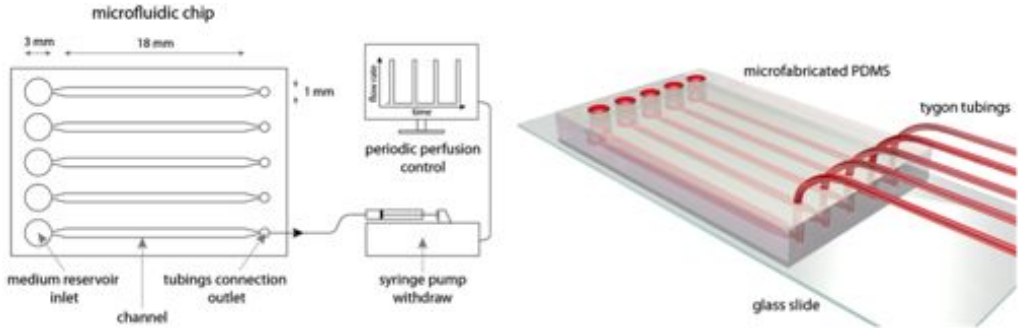

Figure E.3.1 – Schematic top-view and rendering of the microfluidic platform. The microfluidic platform consists on a PMDS layer (5 mm thick) with five parallel channels (18 x 1 x 0.1 mm) and a bottom glass slide which serves as sealing surface for cell culture adhesion and proliferation. Wells (3 mm wide) serve as fresh medium reservoir upstream and Tygon tubings are connected downstream through pinholes. Tubings ends are connected to a set of syringes which are loaded on a withdraw pump.

sterilized via autoclave treatment. Finally, tubings were rinsed with sterile culture medium and incubated for at least 1 hour prior to the platform assembly. Sterile syringes to be connected to the outlets of the platform were filled with sterile medium in order to avoid the elastic effect of the air, and then connected to the pinholes exiting of the platform. The entire chip was embedded in a Petri dish providing a water bath to limit medium evaporation. We considered a continuous and a periodic medium delivery. These strategies were defined by a parameter $\phi = t_{perf}/t_{cycle}$, which is the ratio between the perfusion time and the duration of a single cycle. Three cases were taken into account: a continuous strategy (C1), characterized by $\phi = 1$; and 2 periodic strategies, one with a long medium pulse (P1/P1'), ϕ = 0.25-0.5 and one with a fast medium pulse (P2/P2'), ϕ = 0.02-0.033. Pumps were controlled through the serial port by a customized software developed in LabVIEW (National Instruments) in order to setup the flow rate, the time of perfusion, the time of pause, and the number of cycles, and to establish different operative conditions inside culture channels. Microfluidic cell cultures were monitored using image acquisition in a controlled environment (37 and humidified 5% CO_2, Pecon) on a motorized DMI6000B fluorescent microscope stage (Leica). Glucose measurements were taken with a diabetes-grade sensor (Abbott) and data were collected withdrawing downstream tubings at the end of the continuous set up experiments.

E.3.3 Computational model

In the microfluidic cell culture chip, cells adhere at the bottom of the channel, which is perfused by fresh medium. Convection and diffusion regulate the species mass transport. Because of the cell metabolism, there is a concentration gradient between cells and the medium bulk, hence a flux of nutrients from the bulk to the cells; on the other hand, cells secret factors causing an inward flux. Because microfluidic systems are typically made in PDMS, an inward oxygen flux must be considered during the overall experiment duration due to the high gas-permeability of the PDMS (Fig. 3a). Two different operative conditions were analysed, continuous and periodic medium delivery. The system was described by the mass transport equations and cell growth; in addition the Navier-Stokes equation was applied during the medium perfusion. A 2D model was used since we assumed that all concentration profiles along the width of the culture chamber are negligible. The medium fluid dynamics in the culture chamber was described by the Navier-Stokes equations for incompressible fluids (Eq. 1):

$$\rho\frac{D\nu}{Dt} = -\nabla p + \mu\nabla^2\nu + \rho g \tag{E.3.1}$$

where ρ is the medium density, v is the velocity field, p is the pressure, μ the medium viscosity, and g the gravity. At the inlet a parabolic profile was imposed consistent in the limit at low Reynolds number, while at the outlet the pressure was set to zero. The convection-diffusion equation was used to study species temporal concentration profiles and no reactions occurred in the medium. Since cells are seeded at the bottom of the channel, their cellular activity (uptake and secretion) can be assumed as a flux (outward and inward) at the cell/medium interface. The species mass transport was expressed by:

$$\frac{\delta c_i}{\delta t} = -\nabla N_i \tag{E.3.2}$$

In Eq. 2, c_I is the species concentration, and Ni is the flux which considers both convection and diffusion phenomena:

$$N_i = \nu c_i - D_i \nabla c_i \tag{E.3.3}$$

where D_i is the species diffusion coefficient in medium at 37 °C. The mathematical model was coupled with phenomenological expressions for the oxygen flux at the top of the chamber (N_{ext}), and for the kinetics of uptake and secretion (R_i). The inward oxygen flux through the PDMS follows [16]:

$$N_{O_2}^{ext} = K_0(p_{O_2} - k_{O_2} c_{O_2}) \tag{E.3.4}$$

where K_0 is the global mass transfer coefficient ($K_0 = P_m/\sigma, P_m$ is the oxygen permeability in PDMS [18] and σ is the PDMS thickness), p_{O_2} is the oxygen partial pressure in the incubator atmosphere and k_{O_2} is Henry's coefficient for oxygen. The oxygen uptake was described as a Michaelis-Menten equation, as reported in literature for C2C12 cells [19] The glucose uptake was experimentally determined and it was described with a first order kinetic equation.

$$R_{O_2} = \frac{V_{max} c_{O_2}}{c_{O_2} + K_m} \tag{E.3.5}$$

$$R_G = (k_1 c_G + k_2)\rho_{cell} \tag{E.3.6}$$

In Eq. 5, V_{max}, and K_m are the oxygen kinetic parameters and ρ_{cell} is the overall cell density; whereas in Eq. 6, k_1, and k_2 are the glucose kinetic parameters. The secretion rate of a generic endogenous factor was considered constant for each cell, and described as a linear function of the cell number:2

$$R_{EF} = q_{EF}\rho_{cell} \tag{E.3.7}$$

q_{EnF} is the specific production rate. At the beginning, the culture chamber is loaded with fresh cell media ($c_G = c_G^0$) in equilibrium with the incubator atmosphere ($c_{sat} = p_{O_2}/k_{O_2}$), the EnF concentration equals zero. Boundary conditions details are reported in the Supplementary section. The cell growth was described with an exponential law, in addition we took into account the contact inhibition:

$$\frac{d\rho_{cell}}{dt} = \left(1 - \frac{\rho_{cell}}{\rho_{cell}}\right) \tag{E.3.8}$$

Where ρ_{max} is the cell number at confluence, μ is the kinetic constant ($\mu = log(2)/\tau_d$,21 where τ_d is the doubling time). The initial condition was given by the initial cell seeding density. Both the continuous and periodic cases were numerically solved using the finite element method. The solution of the first case is straightforward; however the periodic case requires the solution of several cycles, each of them is composed of two different models, a continuous state and a rest state. All algorithms were implemented in COMSOL Multiphysics 3.5 (COMSOL Inc., Burlington, MA); details are reported in the Supplementary section.

E.4 Results and discussion

E.4.1 Computational analysis of flow rate microfluidic microenvironment

As previously discussed, different phenomena relating to ExF and EnF are involved at cell microenvironment. Accumulation of these extrinsic factors requires different fluid dynamic conditions; high flow rate promotes high ExF concentrations, whereas low or no flow rate favours the increase of EnF concentration. The computational model was used to assist the development of an experimental setup and to define proper medium flow rate. In order to provide a proof of concept of extrinsic factor dynamics under different hydrodynamic conditions, the model describes the temporal evolution of concentration profiles of three species: oxygen, glucose, and a representative endogenous factor secreted by cells (kinetics and mass transport parameters are those of epithelial growth factor, a powerful mESC mitogen factor; see Table S2). Figure 3b-c shows the behaviour of a continuously perfused microfluidic culture system, both under dynamic and steady state conditions; average dimensionless species concentrations were considered. Figure 3b represents a typical case study of a continuously perfused cell culture in a microfluidic system. Both oxygen and glucose have a decreasing profile due to the cell growth that increases the consumption rates of both metabolites. However, oxygen maintains high concentration due

to the continuous inlet oxygen flux throughout the gas-permeable PDMS membrane at the top of the system. On the other hand, EnF concentration increases in time until reaching a steady-state when the EnF production rate equals the EnF washout due to the medium convection. The cell growth follows the characteristic exponential trend until confluence after about 3.5 days (data not shown). The analysis at steady-state conditions (Fig. 3c) shows that the flow rates greatly influence the medium composition within microfluidic channel: for instance, the higher flow rate results in lower metabolites depletion but highest washing out of factors secreted by cells (i.e. EnF). It is worth to underline that this phenomenon take place at relatively low flow rate at which shear stress mechanical stimulation can be neglected; only higher flow rates ($> 10^2 \mu L/h$) produces shear stress capable to affect cell cultures (Fig. S1). In order to evaluate the reliability of the computational model, a comparison between numerical and experimental cell growth and glucose consumption rate for murine C2C12 cells was performed. Glucose concentration was measure at different time points by sampling under continuous perfusion experiments. Computational results fairly described experimental data as reported in Fig. S3. It is clear that the flow rate must be balanced to preserve the endogenous cell microenvironment and avoiding the nutrients depletion. In our studies, we focused on the flow rates where ExF and EnF concentration have intermediate values (Fig. 3c); we used a flow rate equal to 0.6 μL/h as starting point for our experimental investigation; it is obvious that this value is strongly related to the cell type.

E.4.2 Experimental comparison of continuous and periodic perfusion on cell cultures

Three different operative conditions, corresponding to different values of $\phi = t_{perf}/t_{cycle}$ as reported in materials and methods, were exploited to investigate long-term cellular behaviours inside culture channels (Fig. 1, 6a-b). Continuous and periodic flows were applied maintaining a constant medium volume per cycle (Fig. 1). In particular, a continuous flow at 0.6 μL/h (C1, continuous perfusion) was applied in comparison with two periodic conditions, at 2.4 μL/h (P1, long medium pulse) and 30 μL/h (P2, short medium pulse) for 1.5 and 0.12 h, respectively. In each case, a

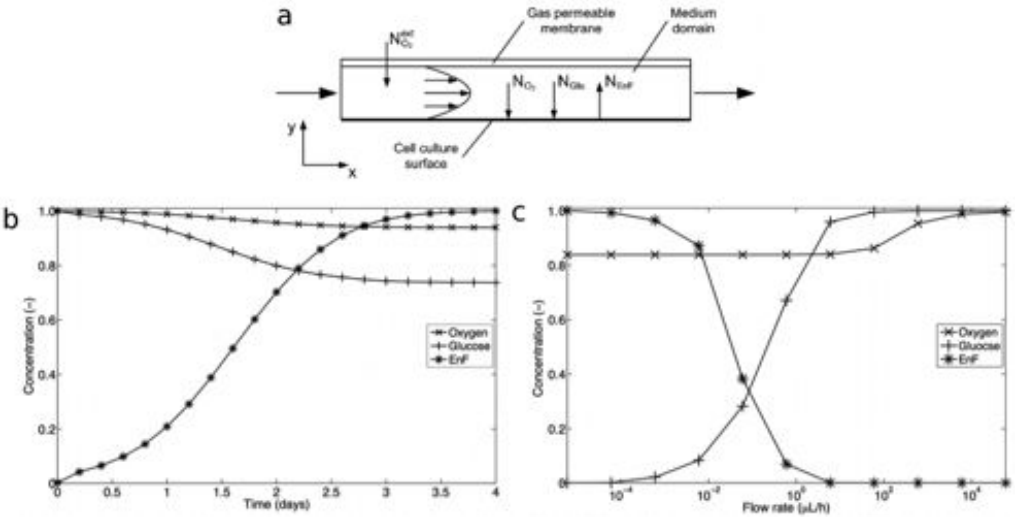

Figure E.4.1 – Concentration profiles of extrinsic factors in a microfluidic channel. (a) Longitudinal section representation of the microfluidic channel. Arrows show the species fluxes: the inward oxygen flux from the external atmosphere through the PDMS, $N_{O_2}^{ext}$, the fluxes of oxygen and glucose from the bulk medium to the cell interface due to their metabolism, N_{O_2} and N_{Glut}, and the endogenous factor secreted by cell, N_{EnF}. (b) Temporal evolution of species concentration in the continuously perfused system (flow rate 0.6 $\mu l/h$, seeding density 20 cell/mm^2 for oxygen ($\times$), glucose ($+$) and EnF ($*$); . (c) Steady state behaviour of the system as function of medium flow rate (at 80% of cell culture confluence).

volume of 3.6 μL was perfused during 6 h of a single cycle, corresponding to twice the chamber volume. Murine C2C12 cells were seeded within microfluidic channel and cultured for at least 5 days under controlled perfusion. Shear stress resulted $< 10^{-2}$ Pa at the maximum flow rate, which it is low for inducing any effect on cultures as previously reported.21 Continuous flow (C1) resulted in a heterogeneous cell growth between upstream and downstream side of each channel. Cell proliferation was reduced downstream (Figure 4a-b) where mortality dramatically increased at day 5 (Fig. 4j). Upstream, C2C12 cultures reached confluence within the fourth day, even though cells tended to form agglomerates. Moreover, cells were characterized by perinuclear vesiculation and anomalous morphologies, such as elongated and narrowed protrusions, which were detected along the whole channel (Fig. 4c). Measurements at day four revealed glucose depletion down to 0.2 g/L in steady state conditions. Cultures under a periodic flow at 2.4 μL/h, with a long medium perfusion (P1), presented lower density downstream evidencing mild abnormalities all along the channel (Fig. 4d-f). At day 5, the first two-thirds of the channel were confluent, but the latter third underwent pronounced mortality (Fig. 4k). When a periodic

flow with a short pulse of fresh medium was applied (P2, 30 μL/h for 0.12 h) cells resulted homogeneously dispersed both upstream and downstream until confluence (Fig. 4g-h). Abnormalities were totally absent (Fig. 4i) as well as in a conventional tissue culture dish. Without switching to a myotube-differentiating medium, the fifth day C2C12 myoblast were almost over-confluent (Fig. 4l) and few cells started to detach or spontaneously differentiate as well as in static cultures controls. We next investigated whether these different strategies of medium delivery could be generally addressed to other cell types. We extended the same conditions to human HFF fibroblasts. Similarly to C2C12, HFF cultures were successfully maintained in P2 conditions whereas the low cell viability and vesiculation was observed in C1 and P1 conditions (Fig. 4m-o). It is worth to underline that HFF were robustly maintained at confluence in P2 condition for at least 50 days without passaging (Fig. S 5).

In order to verify if the periodic medium delivery can robustly and efficiently apply to cell culture that are well known to show high sensitivity to environment condition, we applied the same strategy to mouse embryonic stem cells (mESC). Since mESCs grow as dense and thick colonies to avoid dramatic reduction of medium layer above the cells, we increased the height of microfluidic channel to 200 μm and, consequently, we increase medium flow rates to completely change the medium within the entire channel (as reported in Table 1). Experiments were performed maintaining a constant perfusion rate of 2 μl/h (12 μL over a 6-hours cycle). Consistently with previous data, continuously perfused (C1') mESC culture exhibited highly different behaviours between upstream and downstream region of the channel (Fig. 5a). In particular, mESC colony size is remarkably reduced downstream, stemness markers were observed only in compact colonies regardless of their size whereas SSEA-1-negative cells were observed all over the channel. Applying the same volume per cycle with a periodic slow pulse for 3 hours (C1', Fig. 5b), the heterogeneity between upstream and downstream regions is partially reduced whereas differentiated cells were observed as in the previous condition; few colonies were able to expand normally downstream. Consistently, applying a periodic flow with a short medium pulse of 12 μL (C2'), mESC culture was homogeneous between upstream and downstream regions in terms of colony density, morphology, diameter distribution and stemness

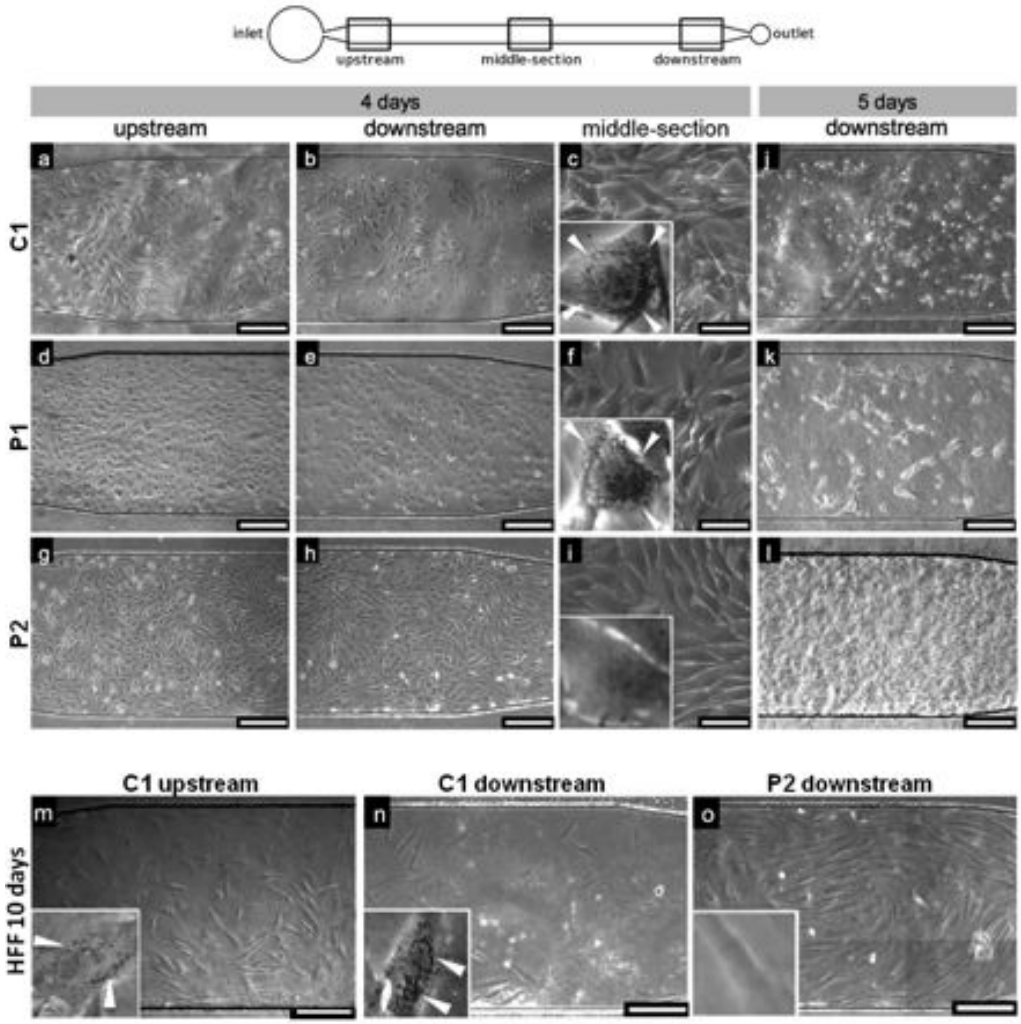

Figure E.4.2 – Microfluidic C2C12 cultures at 4 days. Three different regions of microfluidic channel were analysed, the upstream, the middle-section, and the downstream. Upstream and downstream conditions are reported for C1, P1 and P2. C1 presented marked heterogeneous growth (a-b) and cellular death especially downstream. Altered morphologies resulted all along the channel with marked perinuclear vesiculation (c). P1 determined mild differences between upstream and downstream (d-e) but still influenced cellular morphology and vesiculation (f). Applying the P2 medium delivery, cells grew uniformly along the channel (g-h) and did not present alteration (i). Microfluidic C2C12 cultures at 5 days. C1 cultures reached confluence even with abnormalities but an antithetic situation followed downstream (j), especially compared to P2 downstream channel where culture was over-confluent (l). Insets were taken at half-length of each channel. HFF cultures suffered downstream effects and pronounced vesiculation (m-n) as well as C2C12 while in P2, cultures evidenced normal phenotype (o). White bars are 75 μm (c, f, i), 250 μm (others).

marker expression (SSEA-1 and NANOG) (Fig. 5c).

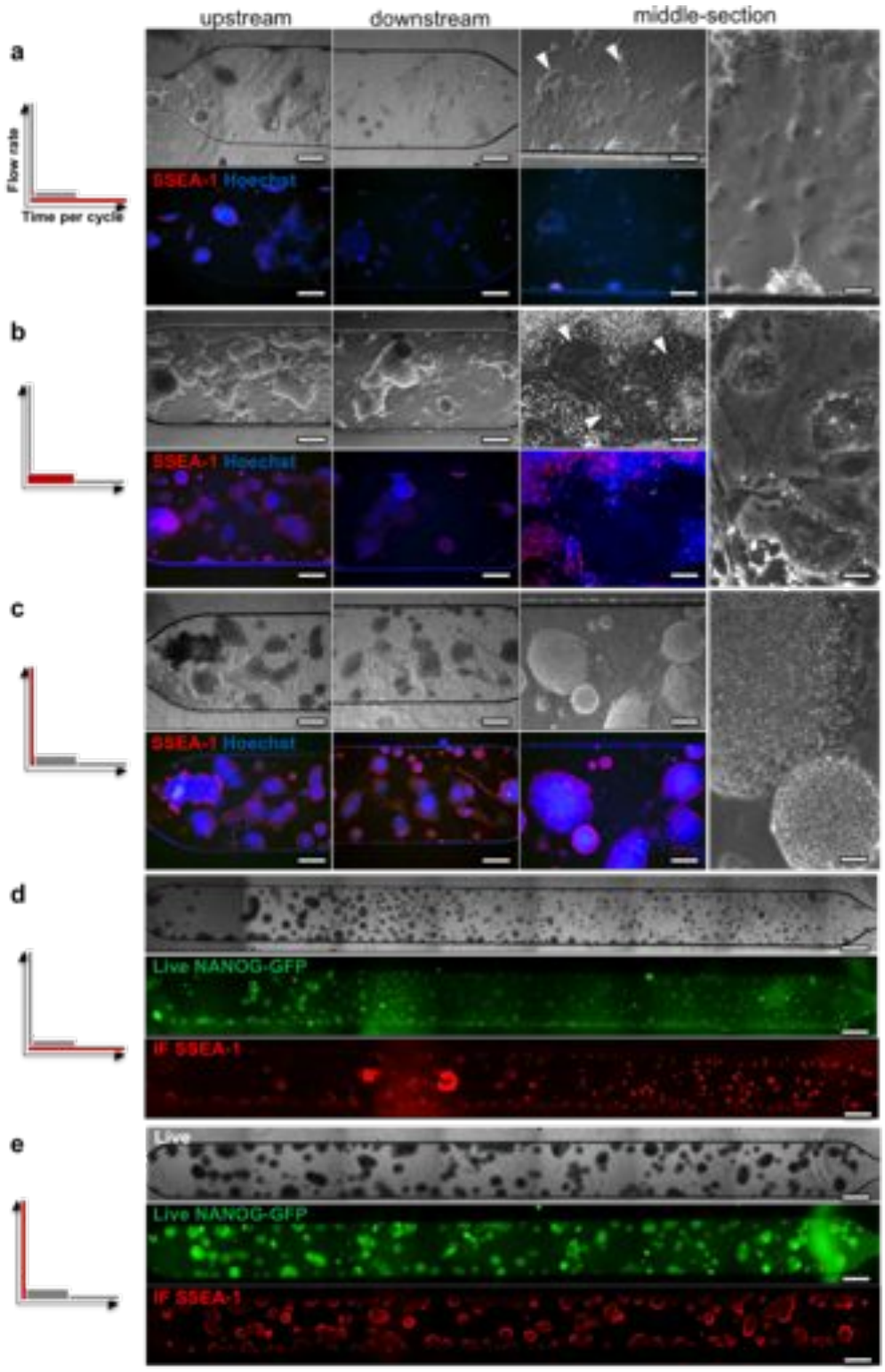

Figure E.4.3 – Microfluidic mESC cultures at 6 days. As reported in Fig. 4 scheme, three different regions of microfluidic channel were analysed, upstream, downstream and middle-section. C1' (a,d), P1' (b) and P2' (c,e) strategies are reported. Bright field, live green fluorescent protein reporter and immunofluorescence (IF) analysis for pluripotency markers (NANOG-GFP, SSEA-1) are illustrated. (a,d) C1' presented marked heterogeneous up-/downstreamgrowth andmarked differentiation with SSEA-1 negative flattened cells (arrows).(b) P1'evidenced mild heterogeneity with a still relevant number of differentiated cells escaping mESC pluripotent colonies. (c,e) P2' resulted in homogeneously and pluripotent compact colonies. Scale bars are 250 μm (a-c, upstream/downstream), 125 μm (middle section, left column), 25 μm (middle-section, right column), 600 μm (d-e).

Our results showed that the medium delivery strategy is extremely relevant for the proper maintenance of cell homogeneity, viability and pluripotent phenotype expression in microfluidic cell culture as depicted from the overall distribution of mESC in microfluidic channel for continuous and optimized periodic medium delivery (Figures 5d and 5e, respectively). A quantification of mESC colony size and pluripotency marker expression is reported in Figures 6a. mESC colonies cultured in P2' condition show significantly higher size and NANOG-GFP expression. In order, P1' and C1' show progressive decrease of size and marker expression, with a heterogeneous upstream/downstream behaviour. Additional quantifications are reported in supplementary Figures S 6 and S 7.

Medium volume and delivery frequency in periodic perfusion We next explored whether a change in frequency and total volume over a cycle affects cell culture quality. A comprehensive scheme of perfusion strategies is proposed in Figure 6b. Regarding mESC, we first verified if the total volume of medium delivered per cycle could be reduced. Using a short pulse periodic perfusion of 12 μL of medium over a 12-hours cycle (Fig. 6c), differentiated cells appeared (morphologically flattened and SSEA-1-negative cells) and colony area was significantly reduced at least downstream (Supplementary Fig. S 8 and S 9). It is likely that a minimum amount per cycle is required to sustain proper mESC phenotype. Next, we asked if a high-quality cell culture could be obtained by increasing the total amount of medium per cycle. Continuous and periodic flows were applied by increasing the volume per cycle of 30 (C3', 60 μl/h) and 4 (P1', 16 μl/h) times respectively. C3' condition corresponds also to a 30-fold volume of P2' one. Interestingly, colonies grew homogeneously upstream/downstream with fair expression of pluripotency markers evidencing an overall improvement in both cases (Fig. 6d-e). Despite size distribution differences

between C3', P4' and P2' is not significant ($p>0.05$), some colonies evidenced a greater area in C3' and P4' (Supplementary Fig. S 8). NANOG-GFP reporter showed a similar expression compared to P2' (Supplementary Fig. S 9). It is worth to underline that C3' continuous perfusion resulted in a 30-fold medium volume (Fig. 6e) consumption. Then, we asked whether C2C12 could be successfully cultivated in similar conditions. We applied a 50-fold continuous perfused volume compared to P1 (C3, Fig 6f). Consistent with mESC C3' condition, C2C12 grew homogeneously over the entire channel but surprisingly, they reached abnormal high cell density probably due to the reduction of contact inhibition proliferation compared to C2 case (Fig. 4l); consistently, we recently reported that C2C12 proliferation can be promoted by reducing the endogenous factor accumulation thought cell micro-patterning techniques regardless of cell density.30 Interestingly, spontaneous myotube formations were observed only in 3-dimensional cell clusters (Fig.6f) where accumulation of endogenous factors is likely to take place. Unfortunately, it is difficult to deeply study at which flow-rate threshold we are expected that efficiently deliver of the ExF contained in serum-supplemented medium can replace those secreted by cells and washed out by the convective flux. Even using a chemically defined knockout-serum replacement supplemented medium, we were not able to dissect the role of EnF and ExF; in particular, C2C12 grew slowly with any periodic perfusion conditions whereas mESC behaviour was fully consistent with the use of FBS-supplemented medium (data not shown). Additional experiments were performed with C2C12 and HFF (additional setups in Table 1, data not shown). A 4-fold gain of the perfused volume per cycle was tested by increasing P2 frequency and by extending P1 perfusion up to a continuous regime. A 4-fold of the medium volume used in P2 (P3) did not affect cell culture of both cell lines. However, a continuous perfusion at 2.4 μl/h (C2) evidenced the same abnormalities seen in C1 and P1, underlining an inadequate medium delivery. Finally, abnormalities appeared even 12 h after a starting seeding of 200 cell/mm^2, indicating no correlations between the culturing progression and the seeding density. We also verified if the cell abnormalities seen in microfluidics can be achieved in standard Petri culture maintaining the same cell density. Not surprisingly, C2C12 evidenced vesiculation and altered morphology even in static cultures

after 4 days in the same medium. Because the available medium volume per cell is 40-fold than the microfluidic system, and the average glucose concentration was still significantly high (0.7 g/L), the altered morphology and vesiculation seem to be due to a secreted factors or waste products from cells rather than a depletion of glucose as it was seen for reduced total medium delivery (Fig. 6c for mESCs and data not shown for C2C12) .

	Regime	Flow rate (μl/h)	Perfusion (h)	Cycle (h)	Medium/cycle (μl)	Optimal strategy
C2C12/HFF	Continuous P1	0.6	6	6	3.4	- -
	Periodic P1	2.4	1.5	6	3.4	-
	Periodic P2	30.0	0.12	6	3.4	+++
	Continuous C2	2.4	6	6	14.4	-
	Continuous C3	30.0	6	6	180.0	+
	Periodic P3	30.0	0.48	6	14.4	++
mESC	Continuous C1'	6	6	6	12	- -
	Periodic P1'	3	3	6	12	-
	Periodic P2'	0.2	0.2	6	12	+++
	Periodic P5'	0.2	0.2	12	12	+
	Periodic P4'	3	3	6	48	++
	Continuous C3'	6	6	6	360	+

Table E.4.1 – Perfusion strategies applied to murine (C2C12 and mESC) and human (HFF) cell lines. A continuous or periodic regime have been applied with a constant total medium perfused per cycle or with a doubled cycle period (P5'). Either the flow rate, the perfusion time or the frequency of periodic flow were changed. Optimal strategy takes into account culture quality and optimal reagent management.

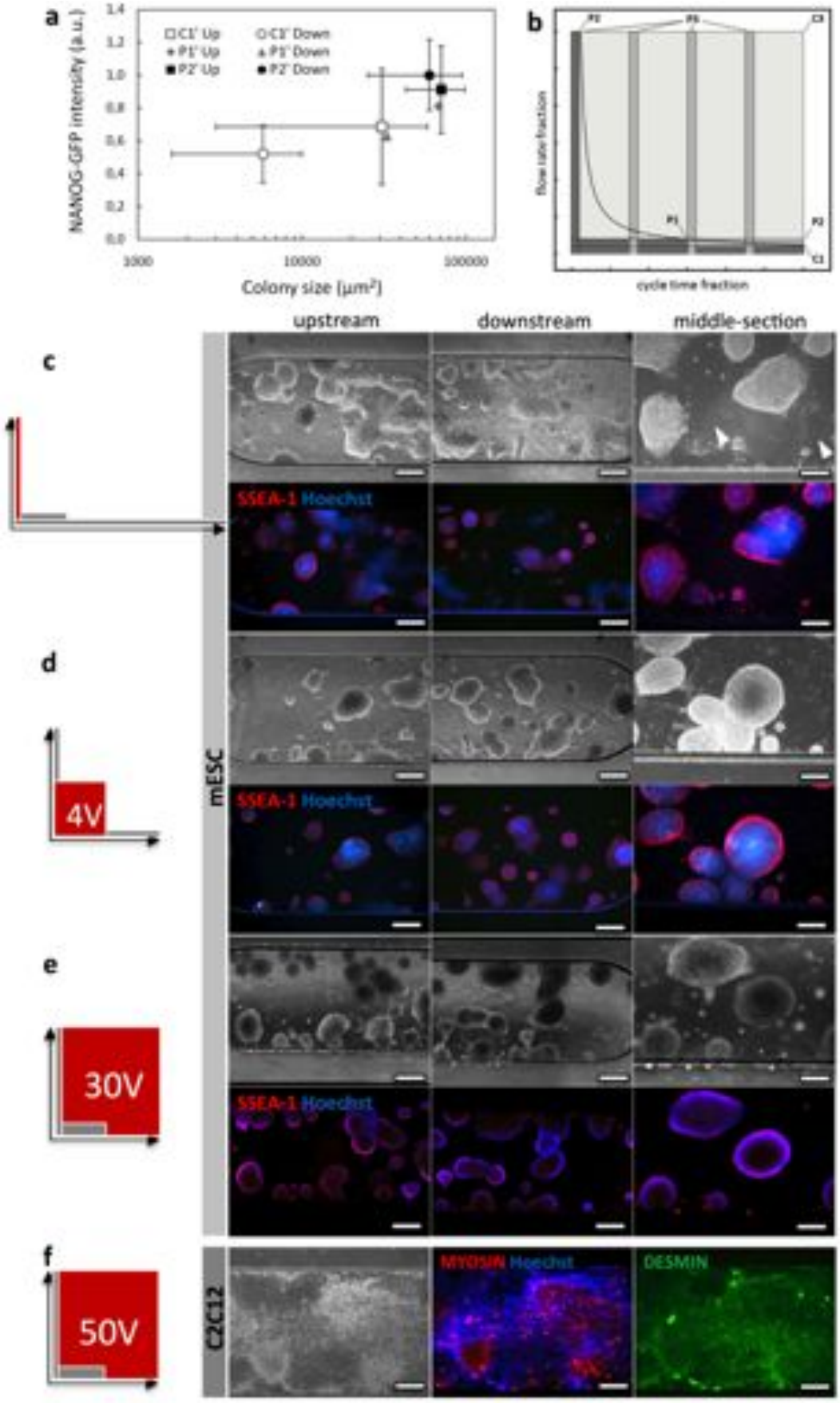
a
NANOG-GFP intensity (a.u.)
C1' Up
C3' Down
P1' Up
P1' Down
P2' Up
P2' Down
Colony size (µm²)
b
flow rate fraction
cycle time fraction
upstream
downstream
middle-section
c
SSEA-1 Hoechst
d
4V
mESC
e
30V
f
50V
C2C12
MYOSIN Hoechst
DESMIN

Figure E.4.4 – Quantification of size and NANOG-GFP fluorescence intensity within colonies at different conditions; P2' data are significantly different (ANOVA $P < 0.05$) for both colony size and marker expression compared to C1'; mean and standard deviation applied, n=25. (b) Comprehensive scheme of perfusion strategies per 6-hour cycle; plot shows generic C1, P1, P2 strategies at a constant volume fitted by an hyperbolic curve; other strategies (C2, P3, C3) have been applied to verify the effect of the total medium perfused per cycle changing either the flow rate, the perfusion time or the frequency of periodic flow (c-e) mESC cultures. (c) Doubling the cycle duration to 12 h, we applied half the volume per cycle compared to P2'.A significant number of differentiated cells appeared all over the channel (arrows).(d-e) Total medium volume per a 6-hour cycle has been increased by 4 and 30 times compared to P1' and P2'/C1' respectively. Cultures have a homogeneous distribution of colony size. (f) C2C12 cultured with 50 times the volume of P2/C3 with a continuous perfusion. Scale bars are 250 μm (c-e, upstream/downstream and f), 125 μm (c-e, middle section).

Altogether, these results evidenced that a time-limited periodic perfusion was optimal to obtain proper cell behaviour, regardless of cell type. Even far from a high shear stress values, prolonged continuous perfusion altered cell morphology and culture behaviours. Cells did not benefit from an increase of the total medium during a single cycle, although this condition provided fresh nutrients. A short medium pulse offered the best condition for a long-term homogeneous and healthy cell culture within the entire channel.

Computational analysis of periodic perfusion The experimental results clearly demonstrated that periodic medium perfusion could strongly enhance the robustness and the efficiency of long-term cell culture in microfluidic devices. However, these biological evidences and their correlations with the dynamic evolution of the microfluidic environment under discontinuous perfusion could be very complex and difficult to understand. For instance, the complex balance between endogenous and exogenous factors is deeply affected by inlet and outlet flux during perfusion and by cellular consumption/production rates during un-perfused phases. The computational model was used to rationally describe the dynamic evolution of microfluidic environment along the cyclic perfusion conditions; as previously, oxygen and glucose were used to simulate metabolite requirement whereas one endogenous factor was used as model of extrinsic cell secreted factor. In the periodic perfusion configuration, the concentration of species oscillate within a range (Fig. 7a and b), the fluctuations increase their amplitude following the increase in cell number until the steady state, when cells reach the confluence. Figure 7a shows the concentration space for all considered species; the black line depicts the cyclic evolution of the

species, which raises its magnitude until cells reach the confluence (red line). It must be highlighted, that the limit-cycle for a periodic system is represented by a whole cycle (red line). At this condition oxygen is almost constant (as already reported in Fig. 3b), therefore we will focus on glucose and EnF that change more significantly. The limit-cycle of two periodic perfusion conditions and the steady-state of continuous perfusion (P1, P2 and C1, respectively) were compared measuring the glucose and EnF concentration upstream and downstream (at 25% and 75% of the channel length, Fig. 7b). Red and black lines depict the upstream and downstream values, respectively. The continuous condition (C1) is represented by two circles on the plot, whereas the limit-cycle of the periodic perfusion is as a closed curve (one for each position along the channel), which shows the temporal evolution of glucose and EnF trajectories for a single perfusion cycle. At P2 (30 μL/h), the culture chamber conditions are more uniform, upstream and downstream curves are overlapped. The rest phase starts from the maximum glucose concentration without EnF. The system evolves following a descending trend (glucose decreases, EnF increases). The perfused phase starts from a minimum glucose value (and a maximum EnF value) and reaches the initial values of the rest phase. At P1 (2.4 μL/h), system behaviour has a different trend than the previous one, with a transition from a convective to a diffusive regime. Although the rest phase follows the same trajectory, maximum and minimum values are, respectively, lower and greater than P2. For example in this case the system cannot reach the maximum glucose concentration and the EnF is always greater than zero. The starting and final slope of the perfusion phase plot is remarkably higher than P2 (e.g. glucose increases rapidly whereas EnF remains almost constant). Finally, as reported by experimental data, the mathematical model show that the lower is the flow rate, the less uniform are the upstream and downstream regions. On the other hand, because we found a transition from a convective to a diffusive regime at P1, not surprisingly, the P1 perfusion shows higher heterogeneity of the culture area along the perfusion direction. Unlike the continuous case, where cells are subjected to a constant steady state concentration of metabolite and growth factors (Figure 7c and d at downstream), the discontinuous perfusion strategy shows an oscillatory behaviour, which periodically exposes the cell cultures to

highest level of both metabolites and extrinsic growth factors. This oscillatory behaviour described by the computational analysis could explain why the time-limited periodic perfusion is more effective to perform long-term cell culture in microfluidic environment.

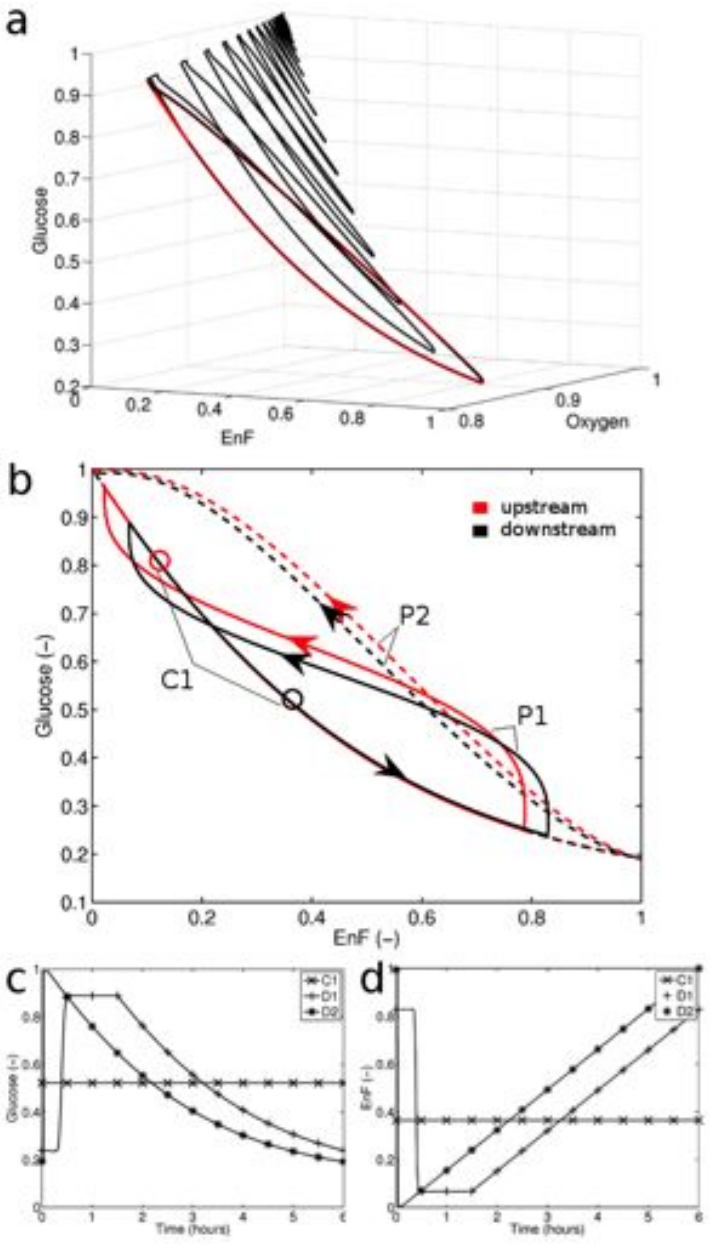

Figure E.4.5 – (a) 3D concentration space of the system evolution, the black line depicts the oscillatory behaviour of the system, the red line depicts the limit-cycle. (b) Glucose and EnF concentration condition at cell confluence (steady state) for three experimental flow rate values - C1, P1, P2. The red colour shows the concentration upstream (x = 4.5 mm), the black colour downstream (x = 13.5 mm). (c) Glucose and (d) EnF temporal downstream evolution per cycle. In C1, cells are exposed to a constant glucose and EnF levels, while in discontinuous cases are characterized by cyclic evolution of species.

E.5 Conclusions

In this work, we investigated how different strategies of medium delivery affect the cell behaviour for a long-term cell culture in microfluidic systems. In particular, continuous and periodic perfusion regimes were used to assess culture behaviour. The mathematical model here developed, was used to rational describe the spatio-temporal profile of different species, nutrients and endogenous factor, along with the cell growth within a microfluidic environments. Moreover, the computational analysis at steady-state perfusion was used to identify the experimental condition at which the flow rates strongly affect extrinsic microfluidic signals. Experimental results show that a stable and uniform long-term microfluidic culture with minimum medium delivery can only be achieved in a periodic regime and with a short flow pulse (below shear stress threshold) followed by a long rest period. Other strategies can result in long-term toxic effects, low viability, upstream/downstream heterogeneity. These results were consistently observed for murine myoblasts, human fibroblasts and murine embryonic stem cells. The improper culture condition observed in continuous perfusion could be partially rescued by a 50-fold increased flow rate, leading to unfeasible medium consumption and abnormal phenotypes for the case of C2C12. In this condition mESC grew homogeneously along the channel with proper cell size and marker expression compared do periodic flow P2' but required more medium per culture area than a Petri dish. Interestingly, the continuous subministration of fresh media with pluripotent leukemia inhibitory factor (LIF) can sustain stemness. In periodic flow, despite the pulse withdraws secreted factors from the cells microenvironment, the static incubation period is sufficient to recover the local secreted factors and cell processes. On the other hand, continuous perfusion results in altered and non-homogeneous culture conditions with negative downstream viability. The management of a microfluidic cell culture should take into account several issues; in this work we study the effect of medium temporal delivery on the cell microenvironment properties. Our experimental and simulated data show that periodic perfusion can improve microfluidic cell culture compared to the continuous condition in term of viability. Low perfusion gives heterogeneous system behaviour along the channel (Fig. 4-6), on the other hand, only a fast cyclic perfusion results in a homogeneous

cell culture proliferation throughout the whole system.

E.6 References

[1] J. El-Ali, P. Sorger and K. Jensen, Nature , 2006, 442, 403.

[2] E. Cimetta, E. Figallo, C. Cannizzaro, N. Elvassore and G. Vunjak-Novakovic, Methods, 2009, 47, 81–89.

[3] E. Figallo, C. Cannizzaro, S. Gerecht, J. Burdick, R. Langer, N. Elvassore and G. Vunjak-Novakovic, Lab Chip, 2007, 7, 710–719.

[4] E. Serena, E.Cimetta, S. Zatti, T. Zaglia, M. Zagallo, G. Keller and N. Elvassore, PLOS ONE, 2012, 7, 1–10.

[5] E. Cimetta, C. Cannizzaro, R. James, T. Biechele, R. Moon, N. Elvassore and G. Vunjak-Novakovic, Lab Chip, 2010, 10, 3277–3283.

[6] P. J. Hung, P. J. Lee, P. Sabounchi, R. Lin and L. P. Lee, Biotechnol Bioeng, 2005, 89, 1–8.

[7] Tourovskaia, X. Figueroa-Masot and A. Folch, Lab Chip, 2005, 5, 14–9

H. Kimura, T. Yamamoto, H. Sakai, Y. Sakai and T. Fujii, Lab Chip, 2008, 8, 741–6.

[8] L. M. Przybyla and J. Voldman, Proc Natl Acad Sci USA, 2012, 109, 835-840.

[9] F. Moledina, G. Clarke, A. Oskooei, K. Onishi, A. Gunther and P. W. Zandstra, Proc Natl Acad Sci USA, 2012, 109, 3264–9.

[10] H. Chen, J. Li, H. Zhang, M. Li, G. Rosengarten and R. E. Nordon, Biomicrofluidics, 2011, 5, 44117–4411713.

[11] S. P. Forry and L. E. Locascio,Lab Chip, 2011,11, 4041–6.

[12] W. Li LM, Wang, S. Zhang, S. Chen, S. Guo, O. Francais, J. Cheng and W. Huang, Anal chem, 2011, 83, 9524–9530.

[13] N. Korin, A. Bransky, U. Dinnar and S. Levenberg, Biomed Microdevices, 2009, 11, 87–94.

[14] W. Gu, X. Zhu, N. Futai, B. Cho, S.Takayama, Proc Natl Acad Sci USA, 2012, 109, 3264–9.

[15] D. Qin, Y. Xia and G. M. Whitesides, Nat Protoc, 2010, 5, 491–502.

[16] E. Cimetta, M. Flaibani, M. Mella, E. Serena, L. Boldrin, P. De Coppi and N. Elvassore, Int j artif organs, 2007, 30, 415–428.

[17] J. Brandrup, E. Immergut and E. Grulke, Polymer Handbook, 4th Edition, Wiley-Interscience, 4th edn, 1999.

[18] G. Mehta, K. Mehta, D. Sud, J. W. Song, T. Bersano-Begey, N. Futai, Y. S. Heo, M.-A. Mycek, J. J. Linderman and S. Takayama, Biomed Microdev, 2007, 9, 123–134.

[19] K. Mehta and J. Linderman, Biotechnol Bioeng, 2006, 94, 596–609.

[20] C. Acevedo, C. Weinstein-Oppenheimer, D. Brown, H. Huebner, R. Buchholz and M. Young, Bioproc Biosys Eng, 2009, 32, 341–351.

[21] E. Figallo, C. Cannizzaro, S. Gerecht, J. Burdick, R. Langer, N. Elvassore and G. Vunjak-Novakovic, Lab Chip, 2007,7, 710–719.

[22] J. Moreira, P. Santana, A. Feliciano, P. Cruz, A. Racher, J. Griffiths and M. Carrondo, Biotechnol progress, 1995, 11, 575–583.

[23] D. Chow, L. Wenning, W. Miller and E. Papoutsakis, Biophys J, 2001, 81, 675–684.

[24] D. Cochran, D. Fukumura, M. Ancukiewicz, P. Carmeliet and R. Jain, Ann biomed eng, 2006, 34, 1247–1258.

[25] M. Haller and W. Saltzman, Pharm res, 1998, 15, 377–385.

[26] D. Brown, W. MacLellan, H. Laks, D. CYet al.,Biotechnol Bioeng, 2007, 97, 962–975.

[27] E. Morsiani, M. Brogli, D. Galavotti, T. Bellini, D. Ricci, P. Pazzi and A. Puviani, Artif Organs, 2001, 25, 740–748.

[28] Y. Toh and J. Voldman, FASEB J, 2011, 25, 1208.

[29] S.Zatti, A. Zoso, E. Serena, C. Luni, E. Cimetta, and N. Elvassore. Langmuir, 2012, 28, 2718–2726.

Appendix F

One-step high-throughput reprogramming and differentiation on a chip

Camilla Luni[1,2,⋆], Stefano Giulitti[1,2,⋆], Elena Serena[1,2], Zambon Alessandro[1,2], Onelia Gagliano[1,2], Luca Ferrari[1,2], Federica Michielin[1,2], Nicola Elvassore[1,2]

1. Department of Industrial Engineering (DII), University of Padua, via Marzolo 9, 35131 Padua, Italy.

2. Venetian Institute of Molecular Medicine, University of Padua, via Orus 2, 35129 Padua, Italy.

⋆ These authors contributed equally.

Article under submission

In this Appendix are reported the detailed methods for the derivation of human induced pluripotent stem cells in microfluidics. The full article is currently under submission.

F.1 Material and methods

F.1.1 Cell culture and hIPS derivation

BJ fibroblast cell line was purchased from Miltenyi Biotech and cultured in EMEM (Life Tecnologies) supplemented with 10% fetal bovine serum (Life Tecnologies), NuFF-RQT (AMS Biotechnology) were seeded at 250 cells/mm2. All cell lines were cultured at 37 °C and 5% CO2 atmosphere. Microfluidic cultures were perfused with fresh medium 24 hours after cell seeding. Modified mRNAs (mmRNA) were provided by Miltenyi Biotech and used according to the Stemgent mRNA reprogramming kit protocol. Opti-MEM and RNAiMAX were purchased from Life Technologies.The RNA transfection complex (RTC) was slowly added to different percentages of supplemented Pluriton medium (PL) relative to the manufacturer's standard with or without B18R (eBioscience) and injected inside each microfluidic channel. Briefly, a 100 $ng/\mu l$ mmRNA stock solution of each factor (OCT-4, SOX2, KLF-4, c-MYC, LIN28, NANOG, nGFP) is diluted 5-fold in Opti-MEM. RNAiMAX is diluted 10-fold in Opti-MEM and added to an equal volume of mmRNA. After 15 minutes of incubation, RTC is combined with PL++ (1:2500 PL Supplement and 200 ng/mL B18R). uF-hIPS were collected either by coring the rubber of the microfluidic chip with a biopsy punch or by a preferential detachment using a high flow rate corresponding to a shear-stress of 250 $dyne/cm^2$. hIPS were mechanically passaged on mouse embryonic fibroblasts (MEF, Millipore) with daily changes of hIPS media (DMEM/F12, 20% knockout serum replacement, 1% NEAA, 1% glutamine, 1% β-mercaptoethanol (all Life Technologies), 20 ng/ml b-FGF (Peprotech)). Karyotype was analyzed by xx (Brescia, Italy).

F.1.2 Microfluidic platform

Microfluidic platforms were fabricated according to standard soft-lithographic techniques and molded in poly-dimethylsiloxane (PDMS). Briefly, Sylgard 184 (Dow Corning) was cured on a 200-μm-thick patterned SU-2100 photoresist (MicroChem) in order to obtain a single PDMS mold with multiple independent channels. The PDMS mold was punched and sealed on a 75x25 mm microscope glass slide (Menzel-Glaser) by plasma treatment. Channels were rinsed with isopropanol and distilled water to check proper flow. Autoclaved chips were eventually treated on the glass bottom of each channel with a 5% water solution of (3-aminopropyl)-triethoxysilane (APTES, Sigma-Aldrich) or 0.3% 3-(trimethoxysilyl)-propyl methacrylate (TMSPM, Acros Organics) in ethanol for 5 minutes. Extracellular matrix proteins were either adsorbed or chemically bound to the silanized bottom of each channel to provide a durable coating for cell culture. Fibronectin (Sigma-Aldrich) was oxidized with sodium meta-periodate (Sigma-Aldrich) in acetate buffer for 1 hour to produce an amine-reactive variant (FnOX). Type-A pork gelatin (Sigma-Aldrich) was treated with methacrylic anhydride (Sigma-Aldrich) in PBS buffer for 1 hour at 60 °C to produce an acrylate-reactive variant (GelMA). A 10 µg/mL FnOX solution was injected and reacted for 1 hour at room temperature in the dark. A TMSPM-GelMA bonding was performed for 15 minutes by adding 0.1% ammonium persulphate and N,N,N',N'-tetramethylenethylenediamine (Sigma-Aldrich) prior to GelMA injection within the each channel. Channels were extensively rinsed with DPBS prior to cell seeding. The microfluidic chip was fully assisted by an automated medium delivery through each culture channel. A periodic10 µL/min perfusion for 30 s was controlled twice a day by Cavro pumps (Tecan) and a lab-made software interfacewritten in Labview(National Instruments). Pluriton-RTC was pipetted inside each reservoir and perfused inside the channels. Fresh PL was added to the reservoirs and automatically perfused after the incubation period.

F.1.3 Immunostaining and RT-PCR

Cells were fixed in 4% (v/v) paraformaldehyde (Sigma-Aldrich) for 10 min and stained with primary antibodies in 5% horse serum with 0.1% (v/v) Triton-X-100

(Sigma-Aldrich). Membrane markers were stained without cell permeabilization. Oct4 and SSEA-4 (Santa Cruz), Nanog (Reprocell), Tra-1-60 and Tra-1-81 (Millipore), Sox2 (Novus Biologicals). AFP and Brachyury-T (Sigma-Aldrich), β-III-tubulin (Abcam). Nuclei were stained with Hoechst 33342 (Life Technologies). Images were acquired with a DMI6000B microscope (Leica). hIPS positive for alkaline phosphatase were detected with AP-staining kit II (Stemgent) with a 10 minutes incubation of the staining solution. RNA extraction was performed with iScript (Bio-Rad). Microfluidic channels are perfused with D-PBS prior iScript injection and solution is collected after 2 minutes. Total RNA was isolated with the RNeasymini kit (Qiagen) and treated with DNase (Life Technologies). RNA (0.1 μg) was reversetranscribed into cDNAby RT (Life Technologies). PCR was performed with Platinum Taq (Life Technologies). Electrophoresis was perfomed in a 2% (w/v) agarose gel.

F.1.4 Differentiation protocols

Embryoid bodies. iPS colonies were treated with CTK ( ) for 30 s and mechanically scratched with a serological pipette e resuspended in EB medium (DMEM/F12, 20% knockout serum replacement, 1% L-Glutammine, 1% NEAA, β-mercaptoethanol (all Life Technologies). EB were cultured in ultra-low adhesive plates (Corning) for 20 days and then transferred on custom-made PDMS micro-wells with a matrigel (BD) coated glass bottom. Characterization was performed after 5 days.

F.1.5 Straightforward differentiation in microfluidics.

Freshly derived uF-hIPS colonies were directly differentiated perfusing media other than Pluriton every 12 hours.

Aspecific differentiation. EB media (without β-mercaptoethanol) was used to randomly differentiate uF-hIPS colonies for 20 days.

Cardiac differentiation. Small molecules were used to promote cardiac differentiation of hiPSC. RPMI with B27 (cardiac basal medium, CBM, Life Technologies) were perfused twice in the first 24 hours with 10 μM Chir. CBM was used in the

following 36 hours and CBM with 4 μM IWP-4 in the next 24 hours. CBM was used thereafter for cardiac maturation.

Epatic differentiation. hiPSC colonies were maintained in Pluriton and expanded over the channel width (1.4 mm). For hepatic differentiation cells were treated with 100 ng/ml activin A and 0.5mM NaB for 3 days in RPMI/B27. Medium was changed to KO-DMEM, 20%SR (both from Invitrogen), 1 mML-glutamine, 1% NEAA, 0.1 mM β-mercaptoethanol, 1% DMSO (Sigma) for 6 days. Hepatic-like cells were maturated with L15 medium (Sigma) supplemented with 8.3% FBS, 8.3% tryptose phosphate broth, 10 μM hydrocortisone 21-hemisuccinate, 1 μM insulin (all from Sigma) and 2 mM L-glutamine containing 10 ng/ml hepatocyte growth factor and 20 ng/ml oncostatin M (both from R&D) for 6 days8.

Appendix G

Protocols

G.1 Functionalization of glass supports and hydrogel preparation

Glass functionalization for acrylc-based hydrogels is performed via silanes. General guidelines for hydrogel production can be found here [111]. Optimization steps for large scale production follows. Glass coverslip are oxidized with oxygen plasma (30 W for 1 minute, Harrick Plasma) and covered for 5 minutes with a thin film of silane solution: a final 0.3% trimethoxy silyl propyl-methacrylate (Acros organics) is dissolved in ethanol and 5% of acetic acid. Glasses are rinsed in ethanol to remove unbound silane and then in distilled water. Once dry, coverslips can be used to polymerize hydrogels. Large stocks of functionalized glasses can be stored at room temperature and dark in a closed vessel for various days. Poly-acrylamide hydrogels were produced by chemical radical polymerization with 1:1000 TEMED (Sigma-Aldrich) and 1:100 v/v of 10% w/v ammonium persulphate (APS , Sigma-Aldrich). 30x30 cm glass supports previously treated with tridecafluoro-octyl-trichlorosilane vapors were used for the production of hydrogel in large batches. Hydrogels were rinsed for 10 minutes in distilled water and UV sterilized for 15 min. On sterile Parafilm foils 50 $\mu g/ml$ fibronectin (Sigma-Aldrich) drops were spotted and each hydrogel was placed in contact with the solution at 37 °C for 2 hours.

	protein cross-link	pros	cons	suitable for large-scale
sulfo-SANPAH	variable between samples and lots	use of native proteins	expensive, needs UV exposure	no
6-((acryloyl)amino) hexanoic acid	effective and consistent	directly incorporated during polymerization	expensive, cross-link lost in the hydrogel bulk	no
hydrazine/sodium periodate	effective and consistent	cheap, hydrogel activation in large stocks and used as necessary	protein derivation necessary, longer procedure	yes

Table G.2.1 – Functionalization strategies for poly-acrylamide hydrogels. Protein cross-linking was assessed by cell seeding after extensive washes of finalized substrates with fibronectin. Pros and cons are reported for each technique and suitability for large-scale hydrogel production is evidenced.

G.2 Functionalization of poly-acrylamide hydrogels

Functionalization of poly-acrylamide hydrogel have been performed with three techniques: sulfo-SANPAH [111], 6-((acryloyl)amino) hexanoic acid [79] and hydrazine [117]. As reported in Table G.2.1, hydrazine has revealed the most effective and convenient method for a large scale functionalization of poly-acrylamide hydrogels.

Protocol is based on Damljanovic et al. 2005 [117]. Minor changes follow. Single drops of 70% hydrazine hydrate (Sigma-Aldrich) are placed on each hydrogel and leave to reach until dryness in a closed glass vessel. Reaction is usually performed overnight. Two additional water rinses have been added before and after the neutralization with 5% acetic acid to properly restore a neutral pH. Hundreds of hydrogel are prepared at once and are kept in a closed vessel. Fibronectin has been used instead of collagen since it can serve a broader selection of cell types. Since sodium periodate is hygroscopic, must be prepared fresh and few milligrams are sufficient for tens of hydrogels, we opted for preparing a stock solution, easier to dissolve in the protein solution and we performed the reaction also overnight at 4 °C. 40 μl of oxidized protein are placed on a Parafilm foil and treated hydrogels are turned on each drop for 1 h. Hydrogel are rinsed three times with water and then sterilized under 280 nm UV-light for 15 minutes.

	hydrogel integration	hydrogel lamination
diazonium salts [159]	yes	yes
acryl-terminated silanes	yes	yes
methacrylic anhydride	no	-
amine-terminated silane/glutaraldehyde [108]	yes	no

Table G.3.1 – Tested bridging molecules for hydrogel integration in PS Petri dishes. At the end of the polymerization phase some hydrogel did non integrated with the PS surface while others laminated because of swelling few hours after placing the hydrogel in water or buffered solutions.

G.3 Functionalization of PS support

Various techniques and operative conditions have been tested for the polymerization of hydrogel supports on commercially available poly-styrene dishes (Table G.3.1). Poly-styrene has been treated with an oxygen plasma (Harrick Plasma) at 30 W for 5 minutes. A 1% v/v acqueous solution of 3-aminopropyl-trimethoxysilane (Sigma-Aldrich) was used to aminate the surface for 1 h. After several rinses with water, a 1% v/v glutaraldehyde (Sigma-Aldrich) was used to react with the amine terminus. A degassed acrylamide/bis-acrylamide prepolymer was poored inside the functionalized PS vessel to produce a ∼1 mm thick layer. Polymerization was performed at room temperature for 1 h with 1:1000 TEMED (Sigma-Aldrich) and 1:50 v/v of 10% w/v APS (Sigma-Aldrich). Before rinsing the gel in water, hydrogels were dehydrated under the hood for additional 2 hours.

G.4 3D biodegradable hydrogels

G.4.1 Methacrylated HA derivation

Hyaluronic acid of 700 kDa provided by Fidia Farmaceutici s.r.l. (Italy) is derived with methacrylated termini on the primary hydroxyl group available on dimeric unit of HA. HA is dissolved at 0.5% w/v in water and cooled on ice. Methacrylic anhydride is added to reach a 10X molar excess of hydroxyl groups. Reaction is conducted vigorously stirring the solution on ice overnight. Product is distilled in water for 24 hours using a 10 kDa cut-off cellulose membrane.

G.4.2 Methacrylated proteins derivation

Collagen I rat tail or type-A gelatin are dissolved in phosphate saline solution at pH 7.8 at 20% w/v in 60 °C water. A 2X excess of methacrylic anhydride is added for 2 hours at 40 °C. Solution is then diluited in PBS pH 7.4 at 5% w/v to stop the reaction. Functionalized proteins are stored at 4 °C. Since abundant amines groups tend interact with other groups promoting a physical gelation process at high concentration (>2%) and low temperatures (<10 °C), the modification of amines allow the gelation only at lower temperatures. Gelatin methacrylation can be assessed by producing a pure gelatin cross-linked hydrogel. 1:1000 TEMED (Sigma-Aldrich) and 1:100 10% w/v solution of ammonium persulphate (Sigma-Aldrich) are mixed within a gelatin sample. A compact hard gel is produced in <10 minutes.